Implications for Underwater Shock Response of Adopting Simplified Structural Styles in Warships

Nicholas Ian Charles Bradbeer

A thesis submitted for the degree of Doctor of Philosophy

Department of Mechanical Engineering, UCL

2013

I, Nicholas Bradbeer confirm that the work presented in this thesis is my own. Where information has been derived from other sources, I confirm that this has been indicated in the thesis.

Abstract

Over the last two decades there has been increasing interest among naval ship designers to adopt design style elements, standards and practices from commercial shipbuilding. Notable among this is a transition from the highly complex structural styles prevalent during the Cold War to simpler, more readily produced structure. It is generally presumed that this will reduce ship procurement costs, but may also have an effect on operational characteristics, including vulnerability to hostile action.

Many naval weapon systems employ shock from underwater explosions as their damaging mechanism. In severe cases shock can cause catastrophic loss of watertight integrity, but in even moderate cases of shock the resulting acceleration environment inside the ship can damage or destroy vital equipment. The research presented in this thesis attempted to quantify the effect of adopting simpler structural styles upon this damaging acceleration environment.

A number of different frigate structural models were specifically designed, using different structural styles but to meet the same design strength criteria. These models were subjected to simulated underwater explosions using Fluid Structure Interaction Finite Element Analysis techniques and the resulting motions at likely equipment mounting points computed. Results are presented in the form of comparative shock response spectra and also compared against existing shock response prediction techniques.

This thesis concludes that the adoption of certain simplified structural styles in warships can lead to significantly elevated shock response motions, compared to those expected from a ship with a more typical naval structural style. In particular, the adoption of reducing the number of stiffeners, or adopting lower cost stiffener profiles, may result in motions increased by a degree significant enough that they should be taken into account when specifying the shock tolerance or mounting arrangements for on-board equipment.

Dedication

To Lucy, the most supportive wife anyone could ask for.

Acknowledgements

While I as sole author bear full responsibility for the research presented in this thesis, it would not have been possible without the assistance and support of a number of other people.

First, I must thank my supervisors: Prof. David Andrews, for providing guidance and support throughout the research without ever dictating the direction the work should take; and David Fellows, for calm encouragement at the crucial stages and for teaching me the art of asking questions. I am also very grateful to Prof. Paul Wrobel, without whose support over the last two years of the research period this thesis might never have come to be written.

I should also like to express my thanks for the friendship and wisdom of the many talented researchers in the Marine Research Group with whom I have shared offices, conversations and coffee over the last five years, and from whom I have learned a great deal; in particular, Dr Rachel Pawling, Dr Tim MacDonald, Dr Tom Grafton, Lucy Collins and Ian Whitelegg.

I am immensely grateful to Phil Thompson, Kenny Stultz and Andrew Nicholson of Weidlinger Associates, who provided me with their specialist EPSA and FUSE2D software as well as training in its use and continued support throughout the project. Without their generous assistance, this project would simply not have been possible.

I would also like to acknowledge the help and support given by David Manley and Helen Peterson at the Ministry of Defence, who provided initial direction, technical advice and access to data, as well as reviewing the validation work that could not be published in the thesis for security reasons.

Finally, thanks are due (long overdue, in fact) to several individuals at BMT Defence Services Ltd who, with the Engineering and Physical Sciences Research Council, provided the funding that made this research possible. In particular: Roy Quilliam, who sponsored the award of a CASE Studentship; and Matt Roberts, and later Phil Green, who acted as project supervisor.

Table of Contents

List of Figures

Appendix D:

Appendix E:

List of Tables

Nomenclature

Terminology

AMA — Added Mass Approximation; a mathematical model of fluid/structure interaction, suitable for the latter stages of modelling an UNDEX response where loads occur at relatively low frequencies relative to the hull's primary natural frequencies;

As/A — Stiffener material fraction; the proportion of the total structural material cross sectional area in a stiffened panel which is provided by the stiffeners (the rest being in the plating);

CFL — The Courant-Friedrichs-Lewy condition; a condition of stability of many explicit finite element solvers, including EPSA and FUSE2D (Courant, Friedrichs and Lewy, 1967);

CCM — Computational continuum mechanics, the field of numerical modelling which includes finite element analysis and computational fluid dynamics;

DAA — Doubly Asymptotic Approximation; a mathematical model of fluid/structure interaction which is asymptotic to the AMA for low frequency and to the PWA at high frequency loading, and is therefore suitable for modelling all stages of an UNDEX response

DDAM — Dynamic Design Analysis Method; a shock modelling method used by the US Navy (O'Hara, 1965);

EGCS — Environmental Grade Curve Scheme; a shock modelling method used by the UK MoD (Ministry of Defence, 1974);

EPSA — Elasto-Plastic Shell Analysis, an explicit Lagrangian finite element analysis tool with fluid/structure interaction capabilities, for simulating the motions of a structure following a shock event;

FE — Finite element;

FEA — Finite element analysis;

FSI — Fluid/structure interaction;

FUSE2D	Farfield Underwater Shock Effects 2D; an explicit Lagrangian finite element analysis tool for generating an axisymmetric pressure field resulting from an underwater explosion, more generally referred to as FUSE since older versions of the FUSE software are now obsolete;
GRG2	A gradient-reduction based nonlinear optimisation solver algorithm, the basis for the Microsoft Solver nonlinear optimisation function within Microsoft Excel (Lasdon and Waren, 1981);
HBX-1	Hexahydro-1,3,5 Trinitro-8-triazine; a commonly-used explosive;
HSF	Hull Shock Factor, a measure of shock factor which only takes account of the weight and standoff of the charge (defined in Section 2.3 b, p45);
Hydrocode	The class of CCM software which can model fluid/structure interaction problems
Hypermesh	A finite element pre-processing software suite published by Altair Engineering, Inc. (Atkash, Bieniek and Baron, 1983);
Kickoff Velocity	The maximum steady-state velocity reached by a shock-loaded plate, reached when local cavitation occurs;
KSF	Keel Shock Factor, a measure of shock factor which takes into account the angle of inclination of the path to the charge (defined in Section 2.3 b, p45) ;
kT	kiloton of TNT; a measure of the power of large (usually nuclear) explosions;
LS-DYNA	A finite element analysis solver published by Livermore Software Technology Corporation (Livermore Software Technology Corporation, 2013);
LTYMAT	The variable in EPSA defining the choice of material stress/strain model (Stultz, 2009);
MoD	(UK) Ministry of Defence;
NATO	North Atlantic Treaty Organisation
NCRE	(British) Naval Construction Research Establishment, now part of QinetiQ, based at Rosyth;

NFR-90	The NATO Frigate Replacement for the 1990s; a multi-national ship procurement project which reached the feasibility design stage before being cancelled;
NRL	(US) Naval Research Laboratory, based at Washington, D.C.;
NSR2	Lloyds Register's Naval Ship Rules 2; a set of classification society rules intended for the classification of medium-sized surface combatants, for example frigates and corvettes (Lloyds Register, 2008);
Paramarine	A naval architecture software suite, published by Graphics Research Corporation Ltd, A QinetiQ Company (QinetiQ, 2013);
PTV	Peak translational velocity;
PWA	The Plane Wave Approximation; a mathematical model of fluid/structure interaction, suitable for modelling the early stages of an UNDEX response, where the loads occur at relatively high frequencies relative to the hull's natural frequencies;
SSCP-23	Ship Systems Controllerate Publication 23; a MoD publication describing ship structural design methods, based on *The Design of Ships Structures* (Chalmers, 1993);
TCL	Tool Command Language; a scripting language applicable to Hypermesh;
te	Metric tonnes;
TNT	Trinitrotoluene, a commonly-used explosive;
UNDEX	Underwater Explosion;
USA	Underwater Shock Analysis; a hydrocode compatible with a number of FEA solvers;
UPC	Unit Procurement Cost

Mathematical Terms

A Pseudo-acceleration (ms^{-2}), see (Hall, 2002 p. 24.6);

A_w Stiffener web area (m^2);

C Shockwave celerity (ms^{-1}), or a constant depending on ship type or equipment mounting, or the damping matrix in a finite element analysis calculation, or the damping factor of a dashpot;

c Speed of sound in water (ms^{-1});

C_B Block coefficient; the ratio of the volumetric displacement of a ship to the volume of the cuboid with the same waterline length, beam and draught;

C_m Midship section coefficient; the ratio of the area of a ship's midship section below the waterline to that of the rectangle with the same waterline beam and draught;

C_p Prismatic coefficient; the ratio of the volumetric displacement of a ship to that of the prism generated by extruding its midship section over its whole waterline length;

f Response frequency (Hz);

I The second moment of area of a two-dimensional shape;

K The stiffness matrix in a finite element analysis calculation, or the stiffness of a spring;

K_p Dimensionless parameter describing an explosive in Cole's similitude equations (see Section 4.3);

K_θ Dimensionless parameter describing an explosive in Cole's similitude equations (see Section 4.3);

M The mass matrix in a finite element analysis calculation, or a mass;

m_0 Mass per unit area of a plate in Taylor's equation (see Section 4.3), or a dimensionless parameter describing an explosive in Cole's similitude equations (see Section 4.3);

m_θ Dimensionless parameter describing an explosive in Cole's similitude equations (see Section 4.3);

ms Milliseconds;

P Incident pressure arising from a shockwave (Pa);

p_0 Peak pressure of the shockwave (Pa);

Q Quality factor, a measure of system damping;

R Standoff distance from the explosive charge (m);

t Time elapsed (s);

t_0 Time of the shockwave arrival

t_{max} Time for the kick-off velocity to be reached

$x(t)$ Absolute response displacement of a shock mount;

V Velocity (ms^{-1}), or pseudo-velocity (ms^{-1}) , see (Hall, 2002 p. 24.6);

$\bar{V}(t)$ A characteristic velocity/time profile which may be scaled by shock factor (ms^{-1}) (see Section 4.3);

W Charge weight (kg);

Z Section modulus (m^3), typically considered for a stiffener with a quantity of associated plating;

$z(t)$ Displacement of a shock mount relative to the mount's base;

α The mass-proportional damping coefficient in Rayleigh damping ;

β The stiffness-proportional damping coefficient in Rayleigh damping, or a parameter in Taylor's equations;

ζ Damping ratio;

ρ Water density ($te.m^{-3}$);

θ Angle between the line from the keel of the ship to the explosive charge and the horizontal (degrees), or the shockwave decay time constant in Cole's similitude equations (see Section 4.3);

ω Angular response frequency (radians s^{-2});

Chapter 1 Introduction

This chapter provides the context for the thesis, starting with an outline of the perceived research need. The research aims are then laid out and an outline of limits placed upon the scope of the project is presented. The chapter concludes with an overview of the thesis structure.

1.1 The Research Need

In the decades following the end of the Second World War, warships of the Royal Navy (and NATO nations more generally) were built with structures typified by light steel plating, reinforced by a large number of relatively small longitudinal stiffeners, supported in turn by larger transverse frames with sophisticated joint connections (Faulkner, 1964). These structures were relatively complex and expensive to manufacture but lightweight, requiring a relatively small fraction of the ship's total mass and allowing a greater quantity of propulsive and combat systems to be carried. Since the latter years of the Cold War, a trend towards a different style has emerged; accepting increased structural weight for reduced structural complexity, driven by the desire for cheaper ship production.

Structural style can have a significant effect on a ship's ability to withstand the shock loading caused by the underwater explosion (UNDEX) of a mine, torpedo or a near-miss bomb, shell or missile. Shock can damage ships through two mechanisms; in severe cases it can damage the structure badly enough to cause widespread flooding or loss of residual strength (breaking the ship's back). In more moderate cases the structure may be left substantially intact while the resulting motion environment inside the ship could be severe enough to damage equipment and injure personnel. It is possible to design equipment or protective measures to withstand a shock event of a specified severity, if the resulting motions inside the structure are understood.

Models already exist (in the UK, principally the Environmental Grade Curve Scheme (Ministry of Defence, 1974), which is discussed in Chapter 2) to predict the shock response motions inside ships for a given severity of UNDEX, but these models are based primarily upon trials conducted on ships with the lightweight, post-War structural style. It is not clear how valid these results remain as the structural style changes. Should they no longer be valid, then two problems arise. Firstly, if the cost savings of adopting a simpler structure are understood but the performance impact (including the effect of the structural style on shock response) is not,

then a cost-capability tradeoff decision about structural style cannot be made in a fully informed manner. Secondly, if the shock response environment inside the ship cannot be properly predicted then the shock resistance specification for equipment and resilient mountings in the ship is unlikely to be correctly formulated, with resultant operational risk.

1.2 Research Aims

The aims of this research were as follows:

i) - Quantify the changes in shock response motions arising from the adoption of structural styles that depart from the 'classical' post-war frigate/destroyer styles, the main objective being to determine whether they are significant enough to require taking the structural style into account when specifying equipment shock protection levels;

ii) - Provide sufficient data to determine whether the UK Ministry of Defence Environmental Grade Curve Scheme (Ministry of Defence, 1974) remains valid for typical warships with structural styles that depart from the 'classical' post-war arrangements, and if not, to determine the limits of validity;

iii) - Develop and demonstrate a method for modelling the impact of structural style on shock response motions, which could be applied to later work in the same field.

1.3 Scope of Research

It was found in investigating the topic that it was necessary to restrict the scope of the research. Limitations were defined in three main areas, namely the methods of research adopted, limiting the research objectives and restricting the scale of the study.

1.3 a Methods of research

The method of simulating UNDEX response was limited to computational finite element analysis (FEA). Experimental trials using explosive charges or seismic airguns would have been prohibitively expensive, not least because of the need to construct large and complex free-floating structural models. Finite element analysis is considered to be sufficiently mature to provide a model of fluid/structure interaction (FSI) and the resulting structural motions of sufficient fidelity to support decision making, so long as it is validated against full-scale trials (Didoszak, Shin and Lewis, 2004; Mair, Reese and Hartsough, 1999; Shin and Schneider, 2003;

Shin, 2004). The FEA methods selected for this investigation are described in more detail, with a discussion of their relative merits, in Chapter 2.

1.3 b Limited objectives

The objectives of the study were limited in the following five regards:

i) Response motions

The study was limited to comparing the shock response motion environment between different structural styles; no attempt was made to assess the effect of different styles on the hull lethal shock factor (that is, the severity of shock at which structural damage is sufficient to cause catastrophic flooding or loss of residual strength (Ministry of Defence, 1974). Shock factor is discussed in detail in Chapter 2.) The importance of the design of structural details in determining the ability of a structure to withstand catastrophic failure under shock loading is well understood (Chalmers, 1993). Modelling those details with sufficient fidelity would have greatly complicated the structural modelling process and, while it is important to eventually address this, the whole-ship investigation undertaken in this study is seen as a necessary first step.

ii) Choice of shock severity

Shock events modelled in the study were kept to moderate severities; that is, a level was selected which was likely to limit the structural response behaviour to elasto-plastic distortion without rupturing, allowing the structure to be modelled without consideration of the shock responses likely to cause tensile failure. This was seen as the most appropriate way to tackle the significant design issue of equipment and system robustness to the ship shock environment. At the request of the UK MoD, the exact charge size and resultant shock factor used are not detailed in the main body of this thesis.

iii) Shockwave

The investigation only considered the structural response to the initial shockwave, disregarding the loading caused by the later bubble pulse phase (mechanisms described in Section 2.2). This was considered a reasonable limitation since the internal acceleration environment is usually dominated by the shockwave (Keil, 1961), while the effect of the bubble would be more important if whole-ship whipping and hull girder structural failure were being considered (Hicks, 1986; Keil, 1961; Reid, 1996). Disregarding the bubble pulse phase had the additional benefit of allowing the simulation to model a much shorter time period,

which reduced the already considerable computation time required by the simulations presented.

iv) Deep water

All simulations were assumed to represent ship structural behaviour in deep water, which meant that the only paths for shock transmission were the direct path and a single reflection from the free surface. The interaction of multiple shock paths would have created a complex pressure field with constructive and destructive nodes, introducing the possibility that vagarities of the pressure field might have overshadowed the effect of the different structural styles.

v) Internal fluids

Due to the limitations of the modelling tools used, all tanks in the ships modelled were assumed to be empty. This is clearly unrepresentative of a warship in service, and physical trials have shown (Keil, 1961) that pressed full double bottom tanks significantly increase the loading on the inner bottom. However, partially filled double bottom tanks are more likely than fully pressed, and the same studies showed that in such cases the spray thrown against the inner bottom in partially-filled tank states strikes over a sufficiently long period as to avoid significantly loading it.

1.3 c Scale of Study

This research was not intended to be a fully comprehensive study of the topic, but rather to establish whether the magnitude of the problem of different structural styles warranted further studies to be conducted, and to demonstrate a suitable method. The scale and granularity of the study were therefore limited in the following four aspects:

i) Hull type

The investigation was planned using a single ship type, representative of a typical monohull surface escort. (In fact, a second ship type was used for one experiment series, but no attempt was made to present a wide enough range of ships to explore the response motions over a variety of hull sizes and forms.)

ii) Charge size

The investigation was limited to a single charge size and location. No attempt was made to explore the response motions with change in shock severity or charge location.

iii) Range of style parameters

The investigation examined the effect of changing only a limited number of style parameters, i.e. reduction in the number of stiffeners, use of simplified stiffener geometries, and adoption of transverse stiffening in place of longitudinal. These were considered to be the most appropriate choices for an initial study of the wider topic, and are discussed further in the opening section of Chapter 5.

iv) Number of simulations per study

The investigation was limited to the simulation of only two or three structural models for each study of a single style parameter. For example, the examination of reduction in stiffener numbers considered a baseline case, plus one case with moderate reduction and one case with extreme reduction. Since the aim was a coarse determination of the magnitude of the effect on motion responses, this was considered sufficient and is discussed further in Chapter 8 after the results have been presented.

1.4 Outline of Thesis

This thesis presents a description of a structural dynamics simulation-based research project undertaken to meet the research aims just outlined. In summary, the project comprised the following activities:

i) Development of a method to design midship structural sections of equivalent strength but different structural styles;

ii) Production of a number of midship structural sections of equivalent strength in which the structural styles were varied from the 'classical' post-war warship style;

iii) Computational simulation of the response of those structures to an underwater explosion, using fluid-structure interaction finite element analysis;

iv) Scrutinising the resulting motions to identify the effect of the variation in structural style on shock response motions.

The thesis reports the research undertaken in the subsequent eight chapters:

Chapter 2: Underwater Shock. This presents a critical evaluation of previous work done in the fields of ship structural design and shock response modelling, both to place the project in context and to explain how previous work informed many of the decisions made in this research. The chapter also includes a summary of the physical phenomena associated with shock.

Chapter 3: Modelling Warship Structures. This details the method used to produce ship structural sections of a specified strength, represent them in a finite element modelling tool and simulate the effects of an underwater explosion upon them.

Chapter 4: Verification and Validation. This presents the measures taken to give confidence that the chosen modelling and simulation methods produced outputs indicative of the real situations they simulated.

Chapter 5: **Parameter Selection.** This describes the defining parameters chosen for each simulation case; the structural styles selected for assessment, the baseline ships the structures were designed for, and the resulting individual structural models. This chapter also describes the geometry of the single shock scenario that was used for all simulations.

Chapter 6: Methods for Processing and Presentation of Shock Response Motions. This describes the methods chosen to process the raw data from the simulation outputs into a format which allowed ready understanding and comparison.

Chapter 7: Results of Finite Element Analysis of Shock Loading Ship Structural Models: This presents the results from the simulation and makes observations about patterns observed within them.

Chapter 8: Discussion. This considers the results of the project in terms of the research goals, including the implications for the ship designer and the writer of equipment shock specification. A critical examination of the research method is presented, with an assessment of which techniques worked well and which less so.

Chapter 9: Conclusions. This presents a concise summary of the project's results in terms of its original contribution to knowledge and an assessment of the degree to which the research goals have been met, together with suggestions for future work.

Chapter 2 Underwater Shock

This Chapter begins with a brief overview of the history of shock response research in the UK and USA, followed by two sections describing of the physical phenomena which follow an underwater explosion and the resultant effects on nearby surface ships. The Chapter concludes with an overview of the three primary methods of exploring shock response: full scale trials; small scale trials; and computational methods.

2.1 The History of Shock Response Modelling

While research interest in the effects on naval vessels of shock had existed as far back at the mid-19th Century (Clements, 1972; Keil, 1961), prior to the Second World War ship design concerns were mostly focussed on the consequences of shells striking armour as well the not inconsiderable effects of the ship's own guns' blast effects. Shock protection was limited to armour plating and mounting fragile items far from the hull plating where possible, or hung from springs. Underwater explosion research was focussed on the effects of torpedoes and mines exploding in contact with the hull (Keil, 1961).

During the Second World War, several weapon technologies were used which spurred interest into underwater shock. Germany developed influence ground mines capable of damaging even heavy propulsion machinery through shock (Clements, 1972); proximity-fused torpedoes came into widespread use, and the rise of air power saw ships frequently suffer underwater shock effects from near-missed bombs. 44% of Royal Navy destroyers sunk in the war were lost to broken backs; that is, collapse of the main hull structural girder (Brown, 1990). Thus research into the effects of stand-off underwater explosions became a priority, particularly in the US and Britain.

In the last year of the war, and immediately post-war, the US and Britain embarked on a significant programme of instrumented full-scale shock trials: Britain expending 17 destroyers, two cruisers and a number of submarines in tests using mines and ASW mortar depth charges (Brown, 1987a; c; d), while the US subjected several destroyers and a submarine to controlled attack by depth charges (Rich et al., 1961). Realising the potential of the nuclear warhead as a naval weapon, the US undertook the first underwater nuclear test in 1946; Shot BAKER of Operation CROSSROADS, in which a 23kT fission device was detonated underwater in Bikini Atoll, in the vicinity of two aircraft carriers, five battleships, three large cruisers, ten

destroyers, eight submarines and 62 varied amphibious and auxiliary ships (Delgado, Lenihan and Murphy, 1991). Figure 2.1.1 shows the scale of the test.

Figure 2.1.1 - Shot BAKER of Operation CROSSROADS, demonstrating the scale of the underwater nuclear test (US Department of Defense, 1946)

By this point, the behaviour of the water following an underwater explosion was reasonably well understood, and Cole published his seminal book "Underwater Explosions" (Cole, 1948). However, the effect of shock on structure and equipment was less well understood, and full scale trials remained the best way of obtaining understanding of the effects of shock on ship structures.

In the same year, Walsh and Blake at the US Naval Research Laboratory produced NRL Report 3302 (Walsh and Blake, 1948), in which they established that the shock response of a structure was highly sensitive to the structure's natural frequencies and applied earlier work by Biot on buildings' response to earthquakes to the naval underwater shock domain. They described their application of Biot's "earthquake spectrum" to ship-like structures as a "shock spectrum" and presented a practical means by which one could be generated from experimental data. The concept of the shock is described more thoroughly in Section 6.5 as it was central to the way the data from this research was presented.

In 1950, the US Office of Naval Research and the (British) Naval Construction Research Establishment, Dunfermline (now QinetiQ Rosyth) jointly published a three volume compendium "Underwater Explosion Research" (US Office of Naval Research and Naval Construction Research Establishment, Dunfermline, 1950a; b; c) containing an estimated 10-20 percent of all the literature then available in the field of underwater explosion. Volumes 1 and

2 dealt with the behaviour of the shockwave and the gas bubble respectively, while Volume 3 dealt with the effects of shock on structures; the latter largely limited to the analytical assessment of the behaviour of single ship plates or stiffened panels.

In the years after the war, the US adopted the "static g" method, also known as the "shock numbers method", where shock loading on equipment was expressed as an equivalent static acceleration. A "shock numbers" plot is reproduced from (Clements, 1972) at Figure 2.1.2. By selecting the mass of the equipment and the appropriate curve for the direction of loading, a "shock design number" can be read off the graph's ordinate. A force equal to the equipment's weight multiplied by this factor was assumed to act at the equipment's centre of gravity, and static force analysis used to calculate the required strength of mountings, supports and tie-down bolts.

Figure 2.1.2 – A typical Shock Design Numbers graph, from (Clements, 1972)

The static g method was simple but imperfect. It took no account of how or where the equipment was mounted in the ship (beyond the potential to have different sets of curve available for different broad regions of the ship) and it took no account of any interaction between the equipment and the structure upon which it was mounted. O'Hara pointed out these flaws in a since-declassified NRL report (O'Hara, 1958) and an article published in the *Journal of the Acoustical society of America* (O'Hara, 1959), arguing that the latter flaw in

particular was so significant that the static g method should be abandoned. Application of the static g curves to pre-existing ships had implied extremely severe design shock loads, which would have resulted in no equipment remaining effective, and yet many items of equipment subjected to such shock loads in full scale trials had done so.

Analysis revealed that non rigid items of equipment on non-rigid foundations tend to feed back forces into the foundations in such a manner as to act as a mechanical damper around the normal modal frequencies of the equipment in question, causing dips in any spectrum of driving forces around those frequencies (O'Hara, 1958). Since these were the frequencies at which the equipment was most sensitive to excitation, these 'spectrum dips' had a fundamental effect on the response motions of the equipment item. O'Hara argued that modelling equipment items as rigid masses, disregarding this interaction, must inevitably lead to significantly conservative overdesign, and presented an alternative method for predicting shock motions, the Dynamic Design Analysis Method, or DDAM.

DDAM was defined in the 1961 NRL Report 5545, also published as NAVSHIPS 250-423-30. This report is classified US CONFIDENTIAL and was not available to the candidate. However, the general nature of the method is described in other unclassified publications (Cunniff and Pohland, 1993; O'Hara, 1965). Mode theory was used to describe the equipment under consideration in terms of its normal modes of vibration, with corresponding frequencies and modal masses, which was then presented in the form of mass and stiffness matrices. An example of such a model is shown at Figure 2.1.3. Loading was defined by design shock spectra as specified in (O'Hara and Belsheim, 1963), and the resulting motions analysed assuming linear elastic behaviour and a least-energy response. DDAM is still in use by the US Navy, although several revisions have been implemented to the original method (Cunniff and Pohland, 1993).

Figure 2.1.3 – Turbogenerator represented as masses and springs for DDAM analysis of athwartship motions, from (Fisher and Parr, 1967)

The approach that the (British) Naval Construction Research Establishment was taking at the same time is not widely discussed in the unclassified literature, although it is chronicled in a classified UK MoD Book of Reference (Ministry of Defence, 1974). In broad terms, empirical design shock loads were defined for various combinations of equipment, ships and mounting configurations, based upon the results of full scale trials. Greenhorn (1999) provided a rare insight into the British research approach in his summary of the SSVUL vulnerability assessment software, in which equipment survivability following a shock event was determined based on an effective shock factor calculated at the point of mounting. This was a much cruder approach than the DDAM, apparently taking no account of the type of ship, the mounting location (beyond whether hull, deck or bulkhead mounted) or the design of the equipment itself. However, the paper provided a description of the methods in use by an early whole-ship vulnerability assessment code, and the simplicity of the method may have been due more to the limited computational power available than any lack of understanding of the physical phenomena.

The development of finite element analysis (FEA) through the 1960s and 70s brought a fresh approach to the field, although computer processing power initially limited its scope to extremely simplified models. Modern computers allow for the simulation of entire ships at the individual stiffener level, and FEA holds the promise of allowing shock response analysis earlier in the ship design process, as well as dramatically reducing the cost of modelling a new ship's shock response compared to full-scale testing (Shin, Didoszak and Christian, 2005). FEA is the

technique which was used in this investigation, and is discussed in more detail later in Section 2.6.

Weapons employing standoff underwater explosions remain in widespread use throughout the world. Heavyweight torpedoes remain the anti-ship weapon of choice for the naval submarine, and mines continue to provide a cost effective sea denial capability. Designing warships to survive UNDEX attack remains as relevant as it was seventy years ago.

2.2 The in-fluid phenomena following an underwater explosion

The response of a fluid to the detonation of a spherical explosive charge has been well understood since the 1940s, with Cole (1948) publishing the seminal comprehensive examination of the resulting phenomena, based on work conducted while he was the research supervisor at the US Underwater Explosions Research Department at Woods Hole. While the experimental techniques described in Cole's book have been supplanted with the development of more modern transducers, the algorithms produced to predict the nature of the various post-detonation events remain in use today. In particular, Cole's 'similitude equations' are used to predict the resultant pressures, shockwave peak pressure and decay constant and the parameters of the gas bubble, for a variety of different explosives.

Swisdak (1978) provided a very useful and thorough summary of the fluid behaviour following an UNDEX. Notably, this was presented in SI units rather than the US Customary units used in previous US reports. Reid (1996) provided a useful précis of the major phenomena and algorithms to model them, following a year-long exchange placement with the US Navy's Underwater Explosions Research Department at Carderock. Reid's report, which was published openly by the Australian government, offers a good introduction, and contains coefficients allowing for the application of Cole's similitude equations to underwater nuclear detonations. While the fluid behaviour following an UNDEX has been thoroughly described in other publications, it is central to the theme of this investigation and therefore is briefly summarised here. Detonation of an explosive charge underwater has two principal products; a shockwave and a bubble of high temperature, high pressure gas. The timescales over which these two phenomena act differ by approximately two orders of magnitude, so it is often possible to consider their effects independently of one another (Swisdak, 1978).

2.2 a Shockwave

For a 1500lb charge of TNT, approximately 53% of the total energy of the explosion is delivered into the shockwave (Keil, 1961). Of that, 20% is lost to non-adiabatic temperature increase around the wavefront during early propagation (for typical warhead charge sizes, this will usually occur within the first millisecond), leaving 33% radiating in the shockwave. The shockwave is approximately spherical, and initially expands at a celerity related to the explosion pressure by the approximation, from (Keil, 1961):

$$C = c(1 + 870 \times 10^{-6} p_0) \qquad \text{(Eq 2.1)}$$

where C is the shockwave celerity, c the speed of sound in water and p_0 the pressure drop across the shockwave in MPa.

For typical TNT warhead sizes, this pressure is initially on the order of 70MPa (Reid, 1996), resulting in an initial celerity up to 1.06 times the acoustic propagation celerity. As the shock front expands its celerity rapidly falls to the speed of sound in water, approximately 1525ms^{-1}. As the wavefront passes a given point, it causes a near-instantaneous pressure rise (over a few microseconds) followed by an approximately exponential decay period. (In fact, the decay is near-exponential until approximately one decay constant has passed, after which the decay occurs slightly more slowly – a correction .) The decay constant, that is, the time taken for the pressure to fall by a factor of $\frac{1}{e}$ is between 0.25ms and 1.0ms over the typical range of charge sizes (10-500kg TNT) and standoff ranges (10m-100m) of interest, meaning that the thickness of the shock wavefront is on the order of 1m and the rate of increase in shock on arrival is several hundred times the rate of decay.

Cole's similitude equations allow the calculation of peak pressure and decay period in terms of charge weight, explosive type and standoff distance. Different explosive compounds have different specific energies as well as different proportions of the total energy divided between shockwave and bubble, so similitude parameters are specific to a particular explosive.

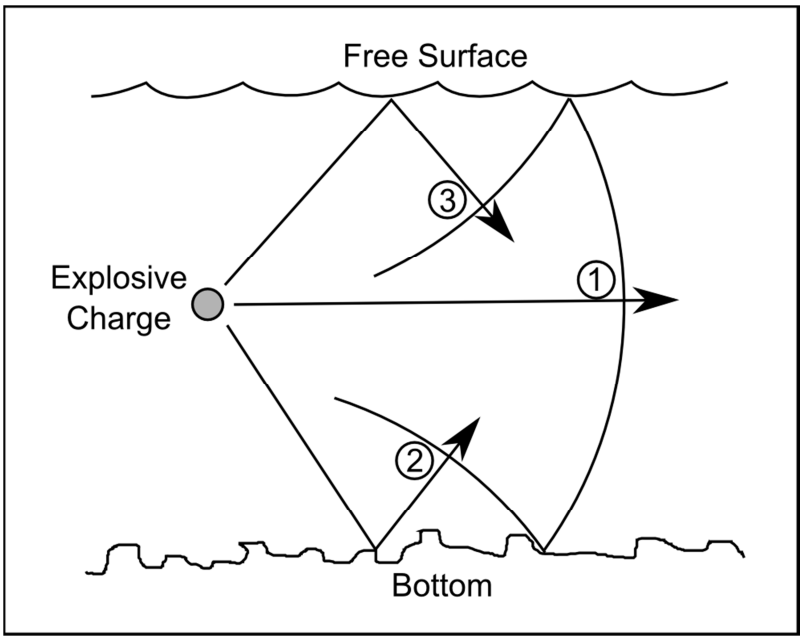

Figure 2.2.1 - Direct and reflected wavefronts

Depending on the depth of water, the shockwave may have three paths to reach a target, as shown in Figure 2.2.1; by direct propagation (1), and by reflection off the bottom (2) or free surface (3). Reflection off the bottom will result in the loss of some energy, so the reflected wavefront will reach a lower peak pressure than the directly propagated wavefront, but it may still provide significant loading to a target. In particular, if the charge is close to the bottom, the reflected wavefront may arrive at a target before the direct wavefront has completely decayed, resulting in a combined pressure loading.

2.2 b Surface cutoff

Reflection from the fluid free surface produces a rarefaction wave. As this wave passes a point in the fluid, it brings a near-instantaneous drop in pressure, followed by a near-exponential decay. This pressure drop acts to cancel the increased pressure brought by the directly propagated wavefront, leading to an abrupt cutoff in the pressure load. This phenomenon is referred to as surface cutoff (Reid, 1996). The relative magnitudes of the two waves are typically such that surface cutoff will reduce the pressure load on the target to near the ambient hydrostatic pressure or slightly below it.

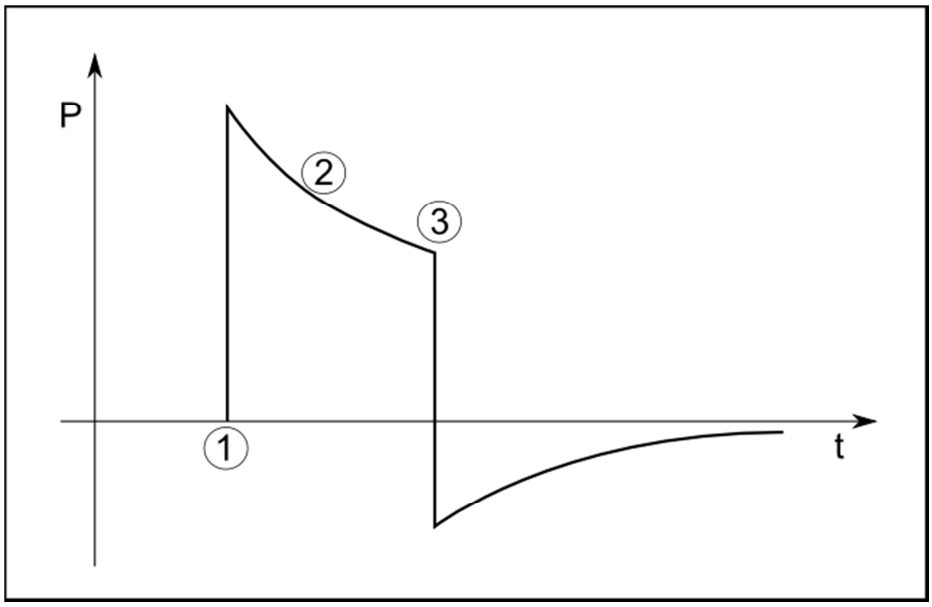

Figure 2.2.2 - Pressure-time plot showing surface cutoff

Figure 2.2.2 shows a typical pressure time history for a fixed point in deep water, including surface cutoff. The directly propagated wavefront arrives at (1) leading to a near-instantaneous rise in pressure followed by a near-exponential decay at (2). The rarefaction wave reflected from the surface arrives at time (3) leading to a near-instantaneous cut-off in the pressure. In moderately deep water, a target near the surface may experience direct loading, then surface cutoff, and then be re-loaded with the arrival of the bottom-reflected wavefront.

2.2 c Bulk Cavitation

A secondary effect of the rarefaction wave is that, near the surface, the pressure behind the wave may fall below the water's vapour pressure. This can lead to cavitation occurring over a volume of revolution with a cross-section similar to that shown in Figure 2.2.3. This is known as bulk cavitation, as distinct from local cavitation which occurs at the point of the shockwave's reaction with a structure. After a period of time, the cavitation region will collapse. This results in a pressure pulse, referred to as the cavitation pulse, being radiated, which can cause re-loading of nearby structures.

Figure 2.2.3 - Bulk cavitation region - from (Shin, 1993) in (Reid, 1996)

2.2 d The Gas Bubble

Aside from the shock wave, the explosion creates a bubble of gas at high temperature and extremely high pressure. There is significant potential energy in this gas; 47% of the total energy of the explosion for a TNT charge (Keil, 1961). As the bubble is initially at significantly higher pressure than the surrounding seawater (between 20 and 50 times the hydrostatic pressure for a typical torpedo warhead explosion), it will expand, eventually reaching an equilibrium pressure. The momentum of the entrained water will continue the bubble's expansion beyond equilibrium until it reaches a maximum size, at which point the pressure differential will cause contraction. Again the bubble will overshoot the equilibrium pressure, reaching a minimum size. The rate of rise of pressure around the bubble's minimum size is much more rapid than around its maximum, and will cause a pressure pulse to be released, referred to as a bubble pulse. The pulse can be quite energetic; in a TNT explosion it will carry 15% of the total explosion energy (Keil, 1961). The bubble may continue to pulsate several times, as illustrated in Figure 2.2.4. For a typical TNT warhead explosion, each pulse will exhaust approximately 60% of the energy remaining in the bubble. The first two pulses therefore expend approximately 84% of the available energy, and subsequent pulses are usually of less interest. The maximum size and period of the bubble can be calculated from Cole's similitude equations (Cole, 1948). Typically the period will be on the order of 1s for charge sizes and charge water depths of interest (Keil, 1961).

Figure 2.2.4 - Bubble pulsation and migration - from (Shin, 1993), in (Reid, 1996)

Due to the difference in hydrostatic pressure between the top and bottom of a large bubble (on the order of 8m for a typical torpedo warhead detonation), during the collapse phase the water at the bottom of the bubble will move faster than the water at the sides or top. As described by Keil (1961), this leads to the formation of an energetic upward-moving water jet which has significant potential for damage if it impacts the underside of a vessel. The action of the jet also means that large bubbles tend towards a toroidal shape around their minimum size, and tend to break up into a cloud of smaller bubbles after a small number of pulsations. If the bubble is formed close to the free surface the jet can cause a large plume, reducing the energy available in later pulsations.

The bubble normally exists long enough (several seconds) for gravity to have a significant effect, and the bubble will rise under its own buoyancy. Due to the momentum of entrained water, it will rise with a maximum velocity when it is near minimum size, and slow almost to a stop when it is near a maximum. This can lead the bubble to rise towards the hull of a target ship, reducing the standoff distance and increasing the pressure loading resulting from bubble pulses. To complicate the bubble's motion further, fluid flow effects act to attract the bubble towards solid objects, while repelling it from fluid free surfaces. These can lead to the bubble "adhering" under the hull of a target vessel, resulting in strong pressure loading from the bubble pulse and increasing the likelihood of bubble jet damage (Cole, 1948, p.332).

2.3 The response of typical ship structures to underwater explosion

It took much longer to understand the motions of ship structures following UNDEX than to understand of the fluid mechanics just described in Section 2.2. By the publication of the Anglo-US compendium Underwater Explosion Research (US Office of Naval Research and Naval Construction Research Establishment, Dunfermline, 1950a; b; c), the fluid mechanics were almost completely developed, while the understanding of structural response was limited to analytical formulae for simple plates, or approximate empirical methods based on full scale trials. Developing this understanding from simple plate reactions to more realistic ship structures took several more decades.

2.3 a Plate loading

Keil (1961) provided one of the few unclassified summaries of the damaging effects of an underwater explosion. It was widely understood that a contact torpedo explosion would rupture the hull over an area perhaps 10m-15m long. Increasing the standoff would decrease the size of the ruptured area until a critical "hull splitting" standoff was reached, beyond which plastic deformation would occur but no rupture of the plating. Increasing the standoff further would eventually reach the critical distance at which all deformation was elastic and no permanent set resulted. Examination of model and full scale tests had given an appreciation for the type of damage likely to result, in qualitative terms. Keil's report included the graph reproduced at Figure 2.3.1, which illustrates the relative timescales of various UNDEX loading phenomena on a wetted shell plate from the midpoint of a compartment.

Examining first the expanded graph in Figure 2.3.1 showing the first 100ms of the response, it can be seen that over the first 20ms the plate maintains a nearly constant rate of deflection, the so-called "kick-off velocity". At the start if this 20ms period, the duration of the incident shock pressure is likely to have been on the order of 1-2ms. Accelerating under this pressure load, the centre of the panel will rapidly exceed the particle velocity of the fluid, resulting in a local pressure drop adjacent to the panel which would be sufficient to cause local cavitation and complete unloading of the panel. The panel therefore continues to deform at constant velocity until decelerated and eventually arrested (over the period from 30-50ms) by the stiffness of the restraining structure. As the panel slows to below the particle flow velocity, the local pressure rises again, and at some point the cavitation region collapses and this "afterflow" reloads the panel. In Figure 2.3.1 this occurs at 65ms, and begins a second period

of panel deflection. The plate subsequently returns elastically to a reduced deformation, shown on the longer plot over the period from 100-200ms, until the first bubble pulse arrives to reload the panel at 1600ms. The diagram illustrates the separation in time of the shockwave-related phenomena from the bubble loading, demonstrating why they are frequently each considered in isolation.

Figure 2.3.1 - Deflection-time history for a panel in the centre of a compartment's sideshell, loaded in a full-scale stand-off UNDEX trial, from (Keil, 1961)

Taylor (1941) provided an empirically-derived method to calculate the kickoff velocity for an infinite flat plate given charge, standoff distance and plate incident angle, a method which is still in widespread use as a validation tool for finite element hydrocodes (Reid, 1996).

2.3 b Shock Factors

Keil (1961) described a simple method to estimate the plastic deformation of a stiffened plate from a kickoff velocity, based on the assumption that the stiffened plate acts as a simple membrane of the equivalent thickness if the stiffeners were spread uniformly over the plate, and demonstrated that it gave results reasonably close to a model test. Noting that the plastic

deflection varied approximately in reverse proportion to the standoff distance, he went on to suggest that a useful predictor of the maximum plastic deformation for a given plate might be:

$$\frac{\sqrt{W}}{R} \qquad \text{(Eq 2.2)}$$

where: *W* is charge weight, in either lb. (for US measurements) or kg (for metric) and *R* is standoff distance from the charge to the hull in either feet (for US measurements) or m (for metric.)

This value is referred to as a shock factor, and remains in use as the most common way to characterise the damaging potential of the shockwave phase of an UNDEX event (Reid, 1996). The customary use of two different unit systems introduces the scope for misunderstandings if the choice of units is not explicitly stated; a shock factor of 1.0 Imperial being equivalent to 2.45 metric. Shock factor is customarily quoted without units, although strictly it should possess units of $kg^{0.5}\,m^{-1}$.

The value given above is referred to as Hull Shock Factor (HSF) and often used when considering the shock effect on a particular hull-mounted item, or when considering the general response of a submarine. When considering ship-wide effects on a surface ship, it is normal to use Keel Shock Factor (KSF) instead, where the standoff R is measured from the charge to the closest point on the keel, and a term is added to take account of the angular position of the charge relative to the ship (see Figure 2.3.2).

For typical warhead charge sizes, KSF is approximately proportional to the Peak Translational Velocity (PTV) imparted to the ship (Reid, 1996), where PTV represents the peak velocity of the average, or rigid body, velocity of a whole hull or section. In simulation, this average velocity may be measured as the motion of the centre of mass of the ship or large ship section.

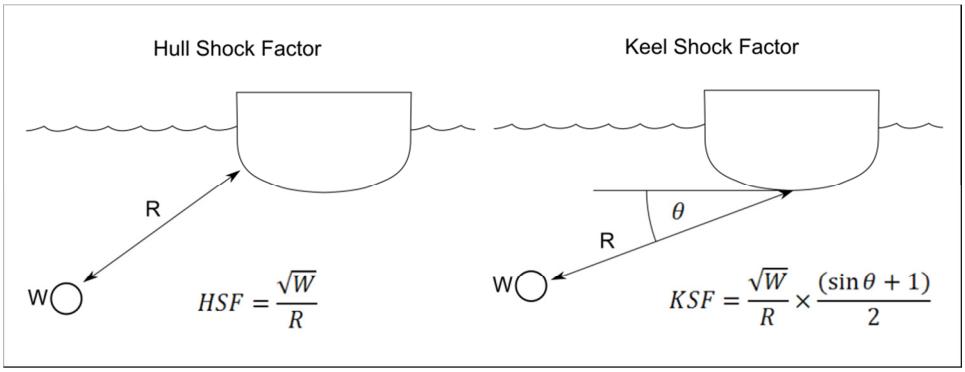

Figure 2.3.2 - Hull Shock Factor and Keel Shock Factor

2.3 c Shock Response Motions

The motion environment inside a ship following a shock arrival is important; in moderate shock events this may be the primary cause of damage to equipment. High accelerations cause damage through brittle failure and overloading of support structures such as mountings, seatings and brackets off primary ship structural members. Large relative displacements between equipment and either structure or other equipment can cause collisions between them, or can break supply connections.

Keil (1961) presented a model for the response throughout the ship following an UNDEX shock, based on an equation of the form:

$$V(t) = C\frac{\sqrt{W}}{R} f(\theta).\bar{V}(t) \qquad \text{(Eq 2.3)}$$

where *V(t)* is the velocity in a given direction with respect to time, *C* is a constant determined by ship type, location aboard ship and type of installation (e.g. deck mounted or bulkhead mounted.) *W, R* and θ are as previously defined. f(θ) might, for example, be defined in the same manner as for KSF for vertical motions; the sine term would be replaced by a cosine for horizontal motions. The $C\frac{\sqrt{W}}{R} f(\theta)$ term can be considered a shock factor. $\bar{V}(t)$ is a characteristic velocity-time history which is then scaled by the shock factor term. In 1961, the only feasible way to derive the characteristic velocity-time histories was to normalise measured results from full-scale trials.

The motions in different parts of the hull may be quite different. While the wetted plating is loaded directly by the shock wavefront with an essentially impulsive load, this load is transmitted through the ship along structure which has a finite stiffness. The structure will therefore deform (elastically or plastically) as it transmits the load which will tend to attenuate accelerations while increasing the period of loading. Locations low in the ship or connected to wetted panels by stiff structure will therefore tend to experience high accelerations for brief periods, while upper decks and other structure connected to wetted panels through long load paths will tend to experience lower accelerations which act over longer periods. Typical velocity-time profiles for the keel, main deck and superstructure of a destroyer subjected to a moderate shock are shown at Figure 2.3.3, reproduced from Keil (1961), where these patterns are clear.

Figure 2.3.3 - Velocity profile through a destroyer following a moderate shock - from (Keil, 1961)

2.3 d Response to bubble loading

The timescales involved in the development of a gas bubble mean that the structure will be settling down from the shockwave loading well before the first bubble pulse arrives. The peak pressure of the first bubble pulse is typically 10-15% of that delivered by the shockwave for a given standoff, although the longer duration means the bubble pulse may deliver a greater total impulse. Additionally, in the case of an under-keel shot, bubble migration may mean that the bubble pulse is delivered from much closer to the hull. If the bubble is close enough to the bottom then the structure may be ruptured, either by the bubble pulse, or the impact of the bubble jet. The mass of water and velocities involved in the jet (which may exceed $100ms^{-1}$, according to Reid(1996)) have the potential to cause significant internal damage and in some torpedo tests may be seen to punch a hole vertically though the ship, for example the exercise sinking of the ex-HMAS Torrens (Australian Collins class submarine torpedo, 1999).

If the bubble is insufficiently energetic or too far from the hull to cause rupture, its most significant effect is likely to be the delivery of sufficient impulse to a localised area of the hull to cause bending of the hull girder, in hogging or sagging depending on the location of the bubble relative to the ship. If the period of the bubble pulsations is close to the first natural frequency of the hull girder (which, for surface escorts is normally in the region of 1Hz) then the bubble loading may excite resonance in the hull girder in longitudinal bending; a phenomenon known as “whipping.” Whipping may result in significant longitudinal bending of

the hull girder, potentially exceeding the buckling strength of the keel, which may well have been weakened by damage from the shockwave or first bubble pulse. Catastrophic buckling of the keel structure results in a loss of overall bending strength and is referred to as having broken the ship's back.

2.4 Full scale shock trials and empirical design data

Before finite element analysis was a mature computational tool, physical experiments were the only way to determine the response of ships to underwater shock loading. Prior to the Second World War there had been little need to design against stand-off underwater explosions, and during the war itself there were few ships that could be spared for such trials. A small number of tests were conducted during the war (Brown, 1987a; Rich et al., 1961), although these trials were usually conducted for very specific purposes and usually conducted on ships rendered unsuitable for service by age or action damage.

In the years following the Second World War, the large number of surplus hulls allowed a relatively large number of full scale explosive trials to take place in both the US and the UK. Brown (1987dc; a; b) described the UK 's post-war shock testing programme. Between 1946 and 1950, seventeen destroyers, two cruisers and five torpedo boats were the subject of shock trials, as well as thirteen submarines and five midget submarines. While the records are incomplete, the trials for which charge data exists subjected the target to Keel Shock Factors of between 0.35 metric and 0.77 metric, with charge sizes of 100lb, 187lb, 1090lb and 6000lb at standoff distances between 90' and 180'. These trials were designed to be non-lethal; the demand for scrap steel was very high at the time, and the instrumentation required re-boarding following the shot to recover data.

The US Navy embarked on a similarly large programme of tests, which became significantly larger when the underwater applications of nuclear weapons were tested. As well as the 1946 Shot BAKER of Operation CROSSROADS (see page 33), the 1958 Shots WAHOO and UMBRELLA of Operation HARDTACK used another eight target vessels (Rich et al., 1961).

No comprehensive record of US Navy shock trials using conventional explosives in the post-war years could be found in the open literature, although references were found to a number of individual trials:

- 1952 - Tests on the submarine USS ULUA and 'Guppy' and 'Minnow'-type submarine models targets (O'Hara, 1965);

- 1957 – A shock test of guided missile destroyer USS GYATT (DDG-1)'s missile systems, for which the ship was nonetheless fully instrumented (Rich et al., 1961);
- 1957 – At least one Liberty ship was tested to lethal shock levels, with remote telemetry (Keil, 1961; Rich et al., 1961);
- Tests on the attack transport USS NIAGARA (APA-87), guided missile cruiser USS BOSTON (CAG-1) and a number of wooden-hulled minesweepers prior to 1961 (Rich et al., 1961);
- 1960 – Shock trials conducted on the destroyer USS FULLAM (DD-474) to support validation of the DDAM(O'Hara, 1965).

Since 1960, far fewer full scale trials have been undertaken, in either the US or UK. The trials are very expensive; Shin and Schneider (2003) quoted costs of $30M for the four shot trial of USS JOHN PAUL JONES (DDG-53) in 1994 and $20M for the three-shot trial of USS WINSTON S CHURCHILL (DDG-81) in 2001. Aside from the direct costs of arranging the trial, the unavailability of the ship during the trial period and during any required repairs add opportunity costs. As navies operate with fewer, more expensive ships, the relative cost of removing one from service for shock trials becomes greater and greater. Since 1960, the US and UK have adopted similar policies, and now generally undertake shock qualification trials on only the first ships of each new class.

Grzeskowiak (1988) presented a report on the US Navy's shock trial of USS KAUFFMAN (FFG-59) which presents an illuminating comparison of the differences between the US and British approach to shock qualification trials. (USS KAUFFMAN was not the first of her class; the trial was intended to assess shock-hardening techniques which had been applied to the FFG-7 class frigates since their first of class shock trial, ten years previously.) The report highlighted three primary areas of difference. First, the British approach was to use relatively small charges (up to 500kg according to Brown and Tupper (1989)) placed close to the ship, while the US Navy use much larger charges (on the order of 5 tonnes of HBX-1) at a much greater standoff, presenting the ship with a shockwave which is much closer to planar upon arrival. The latter results in greater excitation of the whole ship girder, while the UK approach loads a smaller region of the hull, although it requires very deep water and a large exclusion zone (the trial reported by Grzeskowiak occurred 65 miles offshore in 600m of water, whereas British trials were often conducted in the Firth of Forth, just outside a naval base.) Secondly, the US Navy tests to a higher shock factor than the UK, accepting a risk of increased damage from the trial for greater confidence in the thoroughness of the qualification. (Didoszak et al (2004) state the maximum shock factor used in US Navy trials as two-thirds the design shock factor, which sounds rather severe.) Finally, the US Navy ship undertakes combat systems exercises

throughout and after the trial, to demonstrate the ability to fight the ship following a shock load. In summary, the US approach is more demanding, but considerably more expensive than the British approach. To allow better comparison with empirical data, the current study assumed a charge arrangement more typical of the British trials practice.

The expense of full scale trials has led to pressure to examine alternative means of designing and qualifying ships against shock loads. Weidlinger Associates (www.wai.com) has pioneered the use of seismic airguns to dramatically reduce the cost of full-scale trials (Thompson, 2003), and numerous parties have and continue to investigate finite element modelling of shock response, with the aim of removing the need for physical trials entirely.

2.5 Small-scale shock trials

With the expense of full-scale trials, conducting physical experiments at smaller scale is seen to be an attractive proposition. Keil (1961, p.24) described model testing as "one of the tools, and perhaps the most important one" to understand structural shock response. Keil claimed that scaling all linear dimensions, including charge standoff and diameter, give dependable results, and advocated a programme of scaled tests to understand the qualitative behaviour of ship structures validated against a smaller number of full-scale trials. Even so, he acknowledged that the effects of weld size, fatigue, gravity and ductility do complicate the matter as they do not follow the same scaling rules (resulting in models which tend to be stronger than their scaled-up equivalent structures.)

Brown (1987a) also acknowledged the difficulties inherent in model testing, considering model tests to be useful for exploring new ideas but reaffirming the importance of confirming them with full scale experiments. Hammond and Saunders (1997) presented a more thorough examination of scale models as a possible strategy for Australian naval research into shock. They too concluded that while scale models offer significant utility, difficulties in scaling behaviour at very high strain rates, at very low shock levels and during material failures mean that small scale experiments should not exclusively be relied upon so numerical modelling and/or limited full scale trials will still be required.

2.6 Computational modelling

Computational continuum mechanics (CCM, including computational fluid dynamics (CFD) and structural finite element analysis (FEA) as sub-fields) is a mature analytical field now widely

applied to the modelling of structural and fluid problems. Most CCM codes deal solely with the simulation of either solid or fluid materials; problems which include both are often referred to as fluid-structure interaction (FSI) problems, and the codes which can deal with them are known as hydrocodes. There are a significant number of hydrocodes in use; Mair (1999) provides a review, grouping the various codes by solver method to form a simple taxonomy.

This investigation used the FUSE2D and EPSA codes, which were provided to the candidate by Weidlinger Associates Ltd. FUSE2D (Farfield Underwater Shock Effects 2D) is a fluid solver used to generate the fluid pressure field resulting from an underwater explosion (Stultz, 2009). EPSA (Elasto-Plastic Shell Analysis) is a solid solver used to determine the response of the structure to that pressure field, including approximating the changes in the pressure field acting upon the structure which result from fluid-structure interactions (Stultz, 2009; Weidlinger Associates, Inc., 1999).

There are a variety of different types of solver available, which can be divided by the categories described below. Both EPSA and FUSE2D are direct, explicit Lagrangian solvers, and they are connected without full coupling. Many of the choices made during the development of EPSA derive from the fact that it is a relatively old code; development began in 1976, and the limited computational power then available implied a requirement to design the code for efficient use of both processor cycles and memory.

2.6 a Direct vs. modal solvers

Direct solvers are those which calculate the time-domain response of a dynamic system by direct integration of nodal accelerations, rather than expressing the response as a superposition of modal vibrations.

2.6 b Explicit vs. implicit solvers

Within the field of direct solvers, explicit direct solvers are those which compute each time step purely in terms of the state of the model at previous timesteps, as opposed to implicit direct solvers which compute properties at each timestep based on the model state at the previous and current timesteps. Explicit solvers are conditionally stable; that is to say, if the timestep exceeds a certain critical value then errors in the solution will grow exponentially. In the case of EPSA and FUSE (both explicit solvers), the solution must comply with the Courant-Friedrichs Lewy condition (Courant, Friedrichs and Lewy, 1967), which in simple terms means that the timestep must be small enough such that a sound wave cannot propagate between the closest two nodes in one timestep. Implicit solvers are unconditionally stable, but must

perform a computation to balance the internal and external forces at each timestep. Explicit solvers therefore generally require smaller timesteps but each timestep requires less computation (Astley, 1992).

When modelling an underwater explosion, to capture the passage of the shockwave requires very short timesteps in any case, so explicit solvers tend to be more computationally efficient. However, when modelling the bubble pulse, the longer timescales and lower velocities favour implicit solvers. Research has been undertaken into linking two solvers, one of each type, allowing the explicit solver to solve during the shock period and the implicit solver to solve for the bubble period (Wright, Sandler and Sussman, 2002). Since the current research was concerned solely with the shockwave phase, an explicit solver was considered preferable.

Explicit solvers have a secondary advantage for shock modelling, in that the lack of requirement to balance internal and external forces at each timestep allows for the modelling of a free-floating body which can acquire free body motions during the solution. The use of an implicit solver usually requires boundary conditions which restrain at least part of the model; an unrealistic representation of a floating body which can introduce unwanted reaction forces if not done with care.

2.6 c Lagrangian vs. Eulerian solvers

Lagrangian solvers use a mesh which is material-fixed. As the material distorts, so the mesh distorts with it. Since no material crosses mesh boundaries during the solution, the computation is relatively straightforward and therefore fast (Mair, 1999). However, large displacements of the material distort the mesh with it, and this can lead to a poor representation of large distortion problems.

Eulerian solvers use a spatially-fixed mesh, where material can flow between cells from timestep to timestep. The usual method is to perform a Lagrangian solution step, then a "remapping" step to move material between mesh cells to return the mesh to its original shape. Eulerian codes are more computationally intensive than Lagrangian codes, but avoid the distortion problems present in large distortion problems. They are also better able to model the appearance and disappearance of free surfaces, bubbles and cavitation regions. The use of Eulerian solvers has lagged behind Lagrangian solvers by five to ten years due to the former being subject to stricter security classification (Benson, 1992).

2.6 d Fully coupled vs. coupled fluid-structure interaction solvers

The fully coupled approach to fluid-structure utilises a two-way interface between a fluid solver and a solid solver. The fluid solver computes a timestep, the resulting pressure field is passed to the solid modeller which computes one timestep of the structural reaction, the resulting boundary motions are passed back to the fluid solver and the cycle is repeated.

FUSE2D and EPSA use a simplified approach (referred to as coupled, as opposed to fully coupled) where information is passed one way only, from FUSE2D to EPSA. The assumption is made that the response of (and indeed the presence of) the structure does not significantly alter the far-field pressure field, so the fluid-structure interaction effects can be approximated within EPSA's solution of the structural response. While the far-field pressure remains unchanged, the pressure loads acting upon wetted panels are adjusted based on the motions of the panel and the adjacent fluid particle velocity. This allows for the approximation of local cavitation and reloading (Stultz, 2009).

The fluid-structure interaction is approximated by EPSA using one of three methods: the plane wave approximation (PWA); added mass approximation (AMA); or doubly-asymptotic approximation (DAA). The PWA is suitable for high frequency applications, such as during the shockwave loading phase. The AMA is suitable for low frequency loading phases, such as the bubble pulse phase. The DAA is a combined approximation which is asymptotic to the PWA at high frequencies and the AMA at low frequencies (Geers, 1994). Since the investigation was purely concerned with the shockwave loading phase, and both the AMA and DAA required, prior to solution, an additional computational process (the creation of an added mass matrix) the PWA approach was used throughout the current research.

Chapter 3 Modelling Warship Structures

Having outlined the shock environment, this chapter discusses the issue of structural style and how it can be applied to models of warship structures. The approach taken in this study was to construct models of sections of ships' structures and simulate their response to explosions using computational methods. By creating models of structures designed to equivalent strength requirements, but of different styles, the effect of style on response could be established. Creating these models was a two-stage process. First, the midship section structure was designed for each ship; a process of selecting the size, thickness and spacings of the plate, stiffeners and frames. With the structures designed, the second stage was to model them in a form suitable for finite element analysis.

This chapter is divided into three sections. The first deals with structural style and how the styles in use in warships are changing. The second describes the process by which the structures for simulation were designed, and third describes how those designs were translated into finite element models.

3.1 The issue of structural style

Structural style is a term which is widely used, but difficult to find an accepted definition for. In the current research, the term structural style is used to describe those elements of a structural design which were the subject of choices made by the designer, as opposed to those determined by numerical calculation. Typically, the designer will make such choices early in the design – what material to use, whether to adopt thin plate with close stiffening or heavier plate with wider stiffening, whether to avoid the use of double curvatures, and so on. These choices drive the design calculations which determine factors such as required plate thickness and frame size. The summation of these initial choices could be considered to be the structural design style adopted.

While there is significant variation between navies, and between individual ship classes, certain broad trends in warship structural styles can be observed. Table 3.1.1 shows the spacing of longitudinal stiffeners and transverse frames in ten NATO warship classes entering service between 1961 and 1982. While variation is evident, it can be seen that the longitudinal stiffeners were typically spaced at 610mm ±160mm, while the frame spacing was typically around three times the longitudinal spacing.

Table 3.1.1 - Stiffener spacing in some early Cold War NATO warships

Ship Class	In Service	Design Displacement	Typical longitudinal stiffener spacing	Typical transverse frame spacing	Ref
Type 81 FF – TRIBAL	1961	2,720 te	680 mm	(Unknown)	[1]
County DLG - DEVONSHIRE	1962	6,310 te	770 mm	(Unknown)	[1]
Improved Type 12 FF - LEANDER	1963	2,930 te	500 mm	1,400 mm	[1]
Type 82 DDG – BRISTOL	1973	7,000 te	530 mm	630 mm	[1]
Type 21 - AMAZON	1974	3,200 te	450 mm	1,350 mm	[1]
Type 42 DD - SHEFFIELD	1975	3,720 te	610 mm	2,130 mm	[2]
FFG-7 OLIVER HAZARD PERRY	1977	4,200 te	686 mm	2,290 mm	[2]
C70 GEORGES LEYGUES	1979	4,500 te	686 mm	1,700 mm	[2]
F122 - BREMEN	1982	3,680 te	600 mm	1,400 mm	[2]
MAESTRALE	1982	3,100 te	520 mm	1,800 mm	[2]

A study at the (British) Naval Construction Research Establishment (Smith, 1976) examining grillages "representing warship single-bottom and deck structures" used a longitudinal stiffeners spaced at 300mm or 600mm with frames spaced at 1,200mm or 1,500mm, consistent with the majority of the ships in Table 3.1.1 This "NATO Style" of structures was typified by complexity and high efficiency, with closely stiffened light plating allowing a structural weight fraction in the region of 30% of design displacement (Mulligan and Courts, 1998) but expensive, particularly in welding labour hours. Brown and Tupper (1989) made

[1] Purvis (1974)
[2] Kehoe et al (1983)

reference to this style being selected for the WHITBY and later class frigates for its good shock resistance, following the British post-war destroyer shock trials.

The price of warships is increasing rapidly. Arena et al (2006) found that the Unit Procurement Cost (UPC) of British and US warships had risen between 1950 and 2000 at twice the rate of inflation, the additional cost being mostly attributable to increases in capability requirements. Andrews and Brown (1982) reported similar rates of increase, identifying a doubling in the cost per tonne in real terms between the procurement of HMS DIDO and HMS BATTLEAXE, again due largely to capability increases.

There is therefore a significant pressure on naval procurement organisations to reduce the cost of warships. The highly efficient structures with specialist steel components were widely regarded as a candidate area to find savings; Brown and Tupper (1989, p.37) stating that "since [their initial adoption] the aim has been to maintain the same strength in a structure with lower through life cost." Mulligan and Courts (1998) declared that the need to reduce costs was forcing shipbuilders to examine alternative structural styles. Van der Struis et al (1996) presented a review of the Netherlands' new LCF command frigates, which adopted a simplified structural style. Vialette and Cottin (1995) presented a cost analysis of the FLOREAL class corvettes, the first ships (aside from auxiliaries) in the French Navy constructed to 'commercial standards' and concluded that the adoption of these standards offered an 8% cost saving beyond those that could be attributed to differences in size, payload or military requirements. Hudson et al (1996) added that warships had often been subject to arbitrary displacement limitations with a view to limiting cost, and that removal of these limitations to allow cheaper, heavier structure could offer cost savings. Chalmers (1986) demonstrated that the potential savings from simplifying structural style were limited, but (correctly) predicted that rising financial pressures were likely to force the adoption of at least some simplifying features anyway.

It should be mentioned that over the same period there has been a trend towards navies adopting commercial Classification Societies to provide technical assurance of ship designs, rather than the traditional approach of in-house expert bodies, as described by Ashe et al (2006). While this process has been driven by the same cost pressures as the adoption of simplified structure, and such structure is often referred to as "commercial" it must be noted that it has been accompanied by the development of warship-specific class rules, so it does not necessarily imply any degradation in the standards to which these warships are built.

3.2 The Process of Structural Synthesis

This section considers the process adopted for ship structural model development from initial conception to the production of a finite element mesh model suitable for finite element analysis. Each step in this process is examined in more detail in a subsection below.

The process was used to develop structural models for two ship designs; one frigate and one corvette. These ships are described in more detail in Chapter 5.

3.2 a Choice of co-ordinate system

Two co-ordinate systems were used; a model-fixed system and a charge-fixed system.

The model-fixed co-ordinate system used the following convention:

i. X positive forward, with X=0 at the aftermost point of the model.
ii. Y positive to port, with Y=0 on the centreline.
iii. Z positive vertically upwards, with Z=0 at the lowest point of the keel.

The charge-fixed system, just used by the FUSE code, was an axisymmetric two-dimensional system:

i. R positive radially outward from an axis aligned vertically through the explosive charge.
ii. Z positive vertically downwards, with Z=0 at the fluid free surface plane.

3.2 b Choice of structural standards

The choice of standards is an important one in any ship design process. The current research included ships designed to two different sets of standards. Some initial designs were developed using the methods and standards described by Chalmers (1993), initially published internally within the Ministry of Defence as Sea Systems Controllerate Publication (SSCP)-23 (Ministry of Defence, 1989). The baseline ship for the study had been selected as the NATO Frigate Replacement for the 1990s (NFR-90), described in more detail in Chapter 5, and it was felt that SSCP-23 was representative of the standards in use at the time of the NFR-90's design. It was therefore hoped they would lead to a structural design which was comparable to that of the NFR-90 design, described in the open literature by Schaffer and Kloehn (1991).

As the work progressed some difficulties in applying the methods in SSCP-23 to unconventionally-styled structures became clear; in particular limits on the aspect ratio of

grillage panels for which the included data sheets remained valid and the lack of a method to assess failure of asymmetric stiffeners in a coupled flexural-torsional mode. The assessment of flexural-torsional failure was particularly problematic. While a number of models had been published prior to 1989, a comparative study between the predicted failure loads between them (Caridis and Frieze, 1989) found variation which was considered too high to choose one method with confidence. Eventually the Naval Ship Rules (Lloyds Register, 2008) produced by Lloyds Register were selected for the experimental series. The NSR rules allowed the flexibility of panel aspect ratio and stiffener profile required for the study, packaged in a single coherent set of rules. Additionally, they are representative of the contemporary Royal Navy warship structural style, having been used on the Type 45 destroyer and Queen Elizabeth class aircraft carrier designs.

Lloyds NSR2 was used to produce all designs subsequently subjected to shock simulation. Some additional designs were produced using SSCP-23 methods to allow comparison with the published NFR-90 structure and give confidence in the method. The implications of this mixed approach to selecting structural standards for the outcome of the shock analysis are discussed in Chapter 8.

It should be noted that this study does not attempt to draw any comparison between the structures designed to NSR2 and SSCP-23. Since each set of standards uses different methods to estimate the loading, while one structure may be heavier than the other, it may also be inherently stronger. Structures designed to the two different standards therefore cannot necessarily be considered equivalent.

3.3 Scantling Design Synthesis

Both Lloyds Naval Ship Rules and SSCP-23 offer procedures for the analysis of structures against various failure modes and guidance by which these can be used to synthesise a structure, rather than mechanistic structural synthesis processes. It is therefore necessary to develop a synthesis method, use it to produce structural designs, assess them against the desired strength, make necessary adjustments and repeat the process until a structure acceptably close to the desired strength is reached. To that end, various decisions were made by the candidate:

i) Minimisation of independent variables

The synthesis method was designed to pre-set as many variables as possible, limiting the choices available to the structural designer in deriving scantlings wherever possible. The intention was to achieve a process where a single independent variable mapped to a single dependent variable, allowing for the production of structures in a coherent series without the choices of the human designer introducing variation. In the end, a method was found which required two independent variables but allowed these to be optimised by an algorithm, thereby avoiding any choice in this regard from the designer which could not be expressed in algorithmic terms.

ii) Structural equivalence within a series of structural designs

The research required the production of series of "equivalent" designs of different structural styles. In something as complex and multivariate as a warship structure, defining equivalence can be difficult. The method chosen was to create structures of equivalent strength; that is, they were all equally capable of resisting a predefined load case. Within a series of designs, each structure was subject to the same set of loads, and assessed for the same failure modes, with the same factors of safety. In each case, the structure was made to be as light as possible while avoiding all failure modes. Each structure therefore represents a weight-optimised solution for a given load case, design style and choice of standards. While two equivalent designs might reach their limit state due to different failure modes, they were both designed to survive the same load case.

iii) The need to assume constant displacement with varying structural configuration

When increasing structural weight, the designer must choose between accepting an increase in ship displacement and making an equivalent weight saving elsewhere; by reducing the design's capability, standards or margins. Structural loading varies with displacement although the relationship between them can be complex, dependent upon hull geometry and longitudinal weight distribution. If the (non-structural) remainder of the ship was kept constant between structural variants, the structural weight, displacement and structural loading would become interconnected, with the possibility that an increase in structural weight would lead to an increase in ship displacement, an increase in structural loads and a subsequent further increase in structural weight to meet the same standards. Therefore, for ease of comparison, the ship's displacement was kept constant between all structural variants.

It was assumed that sufficient changes in capability were accepted to allow this to happen; a somewhat unreal simplification but necessary for the primary (structural) comparison exercise.

3.3 b Panel Discretisation Approach

Both methods (NSR2 and SSCP-23) assessed structure at different levels; as individual plates or stiffeners, as stiffened panels or as the entire ship girder. To keep the number of control variables to a manageable number, the structure was assessed in a simplified form, made of eight shell or deck panels, within each of which the scantlings were homogeneous. These sections are shown in Figure 3.3.1. The passing and top decks in way of the uptakes (inboard of y=3m in Figure 3.3.1) were assumed to be ineffective in resisting longitudinal bending so were excluded from the strength assessment, although they were included in the FE model. The models were in way of machinery spaces which are typically two decks high, so a lower passing deck (between the passing deck and inner bottom) was omitted.

As can be seen from Figure 3.3.1, the curves of the shell plating were simplified to flat sections of similar shape for purposes of determining scantlings. The structure was also assumed to be prismatic in the longitudinal direction.

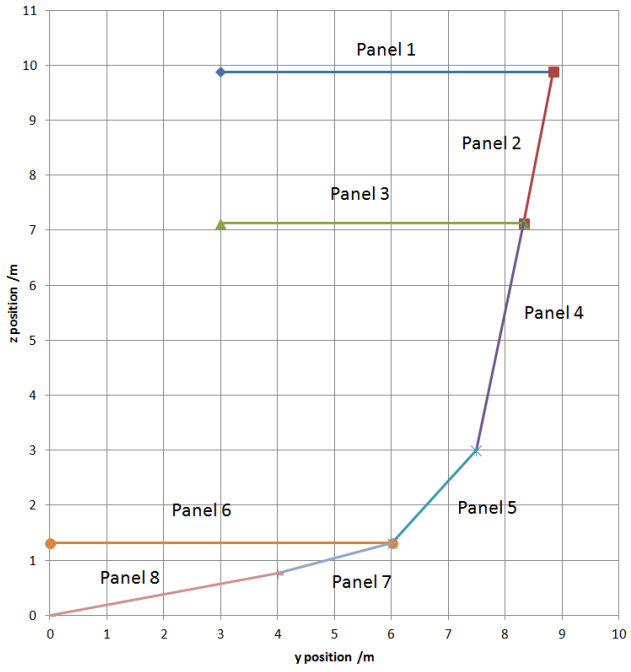

Figure 3.3.1 - Discretization scheme for midship structural section

A spreadsheet was created to perform the strength assessment. Within this spreadsheet, each panel was defined by the following controls:

i. Panel endpoints
ii. Frame spacing
iii. Longitudinal stiffener spacing
iv. Location of longitudinal deep girders
v. Material properties (density, Young's modulus, bulk modulus, yield stress)
vi. Stiffener cross section shape
vii. Smeared panel thickness (as if the stiffeners were averaged over the panel as additional plate thickness)
viii. Stiffener material fraction (cross sectional area of the panel's stiffeners as a fraction of the total cross sectional area of the panel, referred to as As/A.)
ix. Frame depth

All but the last three of these were pre-set for each design and held constant, so designing each panel was simply a matter of setting two control variables for each panel and one for each frame section to find a the minimum weight structure of acceptable strength. Frame design and shell/stiffener design were assessed independently of each other, so they could be treated as two separate optimization problems rather than a single three-variable problem.

3.3 c Pre-set Design Variables

Panel endpoints were defined once for each ship design, to match the discretized model as closely as possible to the shape of the ship's hull.

Frame spacing was set for the baseline ship (1500mm for both the baseline ship designs used; the NFR-90 and a nominal corvette design. Both are described in more detail in Chapter 5.) It was varied as a control in one experimental series.

Longitudinal stiffener spacing was set for the baseline ship (600mm for both the NFR-90 and the corvette structural models.) It was varied as a control in one experimental series.

Longitudinal deep girders were placed in accordance with a simple scheme, replacing the longitudinal stiffener closest to a given point. A single deep girder was located on the sideshell near the waterline oriented with the web horizontal. (A girder is typically included here to transmit berthing loads into the structure; it offers little to longitudinal strength being close to the neutral axis of the hull girder.) Under the top deck, one deep girder was located on the

centreline, with another two spaced as evenly as possible between the centreline and the gunwale. A single deep girder was placed under the passing deck, roughly at one third of the beam out from the centreline. All of the deck-supporting girders were oriented with the web vertical. These girders reflect typical warship design practice, and early simulations found their inclusion to have a significant effect on the shock response of the decks.

A standard material was used for all experimental models; a low carbon crack arrest steel with density of 7750 kg/m3, Young's Modulus of 205 GPa, bulk modulus of 0.3 and yield stress of 300 MPa (Cardarelli, 2008).

Stiffener cross sections were defined with proportions as shown in Figure 3.3.2 and allowed to scale continuously to the size required. The long-stalk tee bars and offset bulb plate profiles were based on data provided by Chalmers (1993) for Admiralty standard tee bars and typical bulb plates from BS4848 (British Standards Institution, 1991). The flat bar proportion was based on the limiting proportions defined by Lloyds Register (2008).

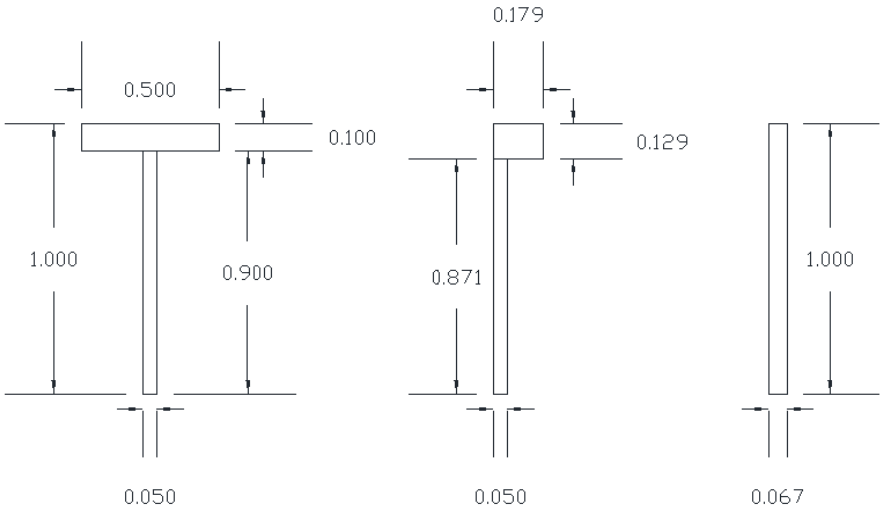

Figure 3.3.2- Stiffener profile proportions

3.3 d Control Variable Values

With initial values chosen for the control variables (that is, smeared panel thickness, stiffener material fraction and frame depth), the resulting structure was subjected to a strength analysis against either NSR2 or SSCP-23. Because the two different methods assess the structure

against different failure modes, the analysis process for each is described separately, in Sections 3.4 and 3.5.

The limiting value for each of the different failure modes may be defined as an allowable stress, a required cross sectional area or bulk modulus. Regardless of the type of variable required, all were presented in dimensionless form as a load factor, which was defined as the ratio of the calculated design value to the acceptable value and arranged so that:

- Load factor < 1 Acceptable
- Load factor = 1 Acceptable, optimum
- Load factor > 1 Unacceptable

The goal was to iterate the control variables until the load factor was acceptable for all failure modes, but just about to fail in one mode. A failure mode was deemed to be on the point of failure when the load factor exceeded 0.99. The use of conditional formatting clearly shows the critical failure mode for each panel.

Iteration to a solution was achieved by one of two methods; manually adjusting inputs, or using the Microsoft Solver utility. Manual adjustment was a relatively time-consuming process wherein the candidate adjusted the smeared thickness up or down in 0.1mm steps, at each step finding the stiffener material fraction value (to three decimal place accuracy) which gives the most favourable load factors.

Seeking a more systematic approach, the Microsoft Solver application was used. This is a plugin for Microsoft Excel that uses the GRG2 gradient reduction algorithm to solve smooth nonlinear programming problems such as the one presented here (Lasdon and Waren, 1981). Comparison of the two optimization methods showed that the GRG2 solver gave optimised scantling schemes very similar to those reached by manual iteration. Given the low number of design cases used, the manual method was used for all simulated designs. However, in a follow-up study using many designs, the use of the GRG2 solver may be more appropriate.

3.4 Scantling assessment using Lloyds NSR2

For structures being designed using the Lloyds NSR2 rules (Lloyds Register, 2008), the structure was assessed using the criteria described in NSR2 Vol 1 Part 6 Chapters 3-5 for the following five areas: a) hull girder under global bending loads; b) plating and longitudinal stiffening; c)

transverse frames; d) longitudinal girders and e) bulkheads. The procedures applied in each area are described in the sub-sections a) to e) below.

Local pressure loads on panels were assessed using the procedures specified in NSR2 Vol 1 Part 5 (Lloyds Register, 2008). Wave-induced hull girder bending moment and shear force were determined by a quasi-static equilibrium calculation balancing the ship on a wave, described in more detail in Chapter 5.

3.4 a Assessment against hull girder loading

Deck/keel peak compressive stress. The allowable peak compressive stresses in the main deck and keel were calculated and compared to a permissible value in accordance with NSR2 Vol 1, Part 6 Chapter 4 Section 2.2.3 (Lloyds Register, 2008).

The stress range (from peak compressive to peak tensile) in the strength deck was calculated and compared to a permissible value in accordance with NSR2 Vol 1, Part 6, Chapter 4, Section 2.2.3 (Lloyds Register, 2008).

The shear stress in each panel arising from wave-induced bending was calculated and compared to a permissible value in accordance with NSR2 Vol 1, Part 6, Chapter 4, Section 2.3.5 (Lloyds Register, 2008).

3.4 b Assessment of plating and longitudinal stiffeners

Longitudinal stiffener profile (tee-bar, offset bulb plate or flat bar) was set depending upon model under consideration.

A required minimum plating thickness was calculated, based on both local loading and buckling under hull girder bending in accordance with NSR2 Vol 1, Part 6, Chapter 2 Table 3.2.1 (Lloyds Register, 2008).

Plate buckling behaviour was modelled in accordance with NSR2 Vol 1, Part 6, Chapter 2, Table 2.4.2 (Lloyds Register, 2008). An assessment was made of whether the plate would buckle plastically, elastically or not at all at the design loading. (Elastic buckling was permitted within limits.)

Requirements for longitudinal stiffener size in terms of required section modulus (Z), second moment of area (I) and web area (A_w) were calculated in accordance with NSR2 Vol 1, Part 6, Chapter 2 Section 2.8.2 (Lloyds Register, 2008).

The buckling of longitudinal stiffeners was modelled in accordance with NSR2 Vol 1, Part 6, Chapter 2, Section 4.5.2 (Lloyds Register, 2008).

Stiffener tripping and flexural-torsional failure was modelled in accordance with NSR2 Vol 1, Part 6, Chapter 2, Section 4.7.3 (Lloyds Register, 2008) to determine that tripping or flexural-torsional failure would not occur until after the onset of unacceptable plate buckling.

3.4 c Assessment of transverse frames

The transverse frames in all models used a long-stalk tee-bar profile. The required frame size was calculated individually for each panel. The largest size required by any side shell frame above the Inner Bottom (Panels 2, 4 & 5 – see Figure 3.3.1) was then used for the entire sideshell, allowing for a simple frame geometry of continuous size. The frames under the Top Deck and Passing Deck (Panels 1 & 3 – see Figure 3.3.1) were modelled at the size calculated.

Requirements for transverse frame size in terms of required section modulus (Z), second moment of area (I) and web area (A_w) were calculated in accordance with NSR2 Vol 1, Part 6, Chapter 2, Section 2.8.2 (Lloyds Register, 2008).

The second moment of area required in the transverse frames to avoid global buckling was calculated in accordance with NSR2 Vol 1, Part 6, Chapter 2, Section 4.9.2 (Lloyds Register, 2008) if the frames were primary structural members or Section 4.8.2 (ibid) if they were secondary structural members.

The critical shear stress to cause the stiffened panel to buckle in shear was calculated in accordance with NSR2 Vol 1, Part 6, Chapter 2, Section 4.6.1 (Lloyds Register, 2008).

A check was made that the transverse frames were at least 40mm deeper than the longitudinal stiffeners, to permit fabrication of the intersections between them, in accordance with NSR2 Vol 1, Part 3, Chapter 2, Section 3.1.2 (Lloyds Register, 2008).

3.4 d Assessment of longitudinal girders

With no requirements given in NSR2 as to the sizing of longitudinal deep girders, the depth of each girder was set as 1.3 times the depth of the intersecting transverse frame, or 360mm, whichever was the greater.

3.4 e Assessment of bulkheads

The bulkhead panel was subject to a smaller set of failure modes:

Minimum plate thickness was calculated in accordance with NSR2 Vol 1, Part 6, Chapter 2 Table 3.2.1 (Lloyds Register, 2008).

Requirements for stiffener size in terms of required section modulus (Z), second moment of area (I) and web area (Aw) were calculated in accordance with NSR2 Vol 1, Part 6, Chapter 2 Section 2.8.2 (Lloyds Register, 2008).

While in practice it might be more realistic with regard to likely ship structural design practice to allow for lighter plating and stiffeners above the Passing Deck, the plating and stiffeners were kept constant across the whole bulkhead. (This greatly simplified the process of integrating the bulkheads into the surface model later, since the points where the bulkhead webs met their supporting stiffeners were coplanar in the XZ plane.) Unfortunately this precluded the inclusion of a thickened margin plate around the edge of the bulkhead. This is a feature which is included to improve strength and stability under explosive loading (Chalmers, 1993) and so is highly relevant to this research. If possible, a margin plate should be included in any follow-up studies concerned with structural failure mechanics. However, the omission was considered reasonable since the current research was primarily concerned with motions at relatively low stresses (below yield) rather than determining the mechanics of structural failure.

3.5 Scantling assessment using SSCP-23

For structures being designed using the procedures in (Chalmers, 1993), the structure was assessed against criteria divided into the following four areas: a) plating and longitudinal stiffening, b) transverse frames, c) longitudinal girders and d) bulkheads. The procedures applied in each area are described in the sub-sections a) to d) below.

Local pressure loads were derived following empirically-derived values given in (Chalmers, 1993). Wave-induced hull girder bending moment and shear force were determined by a quasi-static equilibrium calculation balancing the ship on a wave, described in more detail in Chapter 5.

3.5 a Assessment of plates and longitudinal stiffeners

The algorithms in SSCP-23 assume symmetric stiffeners, so this method was not valid for structures including offset bulb plates. All models constructed using this method used long-stalk tee bar longitudinal stiffeners.

The critical buckling stress for longitudinal stiffeners loaded in compression was calculated and compared to the compressive stress generated in the panel by hull girder loading.

The compressive stress required to cause longitudinal stiffener tripping was calculated, and compared to 1.3 times the applied compressive stress from hull girder loading, the margin included to ensure the avoidance of interaction effects between buckling and tripping.

The peak stress in the longitudinal stiffener flanges arising from bending under local loading was calculated and compared to the material yield stress.

The peak shear stress in the longitudinal stiffener webs arising from local loading was calculated and compared to 0.25 times the yield stress.

The critical stress required to cause stiffener tripping due to local loading was calculated and ensured to be at least four times the applied stress.

3.5 b Assessment of transverse frames

As for the NSR2 method, the transverse frames were always of a long-stalk tee bar profile.

The required frame size was calculated individually for each panel. The largest size required by any side shell frame above the Inner Bottom (Panels 2, 4 & 5) was then used for the entire sideshell, allowing for a simple frame geometry of continuous size. The frames under the Top Deck and Passing Deck (Panels 1 & 3) were modelled at the size calculated.

The maximum stress at the flange face of the transverse frames arising from local loading was calculated and compared to the material yield stress.

To assess global buckling, the critical stress at which the combined frame and plating would plastically buckle was calculated and compared to the stress arising from hull girder bending.

3.5 c Assessment of longitudinal girders

Longitudinal girders were sized by the same method that was used for the NSR2 designs - by setting the depth to 360mm or 1.3 times the depth of the intersecting frame, whichever was the greater.

3.5 d Assessment of bulkheads

The bulkhead panels were subjected to a reduced set of criteria:

The peak stress in the vertical stiffener flanges arising from bending under pressure loading was calculated and compared to the material yield stress.

The peak shear stress in the vertical stiffener webs arising from pressure loading was calculated and compared to 0.25 times the yield stress.

The critical stress required to cause stiffener tripping due to pressure loading was calculated and ensured to be at least four times the applied stress.

As with the NSR2 designs, plating and stiffeners were kept constant over the entire bulkhead, and the same issues relating to the omission of a thickened margin plate around the edge of the bulkhead apply.

3.6 Design of Structural Geometry

With the scantlings numerically designed, the next step was to determine the geometry of the structure, to allow the subsequent creation of a three dimensional mesh model suitable for finite element analysis. The process of determining the geometry contained two main phases: a) adjustment to the stiffener sizes to account for errors in representing solid features with plate elements; and b) construction of a set of two-dimensional drawings defining the geometry of those plate elements. Those two phases are described in the following two sub-sections.

3.6 a Stiffener depth correction

Plate elements represent solid bodies as a surface, thickened to the desired thickness. As shown in Figure 3.6.1, discretizing a typical stiffened plate cross section as thickened surfaces of the same shape results in ‘double counted’ regions and gives a slight increase in total area, of approximately 5%. There is a corresponding increase in second moment of area about the horizontal neutral axis, of approximately 3%. More detailed calculations are provided at Appendix A.

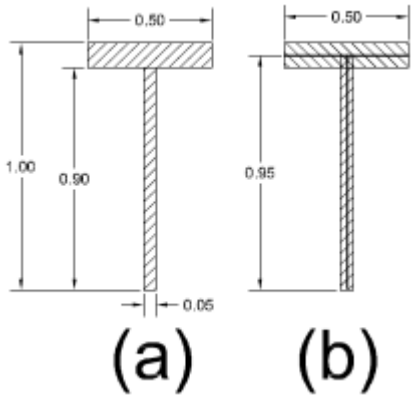

Figure 3.6.1 – Solid (a) and plate (b) representation of tee-bar stiffeners

In a grillage, a certain amount of plating will act with the stiffener to resist bending and buckling; Chalmers (1993) provides a conservative estimate of whichever is the lesser of the stiffener spacing or forty times the plate thickness; taking this plating into account reduced the aforementioned area and second moment of area errors to approximately 1% each.

A correction was made to the depth of each stiffeners to give the equivalent second moment area, assuming that an amount of plating corresponding to Chalmers' prediction acted effectively. This correction was made within the design spreadsheet, in a series of dedicated worksheets, one per panel. The results were collated in a single output worksheet.

3.6 b Production of cross-sectional drawings

Once the numerical design was complete, a series of two-dimensional transverse sectional drawings were created to provide a base for the surface model. The starting point was the hull section outline, taken from (Schaffer and Kloehn, 1991) for the NFR-90 or the Paramarine (QinetiQ, 2013) hull model for the corvette. As shown in Figure 3.6.2, circles of a radius equal to b, the stiffener spacing, were drawn to locate the points at which the shell plates met the longitudinal stiffeners. The arrows show the directions of construction, chosen to ensure even distribution of stiffeners horizontally across the centreline and vertically around the Passing Deck. To ensure vertical bulkhead stiffening, the stiffeners in the Top Deck and Inner and Outer Bottom were located by vertical lines projected from the passing deck.

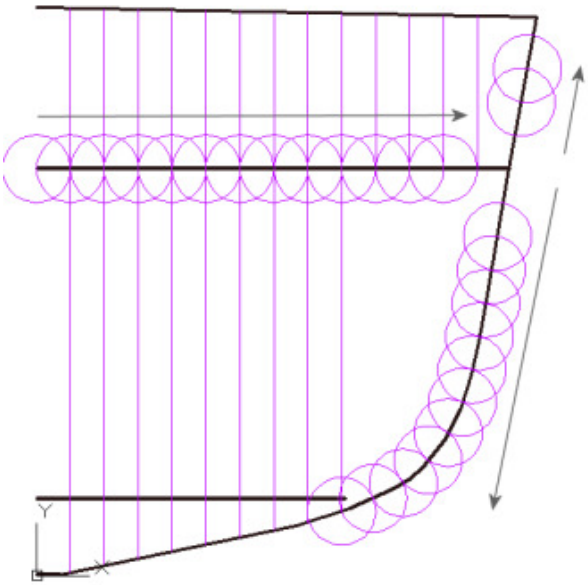

Figure 3.6.2 – Process for determining longitudinal stiffener locations

Next, the shell plates were drawn by joining each intersection between outline and circle. Markers at the panel boundaries were used to guide which panel each plate section was a part of; plates which crossed panel boundaries were assigned to whichever panel the midpoint lay within.

The margin plate[3] joining the inner bottom and outer shell was drawn normal to the outer plating, from the plate end that gave the shortest margin plate of at least 400mm length.

Two intercostal girders supporting the inner bottom were added, joining the inner and outer bottom plate ends closest to y = 1200mm and y = 2400mm, marked X in Figure 3.6.3. (All co-ordinates given in ship co-ordinate system.) These were considered to be a part of the inner bottom so part of Panel 6 (See Figure 3.3.1.)

Longitudinal deep girders were drawn on the Top Deck, Passing Deck and Sideshell. The Top Deck girders were located at the plate ends closest to y=0mm, y=3000mm and y=6000mm and oriented vertically. The inner deck girder was located at the plate end closest to y = 3000mm and oriented vertically. The side shell girder was located at the plate end closest to the waterline at z = 5050mm and oriented horizontally. Longitudinal stiffeners were located at each of the other plate ends. Stiffeners in the Top Deck, Passing Deck, Inner Bottom and Outer Bottom inboard of the margin plate were all oriented vertically. Other stiffeners in the side

[3] Despite the similar terminology, this margin plate is not the thickened region of plating around the bulkhead edge, previously discussed in Section 3.4 e.

shell were oriented normal to the average of the adjacent shell plates. Stiffeners were added at the vertical midpoint of the intercostal girders, oriented horizontally; see Figure 3.6.3.

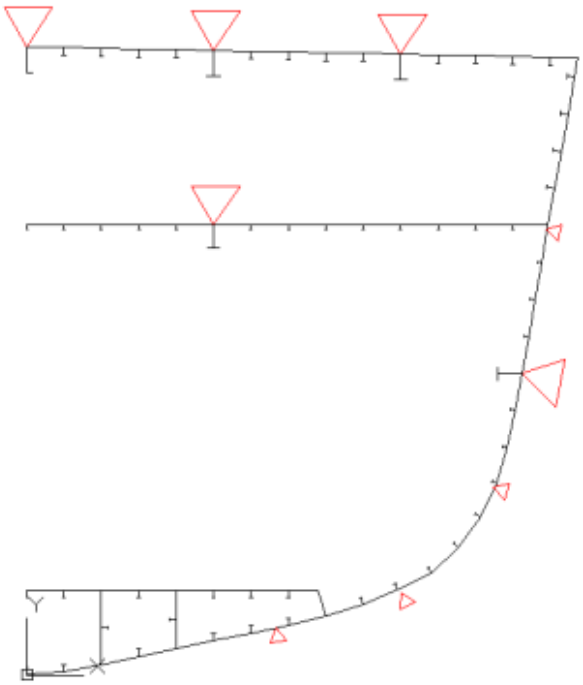

Figure 3.6.3 - Shell plates and longitudinal stiffeners, with the assumed panel boundaries marked

The transverse frames were drawn in, by offsetting the shell plating by the appropriate distance; see Figure 3.6.4. Chamfers of 300mm size were added at the beam knee positions. The frame flange was run horizontal from the level of the inner bottom. Brackets, of length equal to the stiffener spacing, were added to support the deck girders against tripping.

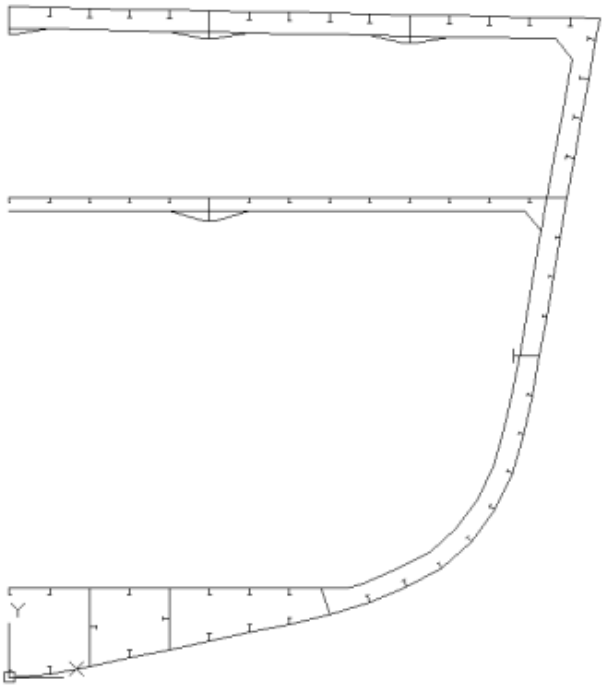

Figure 3.6.4 – Cross sectional drawing defining transverse frame flanges

Some additional detail was added to the frame drawings, as shown in Figure 3.6.5. Experience showed that avoiding concave areas resulted in a better mesh quality, so stiffener flange lines were joined, and some additional lines were added around section transitions.

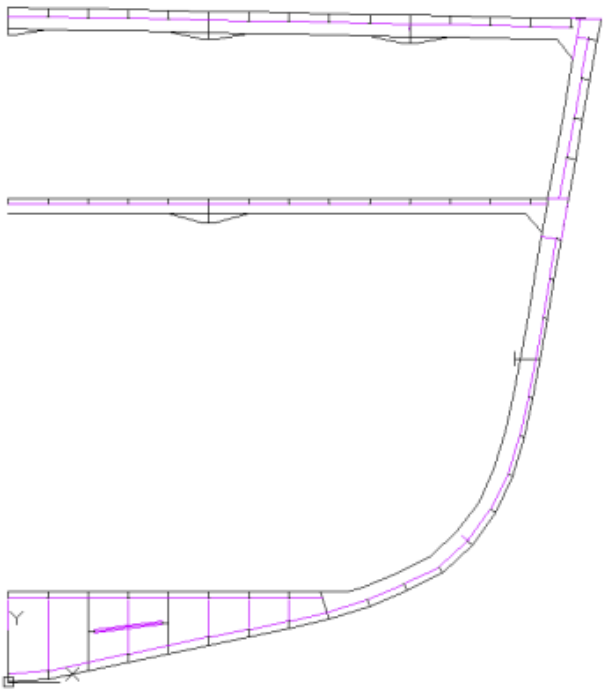

Figure 3.6.5 - Additional detail to frame webs to improve mesh quality

The bulkhead stiffening was then defined by drawing the stiffener web lines, shown in magenta in Figure 3.6.6. Vertical stiffeners were added between the vertically-aligned deck longitudinal stiffeners. Between the upper and passing decks, these ran out as far as the outermost stiffener of the passing deck. Between the passing deck and bottom these ran out as far as the outermost stiffener of the inner bottom. Additional bulkhead stiffeners were projected inwards from the sideshell longitudinal stiffeners, remaining normal to the plating. An oblique stiffener was arranged across the curve of bilge. It was difficult to strictly define how this stiffener should be placed, but it was placed in such a way as to ensure good continuity, while avoiding any very acute or very obtuse angles at stiffener intersections. Aside from being difficult to manufacture in real structures, these angles were noted as a cause of undesirable mesh features.

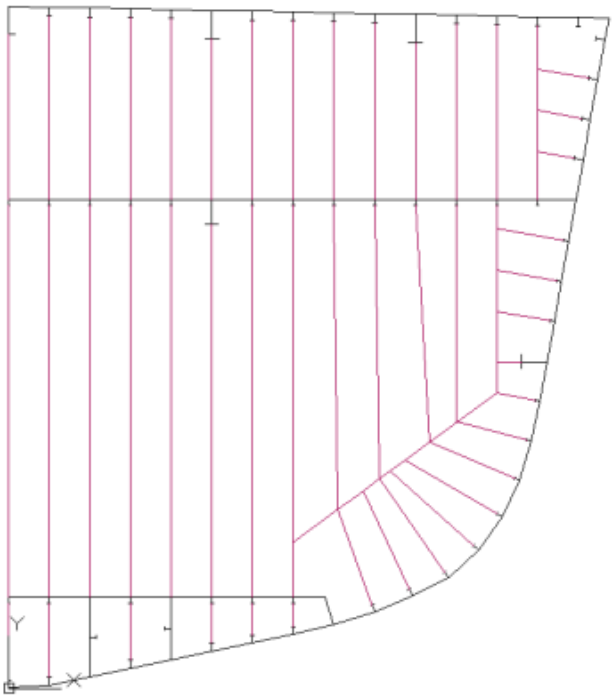

Figure 3.6.6 - Bulkhead stiffening scheme

The bulkhead stiffener flanges were then drawn, as shown in Figure 3.6.7. The flange edges were drawn by offsets from the web lines. Where bulkhead stiffeners ended on a longitudinal stiffener or girder, the flange of the bulkhead stiffener was scarfed up or down at a 15 degree angle to the width of the longitudinal's web.

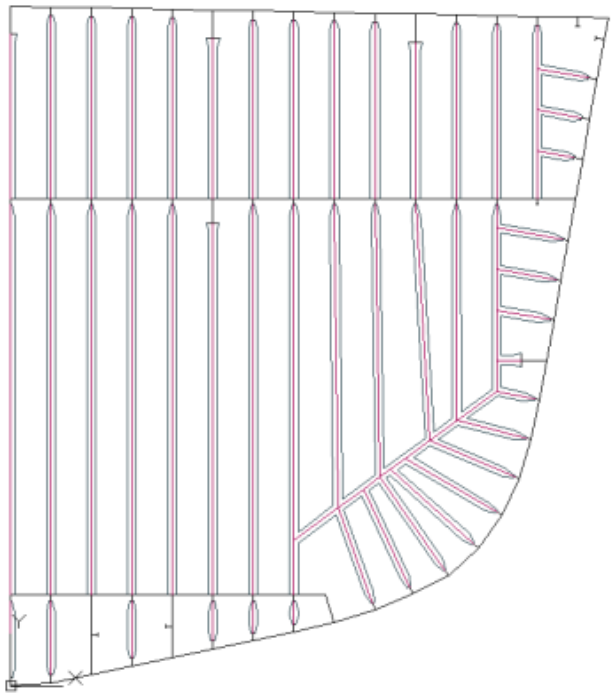

Figure 3.6.7 - Bulkhead stiffener flanges

3.7 Construction of the Finite Element Model

With transfer drawings complete, the next step was to assemble a surface model of the structure, for which the Altair Hypermesh pre-processor software was used (Altair Engineering, Inc., 2011). Construction of the surface model was a three stage process comprising setup, manual modelling of a single frame bay of structure from the sectional drawings just described, then running scripts to expand the single frame bay model into a full surface model.

3.7 a Setup of model parameters

Various model parameters required choices to be made. The most important of those choices related to the following four areas: i) timestep length; ii) damping; iii) material properties; and iv) model hierarchy structure. Each is discussed in one of the following subsections:

i) Selection of timestep

It was necessary to select an appropriate timestep for the simulation. To minimise computation time, this was set as large as possible while ensuring the solution was stable. As

an explicit direct solver (see Section 2.6 b, EPSA is conditionally stable (Weidlinger Associates, Inc., 1999) so long as the Courant-Friedrichs-Lewy condition (Courant, Friedrichs and Lewy, 1967) is met. This condition limited the timestep to be at most half the time taken to travel the minimum inter-nodal distance at the speed of sound in the intervening material. A convenient way to obtain the minimum inter-nodal distance was to run the model through EPSA for a single timestep of arbitrary length and check the summary block of the resulting diagnostics output file. A timestep of 1.5 microseconds was selected, with outputs evaluated every 50 timesteps to limit the size of the output data files. A common timestep was used between all models to simplify processing of results.

ii) Damping

In a welded steel warship structure, energy is dissipated through thermal effects, primarily through material hysteresis (Betts, Bishop and Price, 1976). This dissipation must be represented somehow in the finite element model. Several damping models exist within EPSA, of which the two most appropriate choices were mass-proportional damping and Rayleigh damping.

In the mass-proportional model, the damping matrix is a function of the mass matrix alone, although the magnitude of the damping varies with frequency of oscillation. Some relationship (typically inverse proportionality) is assumed between damping ratio and frequency, scaled by specifying the damping ratio at one specified reference frequency. It can therefore be completely defined by two parameters; the reference frequency and the damping ratio at that frequency.

The Rayleigh damping model adds a stiffness-proportional term (which varies proportional to frequency) and models the damping ratio as the sum of the mass-proportional and stiffness-proportional terms. It is defined by two parameters; the coefficients which control the magnitude of the mass-proportional and stiffness-proportional terms. A Rayleigh damping matrix is typically defined by an equation of the form:

$$C = \alpha M + \beta K \qquad \text{(Eq 3.1)}$$

where C is the damping matrix, α and β are scalar coefficients, M is the mass matrix and K the stiffness matrix.

Shin & Ham (2003) derived Rayleigh damping coefficients for a variety of locations throughout an Arleigh Burke class guided missile destroyer. The USA/LS-DYNA code was then used replicate the full scale shock trial of USS WINSTON S. CHURCHILL, previously referred to in

Chapter 2, using both Rayleigh damping and mass-proportional damping with a damping ratio of 4% of critical damping at zero frequency. Both sets of results were compared to the trials data using Russell's comprehensive error factor (Russell, 1997), a non-dimensionalised metric which compares magnitude and phase errors of two velocity-time histories. The Rayleigh-damped model was found to score significantly better than the mass-proportional damped model; the models scoring similarly on phase error but the Rayleigh-damped model producing greatly reduced magnitude errors. This study therefore used Rayleigh damping, with the coefficients recommended by Shin & Ham's study:

- α (Mass proportional coefficient): 19.2
- β (Stiffness proportional coefficient): 2.09×10^{-6}

iii) Material properties

A number of material models exist in EPSA, defined by the LTYMAT variable on the MATLQ input card. The translator in use (translating Hypermesh outputs into EPSA inputs) allowed a choice from three.

i. LTYMAT = 1; a purely elastic model which defines the material in terms of Young's modulus, Poisson ratio and density. This model assumes linear elastic behaviour up to infinite stress, and therefore overpredicts the strength of the material at high strains.
ii. LTYMAT = 11; an elastoplastic, strain rate-independent model. By adding yield stress as an input variable, the model can allow plastic deformation to occur beyond yield. However, it takes no account of strain rate in computing the stress/strain ratio in the plastic regime, and therefore underpredicts the strength of the material in the plastic regime, under high strain rate loading.
iii. LTYMAT = 12; an elastoplatic, strain rate-dependent model. This takes into account the improved strength many materials display under high strain rates, by varying the plastic flow stress with strain rate, as shown in Figure 3.7.1

Since high strain rate loading is a characteristic feature of underwater shock, the elasto-plastic rate-dependent model was the preferred choice.

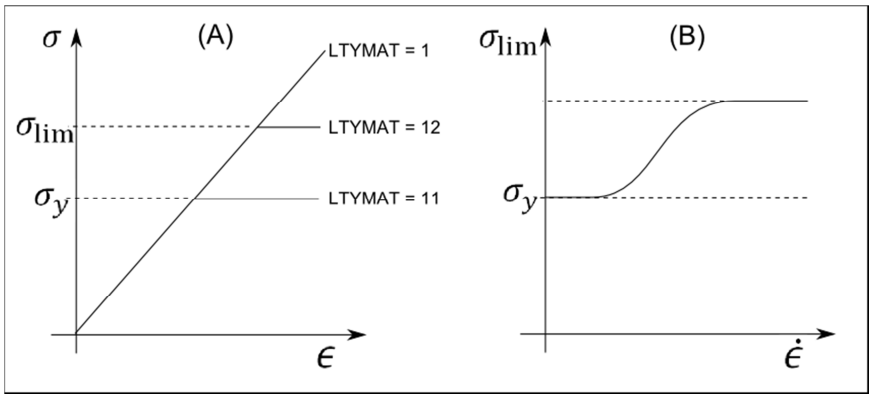

Figure 3.7.1 – Stress/strain relationship for the three EPSA material models (A) and variation in the LTYMAT 12 limiting stress with strain rate (B)

Defence Standard 02-791: Requirements for Weldable Structural Steels (formerly Naval Engineering Standard 791) (Ministry of Defence, 2000) defines four classes of steel suitable for ship structures: mild steel; notch-tough mild steel; 'B-Quality' crack arrest steel; and 'BX-Quality' high thickness crack arrest steel.

The poor fracture strength of mild steel at low temperatures means that most warships are likely to be constructed from notch-toughened or crack-arrest steel (Chalmers, 1993). A B-Quality crack arrest steel as defined by DefStan 02-791 Part 3 (Ministry of Defence, 2000) was selected (equivalent to the British Standard 4360 50EE specification), and the following properties taken from Chalmers (1993): Young's Modulus: 205 GPa; Poisson's Ratio: 0.3; Yield Stress: 300 MPa; and Ultimate Stress: 590 MPa, with density taken from Cardarelli (2008) as 7,750 kg/m3.

The elasto-plastic rate-dependent material model required some further characteristics, to define the relationship between dynamic stress and the strain rate. Such data was available for mild steel, HY-80, HY-100 and HY-130 steels, but not for B-Quality steel specifically. As Billingham et al (2003) made clear, a limited quantity of testing of medium- and high-strength steels at high strain rates has been conducted. While relationships between dynamic and static yield stress in medium-strength steels have been published (Burgan, 2001) they are applicable only to narrow strain ranges and therefore were of little use. Given the paucity of data, the dynamic behaviour of B-Quality steel was assumed to be similar to that of mild steel (or, at any rate, more similar to mild steel than to the higher strength HY-series steels), and the parameters suggested for mild steel by Stultz (2009) were used.

iv) Model hierarchy

Models in Hypermesh contain components and assemblies, where every surface, node and mesh element must be contained within a component and components may be grouped together into assemblies. When converted into EPSA input format, assemblies are converted to sheets. Material settings are applied to each sheet; components within the sheet must use the same material although they may have different thicknesses. Plate elements within a component must all have the same thickness.

Best practice is to minimise the number of assemblies and components in use (Stultz, 2009). Since only a single material was in use, a single assembly was used for the whole model. Forty components were used in each mode, each corresponding to a region of the model as follows:

i. Plating web and flange in each of eight panels
ii. Plating, web and flange in the transverse bulkhead
iii. Web and flange in each of three regions of the transverse frame
iv. Web and flange in three regions of girders
v. One blank component 'transport' used as a temporary storage component by some scripts

A consistent naming convention was applied to the components, to facilitate the production of scripts. Troubleshooting was found to be easier with the full component name included in the EPSA input and output files.

3.7 b Manual creation of a surface model of one frame bay

The choice of a prismatic hull section greatly facilitated the construction of the surface model geometry. A narrow strip of structure was constructed manually, elements of which would subsequently be replicated, translated and scaled in scripted operations to form the complete model.

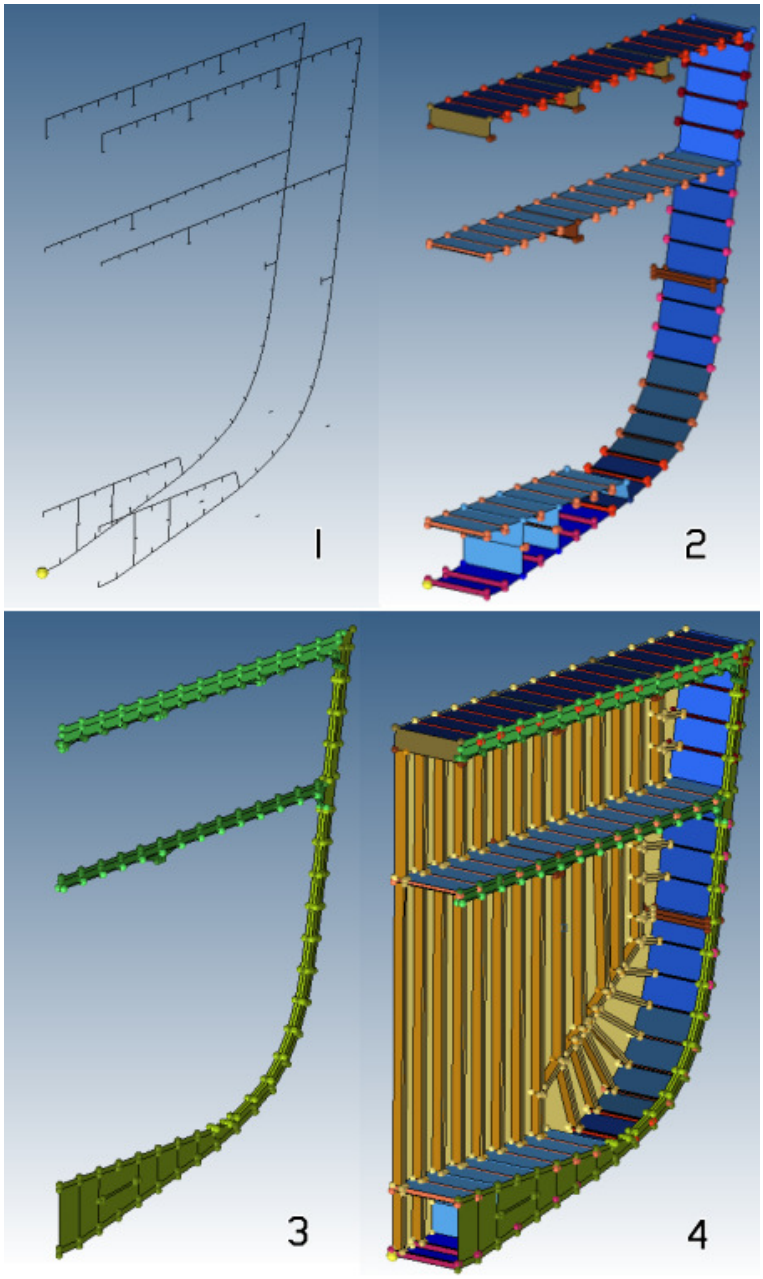

Figure 3.7.2 – Stages in the creation of the initial frame bay surface model

The two-dimensional drawings previously created in AutoCAD were imported into Hypermesh, scaled and translated into the appropriate locations (See Figure 3.7.2 - Stage 1). Surfaces were created to represent a strip of shell plating and longitudinal stiffeners, each assigned to the appropriate component in the hierarchy. (See Figure 3.7.2 - Stage 2). Surfaces were then created for the transverse frame webs and flanges (See Figure 3.7.2 - Stage 3) and transverse bulkheads. The combination of all of these surfaces represented a longitudinal strip of structure one frame spacing long, including one section of shell plate, one section of longitudinal stiffening, one frame and one bulkhead (See Figure 3.7.2 - Stage 4.)

3.7 c Development of strip model into

This structural strip model was then developed into a full three compartments, with between four and eight frame bays per compartment depending on the model. Since the structure was to be prismatic, this required only replication, translation and scaling operations, although a large number of these operations were required. The construction of some early models had illustrated the prohibitive time requirement to build the entire surface model manually, so all subsequent models automated this process using the Tool Command Language (TCL), a scripting language which Hypermesh can natively execute. The process of developing the model from a single frame bay into the full three-compartment structure required the following six steps:

i. Reflection of frame flanges
ii. Replication of frame bays
iii. Integration of bulkhead stiffening with longitudinal stiffening
iv. Reflection of structure about centreline
v. Alignment of shell plating normal
vi. Replication of compartments

i) Reflection of frame flanges

The first script duplicated the transverse frame flanges by reflecting them around the plane of the frame's web (See Figure 3.7.3.)

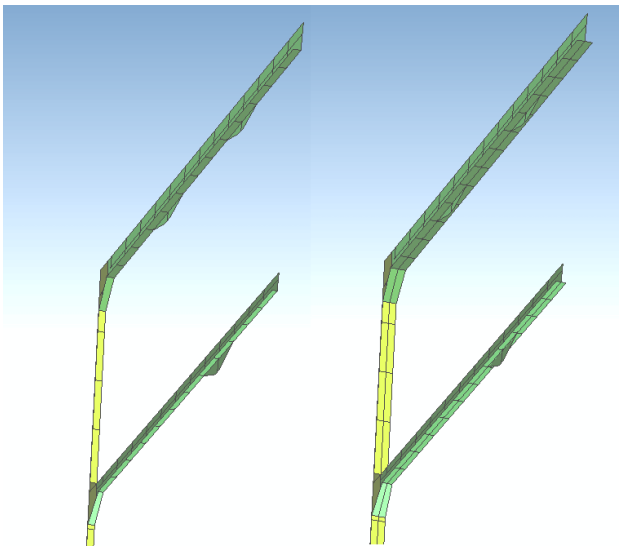

Figure 3.7.3 - Effect of script for reflection of frame flanges (01_FRAME_FLANGES)

ii) Replication of frame bays

The second script replicated the shell plating, longitudinal stiffeners, girders and transverse frames a number of times, translating each copy by the frame spacing. This resulted in a half-width model the length of a single main transverse compartment, as shown in Figure 3.7.4.

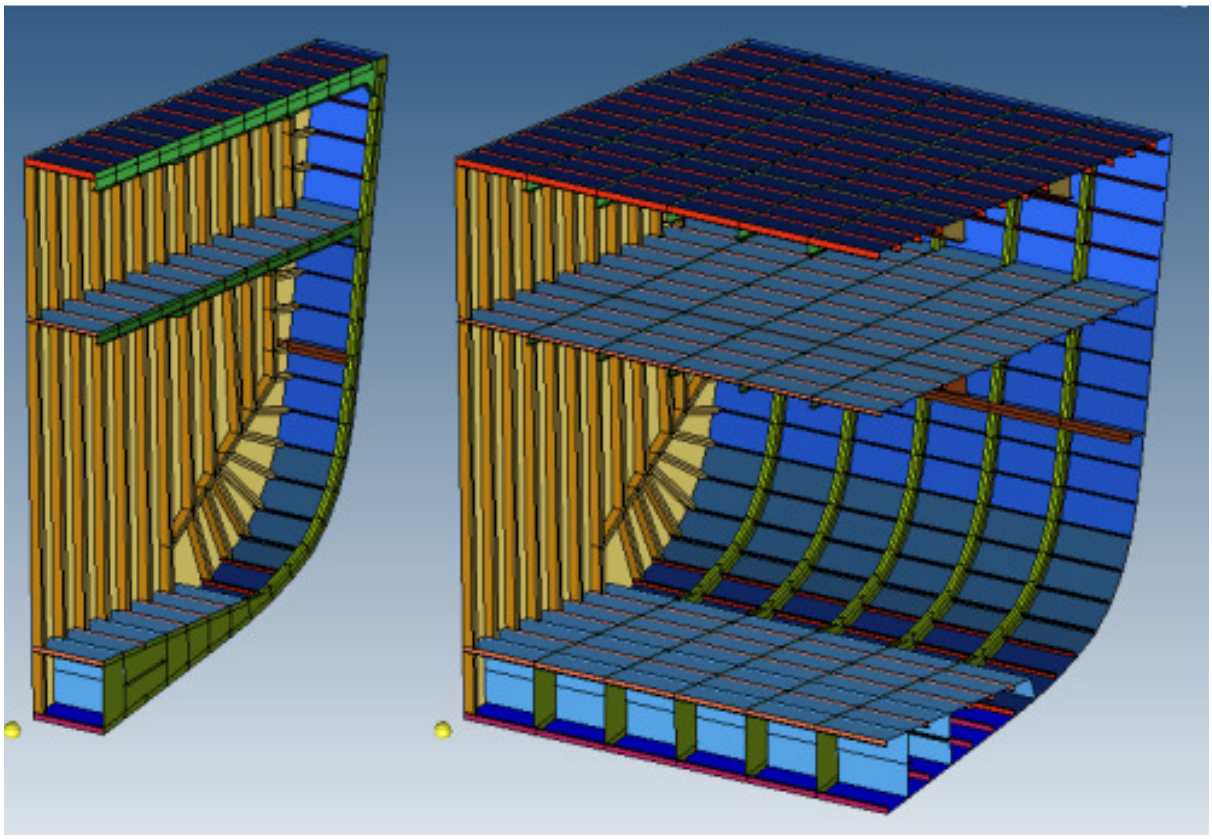

Figure 3.7.4 - Effect of script to replicate frame bays (02_REP_FRAMEBAYS)

iii) Integration of bulkhead stiffening with longitudinal stiffening

The next step was to adjust the shell plating and stiffeners of the frame bay adjacent to the bulkhead, duplicating and scaling in the X-direction to produce edges coplanar with the flange side of the bulkhead stiffeners, as shown in Figure 3.7.5. This step was required to allow the coincident edges of the longitudinal stiffeners and the bulkhead frames to be united for structural continuity.

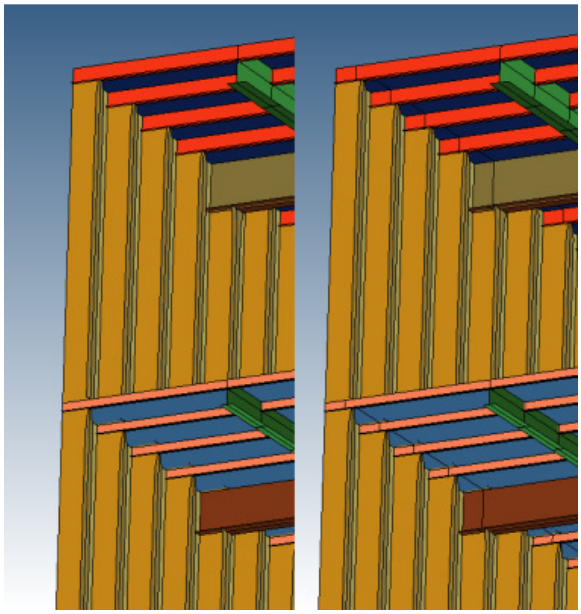

Figure 3.7.5 - Effect of script to integrate bulkhead stiffening (03_INTEGRATE_BULKHEAD)

iv) Reflection of structure about centreline

The structural model was then duplicated and reflected in Y, turning the port-side model into a full-hull model, as shown in Figure 3.7.6.

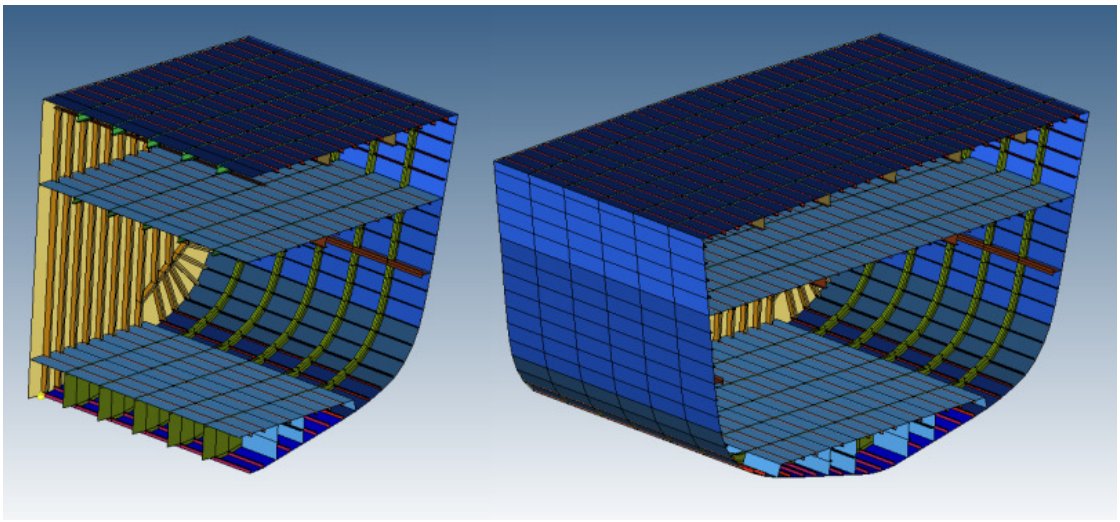

Figure 3.7.6 - Effect of script to reflect structure about centreline (04_MIRROR)

v) Alignment of shell plating normals

To ensure that EPSA applied the fluid loading to elements in the correct direction, it was necessary to ensure that all wetted surfaces were aligned with their normals pointing into the fluid. A group of scripts allowed the normals of individual components to be reversed, or all selected plate sections on one side of the ship's centreline to be reversed together. A combination of these was applied until all shell plating normal faced the wetted side, as shown in Figure 3.7.7.

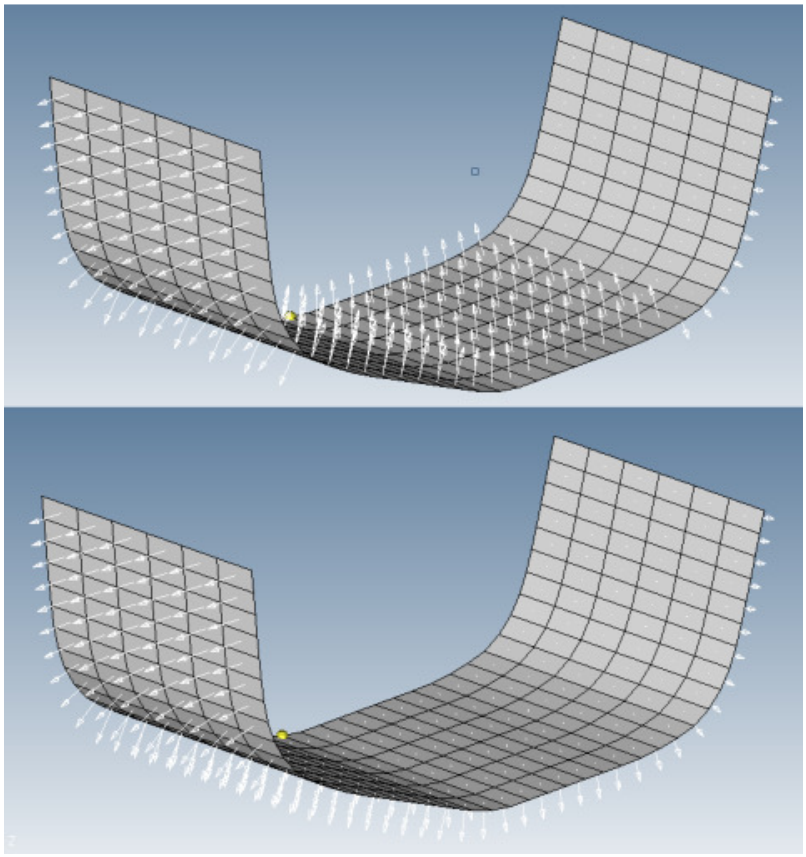

Figure 3.7.7 - Effect of script to align shell plating normal (06_REVERSENORMALS_PLATE_N)

vi) Replication of compartments

Finally, the transverse compartment was replicated and translated in X three times, before all of the final copy was deleted except the transverse bulkhead. This left a complete model with three main transverse compartments and the corresponding four transverse bulkheads, as shown in Figure 3.7.8.

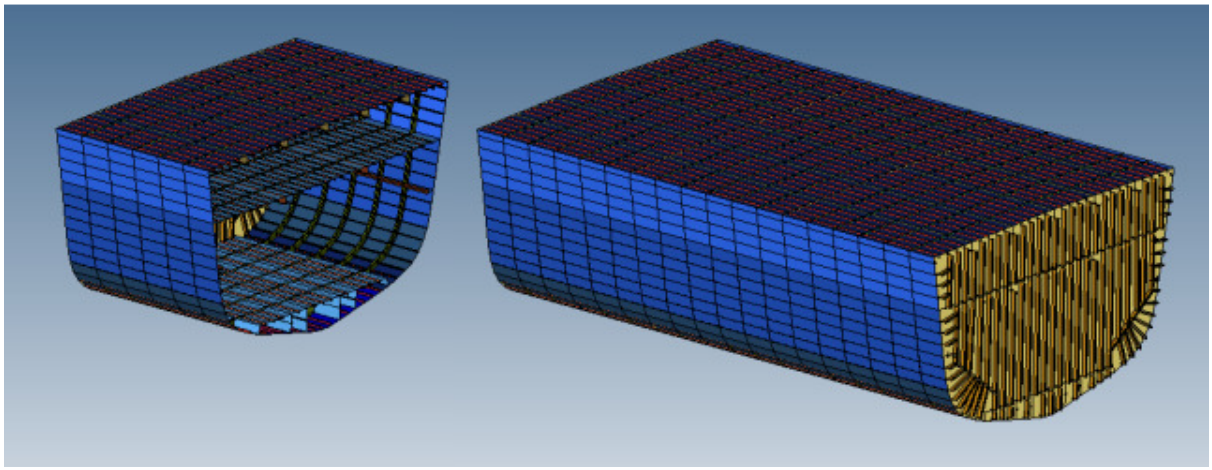

Figure 3.7.8 - Effect of script to replicate compartments (07_REP_COMPARTMENTS)

3.8 Mesh Generation

All coincident edges were unified, representing perfect welded joints of identical strength to the surrounding material. Real welded joints are more complex and may fail at a lower average load than such an ideal joint, since thermally induced distortions in the metal will tend to act as stress concentrators and lead the joint to yield progressively before homogeneous material would. A study examining the failure mechanics of a structure might need to take these effects into account. However, to model welds in more detail would require small features to be represented, and the requirement to comply with the Courant-Friedrichs-Lewy condition (discussed in Section 3.7 ai) would consequently require a smaller timestep, considerations of computation time make it impractical to represent weld detail on the size of model under consideration here. Therefore, a shock factor low enough to be clearly sub-lethal was selected to minimise the effect of this error on the solution, for this study. To take into account weld failure in future studies, a logical approach might be to build sub-models of the region around weld joints, loading them with motions taken from the larger, lower-fidelity whole hull model. This might be a suitable topic for follow-on research work.

Mesh elements were generated using Hypermesh's Automesh function. QUAD4 quadrilateral plate elements were used, with a characteristic size of 0.1m with triangular TRIA elements used where necessary. Because EPSA models a triangular element as a lumped-mass quadrilateral with two nodes coincident, the mass distribution over a TRIA element is incorrect - having half the mass at one corner and one quarter at each of the others, rather than one third at each. It is therefore desirable to limit the number of TRIA elements in use, although they are useful for allowing mesh continuity around areas of complex geometry. Each model typically comprised 200,000 to 250,000 elements.

Elements were checked for concavity (maximum internal angle >180 degrees). Edge connectivity was also checked, and the minimum inter-nodal distance measured to ensure compliance with the Courant-Friedrichs-Lewy condition. The elements comprising the shell plating below the waterline had the WETELM (Wetted Element) flag set, so they would receive loading from the underwater pressure field. Node outputs for recording were selected; in general every node in the deck and shell plating of the central main compartment was set to record vertical velocity. Once complete, the model was exported to the appropriate format for EPSA input.

Chapter 4 Verification and Validation

4.1 Overview

This chapter describes the work that was undertaken to give confidence that the modelling process produced credible results. The chapter is divided into three major sections corresponding to the main aspects considered: verification, validation and sensitivity. The terms verification and validation are treated with a range of different meanings by different authors. The following definitions, from Law and Kelton (1991) were adopted:

> "Verification is determining that a simulation computer program performs as intended, i.e. debugging the computer program. Thus, verification checks the translation of the conceptual simulation model (e.g. flowcharts and assumptions) into a correctly working program."
>
> "Validation is concerned with determining whether the conceptual simulation model (as opposed to the computer program) is an accurate representation of the system under study. If a model is "valid," then the decisions made with the model should be similar to those that would be made by physically experimenting with the system (if this were possible)."
>
> "When a simulation model and its results are accepted by the manager/client as being valid, and are used as an aid in making decisions, we call the model credible."

Credibility was taken as the goal of the simulation, and verification and validation were measures to achieve it. Credibility is a subjective metric, realised by persuading the reader that the code is valid and the conceptual model is an accurate representation of the real system.

Sensitivity analysis is an important tool in the pursuit of credibility. Creating a finite element model requires a number of simplifying assumptions to be made, compared to the real system. Some of these are heavily constrained and/or amenable to analytical selection, for example in this research the relationship between mesh size and timestep being mandated by the Courant-Friedrichs-Lewy Condition (Stultz, 2009). Other assumptions were less obviously constrained and it was seen to be important that assumptions which might have invalidated the model were avoided. Sensitivity analysis allows the designer to understand how sensitive the model outputs are to particular parameters of interest, allowing effort to be focussed on careful selection of the parameters to which the results have the greatest sensitivity.

4.2 Verification

The development of the FUSE and EPSA codes included a thorough programme of verification and validation. Atkash et al. (1983) summarised the early validation work carried out during the development of EPSA, including comparisons of the code's output with classical calculations, other FE codes and experimental measurements, concluding that "excellent agreement was obtained."

Hunter & Geers (2004) summarised the validation work conducted on the theoretical model underlying the FUSE code. Their study identified discrepancies between the model and experimental data after the first bubble pulsation period, for which they suggested corrections, despite excellent agreement in the early phase of the simulation. For the simulations used for the current research, the bubble pulsation period was of the order of one second, well outside the period for which the response was simulated.

The 1983 and 2004 studies gave confidence that the codes themselves were sound and capable of producing results comparable to reality. However, it is entirely possible for a hydrocode operator to use a valid code incorrectly, leading to entirely erroneous results. The candidate, therefore, conducted some further validation studies to give confidence in two additional aspects of the analysis; that the code was used correctly, and that the model types under consideration gave credible results.

4.3 Validation exercises undertaken

Three validation exercises were undertaken by the candidate to evaluate different areas of the simulation process: a) validation of a FUSE/EPSA simulation of a simple flat plate against Taylor's formulae; b) validation of the structural design tools against the NFR-90 structural design; and c) validation of FUSE/EPSA ship hull section models against the Environmental Grade Curve Scheme. Each is described in one of the following sub-sections:

4.3 a FUSE/EPSA Validation – flat plate model

When a shock wavefront strikes an air-backed plate, the increased incident pressure causes the plate to accelerate away from the charge. The wavefront is partially reflected by the plate, which causes the apparent pressure acting on the plate to exceed the incident pressure during the initial period post arrival. As the plate velocity increases relative to the particle velocity of the water the apparent pressure acting on the plate falls, since the water is incompressible. Eventually the plate exceeds the particle velocity, local cavitation occurs, unloading the plate

and resulting in no further acceleration regardless of the incident pressure. This steady state velocity is referred to as the plate's kick-off velocity (Reid, 1996).

Cole (1948) presented a series of equations to model the shockwave arising from an UNDEX, reproduced as Equations (Eq 4.1) - (Eq 4.3), below. These so-called "similitude equations" model the incident pressure at a fixed point as an instantaneous rise followed by an exponential decay. This is a simple model, requiring only two variables to define each case; the peak pressure and a decay time constant. Cole's equations provide an empirically-derived means of estimating these variables for a given charge mass and stand-off distance, for a variety of different explosives. Reid (1996) provided a helpful conversion of the similitude equation coefficients to SI units.

$$P = P_0 e^{\frac{-t}{\theta}} \qquad \text{(Eq 4.1)}$$

$$P_0 = K_p \left(\frac{W^{\frac{1}{3}}}{R} \right)^{m_p} \qquad \text{(Eq 4.2)}$$

$$\theta = K_\theta W^{\frac{1}{3}} \left(\frac{W^{\frac{1}{3}}}{R} \right)^{m_\theta} \qquad \text{(Eq 4.3)}$$

where P is incident pressure in MPa at a time t in seconds, P_0 is the peak incident pressure in MPa, $\theta$is the decay constant in seconds, W is charge weight in kilograms and R is standoff distance in metres. K_p, m_p, K_θ and m_θ are dimensionless constants characterising the behaviour of different explosives.

Swisdak (1978) said that it is widely known that Cole's model under-predicted the pressure during the decay phase, particularly after the duration given by θ, the first time constant, and he gave various methods to correct for this including the use of two exponential curves or invoking the addition of a constant pressure. However, so long as the kick-off velocity is reached within the duration of the first time constant, θ, these corrections are not required.

Taylor (1941) presented a set of equations (reproduced at Equations (Eq 4.4) – (Eq 4.6)) to model the kick-off velocity of an infinite flat plate subjected to a planar pressure wave of instantaneous rise and exponential decay, which Reid (1996) described as allowing "for a quick and reasonably accurate estimation of the velocity of an air-backed plate after being struck by an incident shockwave underwater." Reid went on to present a comparison of experimental results with Taylor's equations and concluded that an error of up to +/-20% is typical.

$$V_{max} = \frac{2\,P_{max}\theta}{(m_p(1-\beta))}\left[e^{-\beta\left(\frac{t_0}{\theta}\right)} - e^{\frac{-t_0}{\theta}}\right] \qquad \text{(Eq 4.4)}$$

$$\beta = \frac{\rho c \theta}{m_p} \qquad \text{(Eq 4.5)}$$

$$t_{max} = \theta\,\frac{(\ln \beta)}{\beta - 1} \qquad \text{(Eq 4.6)}$$

where V_{max} is the kick-off velocity, P_{max} is the peak incident pressure, θ is the decay time constant, m_p the mass per unit area of the plate[4], t_0 the arrival time of the shockwave, ρ the density of water, c the speed of sound in water and t_{max} the time for kick-off velocity to be reached.

As part of the validation process, a simple arrangement of a submerged, air-backed plate subjected to an explosion was modelled in FUSE/EPSA to compare the pressure field and plate kick-off velocity predicted by FUSE/EPSA with those predicted by equations (Eq 4.1) – (Eq 4.6). The plate was a 20cm square of 5mm thick steel plating, arranged normal to a 1kg spherical TNT charge at a standoff of 10m, both charge and plate centre located 10m under the free surface of deep seawater. Incident pressure and horizontal velocity histories were logged at the plate's central node and are shown compared to the Cole/Taylor models in Figure 4.3.1.

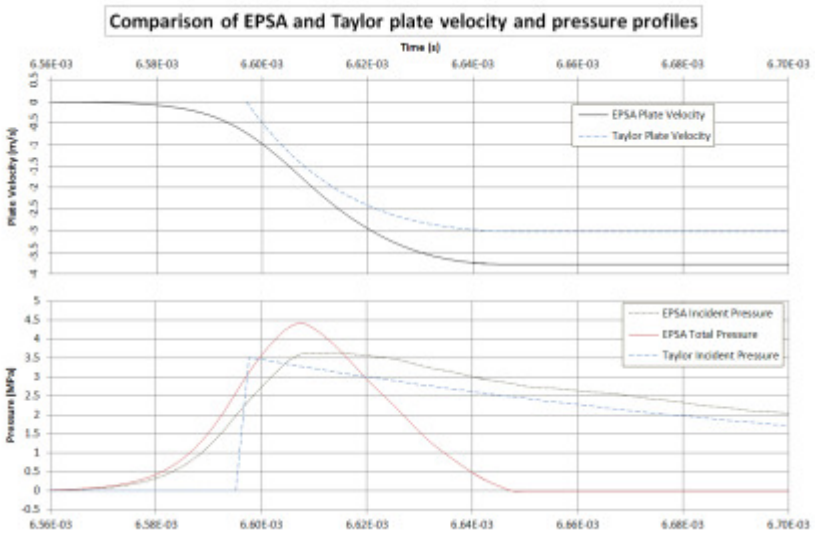

Figure 4.3.1 - Comparison of EPSA plate model to predictions by Cole/Taylor equations, with identical charges

[4] Note that Cole and Taylor used the notation m_p to refer to two different quantities; Cole used it as a dimensionless constant to characterise explosives, and Taylor used it for the area mass density of the plate.

In both the Cole/Taylor and the FUSE/EPSA model the kick-off velocity was reached inside the first decay constant, so there was no need to apply a correction to the similitude equations' decay phase. EPSA predicted kick-off velocity 19.8% higher than that predicted by Taylor's equation (Eq 4.4), but that is within the error band typical for physical experiments. FUSE predicted a peak incident pressure very close to (within 3% of) that predicted by the Cole/Taylor model. The discrepancy in kick-off velocity clearly arose from the different incident pressure profiles assumed by FUSE and by Cole's equations. The areas under the two incident pressure curves in Figure 4.3.1 were compared and it was noted that the FUSE model clearly delivered a greater impulse to the plate.

To check the function of EPSA against Taylor's equation assuming more similar incident pressure profiles, the similitude equations were applied with an enlarged charge, sized to give the same integral of incident pressure over time as that calculated by the FUSE/EPSA model, over the period to reach kick-off velocity. It was found that applying the similitude equations to a charge of 1.63kg of TNT gave a well-matched pressure profile, as shown in Figure 4.3.2.

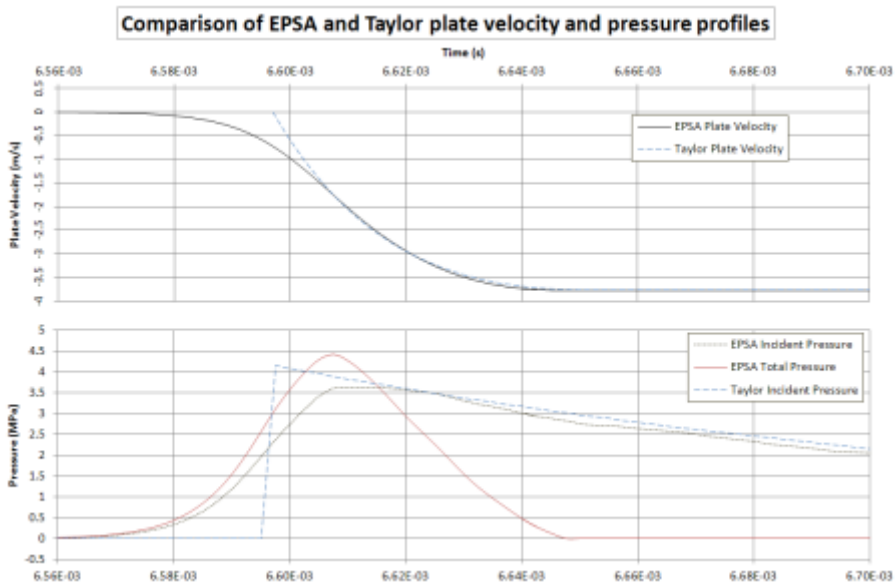

Figure 4.3.2 - Comparison of FUSE/EPSA plate model with predictions by Cole/Taylor equations, with Cole/Taylor explosive charge adjusted to match integral of incident pressure with the FUSE/EPSA model

It was observed that the incident pressure profiles more closely matched each other during the decay phase than in Figure 4.3.1, and that the integral area over the kick-off period was also better matched than in Figure 4.3.1. Given this better-matched pressure profile, EPSA seemed to predict a kick-off velocity in very close agreement with Taylor's equation (Eq 4.4), with an error less than 0.3%.

In conclusion, the pressure field modelled by FUSE predicted a peak incident pressure very close to that predicted by Cole's similitude equations (Eq 4.1) – (Eq 4.3), and gave a kick-off velocity within typical experimental error of that predicted by Taylor's equations (Reid, 1996). Given similar pressure profiles, EPSA gave a very close kick-off velocity to that predicted by Taylor. This gave confidence that EPSA and FUSE were functioning correctly and being operated correctly by the candidate.

4.3 b Structural design method validation

To check that the structural design method, outlined in Chapter 3, gave credible results, the method was used to develop a structure given the same input parameters as the NFR-90 Frigate. This allowed a comparison of the model's output against the output of a real design project, albeit one only developed to the design stage, not detail designed or built. The structure model was developed with the following input parameters, taken from Schaffer & Kloehn (1991):

i) Ship Characteristics

- Waterline length: 133m
- Top speed: 30 knots
- Midship draught: 5.35m
- Block Coefficient 0.484

ii) Loading

- Bending Moment (Hogging): 514 MNm
- Bending Moment (Sagging): -471 MNm
- Shear Force: 9MN

iii) Scantling Design

- Stiffener material fraction (As/A): 20%
- Nominal Longitudinal Stiffener Spacing: 600mm
- Frame Spacing: 1500mm
- Material Tensile Yield Stress: 350 MPa
- Material Ultimate Tensile Stress: 500 MPa
- Material Young's Modulus: 200 GPa
- Material Poisson's Ratio: 0.3

(The material properties chosen for this model differ from those used in the models developed for simulation, since the aim of this model was to replicate a specific design, which had used high strength steel.)

Schaffer and Kloehn's paper, while comprehensive, omitted some necessary data, so values typical for a ship of this type were assumed in the following areas:

- Design Rules: (Chalmers, 1993) /SSCP-23
- Transverse Bulkhead Spacing: 12m
- Stiffener type and aspect ratio: Long-stalk Tee-bar as defined in Section 3.3 c.

Scantlings were designed by manual iteration of smeared panel thickness (Chalmers, 1993). The final thicknesses are given in Table 4.3.1 and compared to those in the NFR-90 midship section presented by Schaffer & Kloehn (1991).

Table 4.3.1 - Comparison of midship scantlings between validation model and the NFR-90 design reported by Schaffer & Kloehn (1991)

	Plate Thickness		**Stiffener Depth**	
Region	**Validation model**	**NFR-90**	**Validation model**	**NFR-90**
1 (Top deck)	14.9mm	12mm & 14mm	153mm	127mm
2 (Upper sideshell)	10.7mm	10mm	130mm	127mm
3 (Passing Deck)	4.9mm	4.5mm & 6mm	88mm	80mm & 100mm
4 (Lower sideshell)	8.2mm	8mm	114mm	100mm
5 (Turn of bilge)	8.2mm	8mm	114mm	127mm
6 (Inner bottom)	7.8mm	8mm	111mm	114mm
7 (Outer bottom)	13.6mm	12mm & 14mm	147mm	127mm & 152mm
8 (Keel)	17.1mm	16mm	164mm	152mm

The plating thicknesses in the validation model fell within +/-7% of the values used in the NFR-90 (where multiple sizes occurred within one region they were averaged) aside from the Top Deck thickness, where the difference was 15%. Similarly, the greatest error in stiffener depth occurred in the Top Deck, where the difference was +20%, while in the other areas the differences fell between -10% and +14%. These larger differences corresponded to the regions where the ratio of stiffener depth to plating thickness varied the most between the models, suggesting that the assumption of a constant As/A ratio (discussed in Appendix B) might explain the deviation.

Given the constraints placed upon the model by the design process, in particular the fact that the regions of constant plate thickness/stiffener size align only approximately between the two designs, it was felt that this represented a reasonably good agreement. Certainly it was felt that the designed model could be considered representative of the same structural style as the NFR-90 Frigate.

4.3 c Whole model FSI validation against the Environmental Grade Curve Scheme

If data had been available for a full-scale shock trial, it would have been desirable to have replicated that trial using FUSE/EPSA and compared the results. However, no suitable trials data was available so an alternative approach was sought.

The UK Environmental Grade Curve Scheme (EGCS) (Ministry of Defence, 1974) was produced based on aggregated data from a number of full scale trials, primarily the series conducted on surplus destroyers and cruisers after the Second World War, described by Brown (1987a; c) and already outlined in Section 2.4. One of those trials was replicated (as far as data was available) and the results compared to those predicted by the EGCS. Given the aggregated nature of the Scheme, it was anticipated that the results would have been similar if perhaps not in perfect agreement. The majority of the post-war shock trials were conducted against surplus destroyer hulls, of which the J/K/N Class accounted for the majority; eight out of fourteen. Consequently a J/K/N Class destroyer hull section was replicated in EPSA and subjected to a shock commensurate in magnitude to those used in the trials. The resulting hull structure motions were logged and compared to those predicted by the EGCS.

Since the EGCS was the accepted method of assessing shock response for ships of the NFR-90's type, a second simulation was conducted using the NFR-90 validation model described in the previous section. The structure was modelled in EPSA and subjected to a sub-lethal shock. As with the J/K/N Class simulation, the response motions at various locations were logged and compared to those predicted by the EGCS.

Elements of the EGCS are protectively marked UK CONFIDENTIAL, and so the calculation cannot be reproduced. A full report of the test was submitted to the UK Ministry of Defence Sea Systems Group's Shock and Vulnerability Section, the UK subject matter experts for shock, in November 2011 for review and comment. A letter from the Head of Section is at Appendix C. In summary this letter states that the analysis in the Confidential Report was sound and shows a good match between the simulation and the EGCS data. This is considered to be sufficient (within the constraints of open access academic presentation) to demonstrate that

the complete modelling and simulation process adopted gives results representative of those observed in full scale trials, and to give credibility to the subsequent computational investigations.

4.4 Sensitivity Analysis

A number of exploratory studies were conducted to determine the sensitivity of the simulation output to various model parameters. In particular, it was necessary to establish an understanding of the following three areas:

i. What proportion of the ship should be included in the model;
ii. What level of detail should be incorporated into the model;
iii. How sensitive the model was to details of bulkhead and frame design.

A range of finite element models were developed based on the engine room region of a Royal Navy Second World War J/K/N-Class destroyer. Their responses to a low shock-factor UNDEX were simulated, allowing a comparison of the vertical motions of indicative points in the upper deck and keel. A more detailed description of these studies is provided at Appendix D, including examples of the models used and results obtained.

These studies informed the choice of model size (three transverse compartments) used for the main research simulations and the level of detail to which the structures were modelled.

Chapter 5 Parameter Selection

Having described the method used to develop structural models, as well as the measures taken to gain confidence in that method, this chapter describes the structural models used for the three selected series of simulations. The ship designs used as the basis for these investigations are described and the structures developed for the three experimental series presented. Each series corresponded to a particular aspect of structural style which appeared to offer the prospect of cost savings:

i. Reduction in the number of stiffeners, proposed by Chalmers (1986) as offering moderate savings in structural costs, principally due to reductions in the quantity of welding work required to assemble the structure;
ii. The use of alternative stiffener profiles to the long-stalk T-bar, again identified by Chalmers (1986) as a likely trend in warship design. The use of commercially available stock profiles as opposed to fabrication of specialist profiles offers potential savings in material cost.
iii. The adoption of a transverse stiffening scheme rather than the more typical longitudinal stiffening scheme. While inefficient in long ships (>100m), where hull girder bending typically dominates the loading case, in smaller ships a transversely stiffened structure seems to offer a significant saving in the quantity of welding required for assembly.

The chapter is divided into six sections, covering the following areas:

i. The ship selected as the baseline for the first two experimental series;
ii. The structural model developed for that ship and used as a baseline for the first two experimental series;
iii. The structures developed for the first experimental series, exploring the effect of adopting a structural style with a reduced number of stiffeners.
iv. The structures developed for the second experimental series, exploring the effects of using lower-cost stiffener profiles in place of long-stalk T-bars.
v. The ship design developed as a baseline for the third experimental series (once it had been determined that the NFR-90 Frigate was not an appropriate baseline for that series.)
vi. The structures developed for the third experimental series, exploring the effect of choosing a transverse stiffening scheme over a longitudinal stiffening scheme.

5.1 Frigate baseline ship design

The majority of the structural models were developed as variants from a baseline design based on the NFR-90 frigate. Generation of the models' structural midsections required definition of the hull geometry amidships and the loads to be carried by each structure. Since main hull girder bending and shear were important load cases, this required the ship design to be developed to a point where the longitudinal distribution of weights within the ship was reasonably well defined. The study did not require development of the ship design beyond that point. It was initially planned to use a frigate design for all experiments, since the frigate is the numerically dominant type of ship in service with blue water navies and is the default basis for most naval ship design standards and practices. Design exploration showed that for some shock response experiments a smaller ship would be more appropriate and so a corvette design was also developed.

The frigate design was based on the NFR-90 Frigate, a common frigate replacement project for eight NATO member navies developed during the 1980s (see Figure 5.1.1). Although the departure of several participating nations led to the programme's cancellation in 1990, extensive design work had been completed, including the overall structural configuration. A comprehensive overview of the project was published by Schaffer and Kloehn (1991), including load descriptions and a structural mid-section.

Figure 5.1.1 - Model of NFR-90 Frigate from Schaffer and Kloehn (1991)

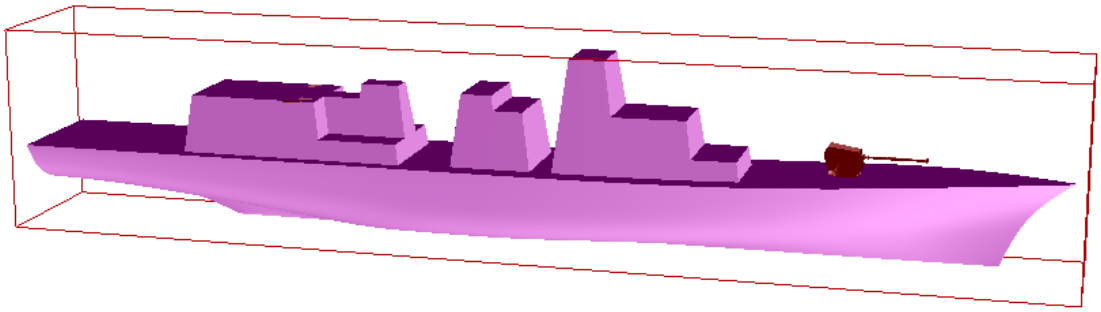

Figure 5.1.2 - Paramarine model of NFR-90 Frigate

The NFR-90 design was of typical size and proportions for a modern frigate, with a waterline length of 133m and a deep displacement of approximately 5,400 tonnes. Frigates currently operated by Western navies typically displace between 3,000 and 6,000 tonnes at full load, with a waterline length of between 100m and 150m. The design was among the last generation of ships designed in the Cold-War period, before the pressures of the post-Cold War "peace dividend" led to force reductions, increased cost constraints and pressure to introduce elements of commercial style into naval structures. It could, perhaps, be viewed as the ultimate development of the Cold War-era NATO frigate design style.

Schaeffer and Kloehn listed a number of design bending moments for the NFR-90, corresponding to various NATO national standards and the initial NFR-90 design. However, they also describe how the initial design was deemed excessively strong by the US Navy and redesigned, without making it clear whether the midship section presented was before or after the redesign, so it was unclear which bending moment that the structure described was designed to carry. The structures developed for the current research were designed to the bending moment value given according to the load case described by Schaffer and Kloehn as corresponding to the 'composite' standards.

As a confidence check, a similar design was developed in the ship design suite Paramarine (Bole and Forrest, 2005) and subjected to hydrostatic analysis. The hullform was generated using the Quickhull Frigate Tool produced by Pawling (2009). This uses a coherency model based on van Griethuysen's work (Van Griethuysen, 1992) to produce a coherent set of primary dimensions based on demanded values of Circular M, prismatic coefficient (C_p), midship section coefficient (C_m) and block coefficient (C_b). Pawling's tool then scales a generic frigate hullform to meet these dimensions as closely as possible.

Superstructure blocks were modelled to approximate the NFR-90 layout. An overall ship's weight distribution was assumed, based on discrete weights for prime movers, generators, gearboxes and main weapons, with all remaining weights distributed assuming constant internal density (see Figure 5.1.3 for the level to which equipment was modelled.) To calculate the bending moment, the displacement was set to 5,991 tonnes, corresponding to the strength displacement limit given by Schaffer and Kloehn (1991) and the ship was balanced on an 8m wave to generate a loading distribution by the quasi-static method. The resulting bending moment and shear force were adjusted upward to that with a 1% probability of exceedance over ship's life level, assuming a 25 year hull life, 180 days per year at sea and an 8 second mean wave period, using the method described by Chalmers (1993).

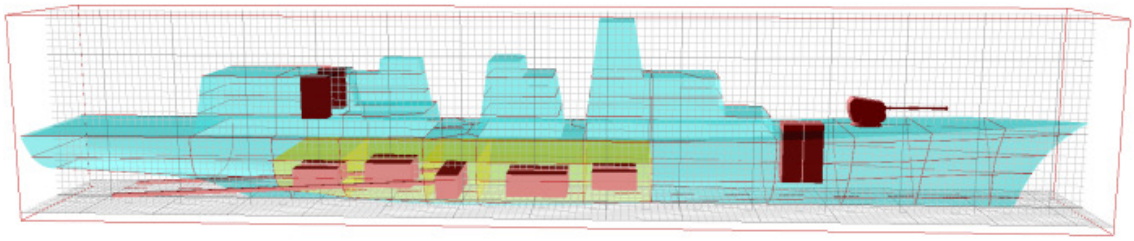

Figure 5.1.3 - NFR-90 Frigate discrete weight items modelled in Paramarine

The shear force amidships was calculated by the SSCP-23 method of plotting the absolute shear force with length and drawing a line between the quarter-point peaks.

The following ship characteristics were taken forward to drive the structural model:

Table 5.1.1 - Principal characteristics of the NFR-90 Frigate model taken forward to drive the structural designs

Bending Moment (Hogging)	357 MNm
Bending Moment (Sagging)	-344 MNm
Shear Force	9.2MN
Rule Length (a term used in NSR2 calculations)	130m
Waterline Length	133m
Top speed	30 knots
Amidships draught	5.35m
Block Coefficient	0.484

The midship section was then discretized into eight panels, as described in Chapter 3. The resulting panel geometry is shown in Figure 5.1.4.

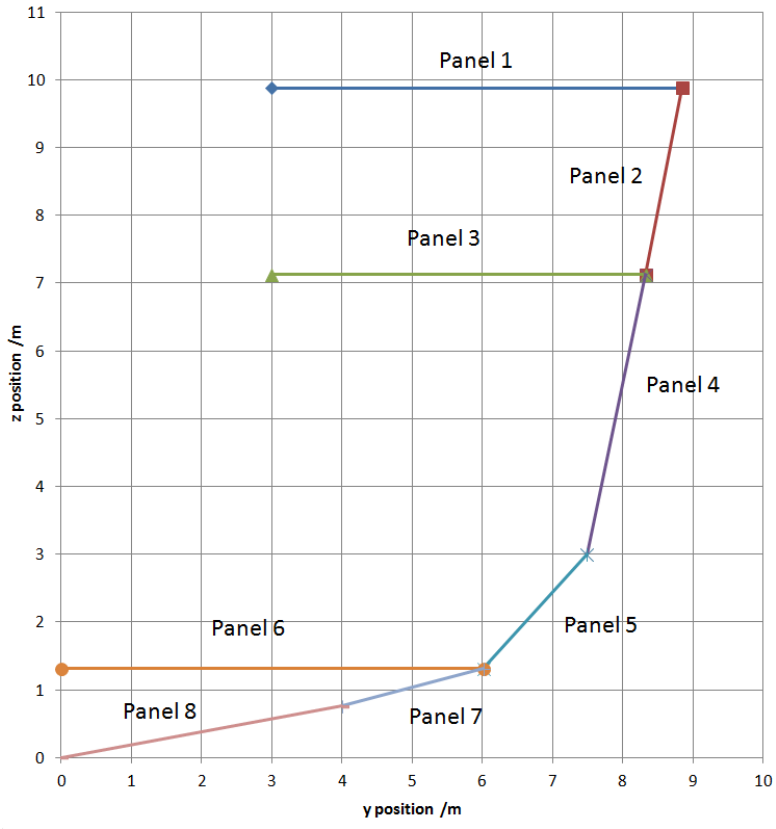

Figure 5.1.4 –Discretized form of NFR-90 Frigate midship section shape

5.2 Frigate Baseline Structural Model

A baseline structural model for the NFR-90 Frigate design was produced, from which the various experimental series variants were subsequently derived.

Structural models produced for this research were assigned reference numbers using the format AABB, where the two digits AA referred to a series of models and BB to a specific model within that series. Seventeen series of models were produced for various preliminary development work, validation and sensitivity studies, so the subsequent experimental models were given numbers in the format 18xx. A systematic approach had been applied to models in preliminary series, some of which had incorporated different combinations of stiffener spacing and stiffener profile types; see Table 5.2.1. To minimise confusion, the same approach was retained for the 18xx series of models, although only Models 1801, 1802, 1803, 1804 and 1807 were developed.

Table 5.2.1 - Systematic naming convention applied to models within Series 18xx (unused numbers in parentheses)

	Close stiffener spacing	Moderate stiffener spacing	Wide stiffener spacing
T-bars	1801	1802	1803
Offset Bulb Plates	1804	(1805)	(1806)
Flat Bars	1807	(1808)	(1809)

The structure was assessed using Lloyds Register NSR2 rules (Lloyds Register, 2008). Since some variants required the use of offset bulb plate stiffeners, a rule set was required which was capable of analysing the performance of asymmetric stiffeners; this ruled out using the Chalmers/SSCP-23 method. Values for the principal ship characteristics required to design the structure by the NSR2 rules (such as rule length, block coefficient and top speed) were taken from Schaffer and Kloehn (1991). Midship section geometry and stiffener spacings were based on the same paper, with frame spacing of 1500mm specified explicitly and characteristic longitudinal spacing of 600mm generalised from the midship section diagram they provided. A main transverse bulkhead spacing of 12m was selected since this is typical of the NFR-90's main machinery spaces. The model was constructed three main compartments long in order to avoid end effects in the compartment of interest (as discussed in Chapter 4.) The main hull girder bending loads and shear force were calculated by quasi-static balance using Paramarine, while the local pressure loads on panels were derived in accordance with the NSR2 procedures. Long-stalk tee-bar stiffeners were used throughout, of the proportions defined in Section 3.3 c. The same cross-sectional proportions were used for all transverse frames, bulkhead stiffeners and deep longitudinal girders. The structural material was assumed to be Admiralty Standard B-Quality crack-arrest steel (to DefStan 02-791 / BS4360 Grade 50EE) (Cardarelli, 2008; Ministry of Defence, 2000). It was further assumed that the material's dynamic behaviour at high strain rates was similar enough to mild steel to permit the use of the mild steel coefficients in the EPSA elastoplastic strain-rate dependent material model.

Table 5.2.2 - Structural parameters of Model 1801 - NFR-90 Baseline

Design Rules	Lloyds Register NSR2
Stiffener material fraction As/A	Calculated optimum for each panel
Nominal longitudinal stiffener spacing	600mm
Frame spacing	1500mm

Transverse bulkhead spacing	12m
Material tensile yield stress	350 MPa
Material ultimate tensile stress	590 MPa
Material Young's modulus	200 GPa
Material Poisson's ratio	0.3
Stiffener type	Long-stalk Tee-bar

The scantling design method, discussed in Chapter 3, produced the structural midsection shown in Table 5.2.3.

Table 5.2.3 - Scantlings for Model 1801 - Baseline NFR-90 frigate design

Panel	**Plate thickness**	**Stiffener Depth**
1 - Top Deck	16.2mm	129mm
2 - Upper Sideshell	16.2mm	129mm
3 - Passing Deck	6.3mm	75mm
4 - Sideshell	10.9mm	72mm
5 - Turn of bilge	13.3mm	97mm
6 - Inner bottom	10.6mm	99mm
7 - Outer Bottom	15.2mm	104mm
8 – Keel	17.6mm	118mm
Transverse bulkhead	11.7mm	251mm

Two standard metrics of structural weight and complexity were defined, which were subsequently used to compare the models in each experiment series: structural weight per metre of ship length; and total weld length per metre of ship length.

Structural weight per metre of ship length was assessed by summing the weight of each panel over one metre of ship length, then adding the weights of a frame and a transverse bulkhead, each divided by their respective longitudinal separation.

Total weld length per metre of ship length was used as a simple measure of structural complexity. It was approximated by summing the total length of stiffener-to-plating joints in one metre of ship length, using a similar approach to that described above to find the weight per metre length. For simplicity, only the plate-to-stiffener and plate-to-frame welds were

considered, since the total length of plate butt welds was likely to be independent of the structural parameters under consideration.

The resulting baseline structural design had the characteristics: weight per metre of length equal to 7.275 te and weld length per metre of length equal to 103.9m, with a midship section as shown in Figure 5.2.1.

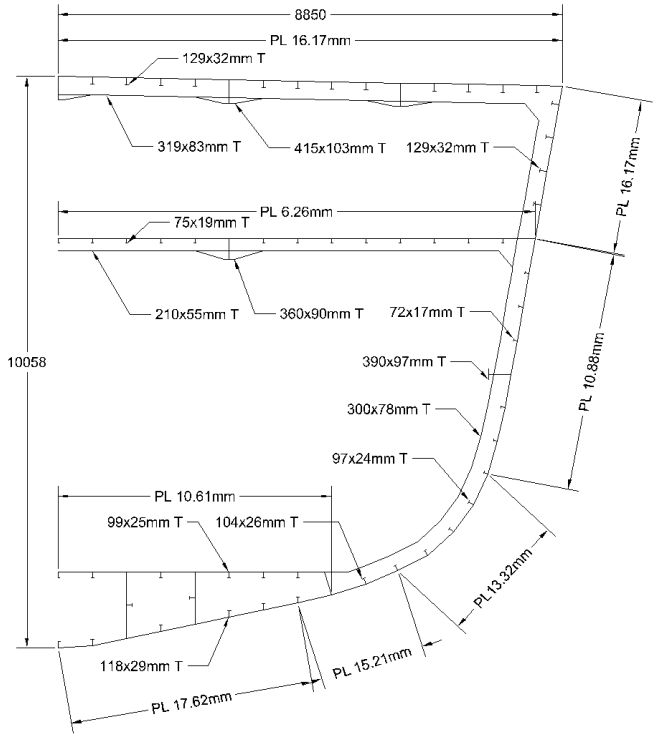

Figure 5.2.1 - Midship structural section synthesised for Model 1801 – Baseline NFR-90 Frigate design

5.3 Experiment Series 1 – Stiffener Spacing

Two variants from the baseline model were constructed to explore the effect of reducing the number of stiffeners; that is, increasing stiffener spacing. In accordance with the naming convention described in Section 5.2, these were named Models 1802 and 1803. Compared to the baseline Model 1801, stiffener and frame spacings were varied, with plate smeared thickness and As/A ratio allowed to vary to retain the same overall strength. The spacings between longitudinal stiffeners and transverse frames were increased in proportion in order to retain the same panel aspect ratio of 5:2. All other design parameters were kept the same.

The selection of spacing intervals was driven by two considerations. First, the series should cover the range from the close stiffening of the NFR-90 to a spacing quite extreme for a warship. Second, spacings were selected which would fit an integer number of frame bays into the 12 metre transverse bulkhead spacing. The panels (as shown in Figure 5.1.4) of the three models had the plate thickness and stiffener depth as shown in Table 5.3.1.

Table 5.3.1 - Scantlings selected for the three models in the first experimental series (varying stiffener spacing)

	Model 1801 (Baseline)		**Model 1802**		**Model 1803**	
	600mm x 1500mm		**800mm x 2000mm**		**1200mm x 3000mm**	
Panel	**Plate thickness**	**Stiffener depth**	**Plate thickness**	**Stiffener depth**	**Plate thickness**	**Stiffener depth**
1 - Top Deck	16.2mm	129mm	18.1mm	156mm	21.2mm	206mm
2 - Upper Side Shell	16.2mm	129mm	18.1mm	156mm	21.2mm	206mm
3 - Passing Deck	6.3mm	75mm	7.1mm	92mm	7.5mm	153mm
4 – Side Shell	10.9m	72mm	10.9mm	100mm	12.0mm	147mm
5 - Turn of bilge	13.3mm	97mm	13.6mm	124mm	16.2mm	185mm
6 - Inner bottom	10.6mm	99mm	12.7mm	119mm	16.5mm	173mm
7 - Outer	15.2mm		15.1mm		17.9mm	

Bottom		104mm		136mm		196mm
8 - Keel	17.6mm	118mm	18.9mm	153mm	21.2mm	206mm
Transverse bulkhead	11.7mm	251mm	11.8mm	273mm	11.8mm	333mm

Table 5.3.2 - Comparison of weights and weld lengths for the three models in the first experimental series (varying stiffener spacing)

Model	Model 1801 (Baseline)	Model 1802	Model 1803
Weight per metre of length	7.275te	7.068te	7.867te
Weld length per metre of length	103.9m	78.0m	52.9m

It can be seen from Table 5.3.2 that Model 1802, with the 800mm x 2000mm spacing, gave the lowest structural weight. A short sensitivity study showed this to be a result of switching from Chalmers/SSCP-23 to Lloyds NSR2 rules. By comparison, under Chalmers/SSCP-23 the lowest weight was obtained around a 600mm x 1500mm spacing - as might have been expected since the NFR-90 designers selected that spacing and were attempting to minimise structural weight The use of NSR2 rules was necessary for the subsequent experimental series and so, to main consistency, was used across all three series of structural style variants.

The midship structural cross sections of Models 1801, 1802 and 1803 are shown in Figure 5.3.1, Figure 5.3.2 and Figure 5.3.3.

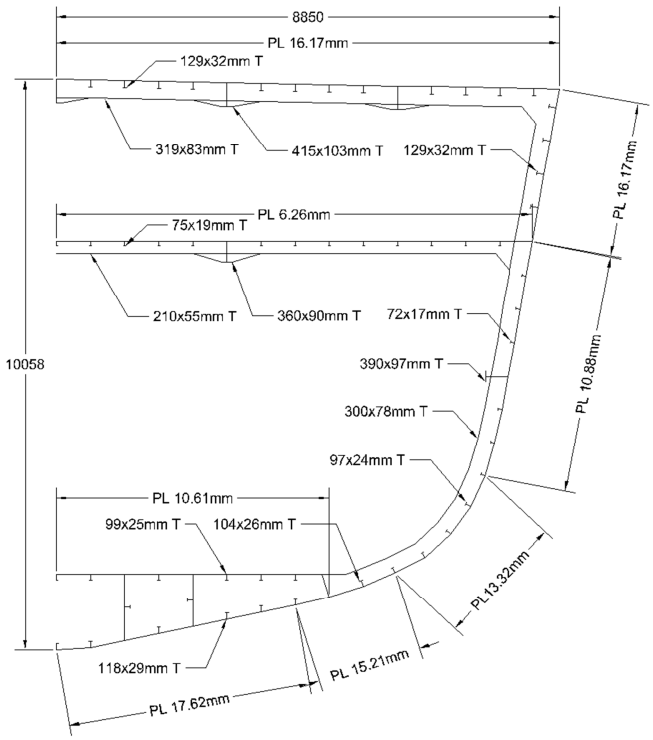

Figure 5.3.1 – Structural cross-section of Model 1801 – Baseline NFR-90 Frigate model (600mm x 1500mm spacing)

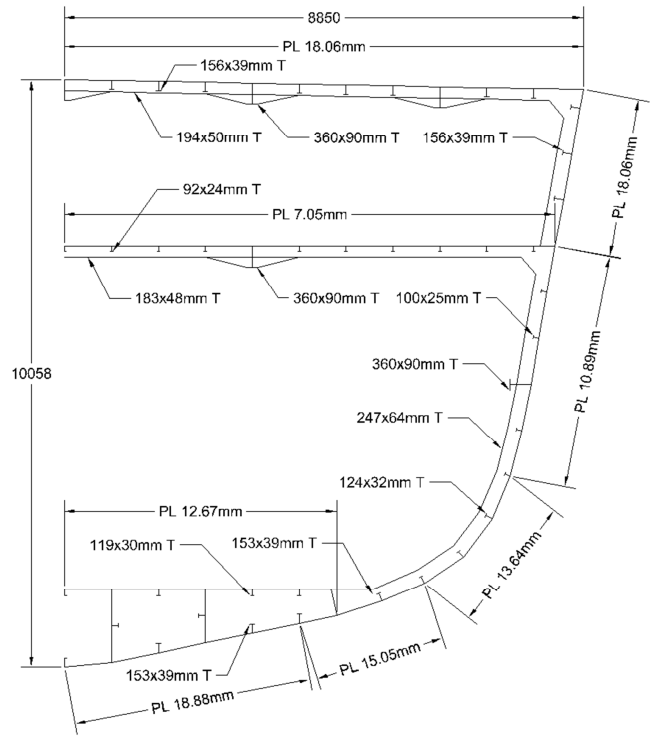

Figure 5.3.2 – Structural cross-section of Model 1802 – NFR-90 Frigate model with moderately increased stiffener spacing (800mm x 2000mm spacing)

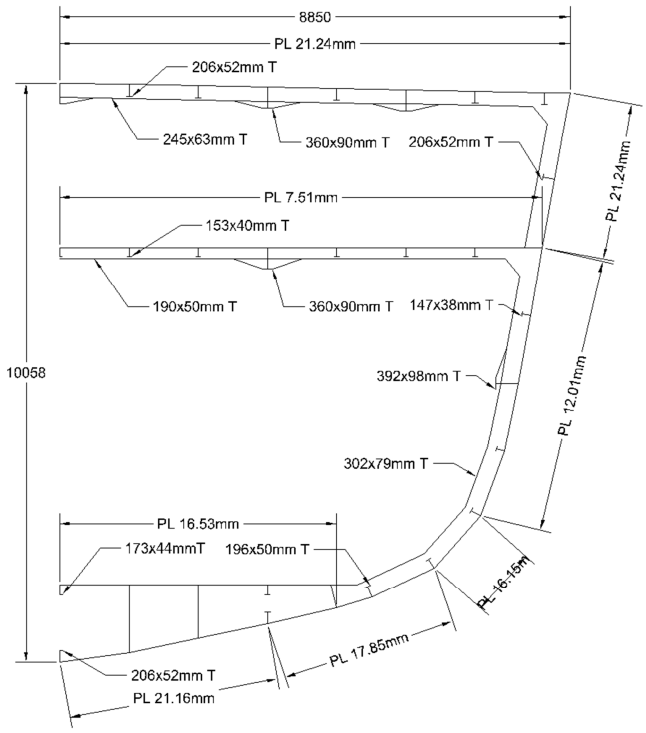

Figure 5.3.3 – Structural cross section of Model 1803 – NFR-90 Frigate with significantly increased stiffener spacing (1200mm x 3000mm spacing)

In Model 1803 the intercostal floors were left unstiffened, since they were of roughly the same length as the characteristic stiffener spacing of 1200mm.

5.4 Experiment Series 2 – Stiffener profiles

Two further variants from the baseline (Model 1801) were developed using alternative, cheaper stiffener profiles. While the baseline used the long-stalk tee-bars typical of traditional warship structural styles, the variants used offset bulb plates (Model 1804) or flat bars (Model 1807) more typical of commercial shipbuilding. Compared to the baseline model, only the stiffener profiles were varied, with plate smeared thickness and As/A ratio allowed to vary to retain the same overall strength. All other design parameters were kept the same.

Table 5.4.1 - Scantlings selected for the three models in the second experimental series (varying stiffener profile)

	Model 1801 (Baseline)		Model 1804		Model 1807	
	Tee bar		OBP		Flat bar	
Panel	**Plate thickness**	**Stiffener depth**	**Plate thickness**	**Stiffener depth**	**Plate thickness**	**Stiffener depth**
1 - Top Deck	16.2mm	129mm	16.8mm	132mm	17.5mm	141mm
2 - Upper Sideshell	16.2mm	129mm	16.7mm	132mm	17.4mm	140mm
3 - Passing Deck	6.3mm	75mm	6.3mm	94mm	6.9mm	91mm
4 - Sideshell	10.9m	72mm	10.9mm	89mm	11.0mm	104mm
5 - Turn of bilge	13.3mm	97mm	13.4mm	105mm	13.4mm	128mm
6 - Inner Bottom	10.6mm	99mm	11.0mm	106mm	11.5mm	119mm
7 - Outer Bottom	15.2mm	104mm	15.3mm	106mm	15.1mm	130mm
8 - Keel	17.6mm	118mm	17.6mm	135mm	18.1mm	143mm
Transverse bulkhead	11.7mm	251mm	11.7mm	278mm	11.9mm	338mm

Table 5.4.2 - Comparison of weights and weld lengths for the three models in the second experimental series (varying stiffener profiles)

Model	Model 1801 (Baseline)	Model 1804	Model 1807
Weight per metre of length	7.275te	7.147te	7.356te
Weld length per metre of length	103.9m	103.9m	103.9m

The midship structural sections of Models 1801 (repeated from Figure 5.3.1), 1804 and 1807 are shown in Figure 5.4.1, Figure 5.4.2 and Figure 5.4.3.

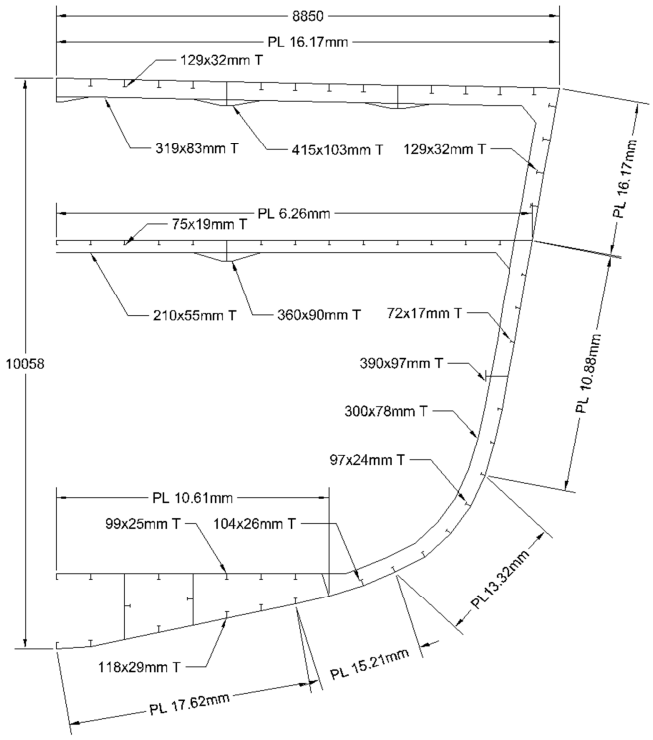

Figure 5.4.1 - Structural cross-section of Model 1801 – Baseline NFR-90 Frigate model (Long-stalk T-bars)

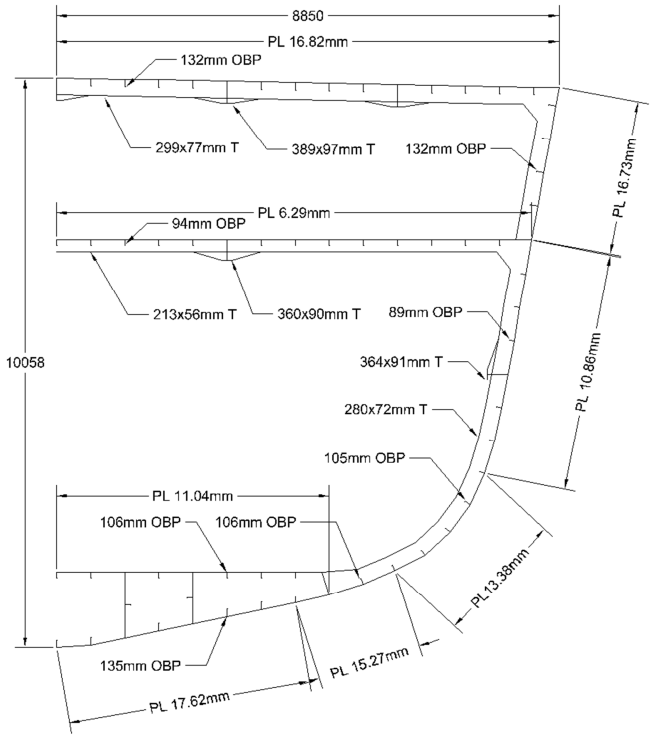

Figure 5.4.2 - Structural cross-section of Model 1804 – NFR-90 Frigate model with Offset Bulb Plate stiffeners

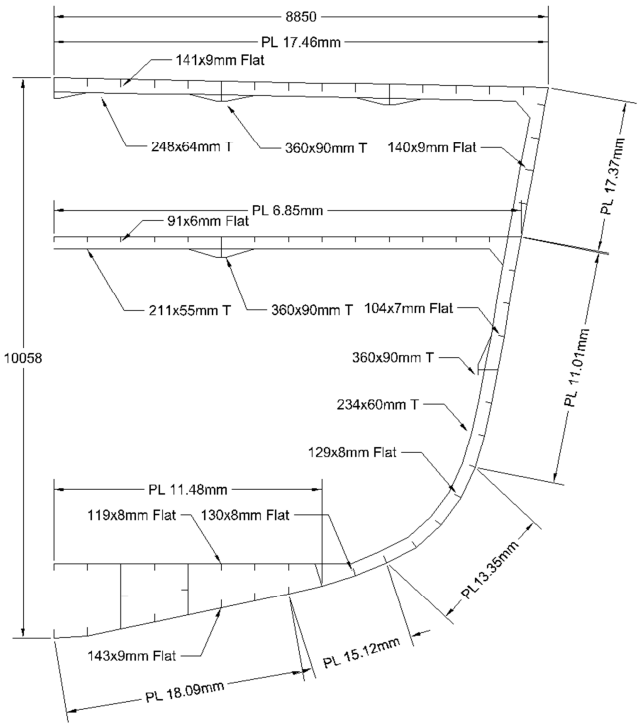

Figure 5.4.3 - Structural cross-section of Model 1807 – NFR-90 Frigate model with flat bar stiffeners

5.5 Corvette Baseline Ship Design

In order to explore the difference in shock response between longitudinal and transversely stiffened structure, it was necessary to design a smaller ship than the NFR-90. In ships longer than approximately 100m, the structural design tends to be dominated by longitudinal bending and shearing of the main hull girder, while in shorter ships local pressure loads dominate. Purely transverse structure is inefficient in carrying compressive loads, so longer ships usually have longitudinal structure in at least the strength deck and keel (although they may use so-called hybrid structure, where the side shell is transversely stiffened.)

Since there was no suitable existing ship for which the required data was readily available, a design was worked up from scratch. The Design Building Block Method (Andrews and Pawling, 2003) was used to develop a weight- and space-balanced model to the 200-block level. Stability, powering, layout and survivability considerations were addressed. The process by which the design was developed is presented in more detail in Appendix E.

Structural weight was estimated, based on scaling formulae (Chalmers, 1993 p103) to allow for design balance before the structure was designed.

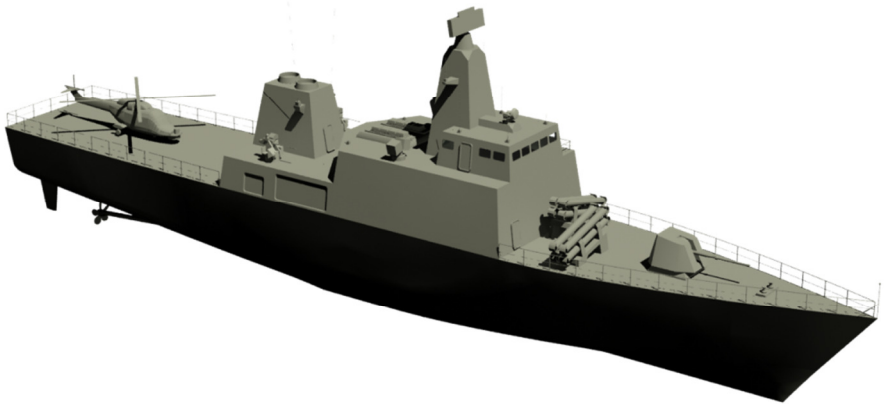

Figure 5.5.1 – Visualisation of the corvette design

Hull girder bending load and shear force were estimated using the tools in ESSD. To calculate a load distribution, the hull was divided into 21 strips. All items having a mass of 3 tonnes or more were allocated to strips as a distributed weight. This accounted for roughly 15% of the deep displacement. The remainder was distributed assuming a constant density throughout the ship. Bending moment and shear force were estimated using the same method as was used for the NFR-90.

The following ship characteristics were taken forward to drive the structural models:

Table 5.5.1 - Principal characteristics of the corvette model taken forward to drive the structural designs

Bending Moment (Hogging)	68.5 MNm
Bending Moment (Sagging)	-98.4 MNm
Shear Force	2.7 MN
Rule Length (a term used in NSR2 calculations)	72m
Top speed	30 knots
Amidships draught	2.9m
Block Coefficient	0.495

It was noted that the bending moment and shear force loads for the corvette were much lower - an order of magnitude lower - than for the frigate, indicating that the structure was unlikely to be driven by longitudinal bending. The corvette's midship cross section geometry was discretized into the same eight panels used for the NFR-90 Frigate model. The resulting panel geometry is shown in Figure 5.5.2, and can be compared with the NFR Frigate model at Figure 5.1.4.

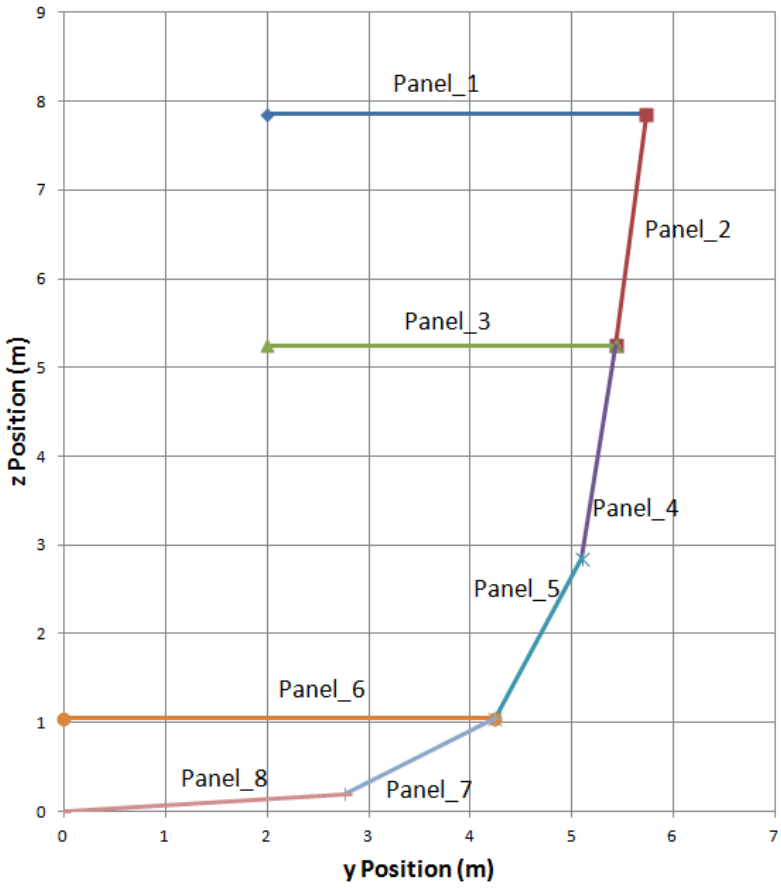

Figure 5.5.2 – Discretized form of corvette model midship section shape

5.6 Experiment Series 3 – Longitudinal / Transverse Structure

A number of different options for stiffener geometry were explored for the corvette, five of which are shown in Figure 5.6.1, which compares the ship structural weight per unit length with the estimated weld length for the stiffening style selected.

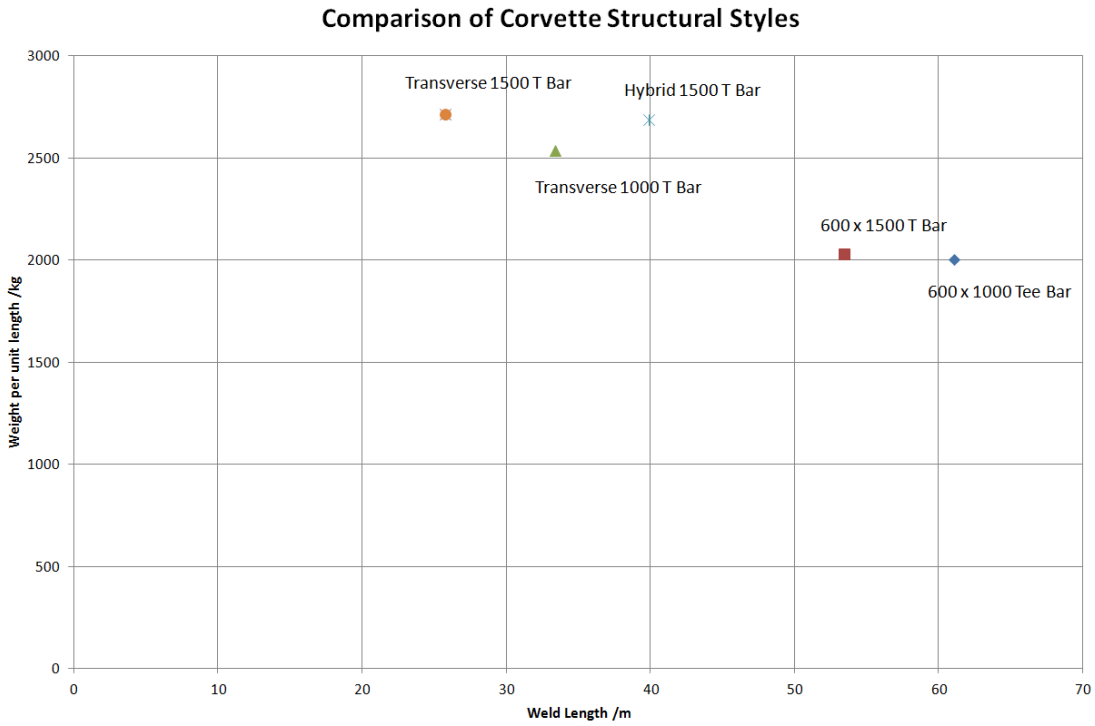

Figure 5.6.1 - Weight and weld length for a variety of corvette structural style options for the corvette model

Longitudinally stiffened options were examined with nominal longitudinal stiffener spacing of 600mm and frame spacings of 1000mm and 1500mm. It can be seen from Figure 5.6.1 that the 1500mm frame spacing option offered a structure requiring significantly less welding than the 1000mm option, for a minimal increase in structural weight.

Purely transversely stiffened structures were considered with the same frame spacing (and no longitudinals at all aside from the deep girders required for deck and superstructure integration, as previously discussed in Section 3.6 b. As can be seen in Figure 5.6.1, the structural weight penalty for adopting a 1500mm frame spacing was more noticeable for the transversely stiffened structures than it was for the longitudinally stiffened ones, but the saving in welding was comparable. It was therefore decided to model the longitudinally stiffened structure with 600 x 1500mm frame spacing and the transversely stiffened structure with 1500mm frame spacing, as these were considered the most likely practical choices.

A hybrid structural style has been adopted in some ships, where the main deck and keel are longitudinally stiffened while the side shell is transversely stiffened. This allows the design to realise some of the simplification (seen in reduced welding requirement) of a transverse structure, while retaining the structural efficiency (and hence low weight) of a longitudinally stiffened structure in the regions which see the greatest compressive loading. A hybrid structure was examined for the corvette, with 1500mm frame spacing, and longitudinals

spaced at 600mm in the Top Deck and Outer Bottom only. However, the benefits were marginal, as can be seen in Figure 5.6.1; the hybrid structure was no lighter than a transverse structure, and somewhat more complex. Since the corvette is a short ship, whose loading is dominated by normal pressure loads rather than compression arising from hull bending this is understandable, but in any case it was not deemed worth simulating the shock response of the hybrid structure.

The two corvette models constructed were assigned the numbers 1851 (for the longitudinally-stiffened) and 1852 (for the transversely-stiffened). In both models, all stiffeners were long stalk tee bars of the standard proportions previously defined. The same material assumptions were used as in the NFR-90 models; B-Quality crack arrest steel, assumed to behave similarly to mild steel at high strain rates.

Table 5.6.1 - Structural parameters of Model 1851 – Corvette baseline (longitudinal stiffening)

Design Rules	Lloyds Register NSR2
Stiffener material fraction As/A	Calculated optimum for each panel
Nominal longitudinal stiffener spacing	600mm
Frame spacing	1500mm
Transverse bulkhead spacing	9m
Material tensile yield stress	350 MPa
Material ultimate tensile stress	590 MPa
Material Young's modulus	200 GPa
Material Poisson's ratio	0.3

Table 5.6.2 - Scantlings selected for the two models in the third experimental series (longitudinally vs. transversely stiffened structure

	Model 1851		Model 1852	
	Longitudinal		Transverse	
Panel	**Plate thickness**	**Stiffener depth**	**Plate thickness**	**Stiffener depth**
1 - Top Deck	10.9mm	105mm	16.9mm	-
2 - Upper Sideshell	10.8mm	104mm	16.9mm	-
3 - Passing Deck	5.2mm	52mm	6.3mm	-
4 - Sideshell	8.1mm	62mm	7.1mm	-
5 - Turn of bilge	9.8mm	73mm	12.1mm	-
6 - Inner Bottom	7.5mm	63mm	12.0mm	-
7 - Outer Bottom	11.4mm	79mm	14.4mm	-
8 - Keel	12.0mm	87mm	14.4mm	-
Transverse bulkhead	10.7mm	181mm	10.7m	261mm

Table 5.6.3 - Comparison of weights and weld lengths for the two models in the third experimental series (longitudinally vs transversely stiffened structure)

Model	**Model 1851 (Longitudinal)**	**Model 1852 (Transverse)**
Weight per metre of length	2.030te	2.719te
Weld length per metre of length	53.46m	25.74m

The midship structural sections for Models 1851 and 1852 are shown at Figure 5.6.2 and Figure 5.6.3:

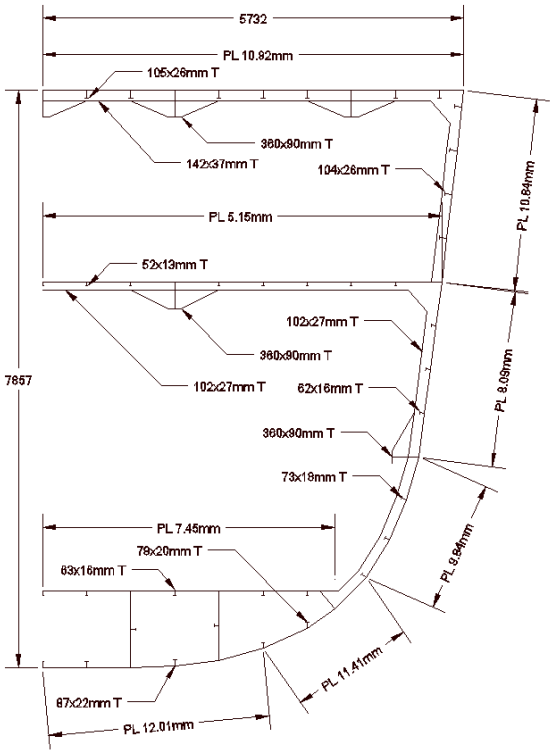

Figure 5.6.2 - Structural cross-section of Model 1851 – corvette model with longitudinal stiffening

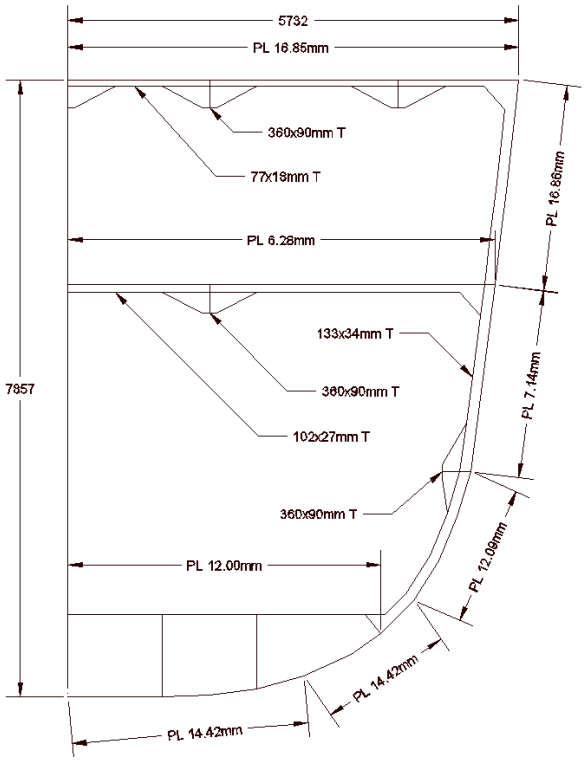

Figure 5.6.3 - Structural cross-section of Model 1852 – corvette model with transverse stiffening

5.7 The UNDEX Pressure Field and FSI Simulation

A common UNDEX scenario was used for all model runs. A spherical TNT charge of fixed size was located 47.42m below the surface of the water (that is, 42.42m below the keel of the NFR-90 frigate model) and 42.42m from the ship's centreline, giving a standoff slant distance of 60m at 45 degrees from the vertical. The charge was aligned in the X direction with the midpoint of the central main transverse compartment (see Figure 5.7.2.)

A geometrically simpler case would have placed the charge directly below the ship's keel. This was precluded by a limitation of the FUSE2D program (Weidlinger Associates, Inc., 2009). Because the code assumes constant speed of sound in water, it does not correctly model the period immediately following detonation, where the extremely high pressure across the shockwave results in a significant increase in wavefront celerity. To avoid this leading to errors in the output, the FUSE2D program does not permit any output recording points to be located either within 15 charge radii of the charge centre or anywhere directly above that region. The chosen geometry remains simple, places the ship well clear of the 15 charge-radii region and generates both vertical and athwartship response motions. Due to security requirements imposed by the Ministry of Defence, the charge size and resulting shock factor cannot be discussed here. These values and the resulting calculations were presented in the Confidential report submitted to MoD (see page 94) and referred to in the MoD letter at Appendix C.

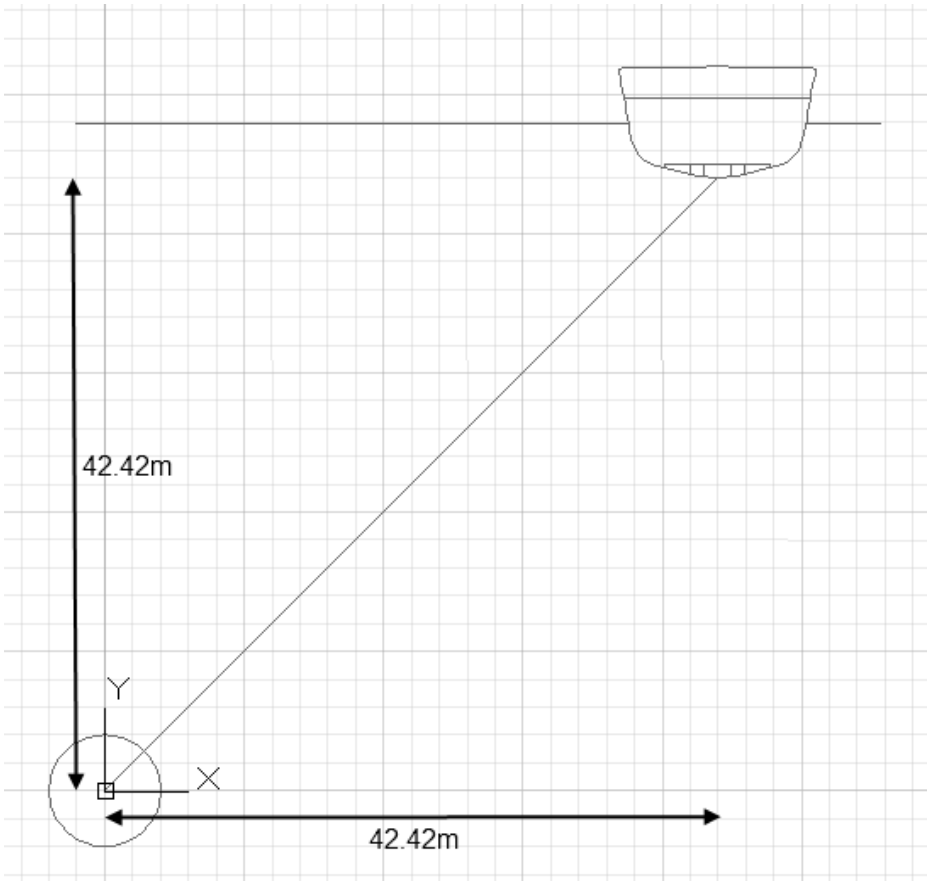

Figure 5.7.1 - Shot geometry used for all simulations, viewed from astern

The input file for FUSE2D was created using the PreFUSE package (Weidlinger Associates, Inc., 2005). FUSE best practice, based on accumulated experience at Weidlinger (Weidlinger Associates, Inc., 2009) makes recommendations for mesh size; namely that mesh elements should be small enough that the arrival (rising pressure) portion of the shock wavefront should cover six FE elements in locations where modelling the wavefront arrival is important to the analysis. For this particular scenario, this resulted in a maximum mesh size of 34mm.

To minimise runtime, it was desirable to choose the largest timestep compatible with the Courant-Friedrichs-Lewy condition (Courant, Friedrichs and Lewy, 1967), which in this case was found to be 1.5×10^{-5} seconds. The simulation was set to run for 15,700 timesteps, which allowed approximately 35ms for the shockwave to cover the 60m standoff distance, and an additional 200ms for the initial hull response.

A single fluid type was defined, using the PreFUSE default values for seawater, namely density equal to 1025.18 kg/m3 and bulk modulus equal to 2247.69 MPa. The water depth was set to 71.5m; that is, just over 1.5 times the charge depth. While the fluid bottom was defined as

transmitting (i.e. representative of very deep water) even transmitting boundaries cause weak reflections due to numerical artefacts (Weidlinger Associates, Inc., 2009). By including a depth margin below the charge the effects of these reflections on the solution were limited. Best practice when using the FUSE2D program suggests setting that margin to 50% of charge depth (Weidlinger Associates, Inc., 2009). A single fluid layer was defined, 71.5m deep and divided into cells vertically by 2148 nodes to give a cell height of 33mm.

A grid of output recording locations was arranged such that the resultant volume when swept around the vertical axis through the charge would encompass the entire wetted region of the structural model, as shown in Figure 5.7.2. The maximum mesh radius was set to be 20% greater than the largest radius used for an output location, again in accordance with the best practice advised in (Weidlinger Associates, Inc., 2009).

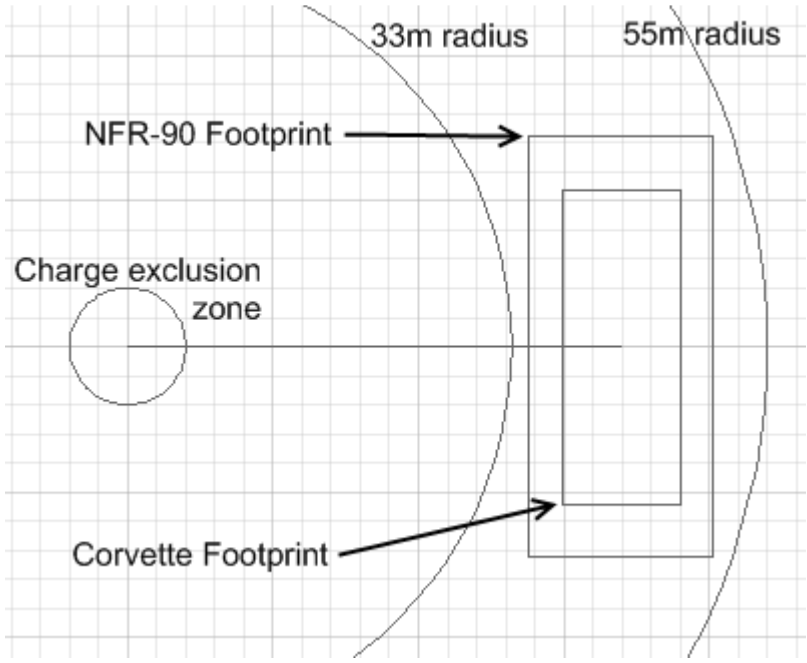

Figure 5.7.2 - FUSE2D data collection regions

PreFUSE created a FUSE input file, which was then processed by FUSE2D. The FUSE2D run took approximately three days on a computer with a 2.4GHz processor. Outputs were delivered in the form of four input files, of approximately 24Gb total size, for the EPSA solver program.

With input files created defining the structural mesh and the fluid pressure field, all the data required to perform an EPSA fluid-structure interaction simulation was in place. For the simulations conducted in this research, EPSA runtime was typically 28 hours on a computer with a 2.4GHz processor. While EPSA was not able to use more than a single processor core in

any given run, the use of a quad-cored processor allowed three EPSA runs to execute simultaneously with no loss of computation speed.

Fluid-structure-interaction was computed using the Plane Wave Approximation (PWA – see Section 2.6 d. The short timescale of the simulation (an order of magnitude shorter than the bubble pulse frequency) meant that there was little advantage to using the Added Mass Approximation or the Doubly-Asymptotic Approximation. Using the PWA also removed the need to pre-calculate a fluid mass matrix, reducing computation time. EPSA provided outputs in the form of a file containing summary and diagnostic data for the run, and a file containing the velocity/time data for the requested output nodes. The large number of nodes and timesteps meant that the latter was a large file; typically in the region of 200Mb.

The process used for reading results from the EPSA output files and processing them into a useable form is described in Chapter 6.

Chapter 6 Methods for Processing and Presentation of Shock Response Motions

This Chapter describes the typical motions of the modelled ship structures following the design shock event, as well as summarising the process by which data was read from the EPSA output files and processed into a useful form for presentation.

6.1 Overall hull response to shock

A broad overview of the response of a ship structure to an UNDEX shock is presented in Figure 6.1.1 through Figure 6.1.3. The figures are taken from 3D visualisations of Model 1801 subjected to the test shock, and coloured according to the Cauchy J2 stress which, according to von Mises' yield criterion, can reach the square of the pure shear yield stress of the material before the material will yield (Ragab, 1999).

Figure 6.1.1 shows the ship very shortly after the arrival of the shock wavefront, which occurred roughly 5ms after the start of the simulation. It can be seen that the charge was located below and abeam of the hull. A roughly elliptical region of shell plating was stressed, but the stress travelled more quickly through the steel than the water. Initially, the plating in the centre of the ship section began to bow inward under the pressure of the shock wavefront, but the shape of the envelope of stressed plating was influenced by the pattern of stiffening under the plate.

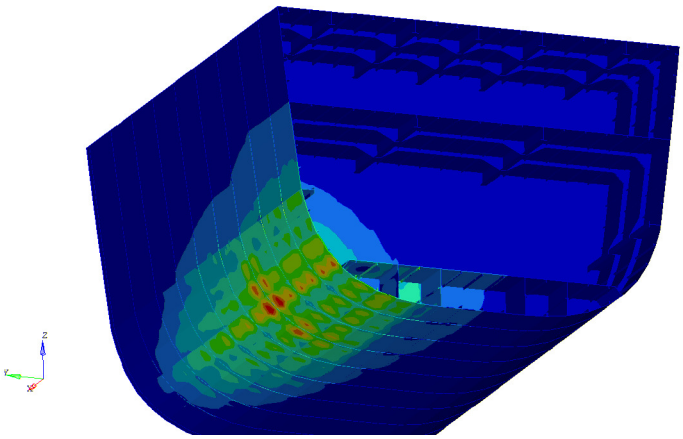

Figure 6.1.1 - Cauchy J2 stress from EPSA finite element analysis of midsection of corvette Model 1851, 7ms after simulation start

As time passed, the stress continued to travel outward through the structure, loading the upper side shell and the higher decks. Figure 6.1.2 demonstrates this, with the displacements magnified by a factor of 100. It can be seen how the side shell slid upwards and transferred load to the upper decks. Since the load path from the centre of the wavefront's impingement on the shell to the Top Deck edge was a different distance for the two sides, a phase lag was introduced into the excitation of the two edges of the Top Deck.

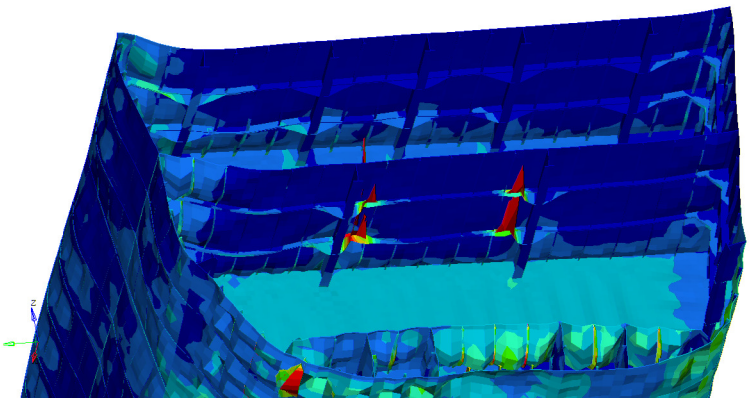

Figure 6.1.2 - Cauchy J2 stress from EPSA finite element analysis of midsection of corvette Model 1851, 10ms after simulation start (displacements magnified by x100)

Once more time passed, the upward velocities of the bottom and lower side shell reduced, following heavy damping due to fluid contact. The two upper decks remained in motion, exhibiting vibration in several modes with low damping. In Figure 6.1.3 the Passing Deck clearly exhibited a strong component of vibration in Mode 3[5], while the Top Deck appeared to be experiencing superimposed Mode 2 and Mode 3 vibration. These vibratory motions were complex, due to the multiple load paths exciting the upper decks, the lack of fluid damping and the low stiffness of the deck structures between the gunwales and transverse bulkheads relative to the more closely-supported transverse bulkheads and bottom structure.

[5] Where normal modes of vibration are described by referring to the number of half sine waves exhibited over the length of the vibrating body.

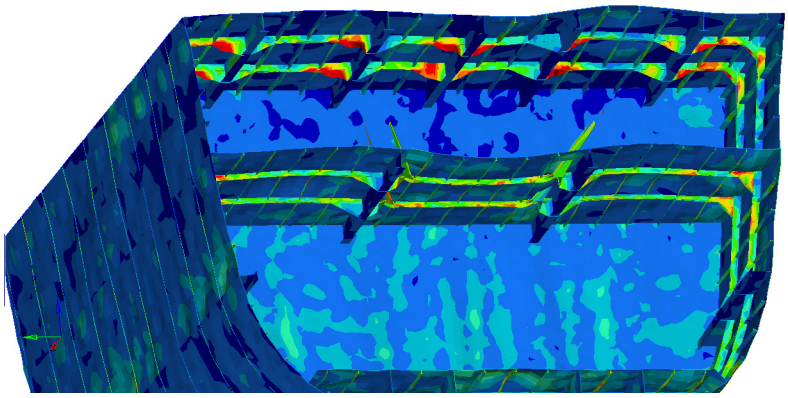

Figure 6.1.3 - Cauchy J2 stress from EPSA finite element analysis of midsection of corvette Model 1851, 28ms after simulation start (displacements magnified by x20)

6.2 Choice of Metrics and Shock Regions

Since designing shock protection into a warship is usually a matter of strengthening equipment against acceleration or designing resilient flexible mountings, the ship designer responsible for shock protection features usually needs to understand the shock environment in terms of acceleration and displacement. Acceleration, since the resulting inertial forces may load equipment components or fastenings beyond breaking point, and displacement since mounting arrangements must include sufficient travel, as well as sufficient clear space around equipment to allow free movement. EPSA provided output data in the form of vertical velocity-time histories, from which acceleration and displacement histories were able to be obtained by differentiation and integration respectively. The output files created by EPSA recorded the data in a proprietary format, so it was necessary for the candidate to pre-process these files to extract the data and convert it into a more format more useful for analysis. This was achieved using MATLAB scripts as described in Appendix F.

Figure 6.2.1 shows acceleration-time, velocity-time and displacement-time histories for two nodes; one typical of the outer bottom and one typical of the Top Deck in the baseline frigate structural Model 1801, following the design case shock loading. That there were significant differences between the shock response environments in those two locations was apparent. These differences underscored the need to account for the location of a node of interest within the ship. The typical method of accounting for this is to divide the ship into a number of regions of similar response. Ideally the number of regions would be small enough to allow the method to be applied without precise knowledge of an equipment item's location, yet include

enough regions so that the response environment within each could be considered reasonably homogeneous.

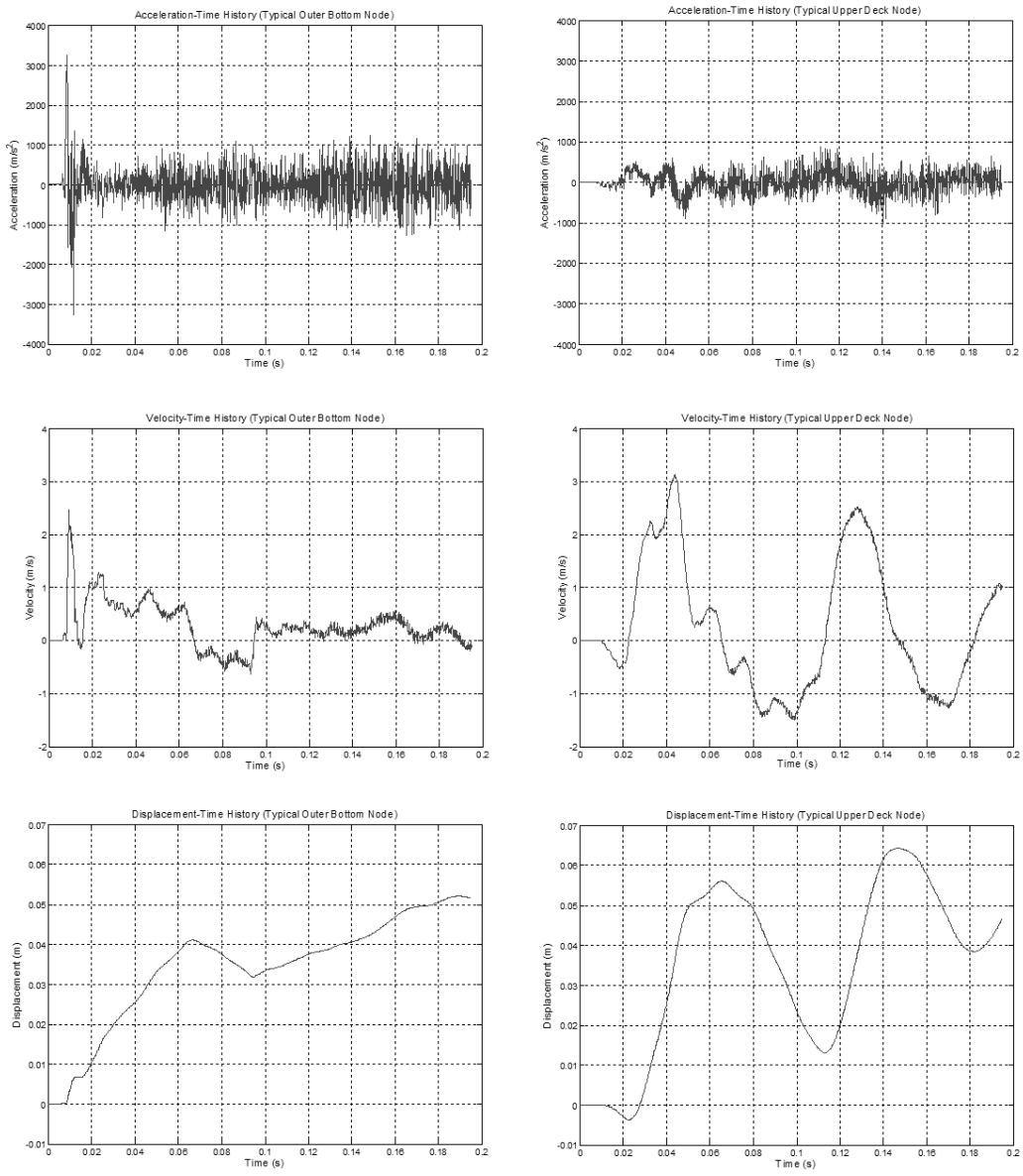

Figure 6.2.1 – Plots of acceleration, velocity and displacement with time for two typical nodes in the Outer Bottom and Top Deck of the baseline NFR-90 frigate Model 1801

Nodes around the transverse cross-section of Model 1801's structure were examined, and the structure divided into six regions, as shown in Figure 6.2.2; namely, Outer Bottom, Inner Bottom, Side Shell below the waterline, Side Shell above the waterline, Passing Deck and Top Deck.

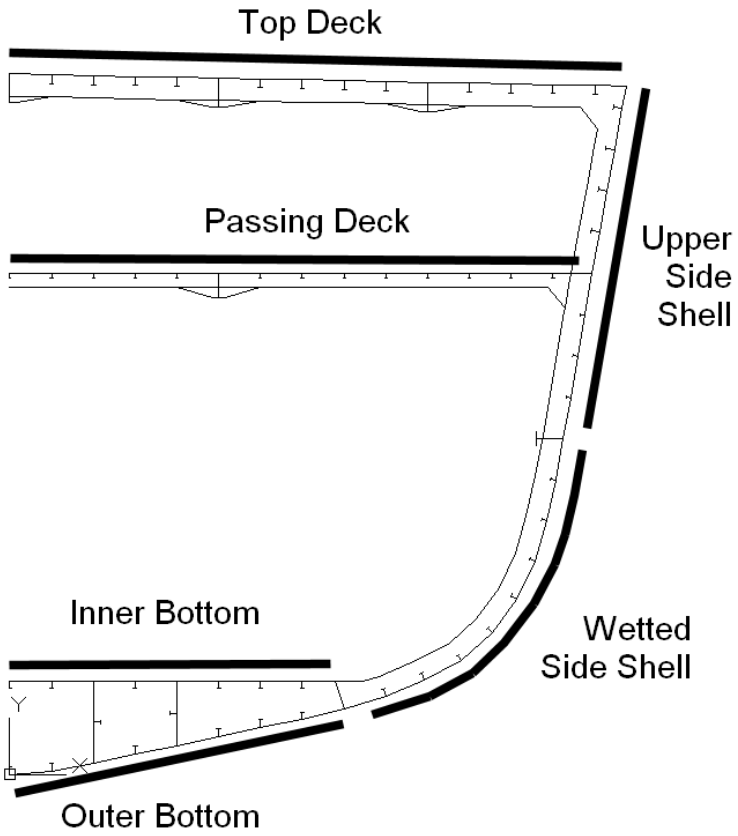

Figure 6.2.2 - Regions of the hull used for division of all subsequently examined outputs from EPSA simulation of ship structures under design shock load

Velocity-time histories for representative nodes within four of the regions in the frigate baseline Model 1801 are presented in Figure 6.2.3 to Figure 6.2.6. While some variation clearly remained within each region, particularly among those higher in the ship's hull where multiple modes of vibration developed, the candidate judged this selection of regions to represent those distinct areas with fundamentally different response behaviours.

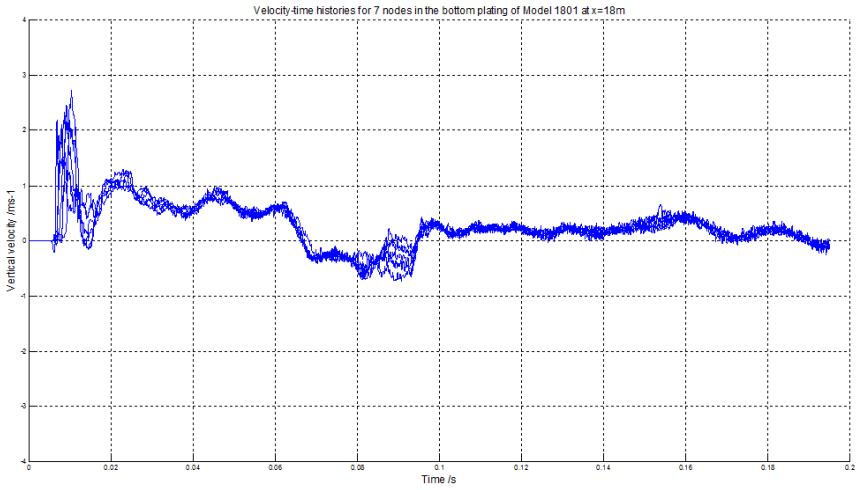

Figure 6.2.3 - Velocity/time histories for typical nodes in the outer bottom of Model 1801 at x=18m

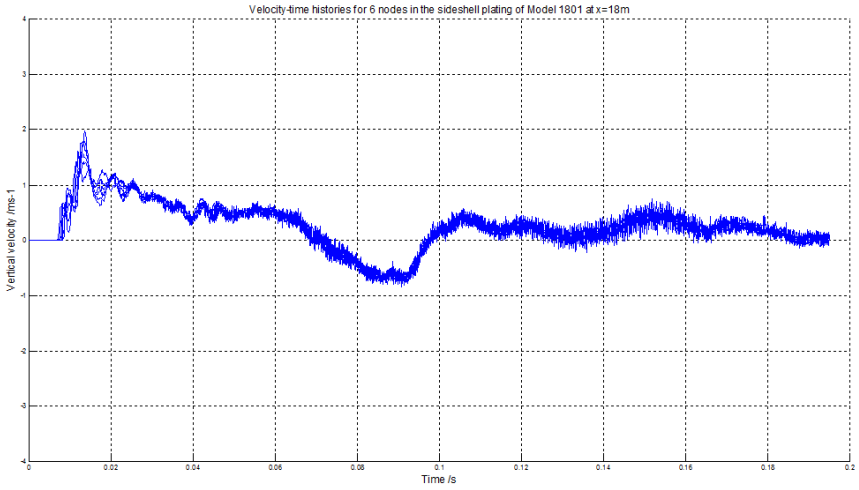

Figure 6.2.4 - Velocity/time histories for typical nodes in the sideshell of Model 1801 at x=18m

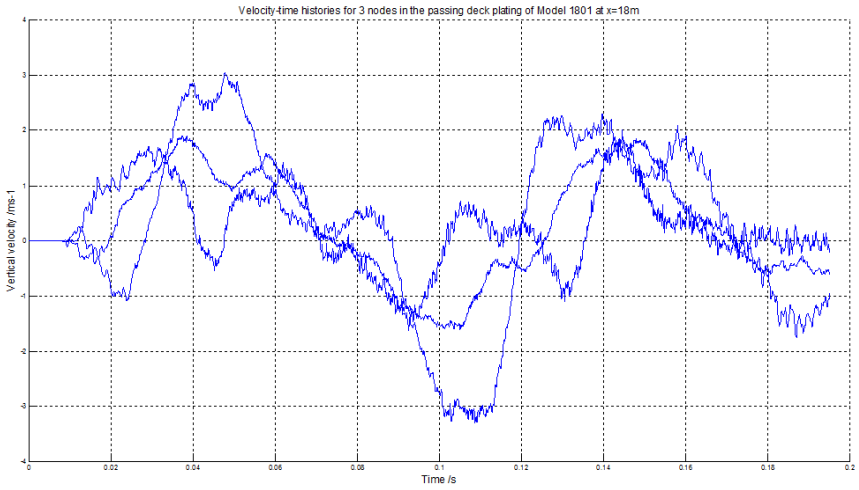

Figure 6.2.5 - Velocity/time histories for typical nodes in the passing deck of Model 1801 at x=18m

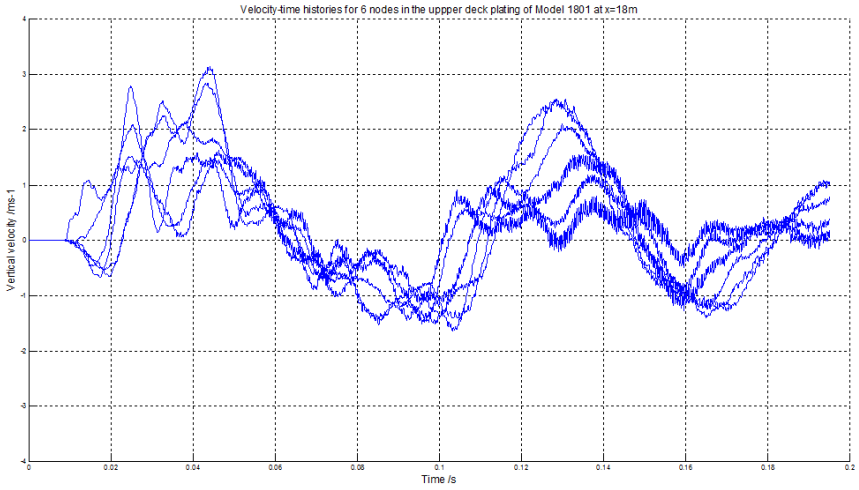

Figure 6.2.6 - Velocity/time histories for typical nodes in the Top Deck of Model 1801 at x=18m

The process of selecting the region boundaries was assisted by the use of several other graphical forms of presenting the data. Overlaid time histories present too much data to be easily readable once more than a dozen or so nodes are presented at once, so methods of data reduction were sought.

Figure 6.2.7 shows a “beard plot”, one such data reduction tool for a transverse cross section. Since the equipment designer is most interested in peak values of acceleration, velocity and displacement, this plot displays only the peak value for each FEA node in a transverse cross-section, plotted against the node’s Y and Z co-ordinates (athwartship and vertical in the body reference co-ordinate system.) While this could be seen as a crude measure of response, the

plot does usefully show the sharp change in peak response between the upper sideshell and the decks.

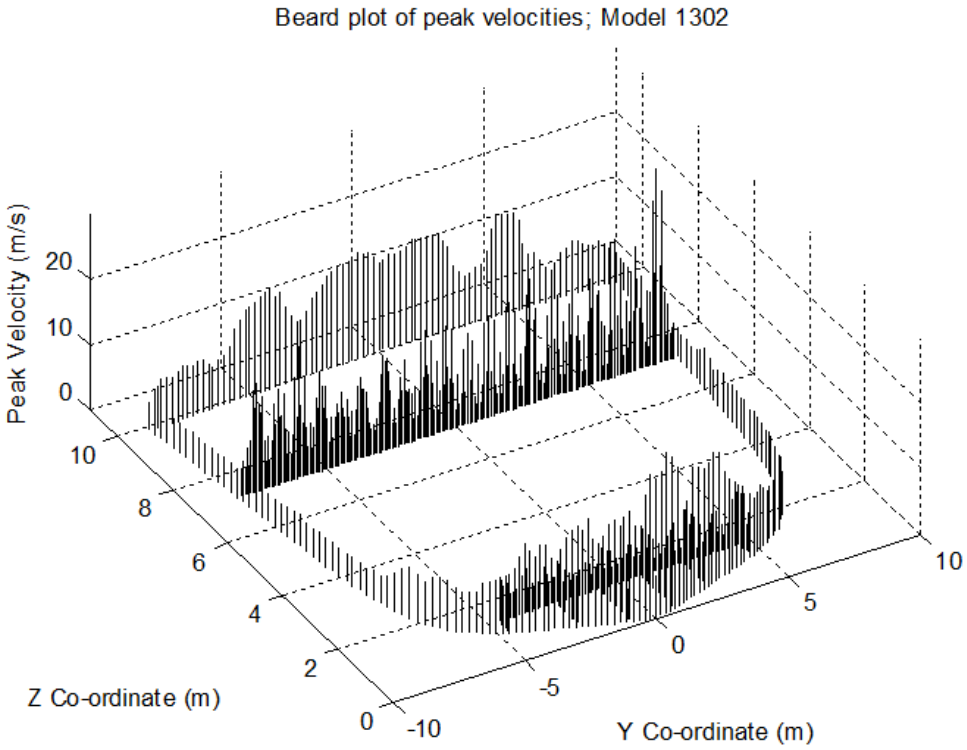

Figure 6.2.7 - Beard plot of peak velocities in a transverse cross section (at x=18m) of a NFR-90 Frigate model (from Series 13, a preliminary series modelled during early exploratory work.)

6.3 Variation in response with longitudinal position

While it was not taken into account in the choice of shock regions, it is worth noting that some regions, particularly those higher in the ship, showed significant variations in response with their location along the (12m) length of the central compartment from which measurements were taken. This is illustrated in Figure 6.3.1 which shows velocity-time histories for 17 nodes in Model 1801. The nodes were spaced evenly along the longitudinal centreline of the Top Deck, between the two boundary transverse bulkheads. The response of the seventeen nodes varies considerably, in peak amplitude, phase and general shape.

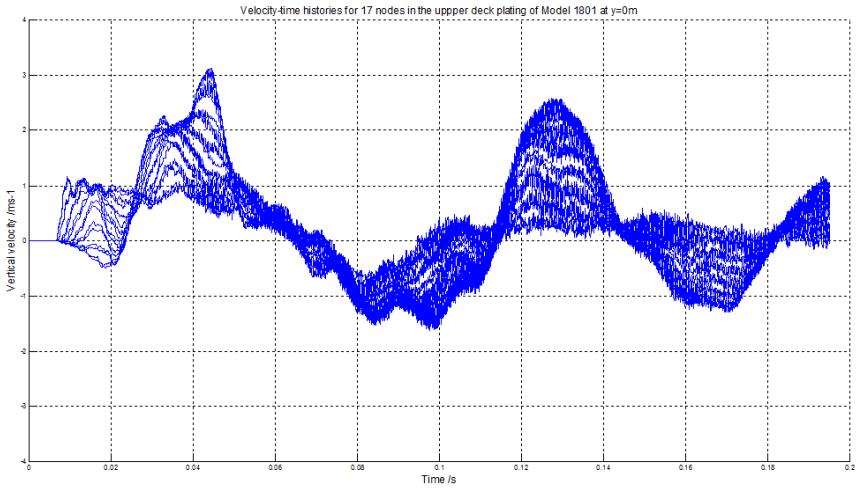

Figure 6.3.1 - Velocity-time histories for 17 nodes in the Top Deck plating of Model 1801 at y=0m, evenly distributed between the model's central two transverse bulkheads

The reason for this variation becomes clear when the mode shapes of the Top Deck vibration are examined, as shown in Figure 6.3.2. The nodes near the bulkheads are more constrained than those in the centre, which are subject to motions of greater displacement.

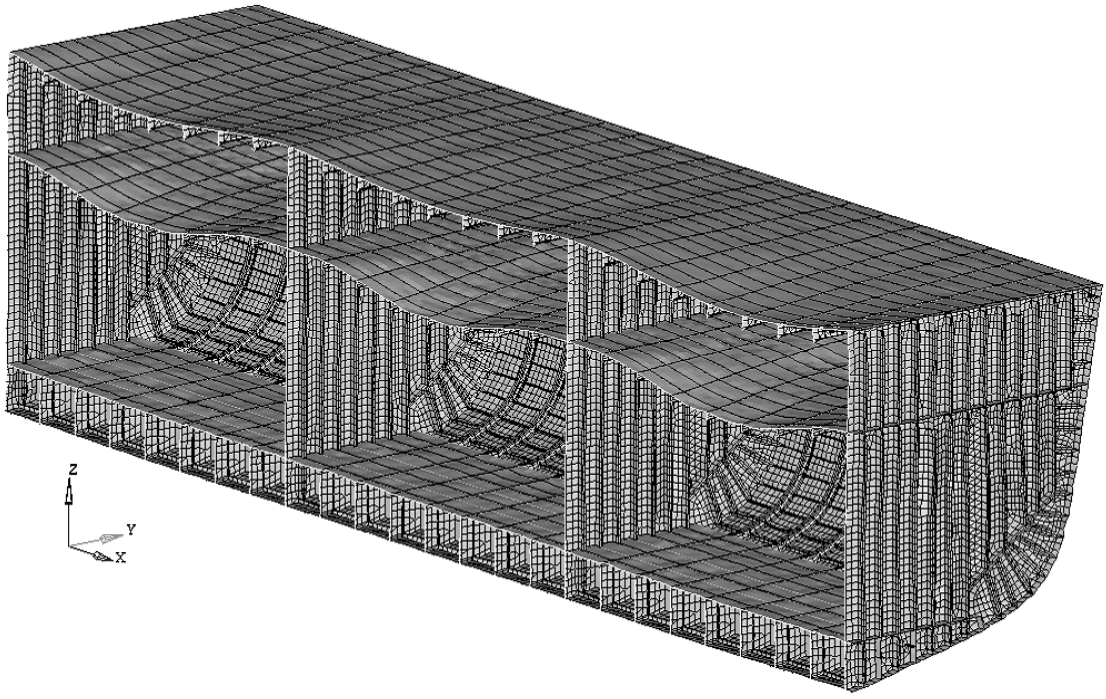

Figure 6.3.2 - Mode shapes in the Top and Passing Decks of Model 1801 following a shock event (Displacements magnified x20)

6.4 Statistical presentation of results

The designer of a piece of equipment to be mounted in a new ship is unlikely to know where exactly within a given shock region the equipment is to be located, so it would be very helpful to treat the entire region as one and provide peak design criteria which apply over the whole region. A simple way to do this would be to provide the acceleration-time histories of every node within the region, calculate the peak acceleration of each and then specify the design criterion as resisting the largest peak acceleration to occur within the region. This approach would have a downside; from inspection of the results in the current research the candidate observed that in many cases a few outliers exhibited a response significantly higher than the rest of the region – often several times higher. Designing for those outlier nodes will result in overdesign in the equipment in all other locations, which are likely to be a significant majority. It is therefore common naval ship design practice (Ministry of Defence, 1974) to treat the peak response values within a shock region (such as those defined in Figure 6.2.2) as a statistical population, and define the shock design criterion such that in a predefined majority of cases, that criterion would not be exceeded.

For the purposes of the current research, the candidate decided to choose the 80th percentile value as the cut-off threshold; that is, the highest 20% peak responses within each region were ignored, and the highest of the remainder was given as the "design level" for the region. Assuming that equipment designed to this level was placed on an arbitrarily chosen node within the region, there was an 80% chance of it surviving the simulated shock event.

Figure 6.4.1 is a histogram of the peak accelerations in the Top Deck region of a typical frigate model, grouping the peak accelerations at the regions nodes into buckets, sized by frequency of occurrence. The 80th percentile peak acceleration is highlighted, illustrating that designing to cope with the top 20% peak values would increase the design criterion from 1,660ms^{-2} to over 6,500ms^{-2} – a more than fourfold increase.

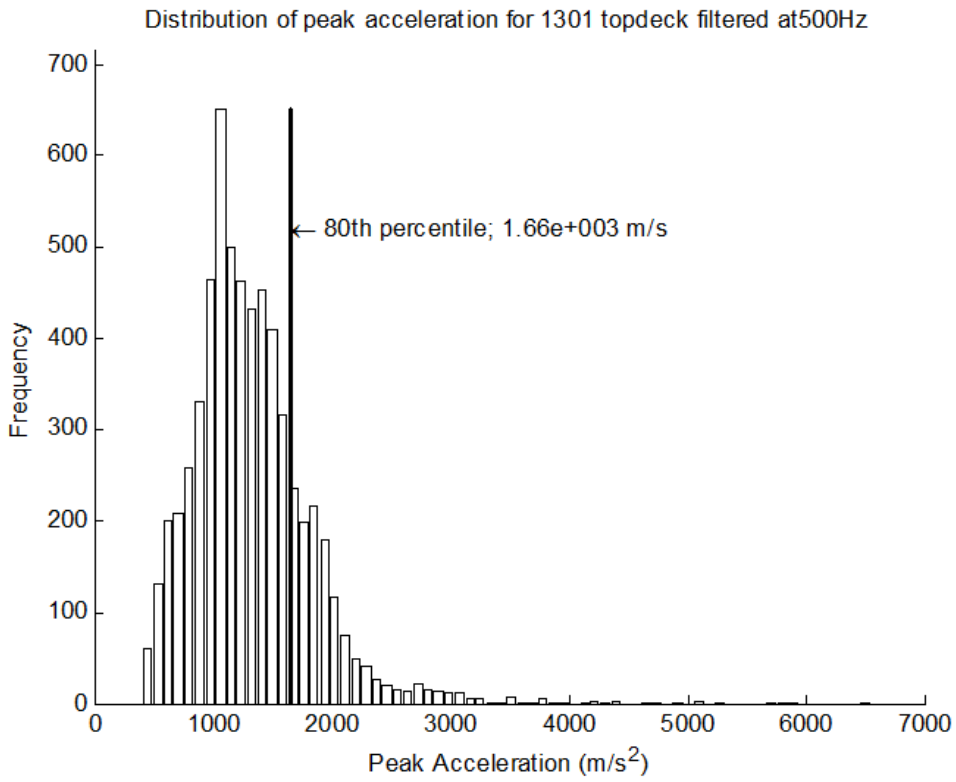

Figure 6.4.1 - Histogram of nodal peak acceleration distribution through the Top Deck of a model following the design shock load

The 80th percentile peak accelerations were calculated for each region of each model and presented as a measure of shock severity in that region. However, while initial conclusions were drawn and presented (Bradbeer and Andrews, 2012b; a), it was discovered that these values were highly sensitive to the method of filtering applied to the raw data. The acceleration-time history of most nodes in the FEA models analysed included very high frequency transient components, which were high in amplitude but of very short period. Since work done on a mass under acceleration varies with the second power of the time under acceleration, these very high frequency components would have been delivering negligible energy into mounted equipment, yet showed as very high peak accelerations. It was considered desirable to remove these high frequency components by applying a low-pass filter to the acceleration-time history. A tenth-order Butterworth filter (The Mathworks, Inc, 2013a) was used, which was selected for its rapid cutoff and low attenuation of the passed signal. It was not clear what the threshold frequency of the filter should be, so a sensitivity study was conducted, applying threshold frequencies between 200Hz and 2kHz to nodal time history data, the results of which are illustrated in Figure 6.4.2 through Figure 6.4.6.

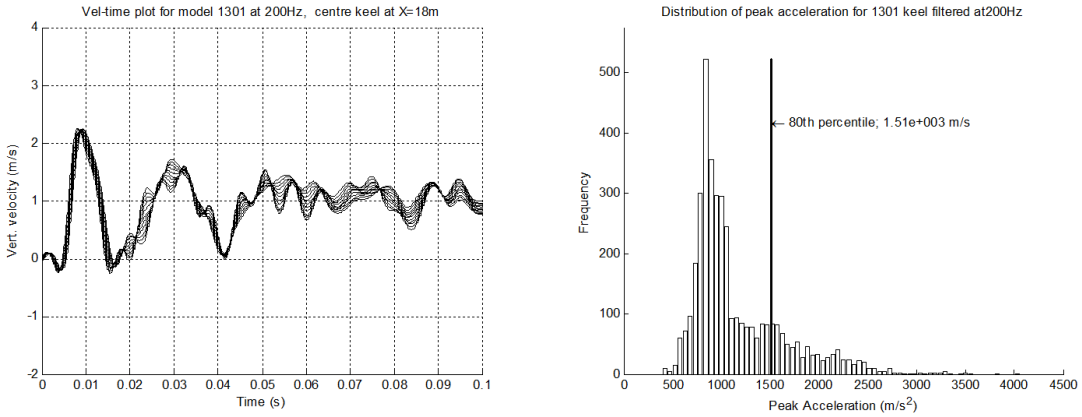

Figure 6.4.2 - Velocity/time history and peak acceleration histogram for nodes in the keel region of the baseline NFR-90 frigate Model 1801, following a 10-pole Butterworth low-pass filter with a threshold frequency of 200Hz

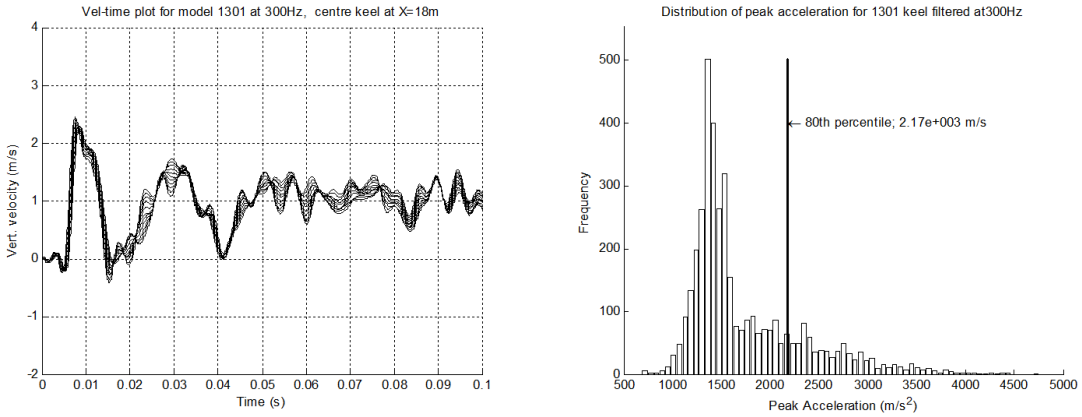

Figure 6.4.3 - Velocity/time history and peak acceleration histogram for nodes in the keel region of the baseline NFR-90 frigate Model 1801, following a 10-pole Butterworth low-pass filter with a threshold frequency of 300Hz

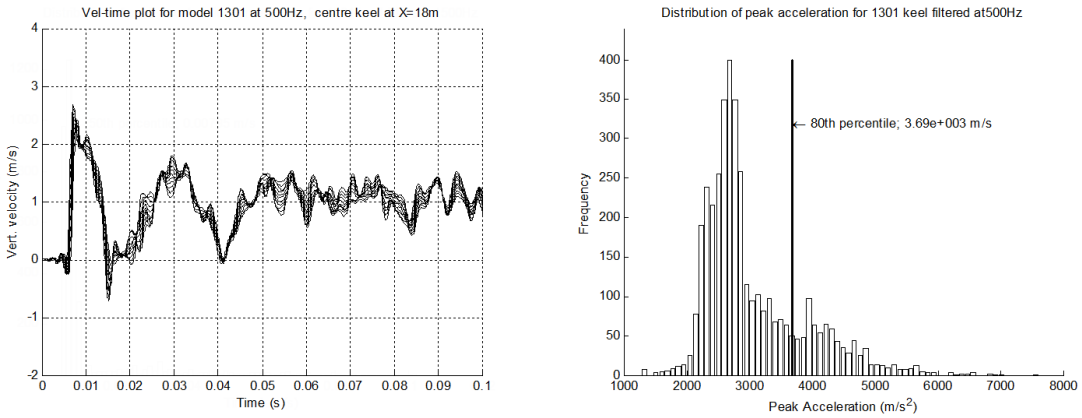

Figure 6.4.4 - Velocity/time history and peak acceleration histogram for nodes in the keel region of the baseline NFR-90 frigate Model 1801, following a 10-pole Butterworth low-pass filter with a threshold frequency of 500Hz

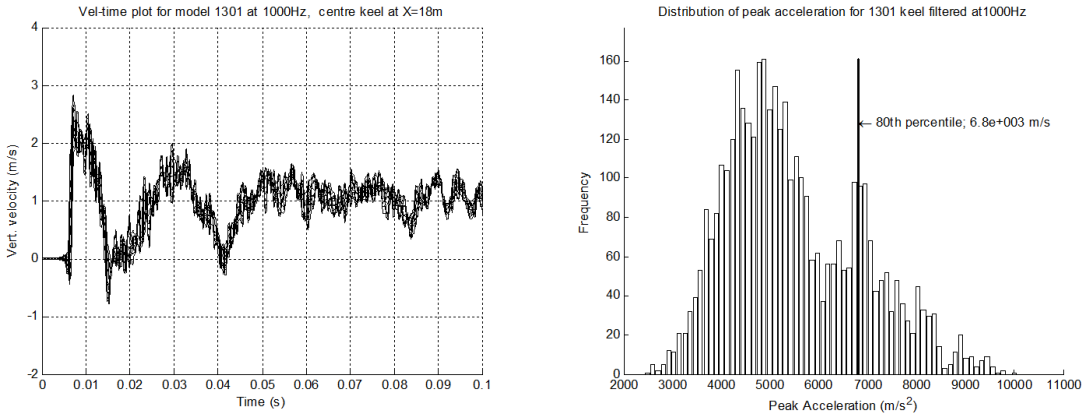

Figure 6.4.5 - Velocity/time history and peak acceleration histogram for nodes in the keel region of the baseline NFR-90 frigate Model 1801, following a 10-pole Butterworth low-pass filter with a threshold frequency of 1kHz

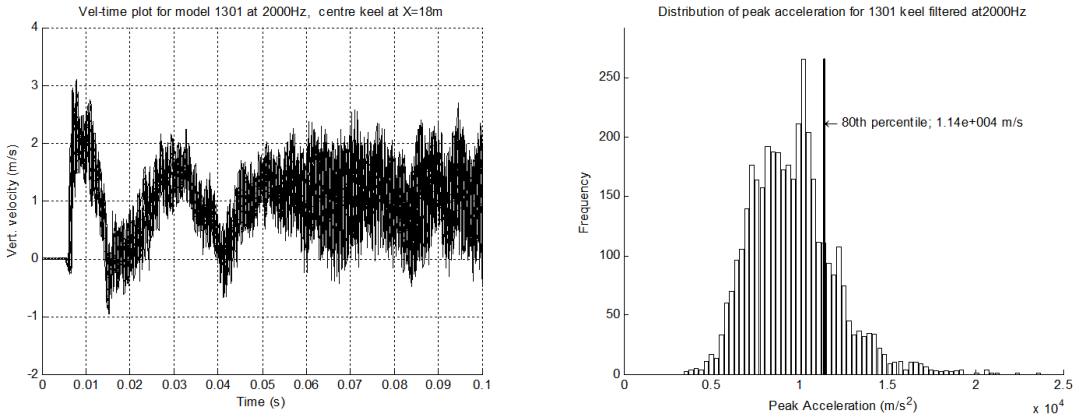

Figure 6.4.6 - Velocity/time history and peak acceleration histogram for nodes in the keel region of the baseline NFR-90 frigate Model 1801, following a 10-pole Butterworth low-pass filter with a threshold frequency of 2kHz

As Figure 6.4.2 through Figure 6.4.6 show, varying the threshold frequency from 200Hz to 2kHz results in an increase in the 80th percentile peak acceleration from 1,510 ms^{-2} to 11,400 ms^{-2}, an increase by a factor of 7. Determination of an appropriate filter threshold frequency is problematic, yet it is clearly crucial if this method of data presentation is to be used.

An alternative method was required to avoid this difficulty, namely the presentation of the results in the frequency domain, using shock response spectra, as outlined in Section 6.5.

6.5 Shock Response Spectra

The shock response spectrum (SRS) is a useful method of presenting shock response data since it takes response frequency into account. A helpful summary of the SRS is given by Alexander (2009) while more complete descriptions including the underlying mathematics are provided by Irvine (2012) and Rubin (2002). This section provides a brief summary of the principles underlying the SRS.

Most vital equipment on a naval ship will typically be protected from shock (up to the design shock level) by resilient mounts, which can generally be represented as a single-degree-of-freedom (SDOF) system with a mass, spring and damper attached to an excited base. Such a system is shown in Figure 6.5.1, with a mass M mounted via a spring of stiffness K and a dashpot of damping coefficient C to a base. The absolute vertical displacement of the base is u(t), the absolute vertical displacement of the mass is x(t) and the relative displacement of the mass from the base is z(t).

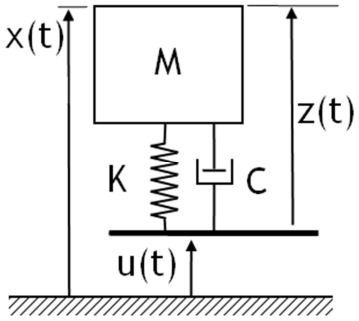

Figure 6.5.1 - A single degree of freedom mass-spring-damper system to represent the motions of a shock-mounted item of naval equipment

The system can be categorised in terms of natural frequency and some measure of damping. Natural frequency is expressed either as *f* (in Hertz) or ω (in radians per second.) Damping is often expressed as the damping ratio *c*, although it is conventionally represented on a shock response spectrum as a "quality factor" *Q*, where the relationships in (Eq 6.1) to (Eq 6.4) apply:

$$\omega = \sqrt{\frac{K}{M}} \qquad \text{(Eq 6.1)}$$

$$f = \frac{\omega}{2\pi} \qquad \text{(Eq 6.2)}$$

$$\zeta = \frac{C}{2 M \omega} \qquad \text{(Eq 6.3)}$$

$$Q = \frac{1}{2\zeta} \qquad \text{(Eq 6.4)}$$

The motions of the system can be described by the differential equation:

$$M\ddot{x}(t) + C\big(\dot{x}(t) - \dot{u}(t)\big) + K\big(x(t) - u(t)\big) = 0 \qquad \text{(Eq 6.5)}$$

Given known values for M, K and C and an arbitrary shock input time history u(t), (Eq 6.5) can readily be solved by numerical integration to give a time history for x(t) and z(t) as well as their derivatives.

It is presumed that the main intent of the designer of such mounts in a naval ship would be to limit the response (probably both the relative displacement and the acceleration) of the mounted equipment, and, while they cannot easily adjust the mass of the equipment, the stiffness, and hence the natural frequency of the mounting could be adjusted by changing the type or number of mounts. It would therefore be useful to present peak response acceleration and displacement in terms of natural frequency, to allow the shock mount designer to tune the natural frequency of the system to a point with peak response levels that would be deemed to be acceptable.

A shock response spectrum may be constructed for any location for which the base acceleration time history $\ddot{u}(t)$ is known. A constant damping quality value *Q* is assumed, and the velocity time history $\dot{z}(t)$response of a large number of SDOF systems is calculated. The peak velocity response from each of these histories can then be plotted against the SDOF system's natural frequency *f* as shown in Figure 6.5.2 .

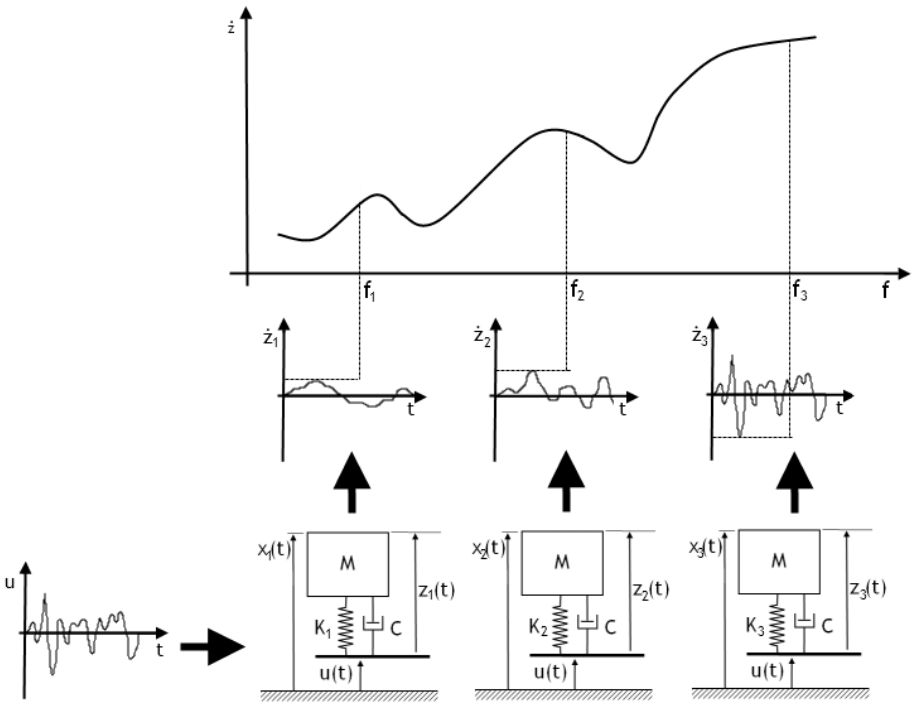

Figure 6.5.2 - Method for constructing a Shock Response Spectrum which was employed in the current research

There are several options when selecting the 'peak value' to record, as Alexander (2009) explains:

i. Maximax spectrum, defined as the maximum absolute value from each response history;
ii. Maximum positive spectrum, defined as the maximum positive value from each response history;
iii. Maximum negative spectrum, defined as the maximum negative value from each response history.

Rather than plotting peak velocity $\dot{z}_{max}$, it is common to plot pseudo-velocity (Hall, 2002), defined in terms of the energy absorption in the system's spring, such that:

$$E_{spring} = \frac{1}{2} M V^2 \qquad \text{(Eq 6.6)}$$

Where E_{spring} is energy absorption in the spring, and V is the pseudo-velocity. The pseudo-velocity is almost identical to the relative velocity $\dot{z}(t)$over high frequencies, although it may deviate significantly at very low frequencies (Hall, 2002). Similarly, the pseudo-acceleration (first derivative of pseudo-velocity) is exactly the same as the acceleration in undamped systems, and is acceptably close in moderately damped systems (Hall, 2002). Pseudo-velocity is useful because of the relationships:

$$V = \omega\, z(t) \qquad \text{(Eq 6.7)}$$

$$A = \omega\, V = \omega^2 z(t) \qquad \text{(Eq 6.8)}$$

Where A is pseudo-acceleration, V is pseudo-velocity, z(t) is the displacement relative to the mount's base, and ω is the angular frequency of excitation. These relationships allow lines of constant relative displacement and constant pseudo-acceleration to be plotted on the SRS. If the SRS is plotted on log-log axes, these will be straight lines rotated at 45 degrees from lines of constant pseudo-velocity (which are parallel to the frequency axis.) This allows the construction of a triaxial plot, from which the (approximate) maximum relative displacement, velocity and acceleration could all be read off a single plot. While there may be a small error between the pseudo-velocity and the true velocity, it is considered that the designer is usually more concerned about the acceleration and displacement. A pseudo-velocity SRS displayed the displacement correctly in all cases, and displays the acceleration correctly in the undamped case. The choice of damping naturally affected the shape of the SRS. Increasing the damping generally reduced the peak responses, as shown in Figure 6.5.3 in which shock response

spectra for the same inputs are plotted with damping ratios from 0 to 0.25 (Q-factors from infinity to 2.0). Aside from the 1Hz-4Hz region where the more highly-damped response curves approached a constant velocity, the undamped response curve marked an outer envelope which included a number of steep peaks between 100Hz and 1.5kHz. The application of just 1% viscous damping removed most of those high-frequency peaks giving a smoother curve. According to manufacturer's data published by Socitec UK (Socitec UK, 2013), naval shock absorber mounts are typically designed for the range of 5Hz upwards with a damping ratio of between 0.08 and 0.25. Since for the range above 5Hz, the response curve with less damping would be more conservative (that is, it would not present unduly reduced peak velocities), a damping ratio of 0.05 (or Q=10) was selected as a compromise. This choice was considered low enough to be conservative for typical shock mounts, yet high enough to smooth the response spectrum in the region above 100Hz, which was considered important to facilitate generalised comparison between curves which might have had high frequency peaks at slightly different frequencies.

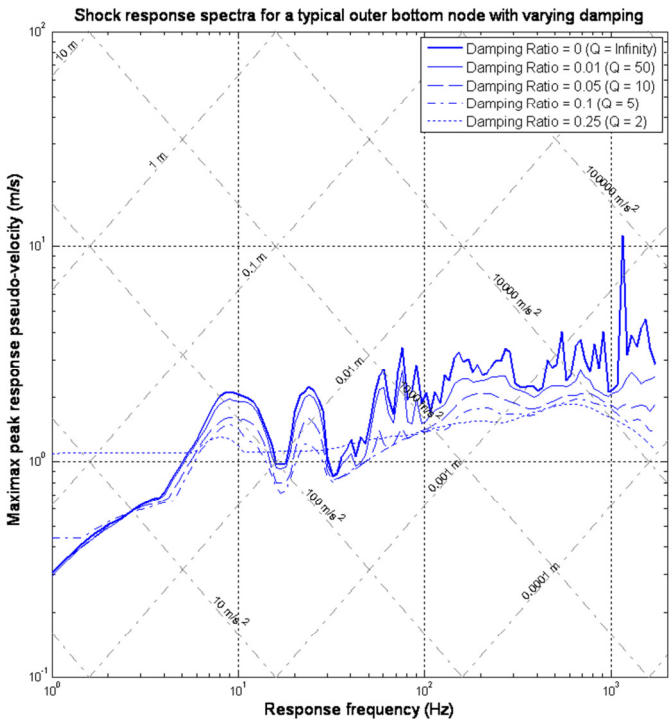

Figure 6.5.3 - Effect of varying the damping ratio on a sample Shock Response Spectrum for a node in the outer bottom of a ship's structure responding to a typical design shock load

A frequency range from 5Hz to 1.2 kHz was selected for the main output plots. The EPSA output data gave one point every 75 microseconds, for a sampling frequency of 13.3kHz. Irvine (2012) recommended using a sampling frequency at least ten times greater than the highest frequency for which a response is plotted in order to minimise errors. The lower bound of 5Hz was selected since the total simulation time of 200ms meant that frequencies below 5Hz would have had insufficient time to complete one complete oscillation cycle, and the confidence in such data would have been low.

The output files generated by EPSA contained base acceleration time histories for each deck/shell FEA node within the area of interest. For each node within a selected region, pseudo-velocity time histories were computed and shock response spectra constructed using MATLAB codes adapted from that produced by Irvine (Irvine, 2006); see Appendix G. Response frequencies were selected at a rate of twelve per octave, for a total of 130 frequencies covering the range from 5Hz to 1.2kHz. This number of response frequencies was considered to be sufficient to give a curve of good resolution, and spreading the points by octave ensured they were evenly distributed along a log/log plot rather than clumped around the upper end of the frequency range. Figure 6.5.4 shows a typical result for a resulting single node SRS plot, with lines of constant relative displacement and pseudo-acceleration marked.

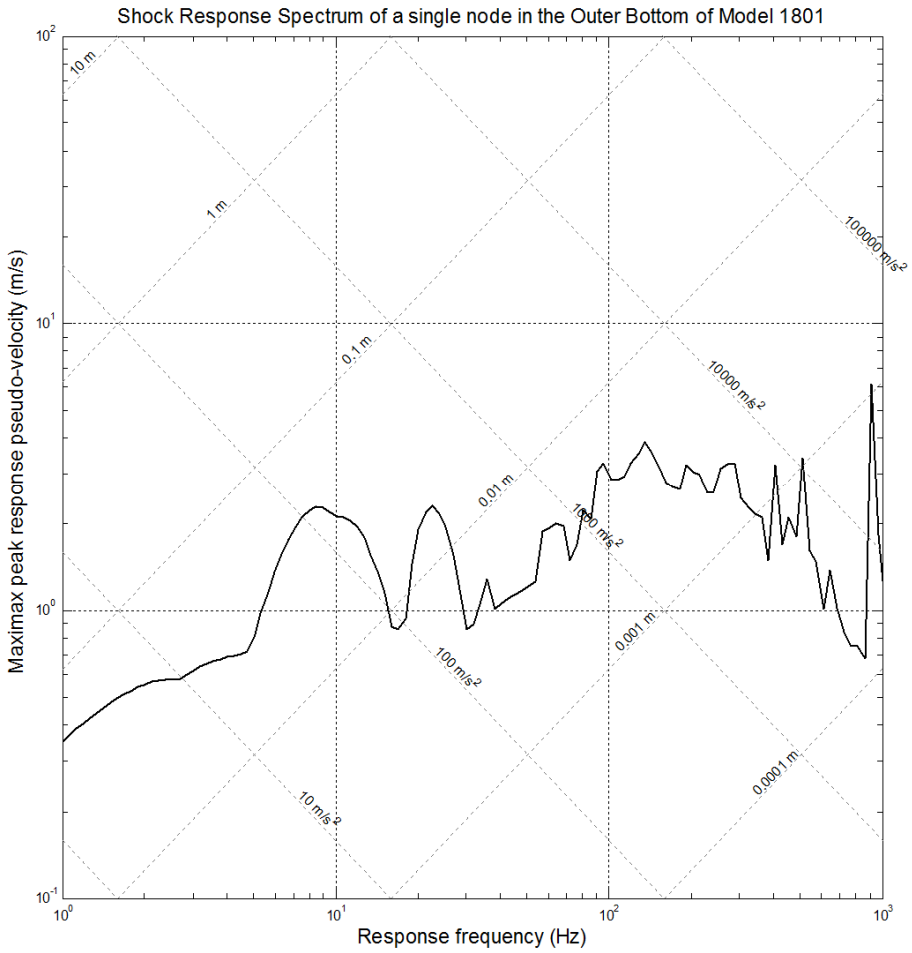

Figure 6.5.4 - Shock response spectrum for a node in the Outer Bottom of Model 1801 responding to a typical design shock load

The naval shock protection or equipment designer does not necessarily know exactly where their equipment will be mounted, or the exact geometry of the UNDEX that may eventually load it. It would therefore be prudent to consider the shock response to numerous FEA nodes throughout the area of structure where the equipment is likely to be mounted. Shock response spectra for multiple nodes may be plotted on the same axes, as shown in Figure 6.5.5, giving the mount/equipment designer an indication of the possible envelope of responses throughout the area of interest.

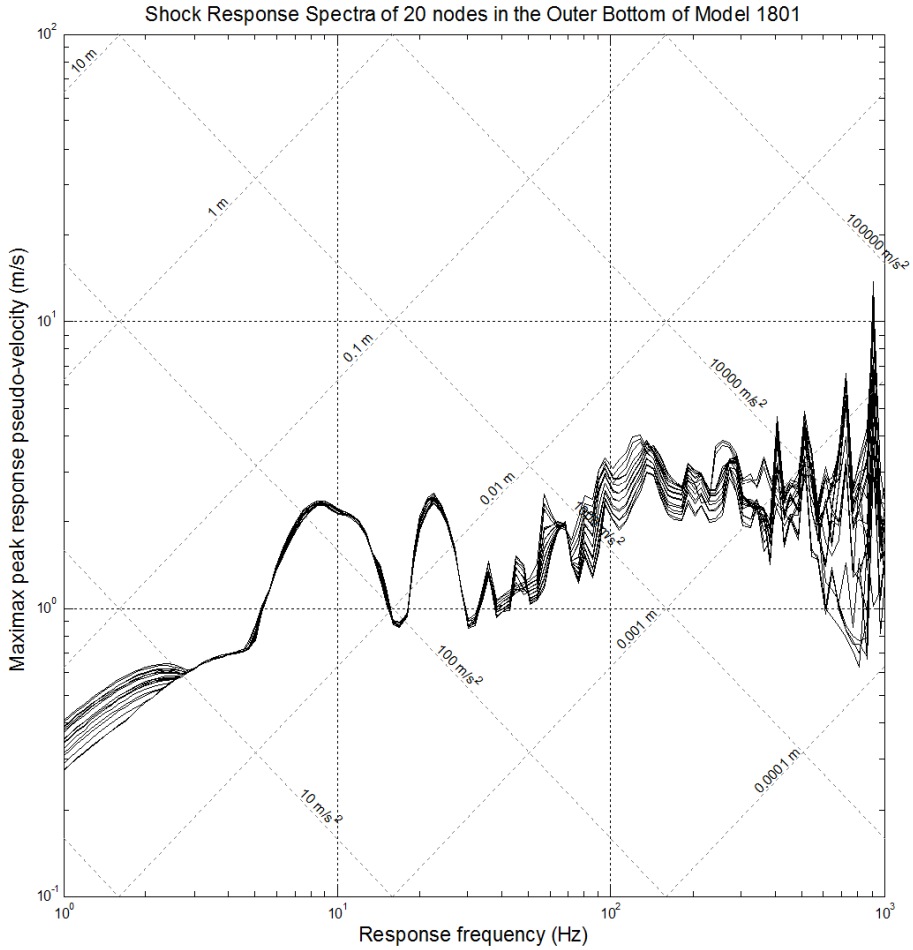

Figure 6.5.5 –Superimposed shock response spectra for twenty nodes in the Outer Bottom of Model 1801 responding to a typical design shock load

Each region within the models used within the present research contained a large number of nodes; in the order of several thousand. Plotting thousands of shock response spectra on the same axes would have been possible but, as shown in Figure 6.5.6, the mass of lines would not give a good idea of their distribution.

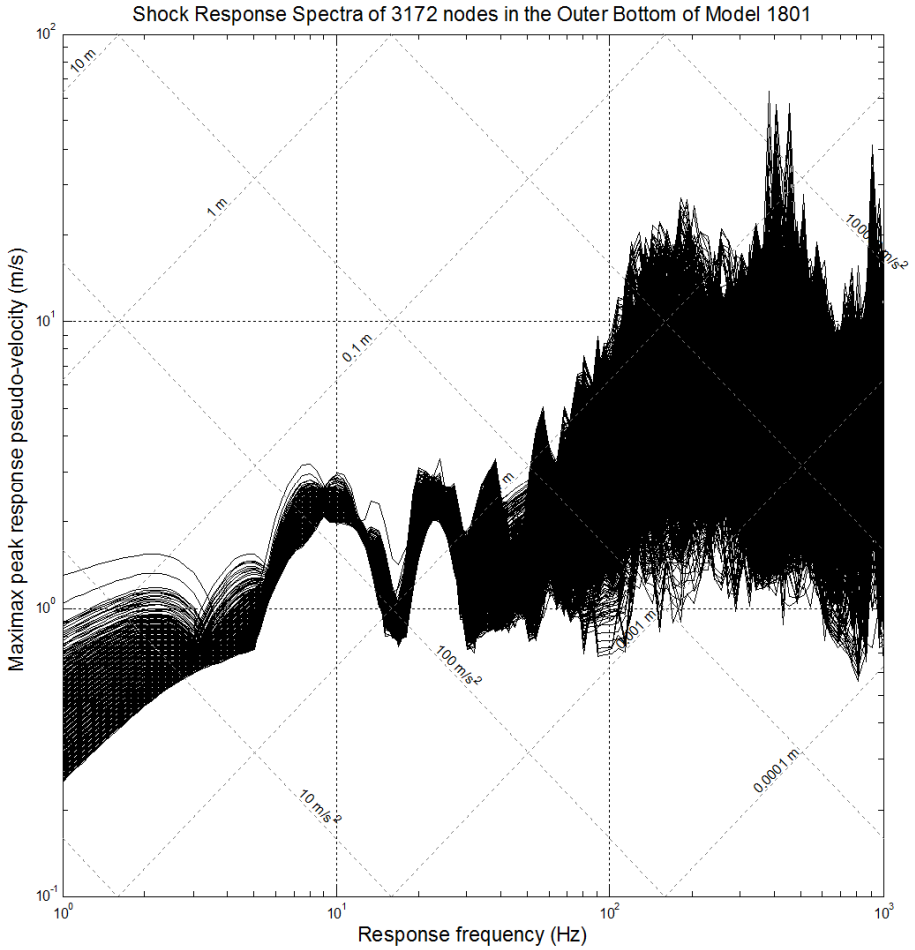

Figure 6.5.6 – Superimposed shock response spectra for all nodes modelled in the Outer Bottom region of Model 1801

It was considered that the presentation in Figure 6.5.7 was a clearer format to present the data. The four lines in Figure 6.5.7 respectively show: the upper and lower bounds of the envelope containing all responses; the mean response at every frequency; and the 80th percentile response (i.e. the response which was not exceeded by 80% of the nodes.) This gave an indication of the mean and extreme values plus a rough measure of the distribution. Plots of this form for each region of every model simulated in this research are presented at Appendix H.

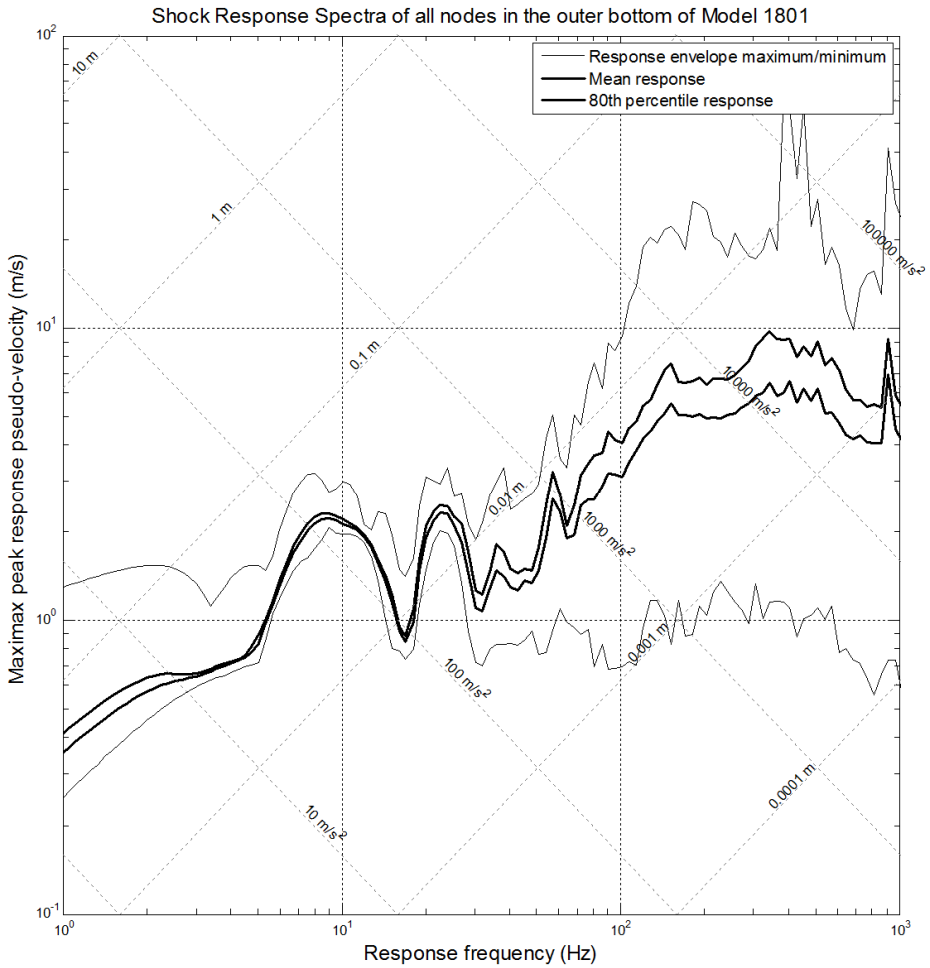

Figure 6.5.7 - Shock Response Spectra distribution plot for a single region of Model 1801

For the purpose of comparing the different models within each series, the 80th percentile response line was selected to represent the response of each region. This use of a single plot line gave an easy comparison between the several plots within a region, as shown in Figure 6.5.8. Since the relationships between peak pseudo-acceleration and peak displacement (defined at Eq 6.7 and Eq 6.8) vary only with frequency, it was considered meaningful to

consider the response motions purely in terms of pseudo-velocity; an increase by any factor in pseudo-velocity at a given frequency must also mean an increase by the same factor in pseudo-acceleration and displacement at that frequency. Comparisons of the results were phrased in the form that "motions increased by a factor of X compared to the baseline" which was derived by dividing one pseudo-velocity by the other, but the same factor will apply to pseudo-acceleration and displacement between the two models at the same frequency.

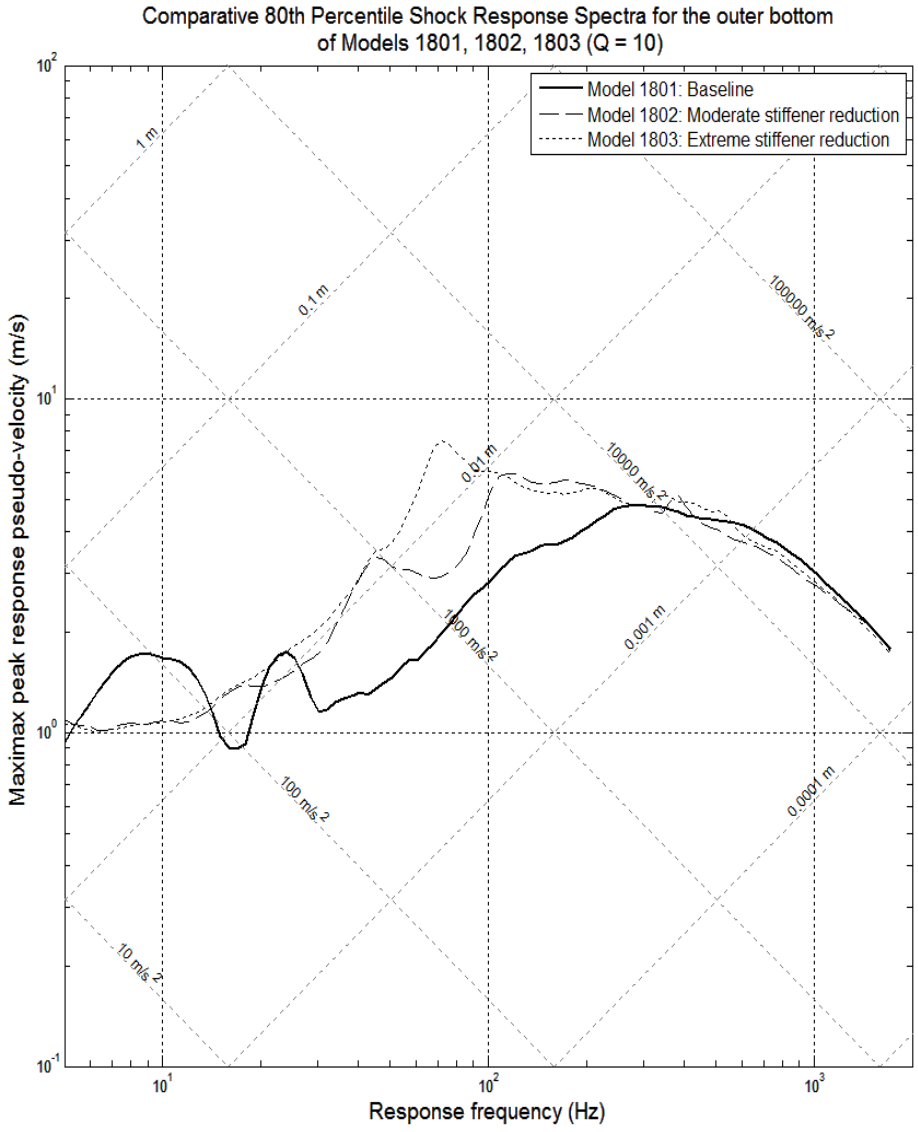

Figure 6.5.8 - Comparative Shock Response Spectra plot for a typical region of the three models within the first experimental series (Models 1801, 1802 and 1803)

Chapter 7 Results of Finite Element Analysis of Ship Structural Models Following Shock Loading

This chapter presents eighteen Shock Response Spectrum (SRS) plots, each one summarising the variation between the ship structural models of a series within a single spatial region (Outer Bottom plating, Top Deck plating, etc.), as described in Chapter 6. The plots each present a comparison of the 80th percentile pseudo-velocity shock response spectra (SRS), with the spectra for all models of the series plotted on the same axes (see Figure 6.5.8.) All the graphs are plotted on axes of a constant scale, to allow for comparison of the results between regions and model series. Each graph is followed by a short list of observations. These are presented in brief and later expanded upon in a summary at the end of each model series.

7.1 Results from Series 1 – Variation in Stiffener Spacing

Series 1 examined the effects of reducing stiffener numbers, accepting heavier plating and deeper stiffeners for a reduction in the quantity of welding required to assemble the structure. It contained three structural variant models, all based on the NFR-90 Frigate (see Section 5.3.)

- Model 1801: The baseline, with 600mm longitudinal and 1500mm frame spacing
- Model 1802: Moderate reduction in stiffeners, with 800mm x 2000mm panels
- Model 1803: Extreme reduction in stiffeners, with 1200mm x 3000mm panels

In every region of the baseline model (especially those below the Top Deck), significant oscillations were present in the response spectra over the frequency range from 5Hz to 30Hz, which were not present in any of the other models simulated and are not typical of a warship structure shock response spectrum. The reason for these oscillations is not apparent, but the frequency range of 8-26 Hz corresponds to the range of natural frequencies associated with a 600mm x 1500mm steel panel of thickness between 10mm and 20mm with simply supported edges vibrating in Mode 1 (Leissa, 1973). It is therefore possible that a strong component of the shock wave loading caused resonance in one or more panels of the baseline model, but not in the other models. However, it is of concern that these oscillations do not appear in Models 1804 & 1807, whose panels might be expected to have similar natural frequencies. Deviations from the baseline response below 30Hz, where these deviations follow the shape of the

baseline's oscillations, have therefore not been included in the comments after each SRS plot. A modal analysis of the structures, such as might be performed to analyse bubble pulse response, would provide useful information to help understand this phenomenon, discussed further in Section 8.3.

7.1 a Series 1 (varying stiffener spacing), Top Deck Region (see Figure 6.2.2)

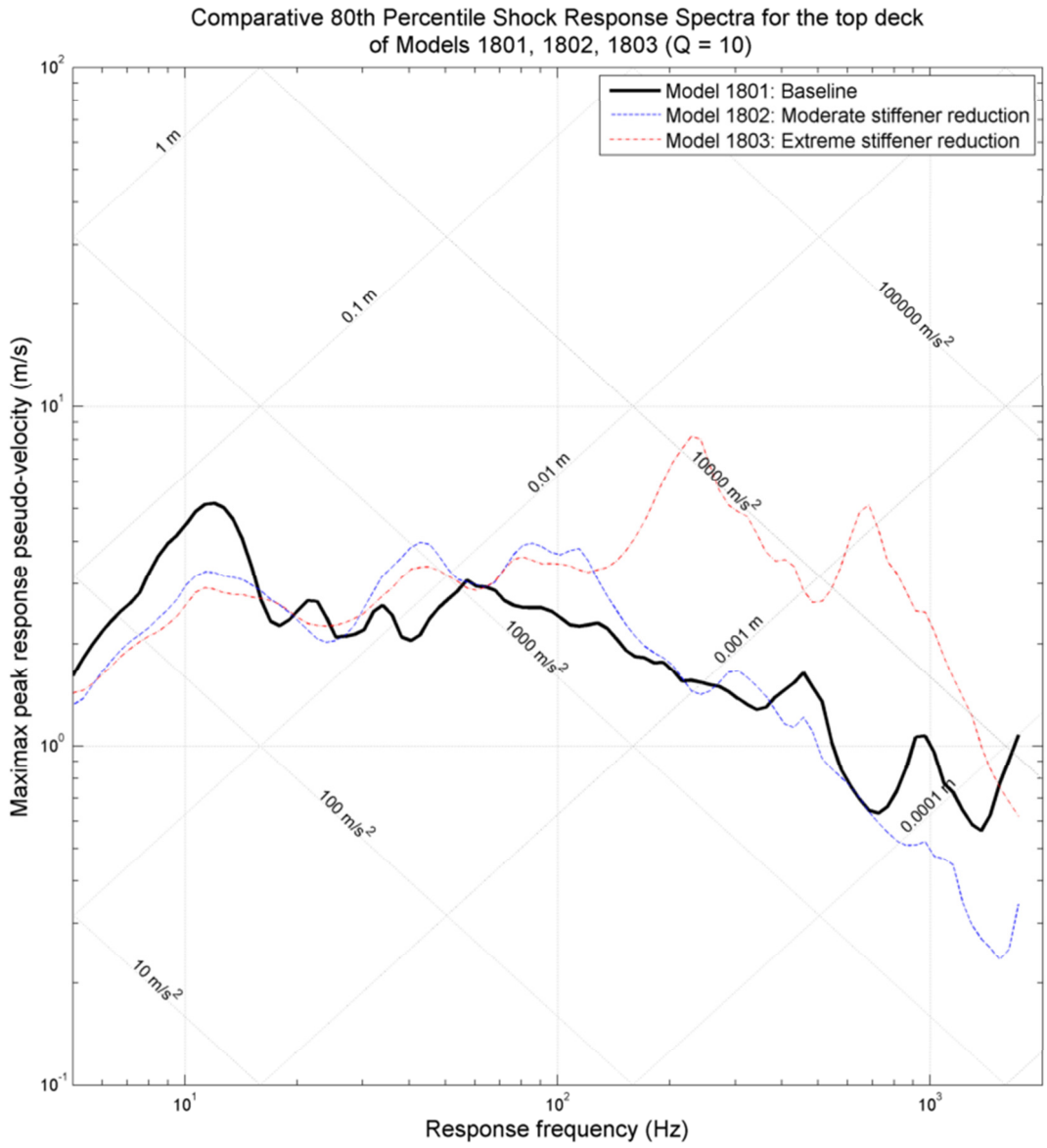

Figure 7.1.1 - Comparative 80th Percentile SRS for the Top Deck region of the first experimental series (Models 1801, 1802 & 1803, varying stiffener spacing)

From Figure 7.1.1, the following observations were drawn:

i. Between 30Hz and 150Hz, both simplified models (1802 and 1803) behaved similarly, exceeding the NFR-90 Frigate Baseline (Model 1801) by a factor of between 1 and 2.

ii. Above 150Hz, the moderately simplified model (1802) behaved similarly to, or better than the Baseline, while the extremely simplified model (1803) experienced motions between 1.5 and 8 times greater than the Baseline model.

7.1 b Series 1 (varying stiffener spacing), Passing Deck region (see Figure 6.2.2)

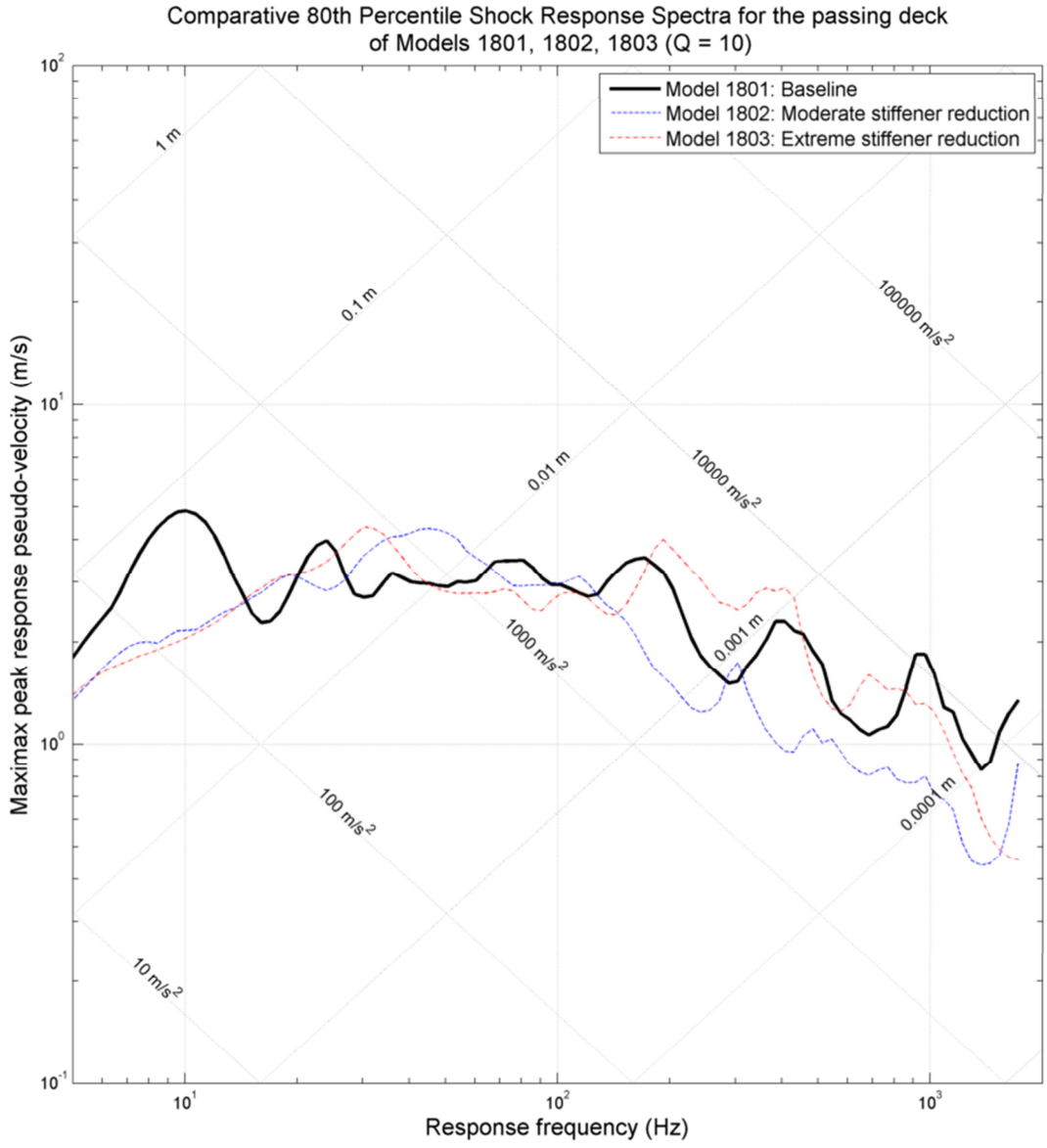

Figure 7.1.2 - Comparative 80th Percentile SRS for the Passing Deck region of the first experimental series (Models 1801, 1802 & 1803, varying stiffener spacing)

From Figure 7.1.2, the following observations were drawn:

i. The three SRS have similar shapes; above 30Hz the simplified models generally remained within 0.4 and 1.6 times the Baseline (Model 1801), which is of similar order to the variations with frequency within each model.

ii. Above 150Hz the moderately simplified model (Model 1802) generally performed better than the Baseline (Model 1801), while the extremely simplified model (Model 1803) generally performed worse.

7.1 c Series 1 (varying stiffener spacing), Upper Side Shell region (see Figure 6.2.2)

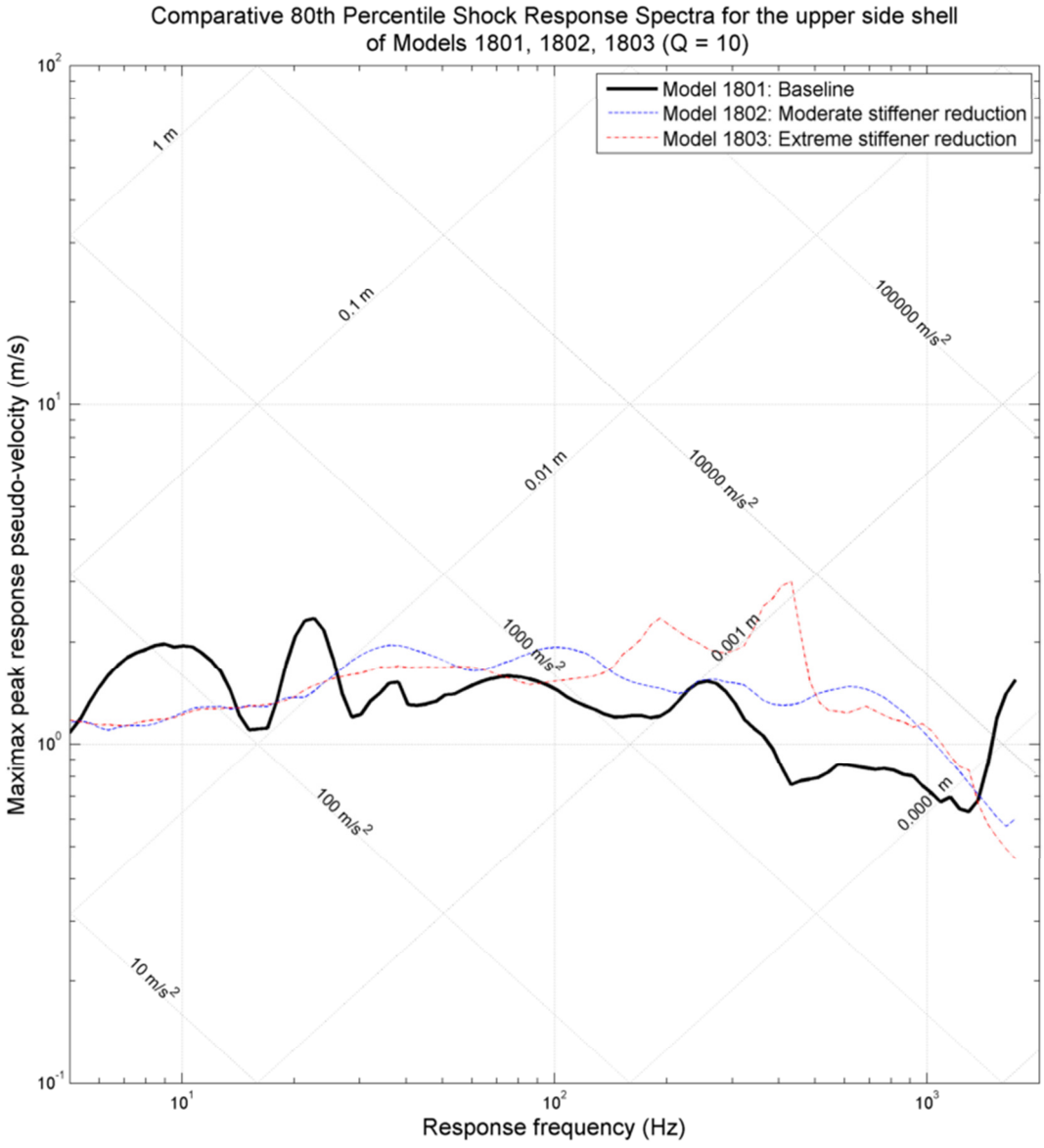

Figure 7.1.3 - Comparative 80th Percentile SRS for the Upper Side Shell region of the first experimental series (Models 1801, 1802 & 1803, varying stiffener spacing)

From Figure 7.1.3, the following observations were drawn:

i. Above 30Hz the moderately simplified model (Model 1802) experienced motions generally larger than the Baseline (Model 1801), by a factor up to 1.8.

ii. Above 30Hz the extremely simplified model (Model 1803) experienced motions generally larger than the Baseline (Model 1801), by a factor generally up to 2, but peaking at 4.

7.1 d Series 1 (varying stiffener spacing), Wetted Side Shell region (see Figure 6.2.2)

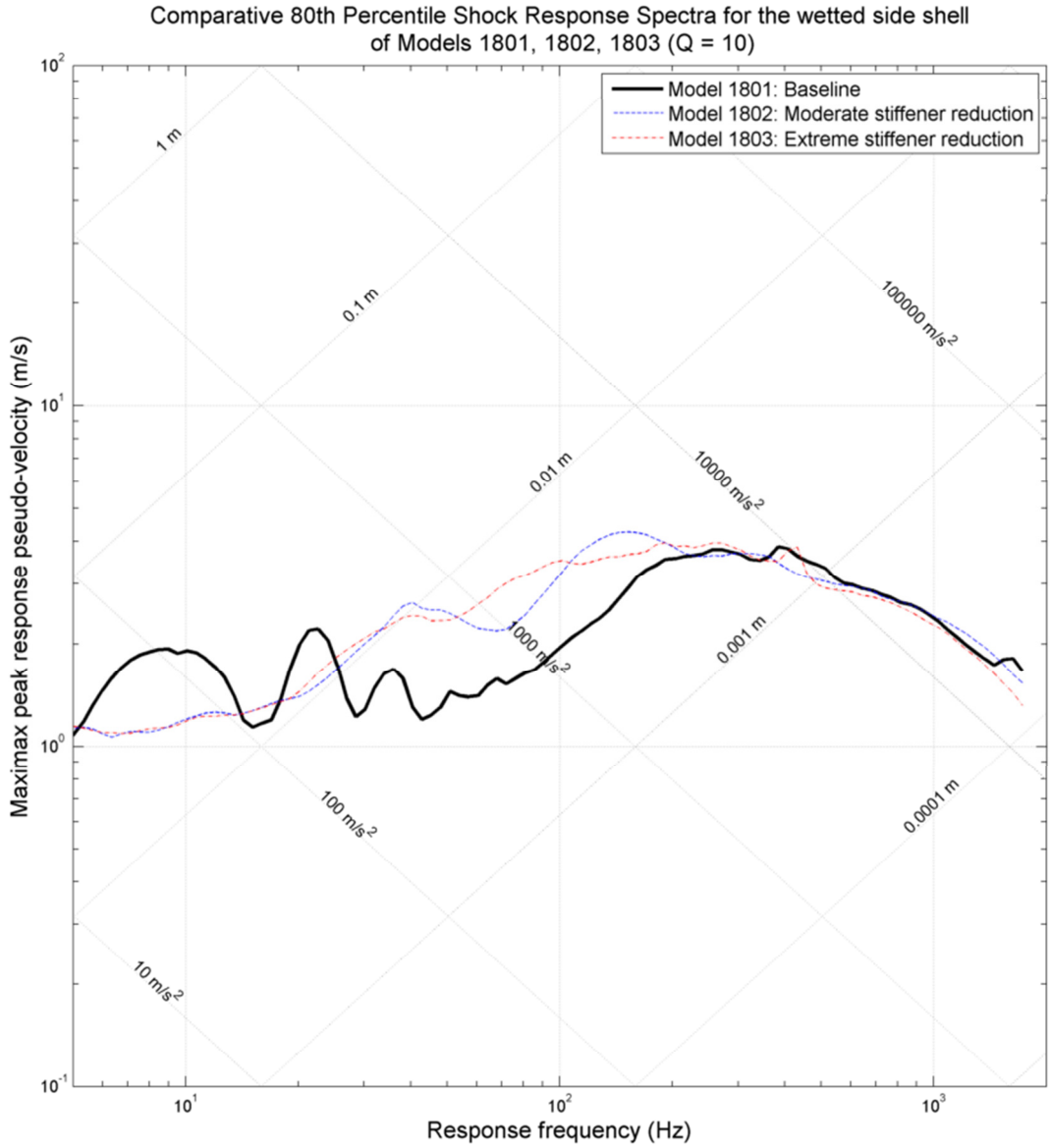

Figure 7.1.4 - Comparative 80th Percentile SRS for the Wetted Side Shell region of the first experimental series (Models 1801, 1802 & 1803, varying stiffener spacing)

From Figure 7.1.4, the following observations were drawn:

i. Between 30Hz and 200Hz both simplified models behaved similarly to one another, experiencing motions larger than the Baseline (Model 1801) by up to a factor of 2.

ii. Above 200Hz both simplified models behaved almost indistinguishably from the Baseline.

7.1 e Series 1 (varying stiffener spacing), Inner Bottom region (see Figure 6.2.2)

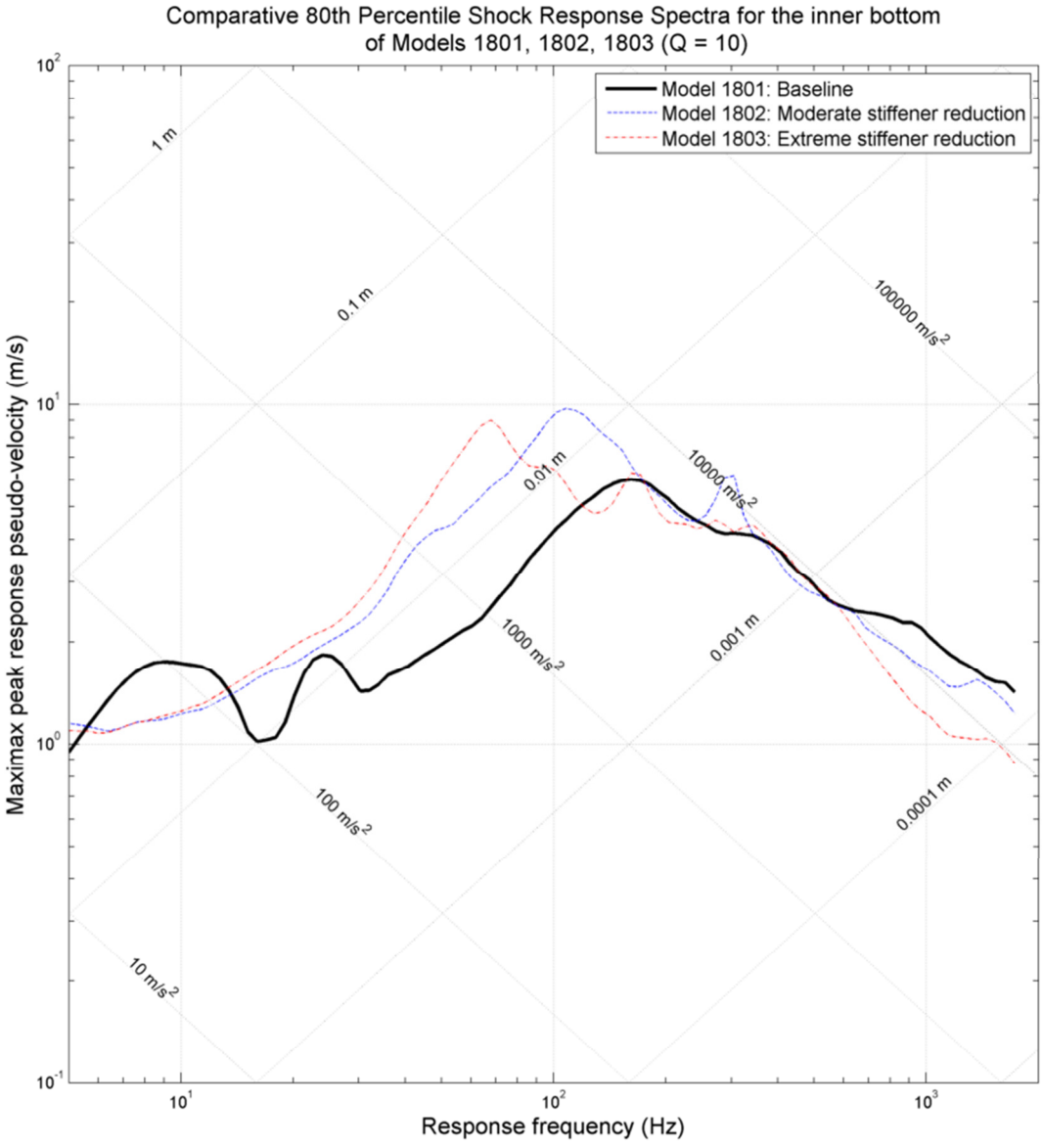

Figure 7.1.5 - Comparative 80th Percentile SRS for the Inner Bottom region of the first experimental series (Models 1801, 1802 & 1803, varying stiffener spacing)

From Figure 7.1.5, the following observations were drawn:

i. Between 30Hz and 150Hz both models experienced motions greater than the Baseline (Model 1801); Model 1802 peaking at a factor of 2.1 greater, and Model 1803 peaking at a factor of 3.8 greater.

ii. Above 150Hz both simplified models behaved generally similar to the Baseline (Model 1801), experiencing lower motions than the Baseline above 600Hz.

7.1 f Series 1 (varying stiffener spacing), Outer Bottom region (see Figure 6.2.2)

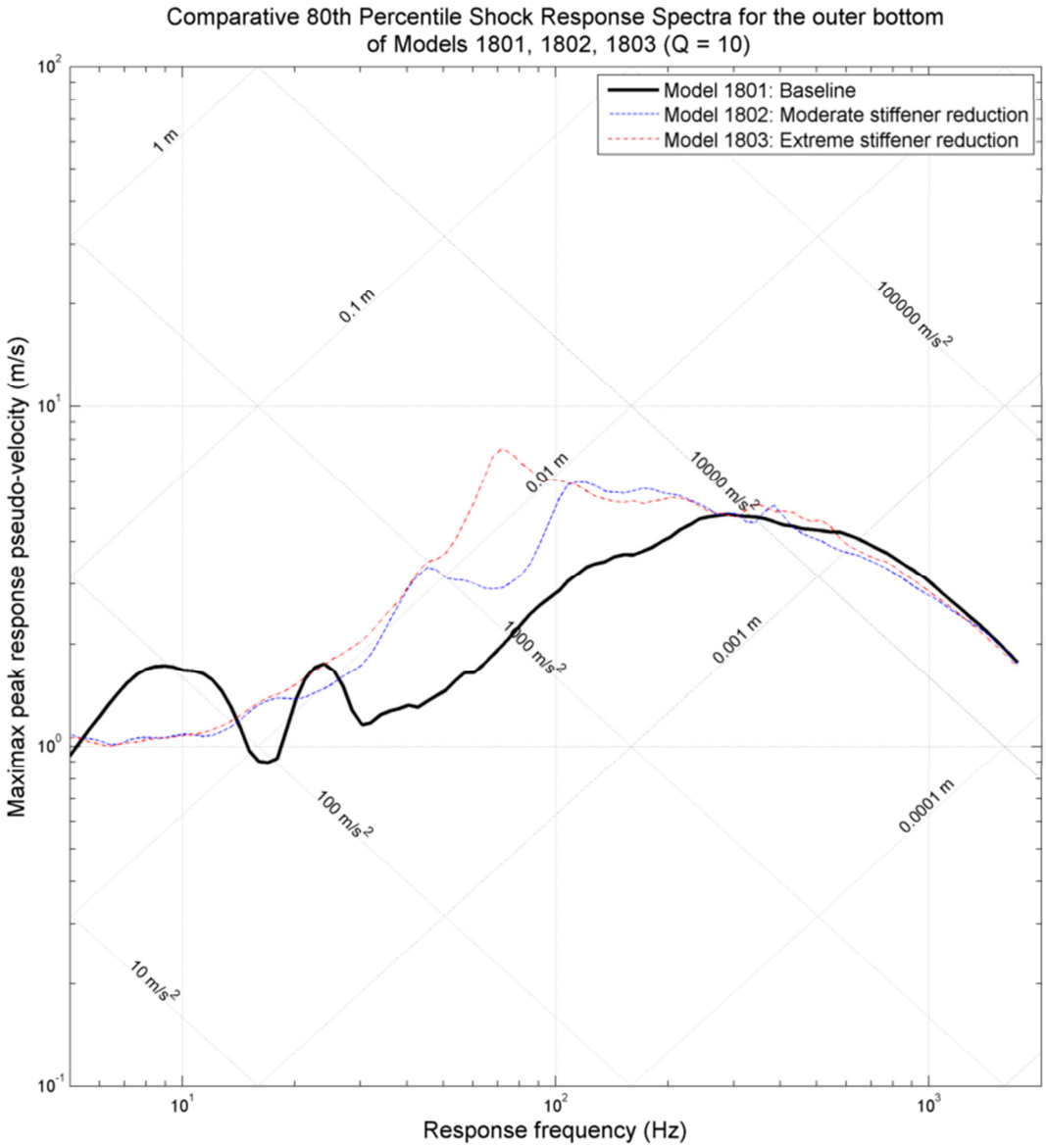

Figure 7.1.6 - Comparative 80th Percentile SRS for the Outer Bottom region of the first experimental series (Models 1801, 1802 & 1803, varying stiffener spacing)

From Figure 7.1.6, the following observations were drawn:

i. Between 30Hz and 250Hz both simplified models experienced motions greater than the Baseline (Model 1801); greater by a factor of up to 2.3 for the moderately simplified model (Model 1802) and up to 4 for the extremely simplified model (Model 1803.)

ii. Above 250Hz both simplified models experienced motions very similar to the Baseline (Model 1801.)

7.1 g Summary of Results from Series 1

Similar behaviour was exhibited across the three lower regions of the structural sections of these frigate models: the outer bottom, inner bottom and wetted sideshell. Each of these exhibited a high frequency range (>150-250Hz) where all three models experienced similar motions and a medium frequency range (<150-250Hz) where the models with simplified structural styles (Models 1802 and 1803) experienced greater motions than the Baseline (Model 1801.) The transition frequency between these frequency ranges was neither clearly delineated nor the same between different models, but appeared to occur somewhere between 150Hz and 250Hz in each model. In the medium frequency range, the moderately simplified model (Model 1802) experienced peak motions up to 2.3 times greater than the Baseline, while the extremely simplified model (Model 1803) experienced motions up to four times greater.

In the Passing Deck (No. 2 Deck in Royal Navy terminology) and Side Shell above the waterline, the response of all three models was broadly comparable. The simplified models experienced motions generally between half and twice those of the Baseline, but this variation was of a similar magnitude to the variations within each model's SRS plot over small frequency ranges. In general the moderately simplified model (Model 1802) performed better than the extremely simplified model (Model 1802) (and frequently better than the Baseline model.)

In the Top Deck (No. 1 Deck in Royal Navy terminology) the moderately simplified model (Model 1802) performed similarly to the Baseline, with all motions remaining in the region of 0.5 to 2.0 times the baseline up to 1kHz. However, the extremely simplified model (Model 1803) experienced greatly increased motions in the range above 150Hz, exceeding the Baseline by a factor of up to 2.0 over most of the range with peaks up to eight times the Baseline.

7.2 Results from Series 2

Series 2 examined the effects of using stiffeners with different cross-sectional profiles, accepting an increase in stiffener depth for a reduction in stiffener material costs. It contained three structural models, all based on the NFR-90 Frigate design (Schaffer and Kloehn, 1991). All had stiffeners and frames spaced at 600mm x 1500mm.

i. Model 1801: The baseline, with long-stalk tee-bar stiffeners

ii. Model 1804: Using offset bulb plates (OBPs)

iii. Model 1807: Using flat bar stiffeners

Since this series used the same Baseline (Model 1801) as Series 1, the low-frequency oscillations previously observed and discussed in Section 7.1 remained present. Therefore, the practice of disregarding deviations from the Baseline model below 30Hz was retained.

7.2 a Series 2 (varying stiffener profile), Top Deck region(see Figure 6.2.2)

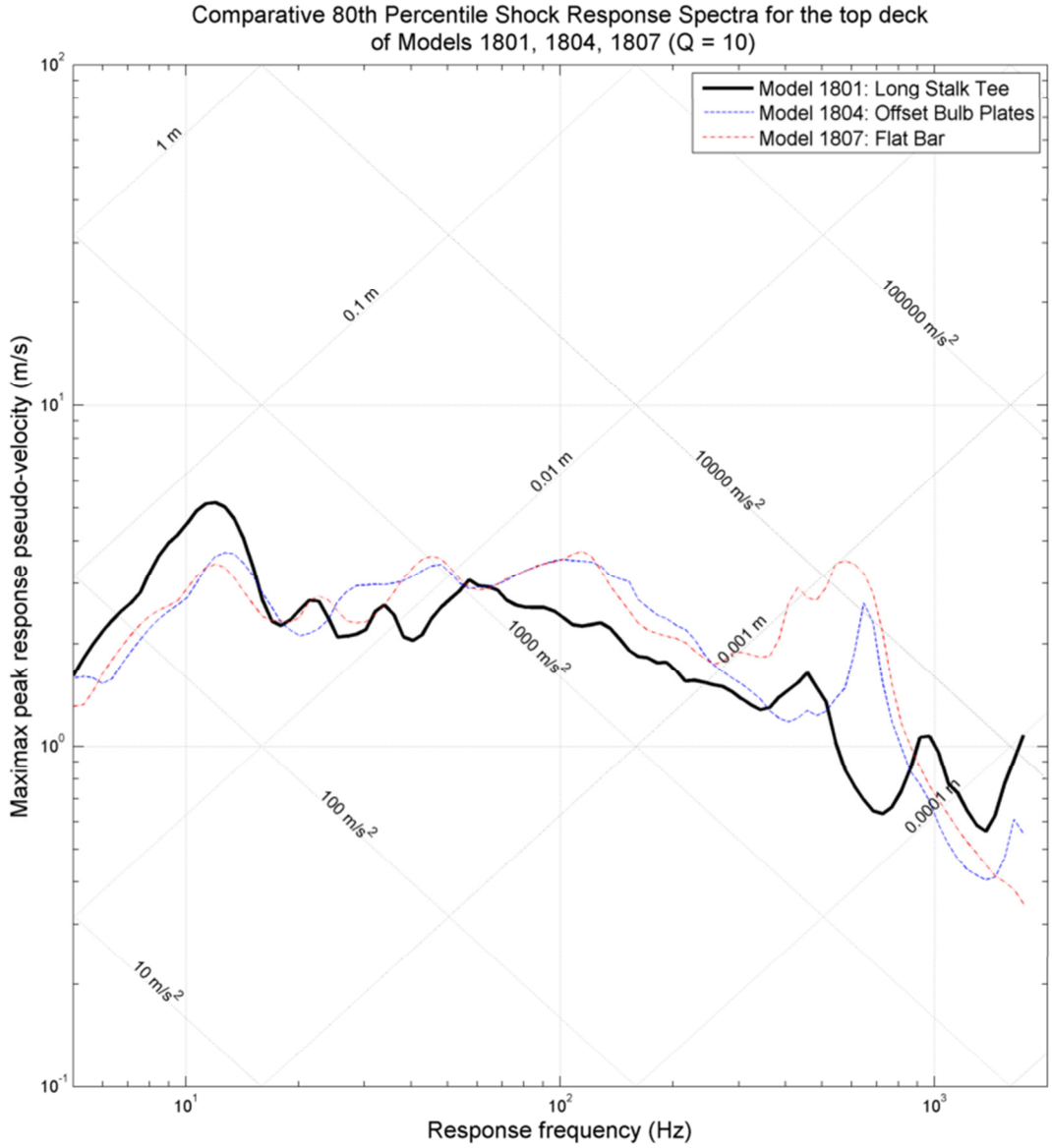

Figure 7.2.1 - Comparative 80th Percentile SRS for the Top Deck region of the second experimental series (Models 1801, 1804 & 1807, varying stiffener profile shape)

From Figure 7.2.1, the following observations were drawn:

i. Above 30Hz, the motions of all models were broadly similar; the motions of the simplified models (Models 1804 and 1807) generally remaining in the range of 0.6 – 1.4 times the Baseline (Model 1801).

ii. Around the 500-700Hz range the response of both simplified models (Models 1804 and 1807) peaked to 3.6-4.6 times the Baseline.

7.2 b Series 2 (varying stiffener profile), Passing Deck region (see Figure 6.2.2)

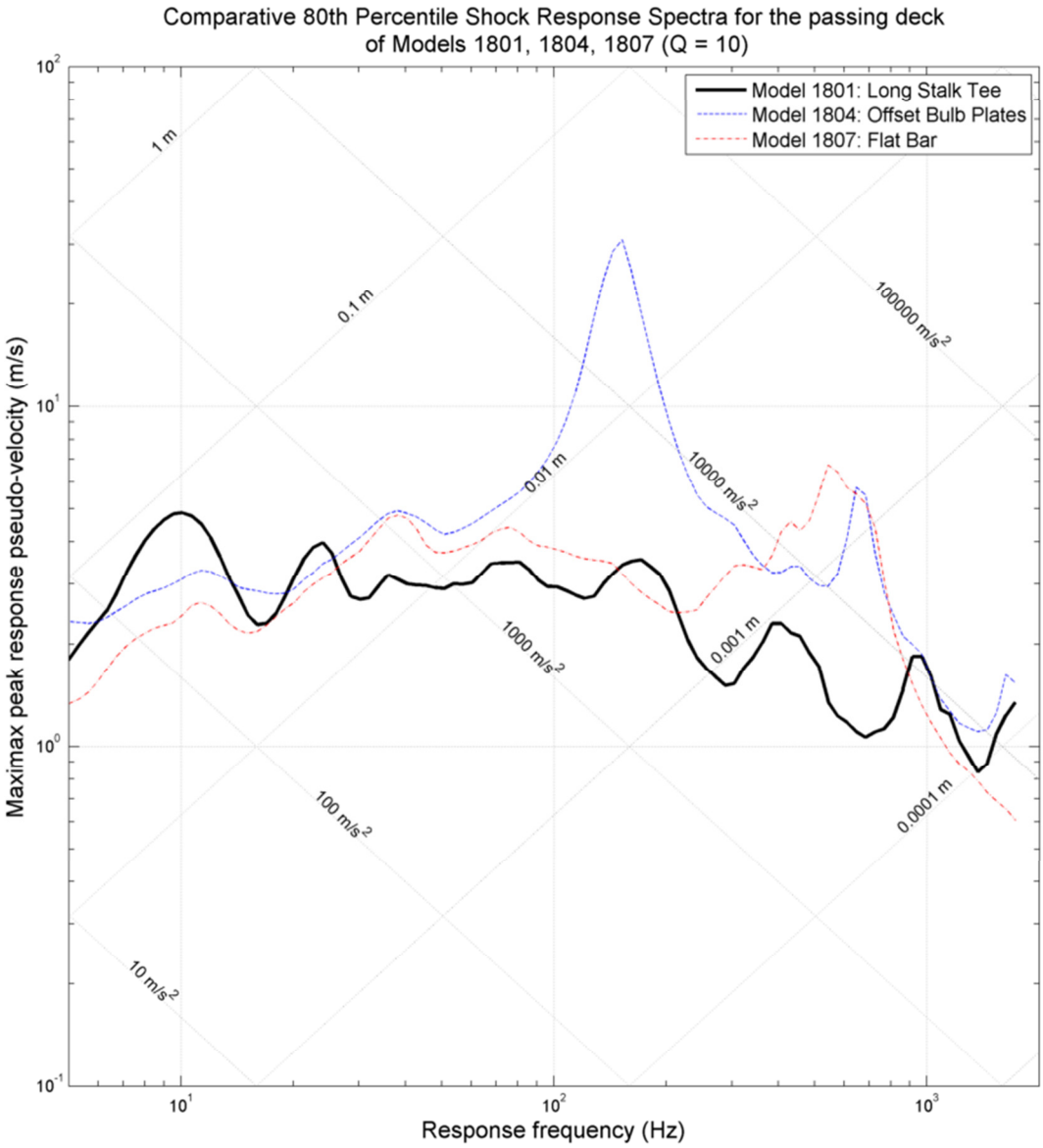

Figure 7.2.2 - Comparative 80th Percentile SRS for the Passing Deck region of the second experimental series (Models 1801, 1804 & 1807, varying stiffener profile shape)

From Figure 7.2.2, the following observations were drawn:

i. Above 30Hz the OBP model (Model 1804) generally experienced motions greater than the Baseline (Model 1801), peaking at nine times greater.

ii. Above 30Hz the flat bar model (Model 1807) generally experienced motions greater than the Baseline (Model 1801) although not so great as Model 1804, peaking at five times the Baseline model.

7.2 c Series 2 (varying stiffener profile), Upper Side Shell region (see Figure 6.2.2)

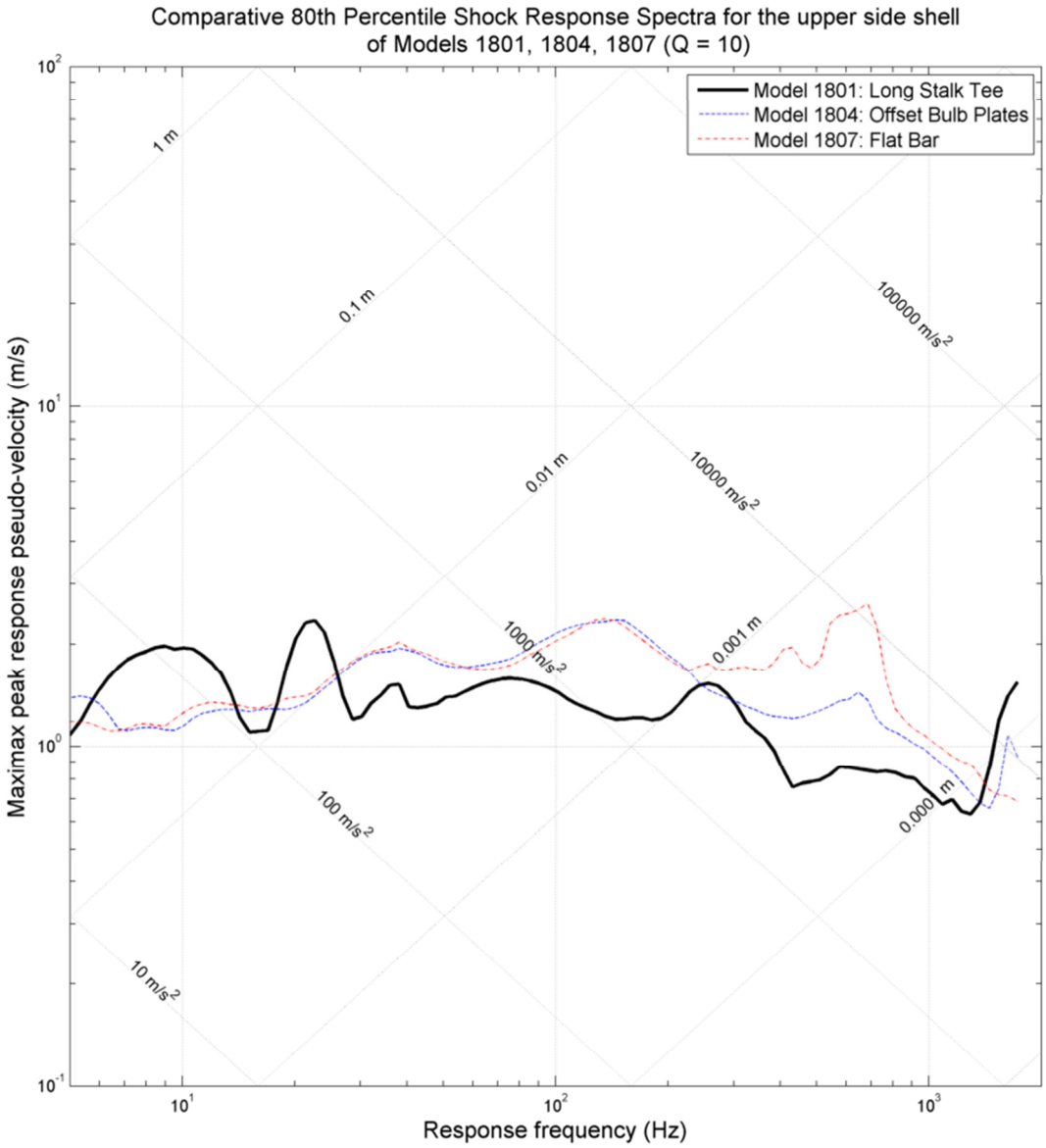

Figure 7.2.3 - Comparative 80th Percentile SRS for the Upper Side Shell region of the second experimental series (Models 1801, 1804 & 1807, varying stiffener profile shape)

From Figure 7.2.3, the following observations were drawn:

i. Between 30Hz and 250Hz both simplified models (Models 1804 and 1807) behaved very similarly, experiencing motions between one and two times the Baseline (Model 1801).

ii. Above 250Hz the OBP model (Model 1804) experienced motions up to 1.5 times the Baseline.

iii. Above 250Hz the flat bar model (Model 1807) experienced motions up to three times the Baseline.

7.2 d Series 2 (varying stiffener profile), Wetted Side Shell region (see Figure 6.2.2)

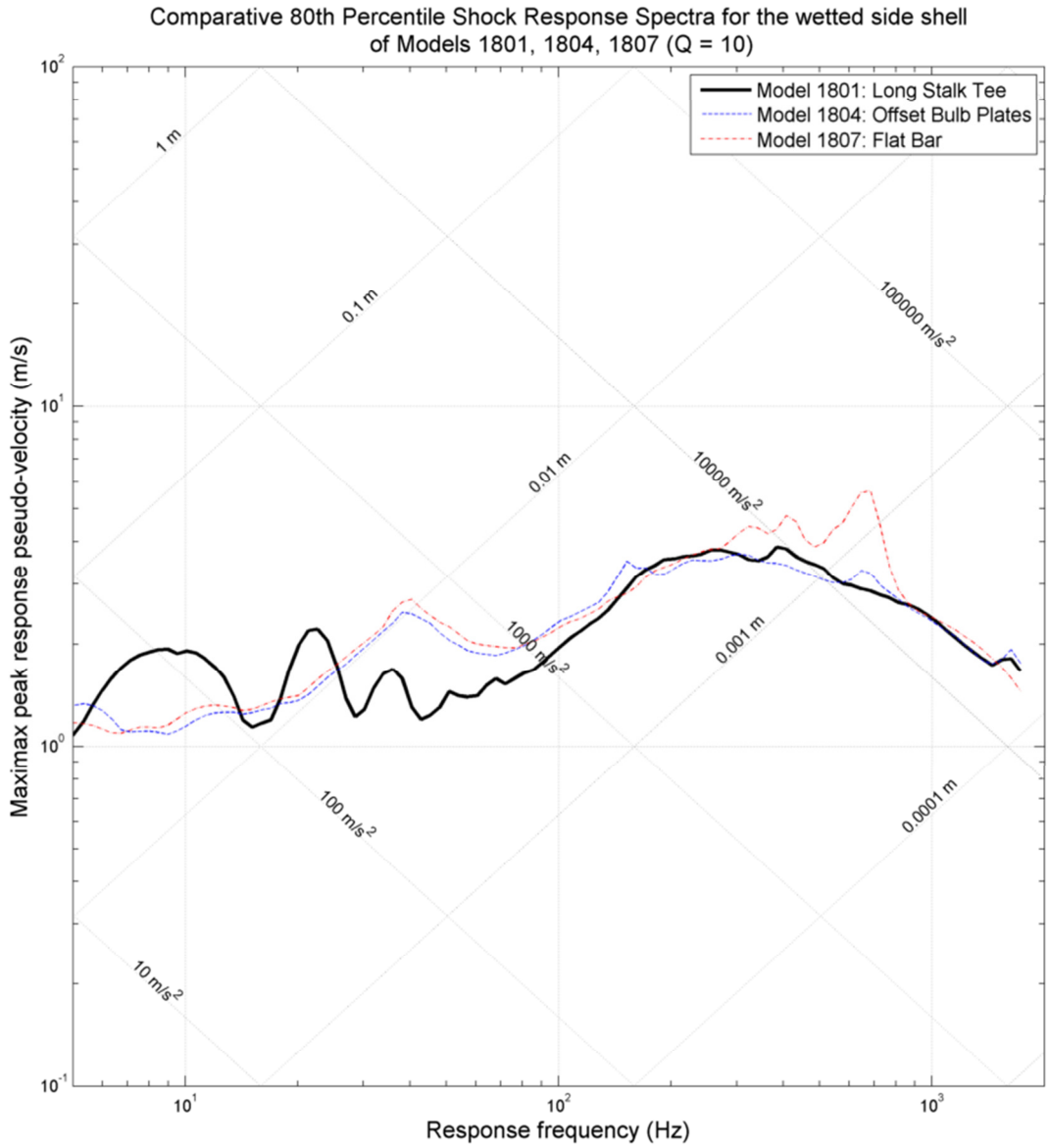

Figure 7.2.4 - Comparative 80th Percentile SRS for the Wetted Side Shell region of the second experimental series (Models 1801, 1804 & 1807, varying stiffener profile shape)

From Figure 7.2.4 the following observations were drawn:

i. Between 30Hz and 300Hz both simplified models (Models 1804 and 1807) behaved very similarly, closely matching the motions of the Baseline model (Model 1801) between 100Hz and 300Hz, and exceeding them by a factor of up to two between 30Hz and 100Hz.

ii. Above 300Hz the OBP model (Model 1804) closely matched the Baseline response.

iii. Between 300Hz and 800Hz the flat bar model (Model 1807) exceeded the Baseline response by a factor of up to two, matching the Baseline closely above 800Hz.

7.2 e Series 2 (varying stiffener profile), Inner Bottom region (see Figure 6.2.2)

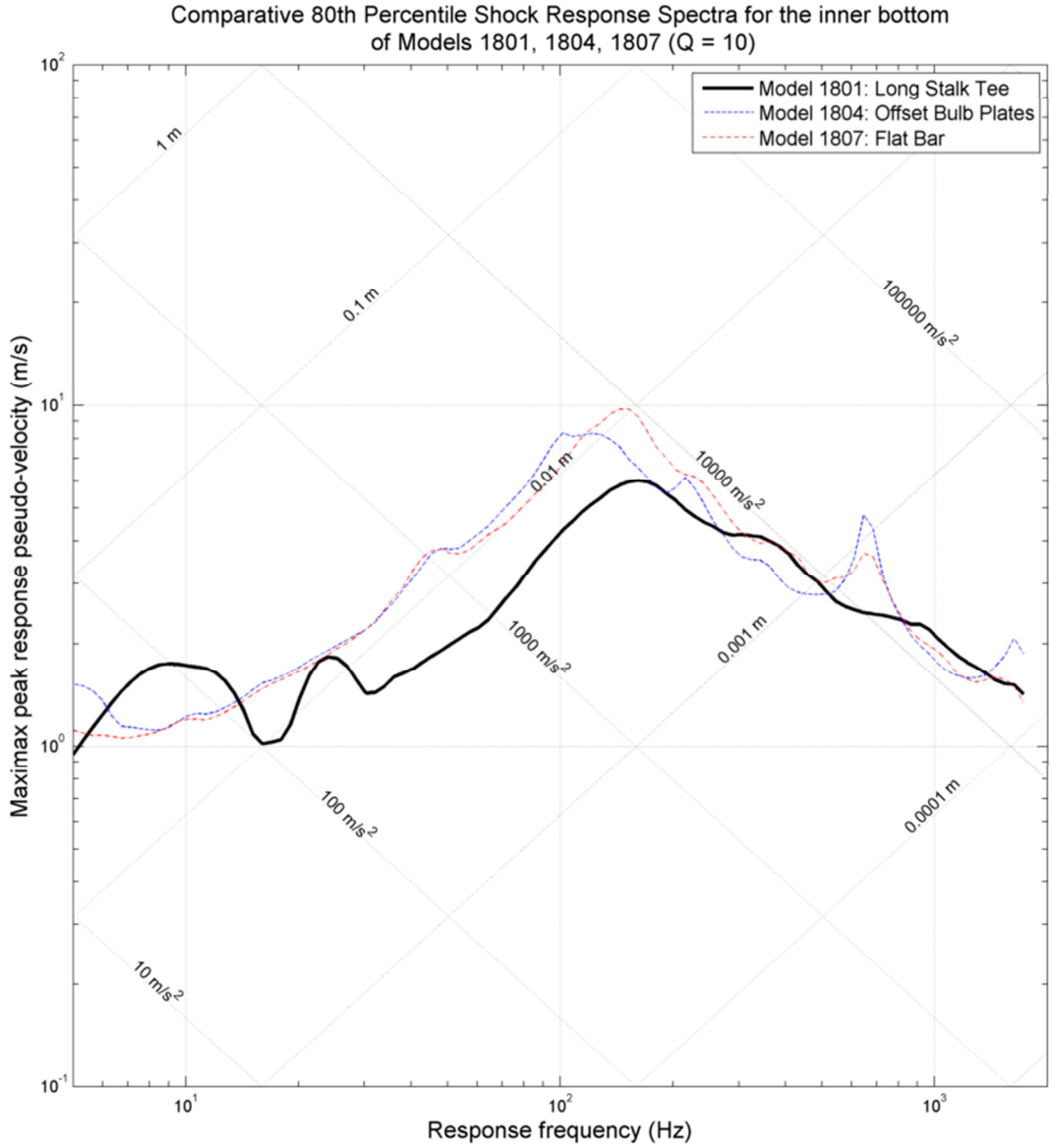

Figure 7.2.5 - Comparative 80th Percentile SRS for the Inner Bottom region of the second experimental series (Models 1801, 1804 & 1807, varying stiffener profile shape)

From Figure 7.2.5, the following observations were drawn:

i. Between 30Hz and 200Hz, both simplified models (Models 1804 and 1807) behaved very similarly, exceeding the response of the Baseline (Model 1801) by a factor of two for much of the frequency range.

ii. Above 200Hz, both simplified models experienced responses similar to the Baseline, aside from a peak (in both models) around the 600Hz-800Hz range up to twice the Baseline response.

7.2 f Series 2 (varying stiffener profile), Outer Bottom region (see Figure 6.2.2)

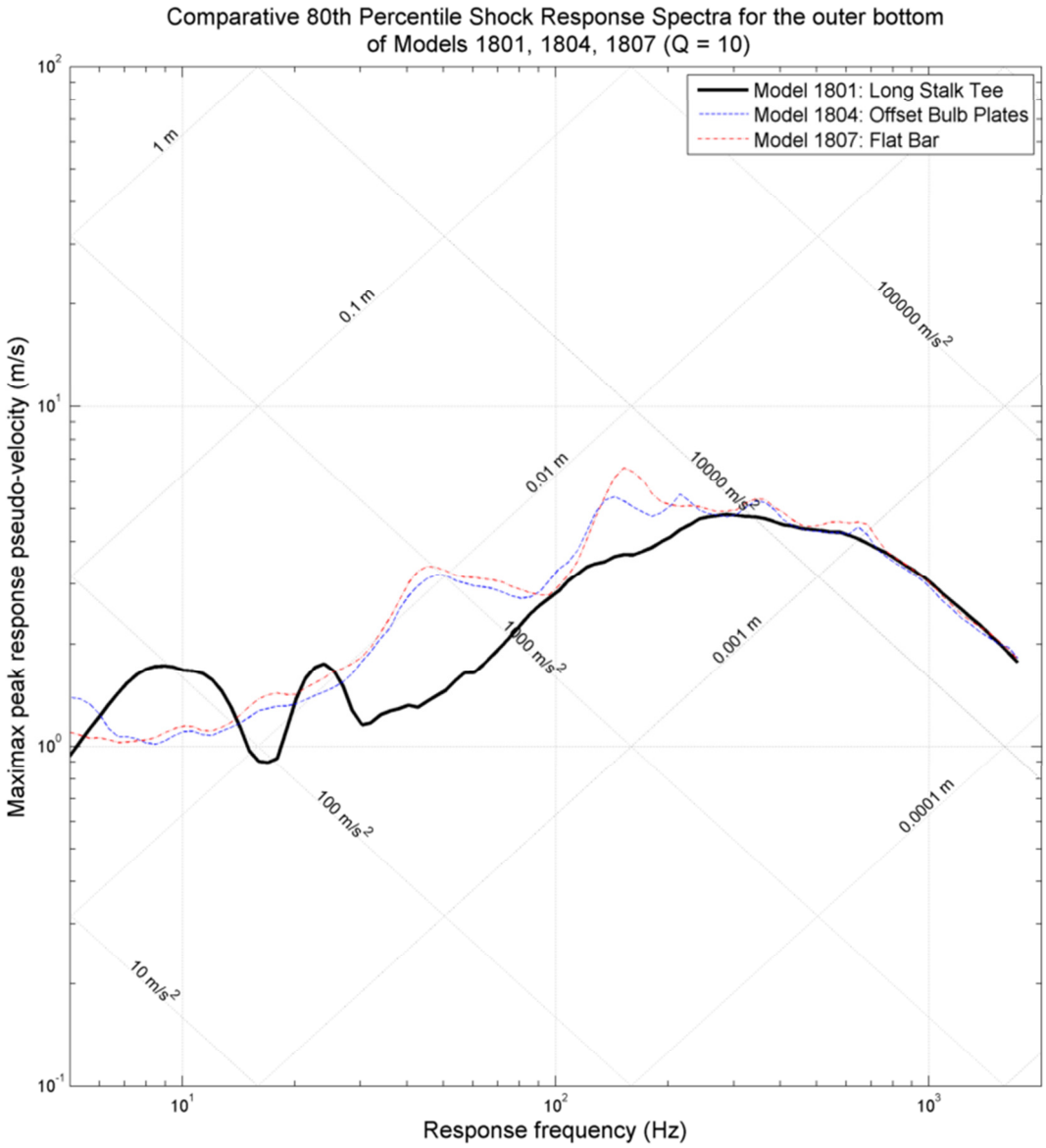

Figure 7.2.6 - Comparative 80th Percentile SRS for the Outer Bottom region of the second experimental series (Models 1801, 1804 & 1807, varying stiffener profile shape)

From Figure 7.2.6, the following observations were drawn:

i. Between 30Hz and 250Hz, both simplified models (Models 1804 and 1807) experienced similar motions, exceeding the response of the Baseline (Model 1801) by a factor of up to around two.

ii. Above 250Hz, the response of all three models was very similar (the response of both simplified models remaining within +/- 10% of the Baseline model's response.)

7.2 g Summary of Results from Series 2

Below the waterline, the Offset Bulb Plate model (Model 1804) generally performed similarly to the Baseline model (Model 1801) at frequencies above 200-300Hz, experiencing response motions up to 2.3 times larger than the Baseline model at lower frequencies.

Above the waterline the response of the OBP model (Model 1804) was more complex. In the Upper Side Shell, motions between 1.5 and 2 times the Baseline model's response were recorded. In the Passing Deck, the model experienced motions generally 15 times greater than the Baseline model, except in the 100-300Hz region where the response varied between 3 and 9 times the Baseline model's and the 600-700Hz range where the response peaked to 5 times that of the Baseline model. In the Top Deck, the motions were at most 1.5 times the Baseline model's response, except for a peak around 600-700Hz where they reached 3.6 times the Baseline model's response.

Below the waterline, the flat bar model (Model 1807) performed very similarly to the OBP model (Model 1804), aside from somewhat larger motions in the wetted sideshell in the 700-800Hz range, and there was little to choose between them. Above the waterline, the flat bar model performed similarly to the OBP model, with the only significant differences being significantly reduced motions in the Passing Deck between 100-300Hz and elevated motions in the upper sideshell between 300-800Hz.

7.3 Results from Series 3

Series 3 examined the effects of adopting a transverse stiffening style as opposed to the traditional warship longitudinal stiffening style. The series contained two models; one longitudinally- and one transversely-stiffened, both based on the corvette design described in Section 5.5.

i. Model 1851: Corvette Baseline - longitudinally-stiffened, with panel size of 600mm x 1500mm

ii. Model 1852: Corvette - transversely stiffened, with frame spacing of 1500mm

7.3 a Series 3 (longitudinal/transverse), Top Deck region (see Figure 6.2.2)

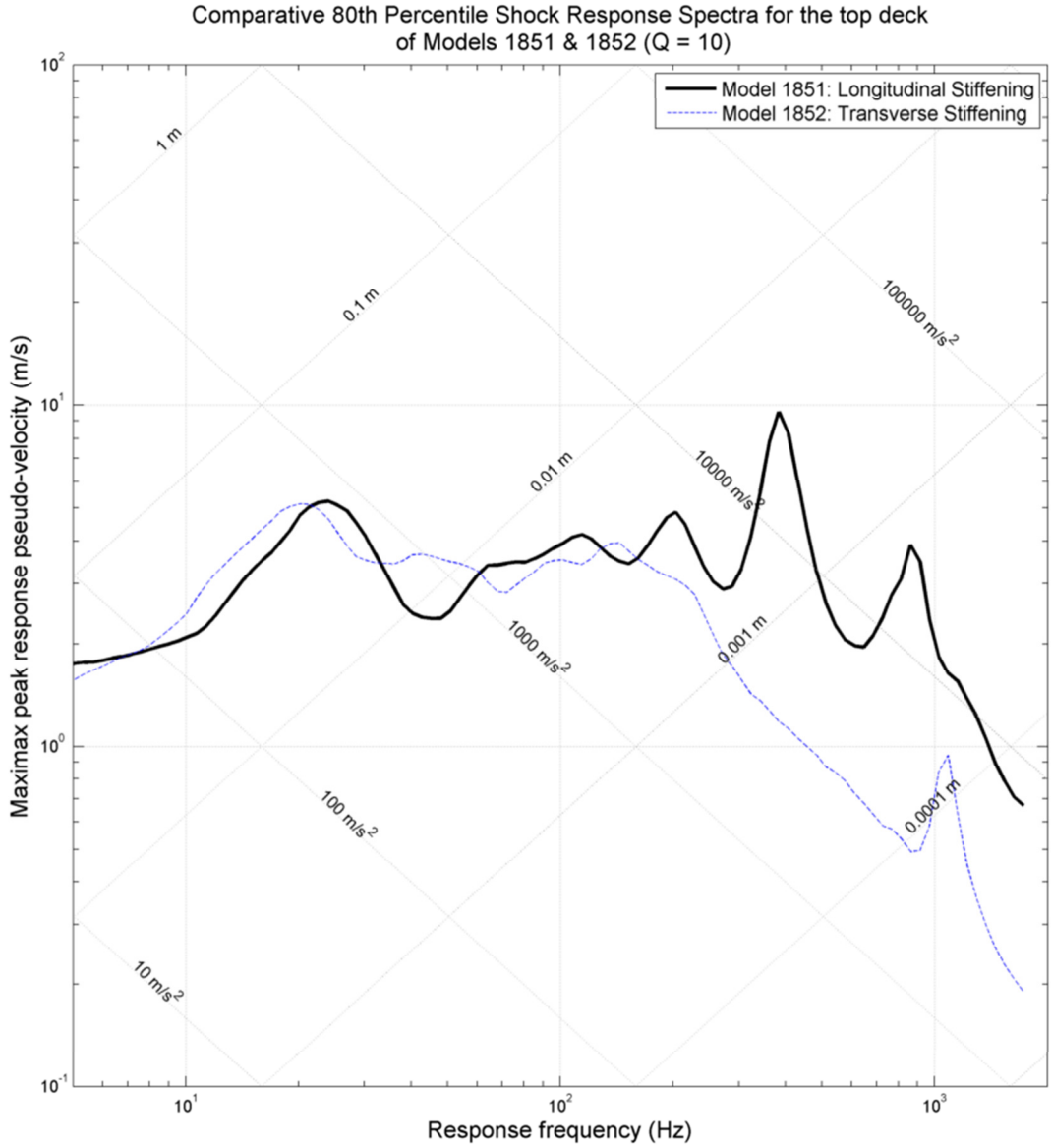

Figure 7.3.1 - Comparative 80th Percentile SRS for the Top Deck region of the third experimental series (Models 1851 & 1852, longitudinal vs. transverse stiffening)

From Figure 7.3.1, the following observation was drawn:

i. Below 200Hz the two models behaved similarly. Above 200Hz the transversely stiffened model (Model 1852) experienced motions much lower than the Baseline Corvette (Model 1851); between 0.15 and 0.7 times the Baseline response.

7.3 b Series 3 (longitudinal/transverse), Passing Deck region (see Figure 6.2.2)

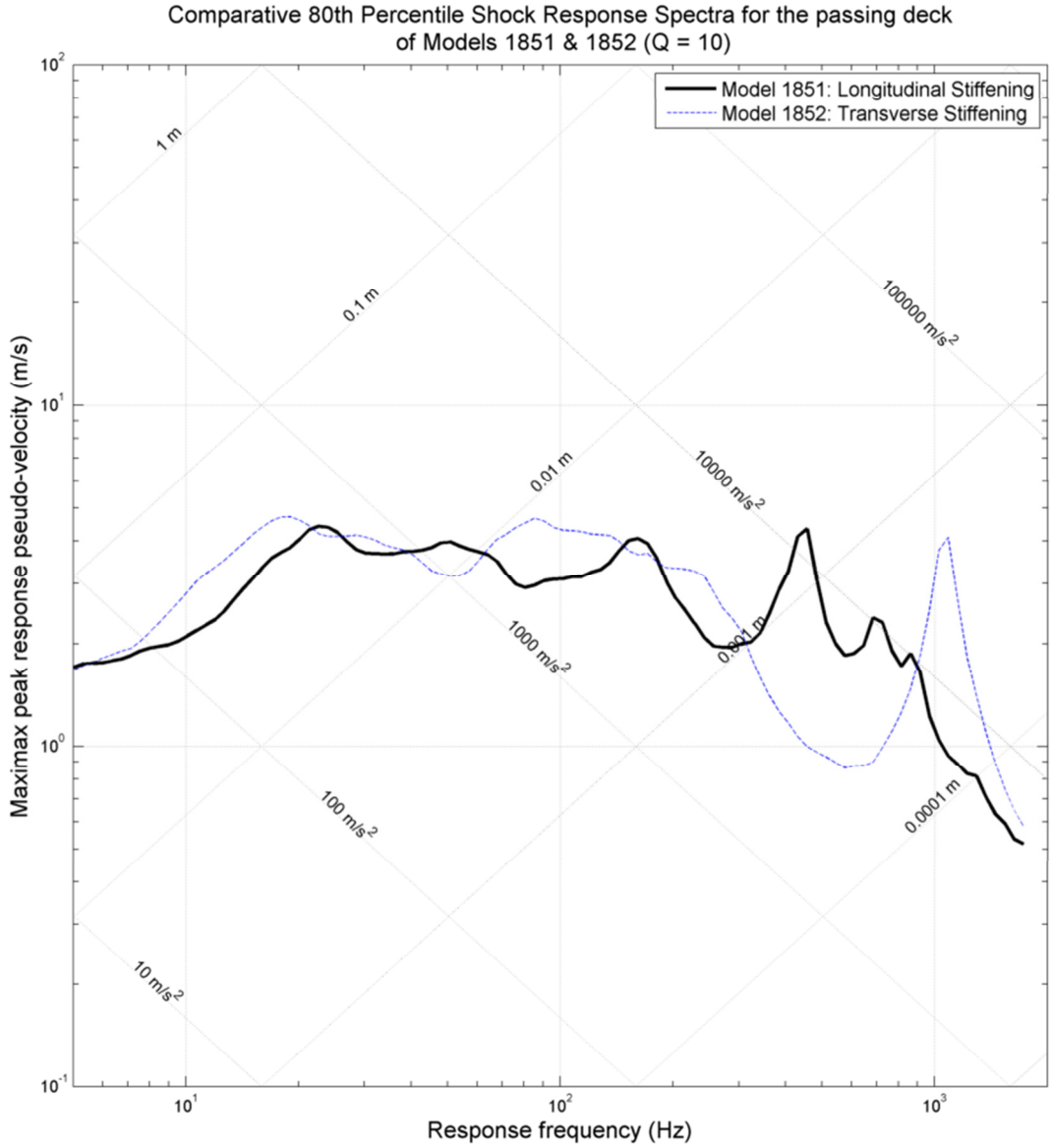

Figure 7.3.2 - Comparative 80th Percentile SRS for the Passing Deck region of the third experimental series (Models 1851 & 1852, longitudinal vs. transverse stiffening)

From Figure 7.3.2, the following observation was drawn:

i. The two models (Models 1851 and 1852) behaved similarly across the whole frequency range. Their peaks and troughs occurred at slightly different frequencies but are of similar magnitudes.

7.3 c Series 3 (longitudinal/transverse), Upper Side Shell region (see Figure 6.2.2)

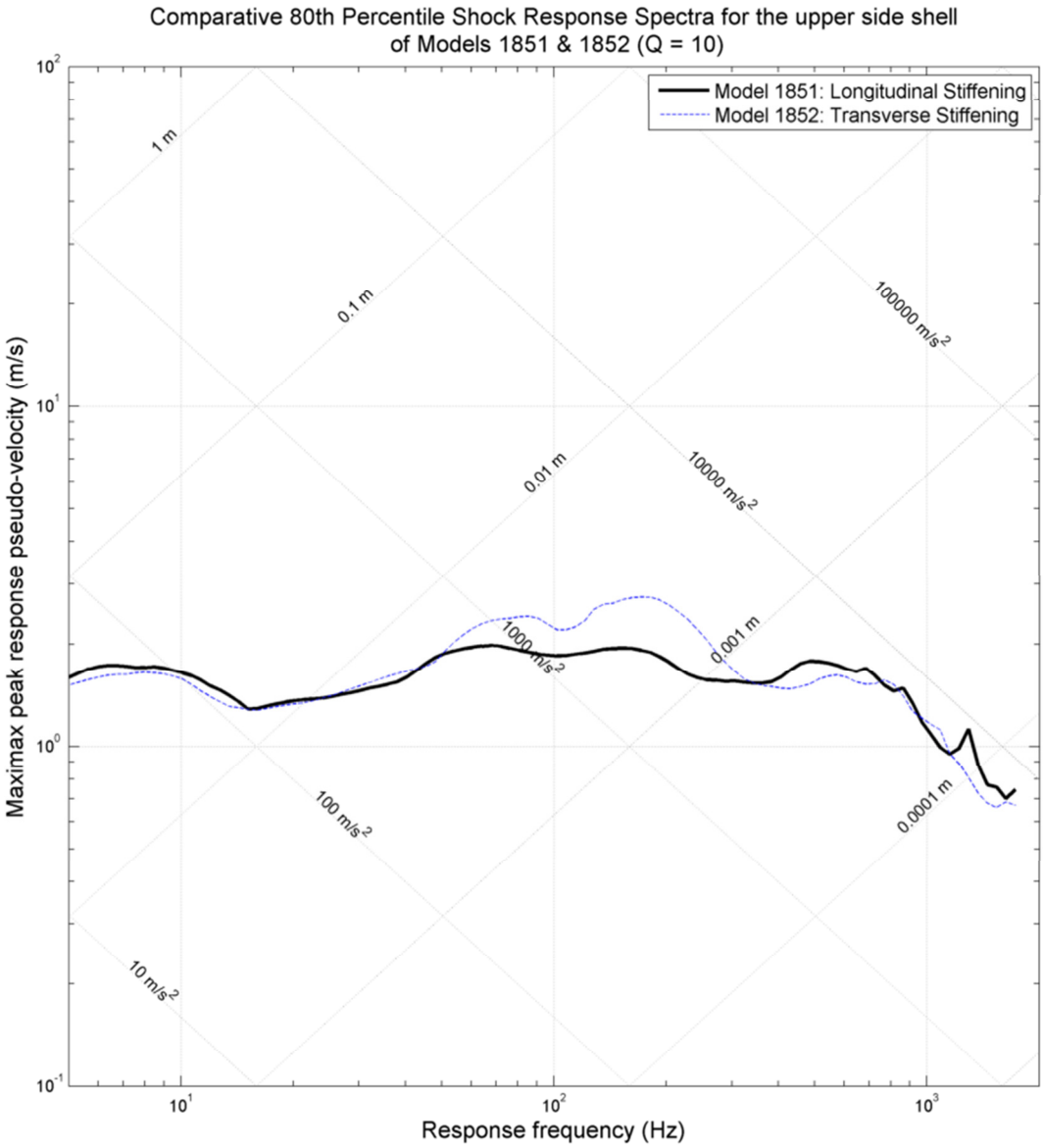

Figure 7.3.3 - Comparative 80th Percentile SRS for the Upper Side Shell region of the third experimental series (Models 1851 & 1852, longitudinal vs. transverse stiffening)

From Figure 7.3.3, the following observation was drawn:

i. The two models (Model 1851 and 1852) behaved very similarly over the entire frequency range; the only deviation of note occurring between 50Hz-300Hz where the transversely stiffened structure (Model 1852) experienced motions up to 1.4 times the Baseline Corvette (Model 1851.)

7.3 d Series 3 (longitudinal/transverse), Wetted Side Shell region (see Figure 6.2.2)

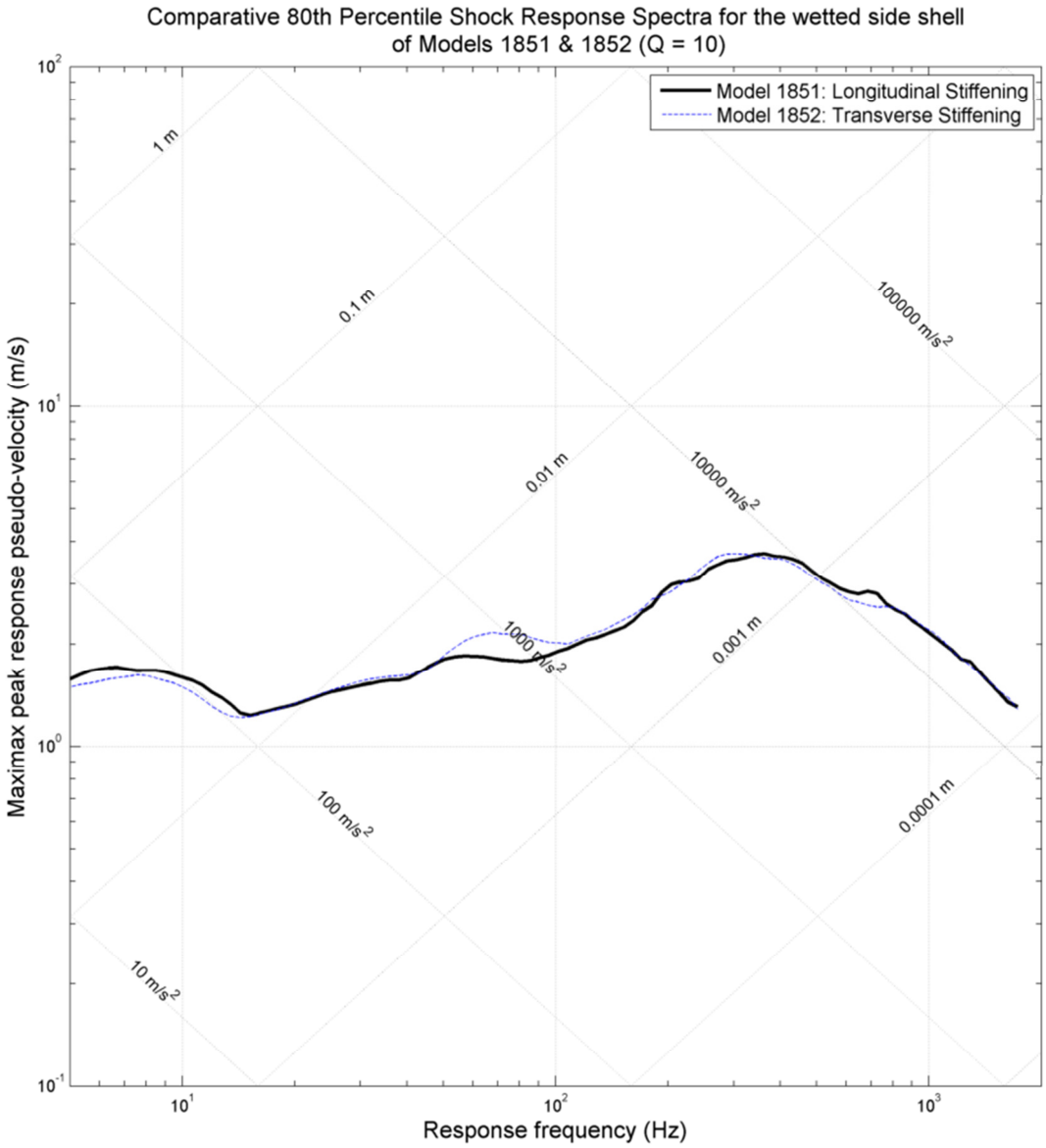

Figure 7.3.4 - Comparative 80th Percentile SRS for the Wetted Side Shell region of the third experimental series (Models 1851 & 1852, longitudinal vs. transverse stiffening)

From Figure 7.3.4, the following observation was drawn:

i. The two models (Model 1851 and 1852) behaved very similarly over the entire frequency range.

7.3 e Series 3 (longitudinal/transverse), Inner Bottom region (see Figure 6.2.2)

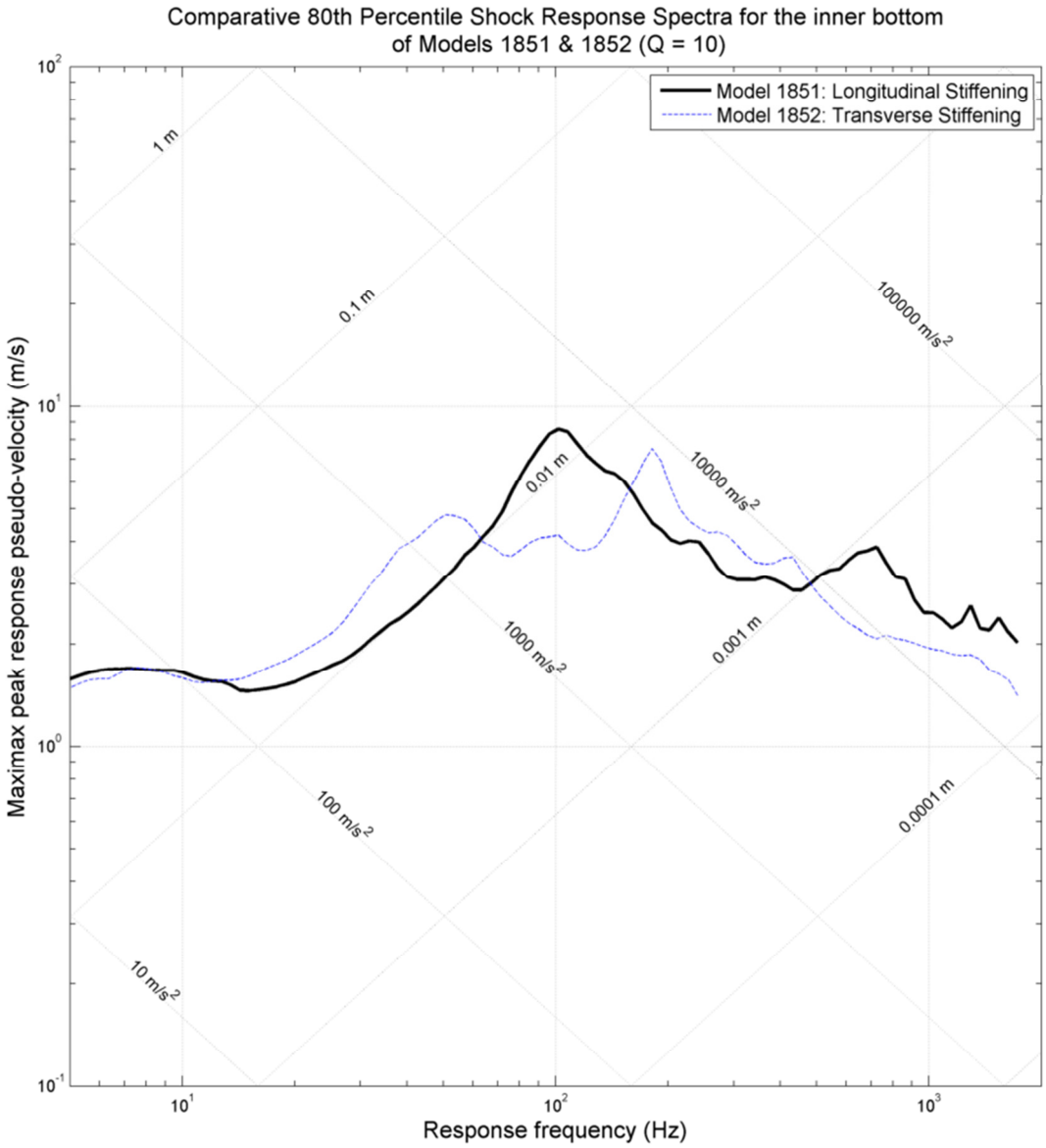

Figure 7.3.5 - Comparative 80th Percentile SRS for the Inner Bottom region of the third experimental series (Models 1851 & 1852, longitudinal vs. transverse stiffening)

From Figure 7.3.5, the following observation was drawn:

i. The two models (Model 1851 and 1852) behaved similarly over the frequency range; the frequencies of response peaks and troughs differed but the magnitudes of response were similar, and the response of the transverse model (Model 1852) remained within 0.45 – 1.6 times that of the Baseline model (Model 1851) at all frequencies.

7.3 f Series 3 (longitudinal/transverse), Outer Bottom region (see Figure 6.2.2)

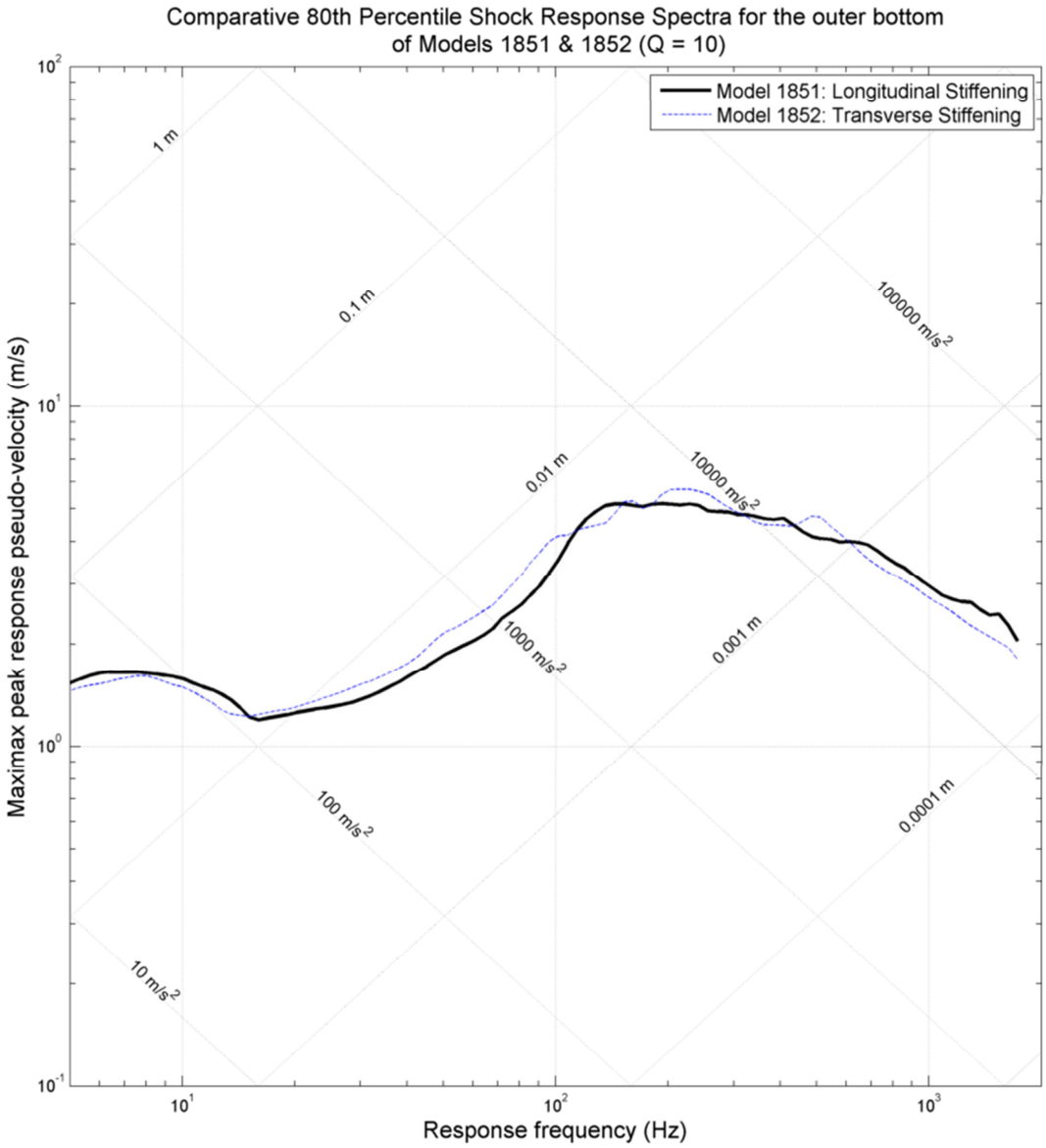

Figure 7.3.6 - Comparative 80th Percentile SRS for the Outer Bottom region of the third experimental series (Models 1851 & 1852, longitudinal vs. transverse stiffening)

From Figure 7.3.6, the following observation was drawn:

i. The response of the two models was similar at all frequencies.

7.3 g Summary of Results from Series 3

Below the waterline, the two models (Model 1851 and 1852) behaved very similarly. There was exceptionally good agreement between the two in the wetted plating of the Outer Bottom and Wetted Side Shell; the difference never exceeding 25% of the Baseline Corvette model's response.

There was good agreement between the two models in the Upper Side Shell; the response of Model 1852 always within the range 0.7 – 1.5 of the Baseline Corvette model's response.

The response spectra of the Inner Bottom and Passing Decks of the two models displayed a similar shape, with similar response magnitudes, although differences in peak and trough frequencies between the two models meant that responses at any given frequency there might be a difference of up to 60% of the Baseline model's response.

The response of the upper decks was similar between the two models, except above 200Hz where the transversely-stiffened model (Model 1852) experienced significantly reduced motions.

Chapter 8 Discussion

This chapter is divided into three sections. First, the results of the study are examined in terms of the research aims defined in Chapter 1, to assess whether those aims had been met by the current research. The chapter then contains an examination of various methodological choices which had been made during the research and considers whether, with the benefit of hindsight, they might have been better made differently. The final section contains miscellaneous observations made during the research which were considered sufficiently interesting to mention.

8.1 Assessment of results in the context of the Research Aims

The research aimed to broadly quantify the impact on shock response motions of the various structural styles considered. This was considered important, primarily to determine whether the consequences of such style differences were sufficient that existing shock response prediction tools would remain valid if such structural styles were adopted, or whether modification to the prediction tools would be required.

Considering each of the three style changes in turn:

8.1 a Series 1 – Reduction in Longitudinal Stiffener Numbers

The results clearly showed that the reductions in stiffener numbers considered could result in significant changes to the UNDEX shock response motions. Table 8.1.1 summarises the general behaviour of the models within Series 1, in terms of their motions relative to the Baseline (Model 1801.) (See Figure 6.2.2 for the arrangement of the regions described.)

Table 8.1.1 - Comparison of the peak shock response motions in the models of Series 1 (reduction in number of longitudinal stiffeners)

Region	**Model 1802** **Moderate stiffener reduction**	**Model 1803** **Extreme stiffener reduction**
Outer Bottom	<250Hz: 1.0-2.5 x baseline >250Hz: Similar to (0.9-1.1 x) baseline	<250Hz: 1.0-3.8 x baseline >250Hz: Similar to (0.9-1.1 x) baseline
Wetted Side Shell	<200Hz: 1.0-2.1 x baseline >200Hz: Similar to (0.9-1.1 x) baseline	<200Hz: 1.0-2.0 x baseline >200Hz: Similar to (0.8-1.1 x) baseline

Inner Bottom	<200Hz: 1.0-2.3 x baseline >200Hz: Similar to (0.8-1.5 x) baseline	<200Hz: 1.0-3.8 x baseline >200Hz: Similar to (0.6-1.1 x) baseline
Upper Side Shell	1.0-1.8 x baseline	1.0-4.0 x baseline
Passing Deck	Similar to (0.4-1.4 x) baseline	Similar to (0.7-1.7 x) baseline
Top Deck	<150Hz: 1.0–1.9 x baseline >150Hz: Similar to (0.3-1.2 x) baseline	<150Hz: 1.0-1.6 x baseline >150Hz: 1.5-7.9 x baseline

In most regions of the ship, there were frequency ranges in which the changing structural style had minimal impact on the shock response motions compared to those of the 'traditional style' baseline frigate. Low in the ship, at high frequencies, the response was almost indistinguishable between all three models. Higher in the ship the response motions tended to vary more with changes in response frequency; the peaks and troughs of these variations occurred at different frequencies in the three models. Thus, even when the average response motions over a frequency range remained similar for all three models, there were usually local differences at any given frequency. In those ranges where responses differed significantly between models (underwater regions at low frequencies (see frequency ranges in Table 8.1.1), Upper Side Shell at all frequencies and Top Deck at high frequencies) there was usually an increase in response moving from the Baseline model to the moderately simplified model (Model 1802), and a further increase moving to the extremely simplified model (Model 1803). It therefore appears that there is a correlation between reduction in the number of stiffeners and increased peak response motions.

Adopting a moderate degree of reduction in stiffener numbers (Model 1802) led to response motions up to approximately twice as severe as those for the Baseline model. Adopting an extreme degree of longitudinal stiffener reduction (Model 1803) led to response motions between two and four times as severe as the Baseline model below the waterline, and up to eight times as severe in the Top Deck. A shock response prediction tool which does not account for this choice of structural style is therefore likely to under-predict shock response motions to a degree unacceptable from a survivability design point of view, even if only a moderate reduction in stiffener numbers was adopted.

8.1 b Series 2 – Stiffener Cross Sectional Profile

Series 2 was not a continuum, but a comparison of two independent alternatives to the Baseline model frigate style of Admiralty standard long-stalk tee-bar longitudinal stiffening. The results showed that using these cheaper stiffener profiles could lead to significantly increased shock response motions at certain frequencies. The results from Series 2 are summarised in Table 8.1.2.

Table 8.1.2 - Comparison of the peak shock response motions in the models of Series 2 (alternate stiffener section profiles)

Region	**Model 1804** **Offset bulb plates**	**Model 1807** **Flat bar stiffeners**
Outer Bottom	<250Hz: 1.0-2.3 x baseline >250Hz: Similar to (0.9-1.1 x) baseline	<250Hz: 1.0-2.5 x baseline >250Hz: Similar to (1.0-1.1 x) baseline
Wetted Side Shell	<100Hz: 1.2-2.0 x baseline >100Hz: Similar to (0.9-1.2 x) baseline	<100Hz: 1.1-2.1 x baseline >100Hz: Similar to (0.9-2.0 x) baseline
Inner Bottom	<200Hz: 1.0-2.0 x baseline >200Hz: Similar to (0.8-1.9 x) baseline	<200Hz: 1.0-2.0 x baseline >200Hz: Similar to (0.9-1.5x) baseline
Upper Side Shell	<250Hz: 1.0-2.0 x baseline >250Hz: 1.0-1.9 x baseline	<250Hz: 1.0-2.0 x baseline >250Hz: 1.2-3.1 x baseline
Passing Deck	1.5-9.0 x baseline	0.8-5.2 x baseline
Top Deck	<250Hz: 1.0-1.6 x baseline >250Hz: 0.6-3.7 x baseline	<250Hz: 1.0-1.7 x baseline >250Hz: 0.8-4.6 x baseline

As with Series 1, the influence of adopting these stiffening style changes was different above and below the waterline. Below the waterline, there was very little difference (especially in the plating directly fluid-loaded) between all three models at response frequencies above 250Hz, yet responses for the “commercially” stiffened models up to twice the size of those for the Baseline model (Model 1801) at lower frequencies, i.e. below 250Hz. Above the waterline there was less frequency dependency, with moderate to substantial increases in response at all frequencies in both the simplified models. While there was a marked difference in response between the Baseline model and both of the simplified models, the two simplified models

behaved similarly to one another, where the only substantial difference between them in response occurred in the Passing Deck.

In general, the use of either OBP or flat bar stiffeners led to motion responses up to twice those seen in the Baseline Model with long-stalk tee bars, with some frequency ranges in the Passing Deck and Top Deck experiencing significantly greater motions (see Table 8.1.2.) A shock response prediction tool, based exclusively upon data from trials of long-stalk T-bar stiffened ships and which does not account for the choice of stiffener profile, may therefore significantly under-predict the motions of a structure which uses OBP or flat bar stiffeners for a given intensity of shock load.

8.1 c Series 3 – Longitudinal and Transverse Stiffening

Series 3 comprised a pair of models, one a baseline with conventional longitudinally stiffened structure (Model 1851) and one with transversely stiffened structure with the same frame spacing. Both models were based on a candidate-developed 92m corvette design (described in Section 5.5) since transversely stiffened structure would have been sufficiently inefficient in a much longer frigate-type ship as to be an implausible design choice. The results from Series 3 are summarised in Table 8.1.3. Generally speaking, there appeared to be no negative implications of adopting a transversely stiffened structure.

Table 8.1.3 - Comparison of the peak shock response motions in the models of Series 3 (longitudinally vs. transversely stiffened structure)

Region	**Model 1852** **Transversely-stiffened structure**
Outer Bottom	Similar to (0.9-1.3 x) baseline (Model 1851)
Wetted Side Shell	Similar to (0.9-1.2 x) baseline (Model 1851)
Inner Bottom	Similar to (0.5-1.6 x) baseline (Model 1851)
Upper Side Shell	Similar to (0.7-1.5 x) baseline (Model 1851)
Passing Deck	Similar to (0.3-4.4 x) baseline (Model 1851)
Top Deck	<200Hz: Similar to (0.6-1.5 x) baseline (Model 1851) >200Hz: 0.1-0.7 x baseline (Model 1851)

On the wetted plating of the Outer Bottom and Wetted Side Shell, the response motions were generally indistinguishable between the two models, with deviations of small magnitude (up to 30%) over specific frequency ranges.

On the Inner Bottom, Upper Side Shell and Passing Deck the response motions between the two models were of similar shape but with greater local deviations. While there was one narrow peak in the Passing Deck (around 1kHz) where the transversely stiffened model's (Model 1852) response exceeded that of the Baseline Corvette Model (Model 1851) by a factor of 4.4, for the most part the response of Model 1852 was within 0.5 - 1.6 times the response of Model 1851.

On the Top Deck, the two models responded similarly at frequencies below 200Hz, above which the transversely stiffened model (Model 1852) exhibited significantly reduced motions, ranging between 0.15 – 0.7 times the response of the baseline Model 1851.

The similarity of response between these two models contrasted with the marked change in response between the models of Series 1. As the stiffener and frame spacing in Series 1 increased, the resulting motions increased as well. In Series 3, moving from small to large spacing between the longitudinal stiffeners, while keeping the frame spacing the same, resulted in negligible increases in response. It is possible that frame spacing has a stronger effect on response motions than longitudinal stiffener spacing for this size of vessel, although a more extensive study, discussed further in Section 9.3, would be required to determine whether or not that was truly the case.

8.1 d The validity of the current (Environmental Shock Grade Curve Scheme) regime over the range of variations in structural style considered

Given the results appeared to show that adopting these structural styles could lead to significantly changed response motions, it was of interest to determine to what degree each style could be adopted before significant changes were observed; that is, whether there was a degree to which a structural design style could be adopted without requiring the style choice to be taken into account in an existing shock response prediction tool such as the Environmental Grade Curve Scheme (EGCS) in use by the UK Ministry of Defence. Elements of the EGCS are Protectively Marked and therefore cannot be considered here, but the effects of the structural style changes on shock response extreme motions can be discussed in general terms.

The results from Series 1 showed that most regions of even the moderately simplified frigate structural model (Model 1802) experienced shock response motions approximately twice those of the Baseline frigate (Model 1801), for certain ranges of frequency. While this was a small study, with only three models, it seemed clear that adopting even the moderate level of reduction in stiffener numbers seen in Model 1802 relative to the Baseline (Model 1801), can

lead to significant enough increases in motions (approximately double the peak motions of the baseline model in most regions) that account should be taken of them in a shock response prediction procedure. A more extensive study, as discussed in Section 9.3, would be required to show whether some degree of simplification of the structural complexity typical of naval combatants could be adopted in future naval ship designs without unacceptable impact upon the shock response extreme motions, and hence on the equipment survivability under shock loads.

The results from Series 2 showed that the use of both OBPs and flat bar stiffeners resulted in significant increases in response motions, compared to the responses of the same strength structure with conventional naval style T-bar longitudinal stiffening. Both simplified models (Models 1804 and 1807) exhibited responses up to double those of the Baseline model (Model 1801) response in regions below the waterline, and up to even greater factors (ranging from 4 – 9 times the baseline) in the regions higher in the ship. Since this series was not changing a continuous variable but rather switching between three discrete choices for stiffener style, it is considered that the evidence is sufficient, without requiring further study, to suggest that use of any non-standard stiffeners may cause sufficient changes in the shock response extreme motions to require that a prediction procedure take such style departures into account.

The results from Series 3 showed minimal impact in moving from longitudinally to transversely stiffened structure; either no significant change or, in the Top Deck, actually resulting in a reduction in the extreme response motions. It appears that existing shock response prediction tools based on data derived from naval-style longitudinally-stiffened structures are likely to remain valid for transversely-stiffened structures of similar size, although it is recognised that the test sample was small at just two models (Model 1851 and 1852) and for one specific naval combatant design.

8.1 e Whether the approach taken in the current research provides a suitable basis for a more extensive investigation of the topic

A number of the aspects already noted in previous chapters are considered worthy of a more extensive follow-up study conducted on a larger number of structural designs and establishing a suitable method for such a study was one of the aims of the current research.

Such a study would allow a better understanding of such issues as to whether there is a degree of stiffener reduction that can be adopted without significant impact on the shock response, or whether the frame spacing has a greater effect on the shock response than the longitudinal stiffener spacing. However, the modelling process described in Chapter 3 was relatively time

consuming to conduct and would require some development before being able to address a study which contained a significantly larger number of structural models. The feasibility of a larger study would rest upon whether the structural model design process could be streamlined and automated, reducing the time to produce each structural model from days to minutes or seconds.

Much of the existing method for producing ship structures meeting equivalent strength requirements but using different structural styles would be relatively straightforward to incorporate into a more automated study, but there are a few areas where more development work is considered necessary. To add an element of automation to the structural assessment process, Visual Basic for Applications (VBA) code could be written to control the structural design spreadsheet. The code could substitute for the actions currently undertaken by the human operator, namely, setting the input variables; running the iteration routine to derive a structure; and exporting the design outputs (see Appendix B). None of these actions are difficult to code in VBA so this is considered to be a low risk task. An automated method for designing bulkhead stiffening schemas would also have to be developed. This is also considered to be a relatively straightforward task, except for designing the bulkhead stiffening to integrate well with the hull shell stiffening around the turn of bilge (See Section 3.6 b, especially Figure 3.6.6.) To reiterate the issues raised in Section 3.6 b, the geometry in this region requires a compromise between good structural continuity, avoiding very acute angles of intersection between stiffeners and ensuring enough space around each joint to enable welding. While it ought to be possible to express this algorithmically, in the current research it was quicker to design each bulkhead manually than to produce an automated tool. This tool would therefore have to be developed from scratch; a task seen as involving moderate risk.

It would be necessary in any more extensive investigation to develop an automated process for generating structural cross section drawings from the outputs of the design spreadsheet. It is felt that this could readily be done using AutoCAD (Autodesk Inc., 2013) script, or by writing MATLAB (The Mathworks, Inc, 2013b) code to directly create a DXF file. Either task would require a fairly significant amount of effort, and a moderate amount of risk. It would also be necessary to write TCL scripts within HyperMesh (Altair Engineering, Inc., 2011) to create the first strip of surface panels from the cross sectional drawings (see Section 3.6 b.) This is likely to require a significant amount of effort and moderate risk.

With the completion of the above four tasks, a complete automated workflow could exist to create ship structural designs of equivalent strength based on a variety of structural styles,

create cross sectional drawings and convert those drawings into a mesh model suitable for FEA. Once the mesh model had been the subject of a fluid-structure interaction shock simulation, the existing automated workflow could be used to convert the results produced into shock response spectrum diagrams such as those produced in the current research, e.g. Figure 7.1.1. Thus, in summary, the method demonstrated appears suitable for scaling up to a more extensive study, but there remain a relatively small number of developmental tasks, which would have to be undertaken to enable a larger scale study to be efficiently performed.

8.2 Critical assessment of modelling choices

This section offers commentary on a number of decisions taken when developing the approach taken in the current research, with the aim of applying the benefit of hindsight to examine whether they were sound choices or whether a different choice might have offered a better solution. They are considered under three broad categories: the scope of the research undertaken; the design and modelling of the ship structures investigated; and the nature of the shock response simulation.

8.2 a Scope of Research

i) Separation of the modelling of internal motions from consideration of structural failure

A decision was made early in the current research to examine the impact of style changes on the internal response motion environment, and not to attempt to model the impact of the style changes on structural failure or the hull lethality shock factor. Two aspects revealed by the results support this decision. Firstly, the investigation found that the internal response motions were strongly sensitive to two of the three style changes considered. The study was therefore considered wide enough in scope to provide some definite insights. Secondly, to have expanded the scope to include modelling of structural failures would have significantly increased the extent of the research. The importance of joint detail design in structural failure under shock loading is widely acknowledged (Chalmers, 1993). If models were to be produced with the required level of high resolution detail in way of structural connections, then mesh size and computation time considerations would almost certainly have pushed towards a sub-modelling strategy, where a whole-ship model at low definition resolved the general motions, which could then have been applied as boundary conditions to a smaller, much more detailed model of the joint, where stresses could be calculated. While EPSA would be capable of modelling whole-ship motions, it has no facility to model motions as boundary conditions so

another package would have to be obtained (or devised) to handle the sub-models. Using a different FEA package, without the in-depth support provided to the candidate by Weidlinger Associates, or having to create interfaces between two packages, would have added substantially to the extent of work required and probably required a much larger research programme.

ii) Extent of each model series

There was a necessary trade-off between the number of simulations within each series, and the number of style changes which could be addressed. It was hoped that using two to three simulations per style investigation would give a reasonable feel for the impact of each style change, while allowing three different style changes to be examined.

Series 2 and 3 examined discrete quantities – adding additional simulations to the study would add breadth rather than depth, by allowing the simulation of additional different types of stiffener profile, or combinations of hybrid longitudinal/transverse stiffening. There were no obvious candidates for additional stiffener types, and exploration of hybrid structural designs by the candidate appeared to show no obvious benefits over either transverse or longitudinal stiffening schemes. Without specific cases of interest, it was not considered worthwhile to expand those particular series.

The models in Series 1 represent points in a potentially continuous series (varying stiffener spacing), so adding more models in would give a better understanding of how the response motions varied as the style changed. However, this series was not truly a continuous one; since an integer number of frame spacings had to fit within the devised 12m transverse bulkhead spacing so only a limited number of design points were possible. (The models in the series fit 8, 6 and 4 frame bays between bulkheads.) A few more design points could be added to the series, but a substantial expansion would require adjustment of the bulkhead spacing which, in turn, would require an additional (albeit useful) study to examine the sensitivity of the results to bulkhead spacing.

The results from Series 1 showed that, in both the variant cases considered, adopting a reduction in the number of stiffeners generally brought increases in peak shock response motions. It would therefore be useful to expand the series, particularly over the region between Model 1801 (the Baseline frigate) and Model 1802 (with moderate reduction in stiffener numbers), to explore whether there might be a region where structural simplifications could be made without negatively impacting the shock response motions. It would also be of interest to vary longitudinal stiffener spacing and transverse frame spacing

independently of one another. However, both of these additions to the study were considered less informative than conducting Series 2 and 3, in what was a first pass at understanding the topic.

iii) Acceptability of using a single shock geometry and size of explosive charge

A single charge was considered to be sufficient to determine that structural style had an impact on shock response motions at one particular shock factor. It would be useful to conduct simulations with larger or smaller charges, and with greater and lesser standoff distances, to determine if the effects revealed in this research remain as significant at other shock factors. It might be of particular interest to see whether the effect of each structural style change on shock response is consistent at lower shock factors, particularly for levels at which the structure remains purely in the elastic stress range. It would therefore be advantageous to undertake additional studies at a range of shock factors, however this remains an option for follow-up research.

iv) Consideration of equipment items of varying mass

At sub-lethal shock factors, for the purposes of the ship's ability to continue functioning, the motions of the structure are of less interest that the motions of equipment items mounted upon it. It can be intuitively appreciated that, while a lightweight piece of equipment might have little effect on the motions of the structure upon which it sat, a heavier piece of equipment might influence the motions of the structure. The effect of a different structural style might therefore have less effect upon a heavier piece of equipment than a lighter one.

It would be useful to the ship structural designer to establish the effect of different structural styles on a variety of equipment of different masses, to determine whether there was an upper mass threshold above which the structural style has little influence, a lower mass threshold below which the equipment mass had little effect on motions, and whether that lower mass threshold varied with structural style.

The greatest difficulty in carrying out such a study is seen to be that, while the motions of several thousand nodes within the structure can be interrogated from within an FE model for analysis, only a few items of equipment could be added to such a model without influencing each other's motions. Furthermore, the motions of each equipment item would be likely to be sensitive to its particular location, so multiple runs with equipment in different locations might be required to give a sufficiently comprehensive picture of its likely response motions. These two factors would combine to require a number of simulation runs significantly greater than those conducted for the current research.

Additionally, the modelling of the equipment mounting arrangements would need to be realistic. For small items (<100kg) which would be mounted at a single point, a clumped point mass would be an appropriate idealisation, which is likely to be possible using EPSA. However, more massive items like gearboxes or prime movers are typically mounted over several frames, requiring a connection between several mounting points, either with rigid rods connected to a point mass, or some form of plate/solid model of the equipment itself. Without some further investigation, it is unclear as to how sensitive the results might be to these different modelling configurations.

Thus, while consideration of equipment item mass would be a desirable subject for a follow-up study, this is seen to be a potentially substantial scope of work.

v) Choice of style parameters for analysis

The structural styles chosen for examination were based on the recommendations made by Chalmers (1986) as the most likely candidates for cost saving in naval ships. From this investigation. these recommendations appear to remain valid. OBPs are already in use in current warships, and their use appears to significantly influence shock response motions (see Section 7.2.) Increased stiffener spacing stands to offer reasonably noticeable initial structural cost savings (Bradbeer and Andrews, 2012a), insofar as any structural style change can give a meaningful saving, given the small fraction of a warship's cost represented by structural materials and fabrication. However, such changes also bring potentially large changes in shock response.

In light of the results, it would be interesting to explore the overlap between Series 1 and 3. In Series 1, the panel aspect ratio was held constant, so stiffener and frame spacing were increased together, and significantly increased shock response motions were measured (typically up to 200% – 400% of the baseline motions in most regions) with increasing spacing - see Figure 7.1.1. In Series 3 the frame spacing was held constant and the longitudinal stiffener spacing varied, with no significant change (usually less than 140% of the baseline motions and frequently much lower) in shock response motions observed. From the limited data from two series, with just five structures modelled, it would appear that choice of frame spacing may affect shock response motions much more strongly than varying the longitudinal stiffener spacing. However, this conclusion relies on a comparison of two series which used markedly different ship designs (a 6,000te frigate and a 1,000te corvette), furthermore one only contained only two data points. It would therefore be interesting to examine the impact of

varying frame spacing and stiffener spacing independently of one another, on a common hull design with more variants.

vi) Selection of hull type

The NFR-90 Frigate hull was selected for analysis on the basis that it was a typical NATO surface combatant design, whose structural style was representative of the NATO Cold War warship style, and for which sufficient detail of structural design was available in an unclassified publication. Each of these aspects was important to the current research, and furthermore there were few other possible candidate ship designs.

The size of Royal Navy surface combatants is increasing. The previous class of destroyers, the Type 42, designed in the 1960s, had a design deep displacement of 4,300 tonnes (for Batch 1 ships) up to 5,350 tonnes (Batch 3 ships). Their replacement, the Type 45 has a design displacement of approximately 8,000 tonnes. Similarly, the currently in-service Type 23 Frigates, designed in the 1980s, had a design deep displacement of 4,900 tonnes, while their planned replacement the Type-26 global combat ship, has had published design concepts displacing between 5,500 and 7,000 tonnes (New and Steven, 2011; Saunders, 2012). With a design displacement of 5,400 tonnes (Schaffer and Kloehn, 1991) the NFR-90 Frigate design fell in the middle of this range, and can be considered representative in terms of size of modern RN surface combatants. The NFR-90 Frigate design is similar to existing RN surface combatants in terms of layout and general ship, but not the style of its structural design.

The need to design a corvette structure to explore the option of transversely-stiffened structure does beg the question of whether it would have been more useful to conduct the investigations of all three structural design style series on a baseline corvette hull design, but the option of the NFR-90 Frigate design allowed for comparison with an existing published design, although it was never developed past the feasibility design phase, and allowed comparison of the simulated results with shock trials data for ships of a similar size and internal configuration.

8.2 b Structural Design and Modelling

i) Choice of modelling method to produce representative ship structures

The structural designs produced by the procedure outlines in Chapter 3 appeared to be reasonably similar to those for real ships. In particular, the NFR-90 Frigate model designed for this research using the UK SSCP-23 method was considered close enough, at the level of detail

developed, to the real NFR-90 design as described by Schaffer and Kloehn (1991) to give confidence in the structural design model.

While the variant structures produced lacked real ships of the same structural style to allow a direct comparison, given that the purpose of the design approach devised was to produce a methodical series indicative of a particular design structural style, this was considered acceptable. It was also considered more important to maintain a consistent approach throughout the series than to adopt changes typical of real designs likely to be introduced for ease of manufacture in a shipyard.

ii) Material property choices

The modelling of the material properties in the shock response simulations used a combination of the low strain-rate properties appropriate for B-Quality crack arrest steel and the high strain-rate properties of mild steel, due to a lack of available data for the high strain rate properties of B-Quality steel. The high strain-rate properties defined the stress level at which the material transitioned from elastic into plastic behaviour and were based on strain rate. It is possible that this introduced errors into the findings of the analysis. It was assumed that the effects of this inconsistency in material properties on the results was small and that the high strain rate behaviour of B-Quality steel is similar to that of mild steel. In the event that better data was made available, it would be a reasonably straightforward task to rerun the models with improved material properties. Since the structural design spreadsheet uses static material properties only, changing the high strain rate properties of the material would not require any changes to the model geometry and the only changes required would be an adjustment to the values of a small number of variables in the EPSA input file (See Section 3.7 aiii)).

iii) The representation of structural connections

The study used idealised joints between all structural components, where the two adjacent components were perfectly bonded with no pre-stress. Real structural connections (particularly the sophisticated arrangements in typical naval structures; see (Faulkner, 1964)) are more complex, with pre-stresses from welding and often with complex local features to reduce stress concentration. Joint design is widely regarded as critical to determining the hull lethal shock factor (Chalmers, 1993). The stresses experienced by the modelled joints were moderate (see Figure 6.1.1.) Much of detail design of structural connections is concerned with allowing the real joint to behave as closely as possible to an ideal connection (Faulkner, 1964). Therefore, while further work to establish the behaviour of structural connections modelled in

more detail would be useful, it is considered that modelling structural connections in more detail would not have materially affected the conclusions of the current research.

Real structural connections also have an important role in damping structural motions (Betts, Bishop and Price, 1976). This was reflected in the Rayleigh damping coefficients used in the study (see Section 3.7 a). The values for these coefficients were based on studies conducted with full-scale warship trials data (Shin and Ham, 2003).

iv) Stiffener depth correction

Some effort was expended in an attempt to correct errors resulting from the representation of solid stiffeners as plate elements. As described in Section 3.6 a, there was a concern that the relatively large thickness of the modelled plates, relative to their width, meant that double-counting of areas around plate intersections might lead to significant errors in the effective second moment of area of stiffeners. A calculation process was built into the structure design spreadsheet to reduce the stiffener web depth in order to give the stiffener (including an area of shell plate acting with the stiffener in bending) the correct second moment of area. It was found that the typical correction was on the order of 1% of second moment of area. Given the magnitude of the change in shock response arising from structural style changes (on the order of 100%-300%) it seems unlikely that the correction would have had any meaningful impact on the results.

It should not be assumed, of course, that a 1% change in second moment of area of a stiffener would correspond to a 1% change in peak response pseudo-velocity. To check the magnitude of the effect of the correction would have required additional simulation runs to compare results, and given the likelihood of the changes having no significant effect on the results, it was felt that this error was not worth additional time and effort in the current research.

8.2 c Shock Response Simulation

i) The use of FUSE/EPSA toolsets to simulate shock response

The combination of FUSE/EPSA (Atkash, Bieniek and Baron, 1983; Weidlinger Associates, Inc., 2009) produced results which were considered to compare favourably to the various validation baselines described in Chapter 4. Fluid/structure interaction by finite element analysis is a mature discipline and widely used for shock response prediction, as outlined in Chapter 2. FUSE/EPSA was selected over other, similar explicit FE solvers (e.g. ABAQUS (Dassault Systemes, 2013), LS-DYNA/USA (Livermore Software Technology Corporation, 2013)) largely on

the basis of availability and support provided to the candidate, but there is no indication that any other solver would have provided an advantage.

The use of an explicit (rather than implicit, see Section 2.6 b) solver had several advantages beyond the primary benefit of reduced solution time for a high-speed impact model requiring many small timesteps. Explicit validity conditions meant that there was no requirement to confirm solution convergence; instead it was merely necessary to comply with the Courant-Friedrichs-Lewy condition (see Section 3.7 a). The lack of a requirement to find an equilibrium between internal and external forces at each timestep allowed the construction of a FEA model without boundary conditions. This was the simplest way to measure the motions of a floating free body, and one which avoided the complication of introducing artificial internal forces resulting from artificial boundary condition constraints. The models constructed for analysis by EPSA conformed to Weidlinger Associates' best-practice guidelines (Stultz, 2009) for element aspect ratio, element internal angle and shape characteristics.

ii) Modelling the shockwave response separately from the bubble pulse response

A similar logic is considered to apply to the choice of modelling the structural response to the initial shock pulse and not the bubble pulse phase. The current research found that there were distinct changes in response motions between different structural styles during the shock phase, so the loading regime chosen was considered sufficient to give useful results. Also, modelling the bubble pulse phase was calculated to have required the simulated time period to have been increased from 200ms to several seconds, raising the computational runtime considerably (i.e. from less than a day to an estimated more than a week per run.)

A follow-up study into the effects of different structural styles on bubble pulse response is considered to be a useful addition, but, since the effect of most concern was considered to be bubble-induced hull whipping (Reid, 1996), that study might well be better served by conducting linear static modal analysis. This could establish the natural frequencies of the hull girder's primary modes of vibration and observe how these frequencies change with changing structural styles, relative to the frequency of the bubble pulse. The EPSA toolset does not offer this capability, so while this is an obvious topic for follow-up research, the effort required is considered to be non-trivial. In addition, Chalmers (1988) strongly suggests that any such change in natural frequency is likely to be very small.

iii) Shock severity level

Given that simulations were only conducted at a single shock factor, it is appropriate to consider the choice of shock factor. The shock factor level applied in the current research was chosen with the intention of providing a stressing level of loading which would have ensured the loaded structure entered the plastic regime but would not have exceeded ultimate tensile stress and ruptured. Examining stress contour plots of the structures post-explosion, plastic deformation is clearly indicated, but the Cauchy J2 stress (Ragab, 1999) remained below the ultimate tensile stress. This suggests the shock was sufficient to induce severe motions as desired, but not so severe as to invalidate the assumptions of the model, which are only valid for the intact case.

8.3 Miscellaneous observations

This section raises some observations which were made during the investigation. These were considered interesting enough to note, but did not relate directly either to whether the investigation had met its aims or to the assessment of choices made regarding the research approach taken.

8.3 a Optimum scantling design dependent upon design rules

Two models of the NFR-90 Frigate structure were developed; the simulation model using Lloyds NSR2 Naval Ship Rules (Lloyds Register, 2008), and the validation model developed using SSCP-23 (Chalmers, 1993). These allowed comparison with the actual NFR-90 Frigate's structural design. In each case, a variety of different stiffener spacings were examined (retaining the same panel aspect ratio, so stiffener and frame spacings were varied in proportion) and the weight of each compared.

Under SSCP-23, 600mm stiffener spacing with 1500mm frame spacing gave the lightest structure. (Encouragingly, this was the same spacing as used in the real NFR-90 Frigate design, which would have used similar design rules.) However, when designing with NSR2, the lightest weight structure was obtained with 800mm stiffener spacing and 2000mm frame spacing. It appears that the reason for this is that NSR2 mandates a minimum stiffener depth (in the forms of web depth and cross sectional area) for a given load, and this minimum depth results in closely stiffened structures being unable to use the smaller stiffeners they would need in order to realise the weight savings that would be possible under SSCP-23. It is therefore questionable as to whether Model 1802 (with 800mm x 2000mm spacing) should have been

considered the baseline design under NSR2, as it seems unlikely any designer would elect for a design which was both heavier and more expensive to achieve just the same strength.

Similarly, the use of offset bulb plate stiffeners actually resulted in a lighter structure than similarly-spaced long-stalk tee bars, which was unexpected. The weight saving was small; approximately 0.75%, but an increase had been anticipated. The majority of the weight savings in the comparison came from the frames and bulkheads. The limit state of the frames was driven by the same failure modes in both structural configurations, so the weight difference was not driven by the increased depth of the OBPs driving up frame depth. Similarly, the two bulkheads were designed to the same stiffener schema. The cause of the weight saving is not clear.

8.3 b Responses at specific frequencies

There were large fluctuations in peak response motion amplitudes in the baseline NFR-90 Frigate model (Model 1801) over the 5Hz-30Hz range. These fluctuations were present throughout the entire model, and entirely absent in all other models. The cause is not apparent.

Many models had a localised peak in response amplitude at around 600-700Hz. This is equivalent to a response cycle period of approximately 1.5ms, which matches the period of the initial shockwave pressure pulse for the charge used. This peak therefore reflects the strong component of the loading corresponding to that initial pressure pulse.

8.3 c Shock Response Spectrum shapes did not match those expected

Typically, shock response spectra are expected to have a shape which has three sections: a near-constant displacement section at low frequencies; a near-constant velocity ‘plateau’ section in the middle of the frequency range; and a near-constant acceleration section at high frequencies (Gaberson, 2012; Hall, 2002). SRS of this shape may be simple characterised by three variables; the frequencies at which the plateau begins and ends, and the pseudo-velocity of the plateau (Gaberson, 2012). The shapes of the SRS generated by the simulations conformed to this shape only very generally. It is possible that this occurred because the shock intensity used in the simulations was higher than that typically used in (British) full-scale trials, and that a simulation at a lower shock factor would give a narrower plateau with more clearly defined constant displacement and constant acceleration regions. It is also possible that the discrepancy arose due to the large quantity of data available from the simulations compared to the data available from a small number of instruments in a full scale trial, to which a smooth curve was subsequently fitted. This could also have been due to the real built structures

containing fabrication details not fully modelled by the simple structural models used in the current research or even the effects of equipment, seatings and distributed systems not modelled.

Chapter 9 Conclusions

This chapter summarises the main conclusions from the current research and makes recommendations for the ship designer in light of those findings, together with suggestions for future work to provide further insight into the topic.

9.1 Summary of the research findings

This thesis suggests that the adoption of certain simplified structural styles in warships can lead to significantly elevated shock response motions, compared to those expected from a ship with a more typical naval structural style.

Most of these simplified structural styles result in motions increased by a degree significant enough that account should be taken of them when specifying the shock tolerance or mounting arrangements for on-board equipment.

9.2 Recommendations for ship structural designers

Cost pressures are continuing to drive warship designers to consider adopting simplified structural styles. The findings of this investigation provide the designer with evidence of the effect those choices appear to have on the structure's shock response motions. Three specific style choices were investigated with each leading to a specific recommendation:

9.2 a Reduction in number of stiffeners

Adopting reductions in the number of stiffeners compared to typical naval structural practice may lead to significant increases in shock response motions. In the cases simulated, moderate reduction in the number of stiffeners (increasing spacing from 600mm x 1500mm to 800mm x 2000mm) resulted in peak accelerations approximately twice as large in most regions of the midship section of a frigate design. More extreme reduction (with a spacing of 1200mm x 3000mm) resulted in peak accelerations up to four times as large below the waterline, and eight times as large in the Top Deck compared to a baseline design of a style more typical of naval structural designs.

Should a structure with a reduced number of stiffeners be under consideration, then it is recommended that the designer takes care to ensure that the shock tolerance and mounting arrangements of on-board equipment is specified to take into account these likely increased accelerations. This may have significant implications for outfit costs.

9.2 b Use of cheaper stiffener cross-sectional profiles

The use of offset bulb plates or flat bar stiffeners instead of long-stalk tee bars may lead to significant increases in shock response motions. In the cases simulated, the performance of the structures with the two alternative stiffener types was similar. Below the waterline, each resulted in peak accelerations approximately twice those of the tee bar structure. Higher in the ship they resulted in peak accelerations up to four times as high, with narrow frequency regions in the Passing Deck even higher.

Should a structure stiffened by offset bulb plates or flat bars be under consideration, then it is recommended that the designer takes care to ensure that the shock tolerance and mounting arrangements of on-board equipment is specified taking into account these likely increased accelerations. This may have significant implications for outfit costs.

i) Adoption of transversely or longitudinally stiffened structure

The use of transversely-stiffened or longitudinally-stiffened structure appeared to have negligible impact on the peak shock response motions, although only structures for a smaller ship, where longitudinal bending was not the driving load case, were conducted in the current research.

The designer might expect that a shock response prediction tool designed to work for longitudinally stiffened structure could also prove appropriate for predicting the response of a transversely stiffened structure. Care should be exercised before extrapolating this result to longer ships where longitudinal bending drives the structural design.

9.3 Recommendations for future work

There are a number of areas in which further work could usefully add to the findings of the current research. These are grouped under the aspects of: extending the scope of the study; and exploring the effect of changing structural style on the hull lethality shock factor.

9.3 a Expanding the scope of the study

While this research would seem to demonstrate that changing the stiffener spacing or its profile can cause significant changes in the shock response motions for a typical naval combatant, this was done for only a limited number of simulations. Undertaking a more extensive set of simulations would offer a better understanding of the relationships between these structural parameters and the shock response motions. The following areas would particularly benefit from further simulations:

i) Expanding the range of stiffener spacings considered

It would be useful to include additional structural models into Series 1, to give a better understanding of the relationship between stiffener spacing and peak shock response motions. At present, with only three data points, it is difficult to have full confidence in the relationship, beyond acknowledging that increased spacing would seem to lead to increased motions. Filling in the gaps, particularly around the Baseline Model's stiffener spacing of 600mm, is seen to be particularly useful. This could identify whether there is a 'plateau' region where spacing can be varied without significant change in response motions.

Additionally, it would be useful to explore the effects of varying the stiffener spacing and frame spacing independently of one another. The contrast between Series 1, where increasing the spacing of both increased the response motions significantly, and Series 3, where increasing the spacing of the longitudinals while fixing the frame spacing had very little effect on the response motions, suggest that the response motions might be more sensitive to the frame spacing than to the stiffener spacing. However, these two series were conducted using distinctly different baseline ship designs, which may also have influenced the results, so additional structures would need to be subjected to shock response analysis before this conclusion could be made with any great assurance.

ii) Expanding the range of ship sizes simulated

All the simulations undertaken used a 130m frigate or a 92m corvette design. It would be useful to determine whether the conclusions that were drawn for these ships can be generally applied over a wider range of displacements, or whether with changes in ship size the shock response motions are consistently sensitive to structural style. In particular, it would be interesting to investigate very large ships, of the 20-60,000 tonne range typical of current Royal Navy capital ships.

iii) Material properties

The simulations conducted assumed that the behaviour of B-Quality crack-arresting steel at high strain rates was similar to that of mild steel at similar strain rates. It would be useful to determine whether this assumption had a significant effect on the results. In particular, it would be important to determine this before attempting to investigate structural failure effects (see Section 9.3 b), as the high strain rate behaviour is likely to have a significant effect on the ultimate strength of the structure.

iv) Different charge sizes

All the simulations conducted used a single charge size, chosen to provide a significant, but sub-lethal, shock factor (the exact level of which cannot be discussed, at the request of the UK Ministry of Defence). Previous work into ship response to underwater shock has found that shock response motions typically vary in linear proportion to shock factor (Keil, 1961; Reid, 1996), so it seems reasonable to assume that the shock response impact of the structural style changes considered in this research could be read across a range of shock factors. However, it would be sensible to extend the research to ensure that assumption is valid by collecting the same set of data at a range of different shock factors.

v) Equipment weights

The investigation did not address the effect of equipment weight on the sensitivity of response motions to structural style changes (see Section 8.2 a.) Intuitively it seems likely that very massive pieces of equipment (namely equipment whose mass would be large compared to the structure on which they were mounted, typically several tonnes in mass) might be considerably less sensitive to style changes, particularly when mounted below the waterline and therefore almost directly fluid-loaded. While very useful, this additional investigation would require some changes in the method of simulation; only a limited number of weighted items could be included in each simulation, and a means of systematically designing mounting arrangements between different structural styles would be required. This seems an important, if complex and extensive, programme of research.

9.3 b The impact of changing structural styles on hull lethal shock factor

The current research did not investigate whether changing structural styles had an effect on the intensity of shock loading that a structure could withstand before undergoing a catastrophic failure, but that is an important consideration, worthy of further investigation. Work would be necessary in two areas, since underwater explosions typically cause catastrophic damage via two different mechanisms: widespread flooding following structural rupture from the shockwave; and loss of structural integrity following whipping of the hull girder.

i) Natural frequencies

Whipping is a phenomenon caused by resonant oscillation of the hull girder (Reid, 1996; Belcher, 2008), one cause of which can be an underwater explosion whose gas bubble pulsation period is similar to a natural period of longitudinal vibration of the hull girder. The susceptibility of a structure to damage is therefore a function of girder strength (in longitudinal

bending) and the associated natural frequency of vibration. Since the structures in the three series presented were designed to have equivalent bending strength, the characteristic of interest is the associated natural frequency. It is therefore of interest to investigate to what degree changing the structural style also changes the longitudinal natural frequencies in low modes of vibration. This is seen to be important as a significant change could tune or de-tune the structure relative to typical torpedo warhead explosions.

This investigation would probably best be undertaken using a linear static finite element solver to perform eigenvalue solution (Astley, 1992). However, the entrained mass of water moving with the hull under the dynamic load is likely to have a significant effect on the solution for modal vibration and may complicate the analysis.

ii) Joint detail modelling and hull lethal shock factor effects

The susceptibility of ship structures to catastrophic failure under shock wave loading requires a far more detailed structural model, particularly in way of stress concentrations, together with a material model which could simulate tensile failure. The conflicting requirements of mesh size, timestep length and simulation time are likely to require either substantially greater computing power than was used in the current research, or the use of a sub-modelling strategy. In the latter case, detailed models of the joints would draw on boundary conditions provided from the motions of a coarser model of the whole structure, such as those generated in the current research, which might therefore provide a starting point for such a study.

References

Alexander, J., 2009. Shock Response Spectrum - A Primer. *Sound and Vibration Magazine*, [online] June 2009. Available at: <http://www.sandv.com/downloads/0906alex.pdf> [Accessed 15 Jan. 2013].

Altair Engineering, Inc., 2011. *Altair HyperMesh - Finite Element Pre Processor*. [Corporate Website] Altair.co.uk. Available at: <http://www.altairhyperworks.co.uk/Product,7,HyperMesh.aspx> [Accessed 15 Jan. 2012].

Andrews, D.J. and Brown, D.K., 1982. Cheap Warships Are Not Simple. In: *Combined Symp. on Ship Costs and Energy*. New York: Society of Naval Architects and Marine Engineers.

Andrews, D.J. and Pawling, R.G., 2003. SURFCON - A 21st Century Ship Design Tool. In: A. Papanikolaou, ed., *Proc. 8th Intl Marine Design Conf*. Athens: IMDC.

Arena, M.V., Blickstein, I., Younossi, O. and Grammich, C.A., 2006. *Why Has the Cost of Navy Ships Risen? - A Macroscopic Examination of the Trends in US Naval Ship Costs Over the Past Several Decades*. [online] Santa Monica: RAND. Available at: <http://www.rand.org/pubs/monographs/2006/RAND_MG484.pdf>.

Ashe, G. et al., 2006. ISSC Committee V.5 - Naval Ship Design. In: *Proc. of the 16th Intl. Ship and Offshore Structures Congress*. Southampton: ISSC, pp.213–262.

Astley, R., 1992. *Finite Elements in Solids and Structures: An Introduction*. Illustrated ed. New York, NY: Springer.

Atkash, R.S., Bieniek, M.P. and Baron, M.L., 1983. Dynamic Elasto-Plastic Response of Shells in an Accoustic Medium - EPSA Code. *International Journal For Numerical Methods in Engineering*, 19, pp.811–824.

Australian Collins class submarine torpedo. 1999. [FLV Flash Video] Directed by Royal Australian Navy. Royal Australian Navy. Available at: <http://www.youtube.com/watch?v=SLrKOOXcOhM> [Accessed 30 May 2013].

Autodesk Inc., 2013. *Autodesk AutoCAD*. [online] Autodesk Corporate Website. Available at: <http://www.autodesk.co.uk/products/autodesk-autocad/overview> [Accessed 4 Jun. 2013].

Belcher, M., 2008. *Survivability Primer - An Introduction to Naval Combat Survivability*. Halifax: Canadian Department of National Defence.

Benson, D.J., 1992. Computational methods in Lagrangian and Eulerian hydrocodes. *Computer Methods in Applied Mechanics and Engineering*, 99(2-3), pp.235–394.

Betts, C.V., Bishop, R.E.D. and Price, W.G., 1976. A Survey of Internal Hull Damping. *Trans. Royal Institution of Naval Architects*, 119, pp.125–142.

Billingham, J., Sharp, J., Spurrier, J. and Kilgallon, P., 2003. *Review of the performance of high strength steels used offshore*. [HSE Research Report] Cranfield, UK: Cranfield University, p.115. Available at: <http://www.hse.gov.uk/research/rrpdf/rr105.pdf> [Accessed 17 Dec. 2012].

Bole, M. and Forrest, C., 2005. Early stage integrated parametric ship design. In: *Proc. 12th Intl. Conf. on Computer Applications in Shipbuilding*. Busan, ROK: ICCAS.

Bradbeer, N., 2010. *Frigate Development Kit*. Unpublished. London: UCL Marine Research Group.

Bradbeer, N. and Andrews, D., 2012a. Affordability, Ship Impact and Shock Response Implications of Simpler Warship Structural Styles (Revised). In: *WARSHIP 2012: The Affordable Warship*. Bath, UK: RINA.

Bradbeer, N. and Andrews, D., 2012b. Shock Response Implications of Lower-Cost Warship Structural Styles. Proc. 11th International Marine Design Conference. Glasgow: IMDC.

British Standards Institution, 1991. *BS 4848-2 - Hot-rolled structural steel sections. Specification for hot-finished hollow sections*. [online] London: British Standards Institution. Available at: <http://shop.bsigroup.com/ProductDetail/?pid=000000000000233418>.

Brown, D.K., 1987a. Post War Trials: Tests against Destroyers. In: *Warship 41*. London: Conway Maritime Press, pp.28–34.

Brown, D.K., 1987b. Ship Trials. In: *Warship 44*. London: Conway Maritime Press, pp.243–248.

Brown, D.K., 1987c. Ship Trials: Tests against Cruisers. In: *WARSHIP 42*. London: Conway Maritime Press, pp.106–108.

Brown, D.K., 1987d. Ship Trials: Tests against submarines. In: *Warship 43*. London: Conway Maritime Press, pp.183–186.

Brown, D.K., 1990. The Battleworthy Frigate. *Trans. NECIES*, 106, pp.117–126.

Brown, D.K. and Tupper, E.C., 1989. The Naval Architecture of Surface Warships. *Trans. RINA*, 131, pp.29–44.

Burgan, B., 2001. *Elevated temperature and high strain rate properties of offshore steels*. [Offshore Technology Report] Ascot, UK: Health and Safety Executive, p.151. Available at: <http://www.hse.gov.uk/research/otopdf/2001/oto01020.pdf> [Accessed 17 Dec. 2012].

Cardarelli, F., 2008. *Materials Handbook: A Concise Desktop Reference*. 2nd ed. New York, NY: Springer.

Caridis, P.A. and Frieze, P.A., 1989. Flexural-torsional elasto-plastic buckling analysis of stiffened plates using dynamic relaxation. Part 2: Comparison with test results and other formulations. *Thin-walled structures*, 7(1), pp.37–72.

Chalmers, D., 1986. Structural Design for Minimum Cost. In: *Advances in Marine Structures*. Intl. Conf. on Advances in Marine Structures`. ARE Dunfermline: Elsevier, pp.650–669.

Chalmers, D., 1988. The Sensitivities of the Resonant Frequencies of Ships' Hulls to Changes in Mass and Stiffness. *Trans. RINA*, 130, pp.329–334.

Chalmers, D., 1993. *Design of Ships Structures*. London: HMSO.

Clements, E., 1972. *Shipboard Shock and Navy Devices for its Simulation*. Washington, DC: US Naval Research Laboratory, p.132.

Cole, R.H., 1948. *Underwater Explosions*. Princeton, NJ: Princeton University Press.

Courant, R., Friedrichs, K. and Lewy, H., 1967. On the Partial Difference Equations of Mathematical Physics. *IBM Journal of Research and Development*, 11(2), pp.215–234.

Cunniff, P. and Pohland, R., 1993. *On the feasibility of a transient dynamic design analysis*. College Park, MD: Department of Mechanical Engineering, University of Maryland, p.40.

Dassault Systemes, 2013. *ABAQUS Overview - Dassault Systemes*. [Corporate Website] Dassault Systemes. Available at: <http://www.3ds.com/products/simulia/portfolio/abaqus/overview/> [Accessed 4 Jun. 2013].

Delgado, J., Lenihan, D. and Murphy, L., 1991. *The Archaeology of the Atomic Bomb: A Submerged Cultural Resources Assessment of the Sunken Fleet of Operation Crossroads at Bikiki and Kwajalein Atoll Islands*. [online] Santa Fe, NM: US Department of the Interior National Park Service and the US National Maritime Initiative Submerged Culture Resources Unit, p.208. Available at: <http://www.nps.gov/submerged/PDF/NNPS_903_D160_[38840]pg0000.pdf> [Accessed 6 May 2013].

Didoszak, J.M., Shin, Y.S. and Lewis, D.H., 2004. Shock Trial Simulation for Naval Ships. In: *ASNE Day 2004*. Monterey, California: ASNE.

Faulkner, D., 1964. Welded Connections used in Warship Structures. *Transactions of the Royal Insititution of Naval Architects*, 106, pp.39–70.

Fisher, E. and Parr, A., 1967. Mathematical model analysis for the dynamic design of machinery. *Experimental Mechanics*, 7(10), p.27a–34a.

Fung, S. and Liebman, L., 1995. Revised speed-dependent powering predictions for high-speed transom stern hull forms. In: *FAST95*. 3rd Intl. Conf. on Fast Sea Transportation. Lubeck-Travemunde, Germany: Schiffbautechnische Gessellschaft, pp.151–164.

Gaberson, H., 2012. Shock Severity Estimation. *Sound and Vibration Magazine*, [online] Jan 2012. Available at: <http://www.sandv.com/downloads/1201gabe.pdf> [Accessed 6 Jun. 2013].

Geers, T.L., 1994. Doubly asymptotic approximations for transient motions of submerged structures. *Journal of Applied Mechanics*, 61, pp.893–906.

Greenhorn, J., 1999. The Assessment of Surface Ship Vulnerability to Underwater Attack. *Trans. Royal Institution of Naval Architects*, 131, pp.233–244.

Van Griethuysen, W.J., 1992. On the Variety of Monohull Warship Geometry. *Transactions of the Royal Insititution of Naval Architects*, 134, pp.277–298.

Grzeskowiak, S., 1988. A U.S. Navy Shock Trial. *Journal of Naval Engineering*, 31(2), pp.351–356.

Hall, W., 2002. Chapter 24: Vibration of Structures Induced by Ground Motion. In: *Harris' Shock and Vibration Handbook*, Fifth Edition. New York: McGraw-Hill.

Hammond, L. and Saunders, D., 1997. *The Applicability of Scaling Laws to Underwater Shock Tests*. [DSTO Public Report] Melbourne, Australia: DSTO Aeronautical and Maritime Research Laboratory, p.27. Available at: <http://www.dtic.mil/cgi-bin/GetTRDoc?AD=ADA342636> [Accessed 11 Jan. 2012].

Hicks, A., 1986. Explosion Induced Hull Whipping. In: *Advances in Marine Structures*. Intl. Conf. on Advances in Marine Structures. ARE Dunfermline: Elsevier Applied Science Publishers, pp.390–410.

Hudson, B., Shepherd, D. and Ferris, J., 1996. Warship design: what's so different? A Canadian experience. In: *Intl. Naval Engineering Conf. 96 - Warship design: What is so different?* INEC 1996. London: Institution of Marine Engineers.

Hunter, K.S. and Geers, T.L., 2004. Pressure and velocity fields produced by an underwater explosion. *The Journal of the Acoustical Society of America*, 115(4), p.1483.

Irvine, T., 2006. *SRS.M*. [MATLAB] Available at: <http://www.mathworks.co.uk/matlabcentral/fileexchange/7398-shock-response-spectrum/content/srs.m>.

Irvine, T., 2012. *An introduction to the shock response spectrum (Revision S)*. [online] Available at: <http://www.vibrationdata.com/tutorials2/srs_intr.pdf> [Accessed 15 Jan. 2013].

Kehoe, J., Brower, K., Meier, H. and Runnerstrom, E., 1983. US and foreign hull form, machinery and structural design practices. *ASNE Naval Engineers Journal*, Nov 1983, pp.36–53.

Keil, A.H., 1961. *The Response of Ships to Underwater Explosions*. Carderock, MD: US Department of the Navy: David Taylor Model Basin.

Lasdon, L.S. and Waren, A.D., 1981. GRG2. *ACM SIGMAP Bulletin*, (30), pp.10–11.

Law, A.M. and Kelton, W.D., 1991. *Simulation modeling and analysis*. New York, NY: McGraw-Hill.

Leissa, A.W., 1973. The free vibration of rectangular plates. *Journal of Sound and Vibration*, 31(3), pp.257–293.

Livermore Software Technology Corporation, 2013. *LS-DYNA | Livermore Software Technology Corporation*. [Corporate Website] Livermore Software Technology Corporation. Available at: <http://www.lstc.com/products/ls-dyna> [Accessed 4 Jun. 2013].

Lloyds Register, 2008. *Rules and Regulations for the Classification of Naval Ships, Volume 1, Part 3-6, Ship Structures*. London: Lloyds Register.

MacDonald, T., 2010. *X-Topology Frigate Hull Generator*. Unpublished. London, UK: UCL Marine Research Group.

Mair, H., Reese, R. and Hartsough, K., 1999. *Simulated Ship Shock Tests/Trials?* Alexandria, VA: Institute for Defense Analysis.

Mair, H.U., 1999. Review: Hydrocodes for structural response to underwater explosions. *Shock and Vibration*, 6, pp.81–96.

Ministry of Defence, 1974. *CB 5012*. UK Protectively Marked: UK Ministry of Defence.

Ministry of Defence, 1989. *Design of Surface Ship Structures*. UK: Sea Systems Controllerate, UK Ministry of Defence.

Ministry of Defence, 2000. *Defence Standard 02-791 Requirements for Weldable Structural Steels*. Glasgow: UK Defence Standardisation.

Mulligan, R.D. and Courts, M.D., 1998. Corvette Design Considerations. In: *WARSHIP 98 - Surface Warships: the Next Generation*. London: RINA.

New, C. and Steven, G., 2011. The contradictions in modern naval asset management and their resolution. [online] IET, pp.23–23. Available at: <http://digital-library.theiet.org/content/conferences/10.1049/cp.2011.0544> [Accessed 10 Jun. 2013].

O'Hara, G., 1958. *Effect upon shock spectra of the dynamic reaction of foundations*. [NRL Report] Washington D.C.: US Naval Research Laboratory. Available at: <http://www.dtic.mil/cgi-bin/GetTRDoc?AD=AD0209366>.

O'Hara, G., 1959. Impedance and Shock Spectra. *J. Acoust. Soc. Am.*, 31(10), pp.1300–1303.

O'Hara, G., 1965. *Background for mechanical shock design of ships systems*. Washington D.C.: US Naval Research Laboratory, p.20.

O'Hara, G. and Belsheim, R., 1963. *Interim Design Values for Shock Design of Shipboard Equipment*. Washington, DC: US Naval Research Laboratory, p.24.

Pawling, R., 2009. Annex A: Hullform Generation Using Quickhull. In: *Paramarine Surface Ship Early Stage Design Training Course for Warship Design*. London, UK: Graphics Research Corporation.

Purvis, M.K., 1974. Post War Frigate and Guided Missile Destroyer Design 1944-1969. *Trans RINA*, 116, pp.189–222.

QinetiQ, 2013. *Paramarine*. [Corporate Website] QinetiQ GRC. Available at: <http://www.grc.qinetiq.com/products/paramarine/Pages/default.aspx> [Accessed 10 Jun. 2013].

Ragab, A.-R.A.F., 1999. *Engineering solid mechanics: fundamentals and applications*. Boca Raton, FL: CRC Press.

Reid, W., 1996. *The Response of Surface Ships to Underwater Explosions*. Melbourne: Australian Defence Science and Technology Organisation.

Rich, H. et al., 1961. *Extract from Operation HARDTACK Project 3.3 - Shock loading in ships from underwater bursts and response of shipboard equipment*. Washington D.C.: David Taylor Model Basin.

Rubin, S., 2002. Chapter 23: Concepts in Shock Data Analysis. In: *Harris' Shock and Vibration Handbook*, Fifth Edition. New York NY: McGraw-Hill.

Russell, D.M., 1997. Error Measures for Comparive Transient Data: Part 1: Development of a Comprehensive Error Measure. In: *Proc. 68th Shock and Vibration Symposium*. 68th Shock and Vibration Symposium. Hunt Valley, MD: Shock And Vibration Information Analysis Centre, pp.175–184.

Saunders, S., 2012. *IHS Jane's fighting ships 2012-2013*. Coulsdon: IHS Jane's.

Schaffer, R.L. and Kloehn, H.G., 1991. Design of the NFR-90. *ASNE Naval Engineers Journal*, 103(2), pp.29–49.

Shin, Y., 1993. Overview of Underwater Shock and DDAM. In: *Short Course:* 64th Shock and Vibration Symposium. Fort Walton Beach, FL: SAVIAC.

Shin, Y., Didoszak, J. and Christian, T., 2005. *NPS Shock Team*. [online] Available at: <http://www.nps.edu/research/Documents/SVCL_web_sanitized.ppt>.

Shin, Y. and Schneider, N., 2003. Ship Shock Trial Simulation of USS Winston S. Churchill (DDG 81): Modeling and Simulation Strategy and Surrounding Fluid Volume Effects. [online] 74th Shock and Vibration Symposium, 2003. .Available at: <http://www.nps.edu/Academics/GSEAS/svcl/docs/saviac%20ship%20shock%20paper%202003.pdf> [Accessed 2 Dec. 2009].

Shin, Y.S., 2004. Ship shock modeling and simulation for far-field underwater explosion. *Computers & Structures*, 82(23-26), pp.2211–2219.

Shin, Y.S. and Ham, I., 2003. *Damping Modelling Strategy for Naval Ship System*. Monterey, CA: US Naval Postgraduate School.

Smith, C.S., 1976. Compressive Strength of Welded Steel Ship Grillages. *Trans. Royal Institution of Naval Architects*, pp.325–359.

Socitec UK, 2013. *Socitec UK Products Overview*. Available at: <http://www.socitec.co.uk/Overview.html> [Accessed 17 Jan. 2013].

Van der Struis, P.M., Janssen, M.C.W.M. and Vries, T., 1996. The LCF Programme: A Step towards an afforable warship. In: *Intl Naval Engineering Conf 96 - Warship design: What is so different?* London: Institution of Marine Engineers.

Stultz, K., 2009. *EPSA Software Seminar*.

Swisdak, M., 1978. *Explosion Effects and Properties: Part II - Explosion Effects in Water*. Silver Spring, MD: Naval Surface Weapons Center.

Taylor, G.I., 1941. The Scientific Papers of G I Taylor, vol III. In: C.U. Press, ed. Cambridge, MA: US Office of Naval Research, pp.287–303.

The Mathworks, Inc, 2013a. *Butterworth filter design in MATLAB*. [MATLAB Documentation Centre] Available at: <http://www.mathworks.co.uk/help/signal/ref/butter.html> [Accessed 3 Jun. 2013].

The Mathworks, Inc, 2013b. *MATLAB*. [online] The Mathworks, In. Corporate Website. Available at: <http://www.mathworks.co.uk/> [Accessed 3 Jun. 2013].

Thompson, P., 2003. *Shock Testing of Naval Vessels Using Seismic Airgun Arrays*. US 6,662,624 B1.

UCL, 2011. *UCL Ship Design Data Book, 2011 edition*. Unpublished. London, UK: UCL.

US Department of Defense, 1946. *Operation Crossroads Baker (wide)*. [Photograph] Available at: <http://commons.wikimedia.org/wiki/File:Operation_Crossroads_Baker_(wide).jpg> [Accessed 28 May 2013].

US Office of Naval Research and Naval Construction Research Establishment, Dunfermline, 1950a. *Underwater Explosion Research, vol 1 - The Shock Wave*. Washington D.C.: US Department of the Navy.

US Office of Naval Research and Naval Construction Research Establishment, Dunfermline, 1950b. *Underwater Explosion Research, vol 2 - The Gas Globe*. Washington D.C.: US Department of the Navy.

US Office of Naval Research and Naval Construction Research Establishment, Dunfermline, 1950c. *Underwater Explosion Research, vol 3 - The Damage Process*. Washington D.C.: US Department of the Navy.

Vialette, P. and Cottin, Y., 1995. *An Analysis of the Influence of Military Requirements on Ship Platform Costs by Comparison of Frigates of the Floreal and La Fayette Classes*. Translated by P. Babler. Glasgow: Defence Researce Information centre.

Walsh, J. and Blake, R., 1948. *The Equivalent Static Accelerations of Shock Motions*. [online] Washington, DC: US Naval Research Laboratory, p.11. Available at: <http://www.dtic.mil/dtic/tr/fulltext/u2/a953478.pdf> [Accessed 28 May 2013].

Weidlinger Associates, Inc., 1999. *EPSA-III Theoretical Guidebook*. New York, NY: Weidlinger Associates, Inc.

Weidlinger Associates, Inc., 2005. *User Guide to PreFUSE*. New York, NY: Weidlinger Associates, Inc.

Weidlinger Associates, Inc., 2009. *Unofficial User's Guide to FUSE*. New York, NY.

Wright, J., Sandler, I. and Sussman, M., 2002. *Advanced Fluid Modelling Capability for Underwater Shock Analysis of Naval Ships*. New York, NY: Weidlinger Associates, Inc.

Appendices

Appendix A Stiffener depth correction

This Appendix provides a more detailed description of the stiffener depth correction process discussed in Section 3.6 a.

Plate elements represent solid bodies as a surface, thickened to the desired thickness. As shown in Figure 3.6.1, discretizing a typical stiffened plate cross section as thickened surfaces of the same shape results in 'double counted' regions and gives a slightly increase in total area, of approximately 5%. There is a corresponding increase in second moment of area about the horizontal neutral axis, of approximately 3%.

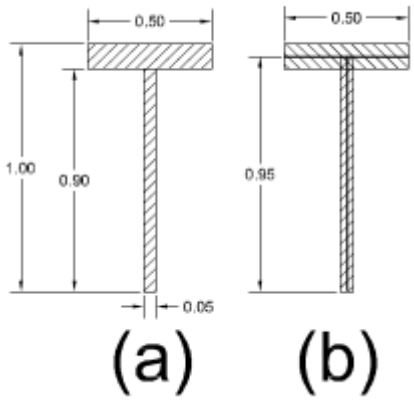

Figure A. 1 - Solid (a) and plate (b) representation of tee-bar stiffeners

The two different representations in Figure A.1 have the following properties:

(a) Area: 9.50e-2, Second Moment of Area: 5.98e-3

(b) Area: 9.95e-2, Second Moment of Area: 6.15e-3

Area error +4.7%, I error +2.8%

Adding in a plate section of thickness 0.08 and width 3.2 (40t), those results change to:

(a) Area: 3.51e-1, Second Moment of Area: 4.54e-2

(b) Area: 3.56e-1, Second Moment of Area: 4.59e-2

Area error: +1.3%, I error +1.1%

How much plating acts with the stiffener varies with geometry and loading, and is not possible to establish for each stiffener prior to the design. Chalmers provides a conservative estimate of whichever is the lesser of b and 40t. The true error is probably therefore somewhere between the bounds described above.

To attempt to reduce this error, the stiffeners were modelled in plate form with slightly reduced depth. A choice had to be made between choosing the web depth to give the correct overall stiffener depth, correct total stiffener area, or correct second moment of area. Another choice had to be made as to how much plating to be assumed to be acting with the stiffener.

Since bending and buckling were likely to be the predominant causes of stiffener failure, it was decided to prioritize second moment of area. A quantity of plate equal to that predicted by Chalmers was assumed to apply, in order to avoid over-correcting.

This correction was made within the design spreadsheet, in a series of dedicated worksheets, one per panel. The results were collated in a single output worksheet.

Appendix B

With the pre-set variables (geometry, stiffener spacings, material properties etc.) entered, initial values were chosen for panel smeared thickness, stiffener material fraction and frame depth. In this example case all panels were set to a smeared thickness of 16mm, with 10% of the material in the stiffeners (30% in the case of Panel 9) and frames 250mm deep. This initial setup is shown in Figure B.1.

	DESIGN	NFR-90 600x1500 T-Bar									
	Nick Bradbeer	5th Oct 2011									
				1	2	3	4	5	6	7	8	9
				1 Deck	Top Shell	2 Deck	Lower Shell	Turn of Bilge	Inner Bottom	Bottom	Keel	BULKHEAD
CHALMERS - LOAD FACTORS												
LLOYDS NSR - LOAD FACTORS												
1	Girder bending peak stresses			0.59							0.58	
	Girder bending stress range			0.92								
2	Plate thickness			0.40	0.63	0.35	0.74	0.93	0.54	1.08	1.15	1.05
	Plate buckling			1.04	1.03	0.47	0.48	0.76	0.76	0.88	1.05	
	--- Plate elastically buckles?			NO	NO	NO	NO	NO	NO	NO	NO	
	Longitudinal Sizing (local loads) - Z			0.10	0.22	0.07	0.37	0.62	0.29	0.71	0.77	2.32
	Longitudinal Sizing (local loads) - I			0.05	0.11	0.03	0.18	0.30	0.14	0.35	0.38	3.86
	Longitudinal Sizing (local loads) - A			0.14	0.30	0.09	0.50	0.84	0.39	**0.97**	1.04	1.03
	Longitudinal Sizing (buckling)			1.19	1.19	0.54	0.55	0.87	0.87	1.01	1.20	
	Plate buckling before stiffener tripping			0.87	0.88	0.87	0.88	0.87	0.85	0.86	0.86	
3	Transverse frame sizing (local loads) - Z			0.14	0.27	0.32	0.70	1.17	0.26	0.64	0.69	
	Transverse frame sizing (local loads) - I			0.08	0.15	0.32	0.47	0.79	0.13	0.31	0.34	
	Transverse frame sizing (local loads) - A			0.17	0.35	0.21	0.73	1.23	0.40	**0.98**	1.05	
	Transverse frame sizing (global buckling)			-4.95	-4.01	2.67	0.42	0.85	0.19	0.33	-3.73	
	Shear buckling of stiffened panels			0.07	0.10	0.03	0.13	0.13	0.05	0.06	0.04	
	(Stiffener Depth + 40mm) / Frame Depth			0.70	0.70	0.70	0.70	0.70	0.70	0.70	0.70	
	Panel weight/m		kg	734.76	351.52	669.45	528.73	281.33	756.11	262.95	511.39	1829.44
	Frame weight /m		kg	122.46	58.59	111.57	88.12	46.89	126.02	43.82	85.23	0.00
	Stiffener Weld Length /m		m	9.75	4.66	8.88	7.02	3.73	10.03	3.49	6.79	24.28
CONTROL VARIABLES												
	Smeared Thickness	ts	mm	16	16	16	16	16	16	16	16	16
	Stiffener Spacing	b	mm	600	600	600	600	600	600	600	600	600
	Frame Spacing	a	mm	1500	1500	1500	1500	1500	1500	1500	1500	7125
	Material Fraction in Stiffeners	As/S		0.1	0.1	0.1	0.1	0.1	0.1	0.1	0.1	0.3
	Frame Depth		mm	200	200	200	200	200	200	200	200	
	Stiffener Type (1=Flat, 2=OBP, 3=T-Bar)			3	3	3	3	3	3	3	3	3

Figure B. 1 - Initial setup of scantling design spreadsheet control panel

Each panel corresponded to a column in the spreadsheet, while rows contained either control variables of load factors for each panel against a particular failure mode. The control input variables are marked in orange at the bottom, while the output load factors are shown in the green and red blocks above. The output blocks are colour coded, thus:

i. Red cells signify a load factor >1.00
ii. Pale green cells signify a load factor <0.95
iii. Bold green cells signify a load factor between 0.95 and 1.00.

The design as shown in Figure B.1 is not in an acceptable state. Most panels have at least one red cell with a load factor in excess of 1.00, indicating that they are under strength. Panels 4 and 6 have only pale green cells, indicating that they are over strength. The desired end state is for each panel to have at least one cell between 0.99 and 1.00, with no red cells.

The output blocks are divided into three sections (marked 1-3 in Figure B.1), grouped by input dependency.

- The top two rows, concerned with hull girder bending stress in the strength deck and keel, are dependent upon the smeared thickness of Panels 1-8.
- The central block of plate and stiffener failure modes are dependent upon smeared thickness and stiffener material fractions. Panels 1-8 are interdependent, while Panel 9 (the bulkhead) is independent of the others.
- The lowest block relates to the transverse frames, and is dependent upon smeared thickness, stiffener material fraction and frame depth. Again, Panels 1-8 are interdependent, while Panel 9 (the bulkhead) is independent of the others.

The solution method used was as follows:

1. Find values of smeared thickness and stiffener material fraction which satisfy the central block (of plate and stiffener failure modes.)
2. Check that these values satisfy the top block (allowable stresses arising from hull girder bending) and increase the thickness of the upper deck and/or keel if necessary.
3. Finally, find values of transverse frame depth which satisfy the lower block.

Paying attention to only the central block, values of smeared thickness were found which give an approximate solution, as shown in Figure B.2. Even adjusting smeared thickness in whole millimetre increments, it is possible to reach a solution where each panel has a cell within 3% of the limiting value.

DESIGN	NFR-90 600x1500 T-Bar										
Nick Bradbeer	5th Oct 2011										
			1	2	3	4	5	6	7	8	9
			1 Deck	Top Shell	2 Deck	Lower Shell	Turn of Bilge	Inner Bottom	Bottom	Keel	BULKHEAD
CHALMERS - LOAD FACTORS											
LLOYDS NSR - LOAD FACTORS											
Girder bending peak stresses			0.55	x	x	x	x	x	x	0.55	
Girder bending stress range			0.87	x	x	x	x	x	x	x	x
Plate thickness			0.34	0.53	0.70	1.00	0.98	0.67	0.98	0.91	0.53
Plate buckling			0.92	0.91	0.71	0.55	0.75	0.83	0.81	0.91	
--- Plate elastically buckles?			NO	NO	YES	NO	NO	NO	NO	NO	
Longitudinal Sizing (local loads) - Z			0.08	0.17	0.20	0.58	0.68	0.40	0.65	0.54	0.84
Longitudinal Sizing (local loads) - I			0.03	0.08	0.14	0.33	0.35	0.22	0.31	0.24	0.99
Longitudinal Sizing (local loads) - A			0.12	0.25	0.18	0.66	0.89	0.48	0.91	0.83	0.53
Longitudinal Sizing (buckling)			1.00	1.00	0.97	0.65	0.86	0.97	0.91	0.97	
Plate buckling before stiffener tripping			0.92	0.93	0.39	0.74	0.84	0.75	0.88	0.93	
Transverse frame sizing (local loads) - Z			0.13	0.26	0.33	0.71	1.17	0.27	0.64	0.67	
Transverse frame sizing (local loads) - I			0.07	0.14	0.39	0.51	0.80	0.14	0.30	0.31	
Transverse frame sizing (local loads) - A			0.17	0.35	0.21	0.73	1.23	0.40	0.98	1.05	
Transverse frame sizing (global buckling)			3.07	2.49	1.41	0.35	0.71	0.15	0.26	1.24	
Shear buckling of stiffened panels			0.06	0.09	0.04	0.18	0.13	0.05	0.07	0.04	
(Stiffener Depth + 40mm) / Frame Depth			0.75	0.75	0.56	0.64	0.69	0.65	0.72	0.76	
Panel weight/m		kg	872.53	417.43	334.72	396.55	263.74	614.34	279.38	639.23	3544.54
Frame weight /m		kg	122.46	58.59	111.57	88.12	46.89	126.02	43.82	85.23	0.00
Stiffener Weld Length /m		m	9.75	4.66	8.88	7.02	3.73	10.03	3.49	6.79	24.28
CONTROL VARIABLES											
Smeared Thickness	ts	mm	19	19	8	12	15	13	17	20	31
Stiffener Spacing	b	mm	600	600	600	600	600	600	600	600	600
Frame Spacing	a	mm	1500	1500	1500	1500	1500	1500	1500	1500	7125
Material Fraction in Stiffeners	As/S		0.1	0.1	0.1	0.1	0.1	0.1	0.1	0.1	0.3
Frame Depth		mm	200	200	200	200	200	200	200	200	
Stiffener Type (1=Flat, 2=OBP, 3=T-Bar)			3	3	3	3	3	3	3	3	3

Figure B. 2 – An approximate solution for scantlings

A useful measure is the structural mass per metre of ship length. This was calculated separately for the panels (shell plating and longitudinal stiffening) and transverse frames and summed. While only one side of the ship was modelled, there was no need to double the weight to serve as a comparative metric.

At the point shown in Figure B.2, the structure had a weight of 4,809 kg/m.

The next step was to find the minimum acceptable smeared thickness for each panel. The relationship between minimum acceptable smeared thickness and stiffener material fraction was of the general form shown in Figure B.3. The minimum point may be found by manual variation of the input variables, but since the relationship was continuous and nonlinear, it lent itself readily to rapid solving using nonlinear programming methods.

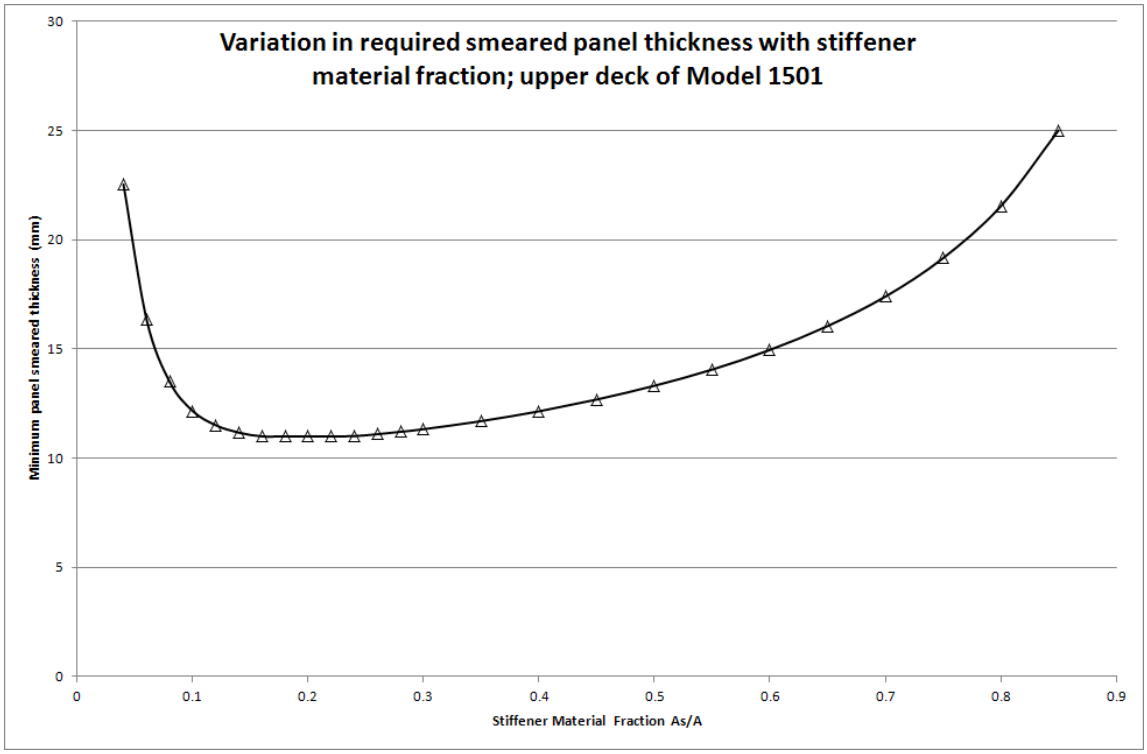

Figure B. 3 - Typical relationship between required panel smeared thickness and stiffener material fraction

Two simple Visual Basic for Applications (VBA) routines were produced to assist with finding the minimum point; Increment() and Decrement(). Each routine either incremented or decremented the panel smeared thickness by 0.1mm, then used the MS Solver plugin to find the stiffener material fraction to give the lowest value of the maximum load factor for the panel. These two functions greatly sped up the process of finding minimum points, although care must be taken to ensure they do not return local minima.

With this process complete, the sheet looked as shown in Figure B.4, with a structural weight of 4,706 kg/m.

DESIGN	NFR-90 600x1500 T-Bar										
Nick Bradbeer	5th Oct 2011										
			1	2	3	4	5	6	7	8	9
			1 Deck	Top Shell	2 Deck	Lower Shell	Turn of Bilge	Inner Bottom	Bottom	Keel	BULKHEAD
CHALMERS - LOAD FACTORS											
LLOYDS NSR - LOAD FACTORS											
Girder bending peak stresses			0.56	x	x	x	x	x	x	0.56	x
Girder bending stress range			0.88	x	x	x	x	x	x	x	x
Plate thickness			0.36	0.57	0.82	**1.00**	**1.00**	0.79	**1.00**	0.92	**1.00**
Plate buckling			**0.95**	0.95	0.82	0.55	0.77	0.93	0.83	0.93	
--- Plate elastically buckles?			NO	NO	YES	NO	NO	NO	NO	NO	
Longitudinal Sizing (local loads) - Z			0.04	0.10	0.16	**0.98**	0.70	0.31	0.65	0.55	0.73
Longitudinal Sizing (local loads) - I			0.02	0.04	0.11	0.66	0.36	0.16	0.31	0.24	**0.98**
Longitudinal Sizing (local loads) - A			0.08	0.17	0.16	**0.97**	0.90	0.40	0.91	0.84	0.46
Longitudinal Sizing (buckling)			**1.00**	**1.00**	**1.00**	0.78	0.89	**0.99**	0.93	**1.00**	
Plate buckling before stiffener tripping			0.90	0.91	0.29	0.74	0.83	0.69	0.88	0.93	
Transverse frame sizing (local loads) - Z			0.13	0.27	0.34	0.71	1.18	0.27	0.64	0.67	
Transverse frame sizing (local loads) - I			0.08	0.14	0.41	0.51	0.81	0.14	0.31	0.31	
Transverse frame sizing (local loads) - A			0.17	0.35	0.21	0.73	1.23	0.40	**0.98**	1.05	
Transverse frame sizing (global buckling)			5.05	4.08	1.34	0.34	0.74	0.16	0.28	2.14	
Shear buckling of stiffened panels			0.07	0.09	0.04	0.18	0.13	0.05	0.07	0.04	
(Stiffener Depth + 40mm) / Frame Depth			0.87	0.87	0.58	0.56	0.68	0.70	0.72	0.76	
Panel weight/m		kg	867.94	413.04	297.07	386.64	260.23	576.54	277.74	636.04	2572.65
Frame weight /m		kg	122.46	58.59	111.57	88.12	46.89	126.02	43.82	85.23	0.00
Stiffener Weld Length /m		m	9.75	4.66	8.88	7.02	3.73	10.03	3.49	6.79	24.28
CONTROL VARIABLES											
Smeared Thickness	ts	mm	**18.9**	**18.8**	**7.1**	**11.7**	**14.8**	**12.2**	**16.9**	**19.9**	**22.5**
Stiffener Spacing	b	mm	600	600	600	600	600	600	600	600	600
Frame Spacing	a	mm	1500	1500	1500	1500	1500	1500	1500	1500	7125
Material Fraction in Stiffeners	As/S		**0.15**	**0.15**	**0.13**	**0.07**	**0.1**	**0.13**	**0.1**	**0.1**	**0.48**
Frame Depth		mm	200	200	200	200	200	200	200	200	
Stiffener Type (1=Flat, 2=OBP, 3=T-Bar)			3	3	3	3	3	3	3	3	3

Figure B. 4 - Scantlings after fine selection of plate thickness and longitudinal size.

With the middle block of load factors satisfied, it can be seen that the first block has also been satisfied, and the designer's attention can be turned to the design of the frames. This was a simple matter of adjusting a single variable for each panel – frame depth – until the third block of load factors is satisfied.

	DESIGN	NFR-90 600x1500 T-Bar									
	Nick Bradbeer	5th Oct 2011									
				1	2	3	4	5	6	7	8	9
				1 Deck	Top Shell	2 Deck	Lower Shell	Turn of Bilge	Inner Bottom	Bottom	Keel	BULKHEAD
CHALMERS - LOAD FACTORS												
LLOYDS NSR - LOAD FACTORS												
Girder bending peak stresses				0.56	x	x	x	x	x	x	0.56	
Girder bending stress range				0.88	x	x	x	x	x	x	x	x
Plate thickness				0.36	0.57	0.82	**1.00**	**1.00**	0.79	**1.00**	0.92	**1.00**
Plate buckling				**0.95**	0.95	0.82	0.55	0.77	0.93	0.83	0.93	
--- Plate elastically buckles?				NO	NO	YES	NO	NO	NO	NO	NO	
Longitudinal Sizing (local loads) - Z				0.04	0.10	0.16	**0.98**	0.70	0.31	0.65	0.55	0.73
Longitudinal Sizing (local loads) - I				0.02	0.04	0.11	0.66	0.36	0.16	0.31	0.24	**0.98**
Longitudinal Sizing (local loads) - A				0.08	0.17	0.16	**0.97**	0.90	0.40	0.91	0.84	0.46
Longitudinal Sizing (buckling)				**1.00**	**1.00**	**1.00**	0.78	0.89	**0.99**	0.93	**1.00**	
Plate buckling before stiffener tripping				0.90	0.91	0.29	0.74	0.83	0.69	0.88	0.93	
Transverse frame sizing (local loads) - Z				0.03	0.08	0.26	**1.00**	0.87	0.73	0.66	0.36	
Transverse frame sizing (local loads) - I				0.02	0.04	0.30	0.77	0.56	0.47	0.32	0.15	
Transverse frame sizing (local loads) - A				0.07	0.16	0.18	0.93	**1.00**	0.80	**1.00**	0.68	
Transverse frame sizing (global buckling)				**1.00**	**1.00**	**1.00**	0.50	0.52	0.51	0.29	**0.99**	
Shear buckling of stiffened panels				0.07	0.09	0.04	0.18	0.13	0.05	0.07	0.04	
(Stiffener Depth + 40mm) / Frame Depth				0.54	0.57	0.53	0.63	0.62	**0.99**	0.72	0.61	
Panel weight/m			kg	867.94	413.04	297.07	386.64	260.23	576.54	277.74	636.04	2572.65
Frame weight /m			kg	317.43	133.58	135.01	69.80	57.77	62.63	42.95	132.11	0.00
Stiffener Weld Length /m			m	9.75	4.66	8.88	7.02	3.73	10.03	3.49	6.79	24.28
CONTROL VARIABLES												
Smeared Thickness	ts		mm	**18.9**	**18.8**	**7.1**	**11.7**	**14.8**	**12.2**	**16.9**	**19.9**	**22.5**
Stiffener Spacing	b		mm	600	600	600	600	600	600	600	600	600
Frame Spacing	a		mm	1500	1500	1500	1500	1500	1500	1500	1500	7125
Material Fraction in Stiffeners	As/S			**0.15**	**0.15**	**0.13**	**0.07**	**0.1**	**0.13**	**0.1**	**0.1**	**0.48**
Frame Depth			mm	322	302	220	178	222	141	198	249	
Stiffener Type (1=Flat, 2=OBP, 3=T-Bar)				3	3	3	3	3	3	3	3	3

Figure B. 5 - An acceptable configuration of scantlings

The structure shown in Figure B.5 represents the desired end state, with a weight of 4,666 kg/m.

Appendix D Sensitivity Analysis

As described in Section 4.4, a number of sensitivity studies were conducted to support the choices of various parameters of the finite element models. In particular, it was necessary to determine what proportion of the ship should be modelled, what level of detail should be incorporated into the model, and how sensitive the results were to details of the bulkhead and frame design. This Appendix describes some of the sensitivity studies conducted.

The studies used a model based on HMS JAVELIN. During the early stages of the research it had been intended to use HMS JAVELIN as the baseline ship for the study's main investigations, although subsequently (for reasons discussed in Chapter 5) the NFR-90 frigate and generic corvette were selected instead. Nevertheless, the sensitivity studies conducted using the HMS JAVELIN model offered useful insights which were transferrable to the other ships modelled.

D.1 The JAVELIN model

The post-war destroyer shock trials described by Brown (1987) included four ships of the J/K/N class, in addition to two A-Class, one B-Class, two Tribal class, two Battle class, one P-class, two unique prototypes and two Narvik class formerly of the German *Kreigsmarine*. While all of these ships were broadly similar in layout, they exhibited variation in armament, engine layouts and structural arrangements. The J/K/N class was selected as most representative of the sample. Enquiries with the National Maritime Museum (NMM) Archives determined that ship plans for HMS JAVELIN (DD 61) were available.

From these plans, a model based on HMS JAVELIN's boiler rooms was constructed. For simplicity the model was made as a prismatic extrusion of the section at Frame 42, with frames spaced regularly at a distance representative of the varied frame spacings used on the ship. Three transverse bulkheads were modelled at a spacing of 10m, with the compartments between them. Note that, as was typical for a destroyer of the period, the boiler rooms occupied the full depth of the hull, with no passing deck.

Figure D. 1 - HMS Kelvin (of the J/K/N class) illustrating the location of the boiler rooms

The section at Frame 42 was digitised from the NMM-supplied plans, which also supplied stiffener dimensions and plating weights. Most of the longitudinal stiffening was C-channel riveted onto the shell plating.

Bulkhead and frame weights were not defined on the available plans, and were estimated (at 6.3mm for bulkhead plating and 10mm for frames.) Studies were conducted to determine the sensitivity of the results to these assumptions, and are described below.

For the studies described below, the main output of interest was vertical velocity, at two points in the structure. The first of these, Node A, was located at the inner edge of the frame web at the keel, one frame spacing in from the central bulkhead. The other, Node B, was located on the same frame, at the inner edge of the web below the main deck, on the longitudinal centreline. It was expected that Node A would receive very severe accelerations for very short periods, while the finite stiffness of the ship's structure would mean that Node B received much lower accelerations (gradient of velocity plot) and greater displacements (integral of velocity plot).

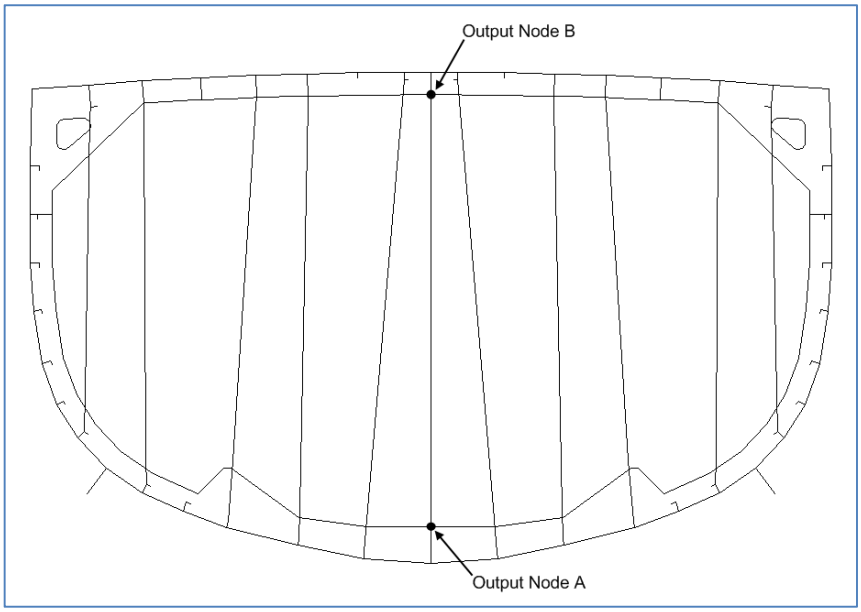

Figure D. 2 - Location of output nodes A & B

D.2 FUSE Shots

Two shots were used during these simulations, Shot A and Shot D, as shown in Figure 3. A FUSE simulation was conducted for each to generate the pressure field resulting from the explosion. Both charges were located in the plane of the central bulkhead, at a depth of 13m. The charge in Shot A was located 20m off the centreline of the target model, while the charge in Shot D was located 55m off the centreline. To comply with national security requirements, the charge masses are not reproduced here.

Shot A was run for 12,000 timesteps of 3.33×10^{-6} each, for a total of 40ms of simulation time.

Shot D was run for 22,000 timesteps of 3.33×10^{-6} each, for a total of 73ms. Since the shock wavefront did not reach the target until approximately 35ms after detonation, the first 10,000 timesteps were disregarded during the structural analysis, the remaining 12,000 timesteps giving 40ms of structural response.

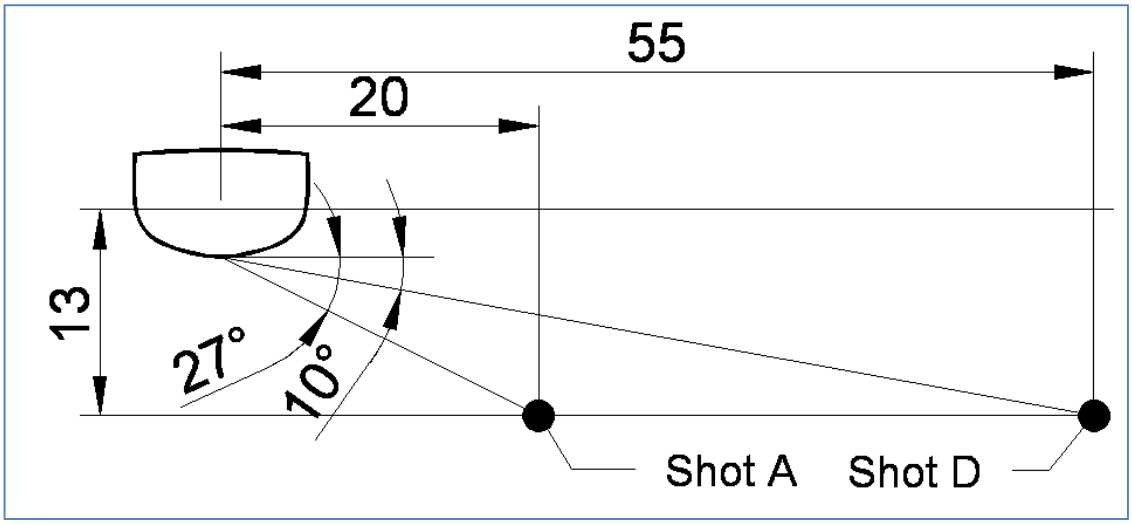

Figure D. 3 - Geometry of Shots A and D

D.3 Parameter Selection

A finite model is a simplified representation of reality, where continuous quantities like time, length and volume are discretised into a finite number of elements or timesteps. When building such a model, choices must be made about how to simplify the reality of the structure modelled; both in the extents of the model and the nature of the elements into which it is discretised. Some of these choices are outside the hands of the operator, driven by mathematical relationships or choices made when the FE solver was coded. Others require the operator to make a choice; in most cases selecting a point somewhere on a tradeoff between accuracy of solution and computational runtime.

D.3.a Solid Mesh detail

As previously mentioned, JAVELIN's longitudinal stiffening was made of C-section channels riveted to the shell plating. It was unclear whether the side of the channel riveted to the shell would have contributed to the structural strength fully, not at all, or somewhere between the two. In order to bound the effect, the two extreme cases were modelled.

Two versions of the JAVELIN model were constructed. Both were 20m prismatic sections containing two compartments. One, the Medium Complex model, modelled the riveted joints as thickened sections of shell plating, assuming the riveted flange of the C-channel to act as a fully effective part of the shell. The other, the Medium Simple model, did not model the outer flange of the C-channel at all.

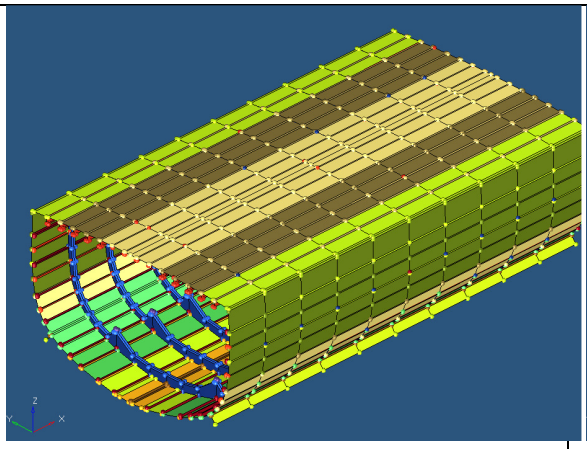

Figure D. 4 - Medium Complex JAVELIN model (transverse bulkheads not shown)

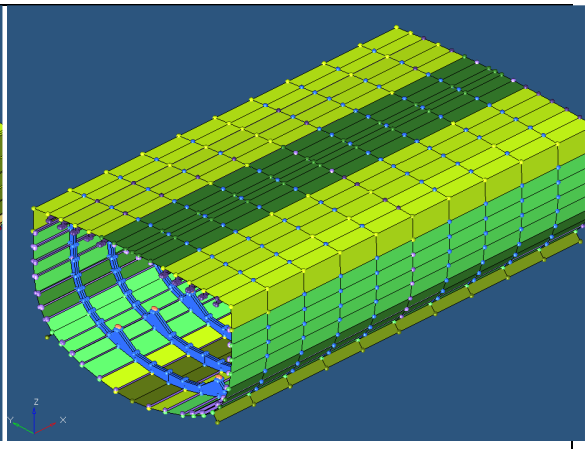

Figure D. 5 - Medium Simple JAVELIN model (transverse bulkheads not shown)

Both models were subjected to Shot D, the results of which are presented at Figures D.6 and D.7.

Runs:

- 0408 – Medium Simple model run with Shot D
- 0410 – Medium Complex model run with Shot D

Comparing the responses of Node A between the Complex and Simple models shows good correlation during the initial velocity spike corresponding to the arrival of the shock wavefront (error between peak velocities <6%) with divergence in the later response. Nonetheless, while the velocity time histories after 6ms differ significantly, the velocity range experienced by both models is similar.

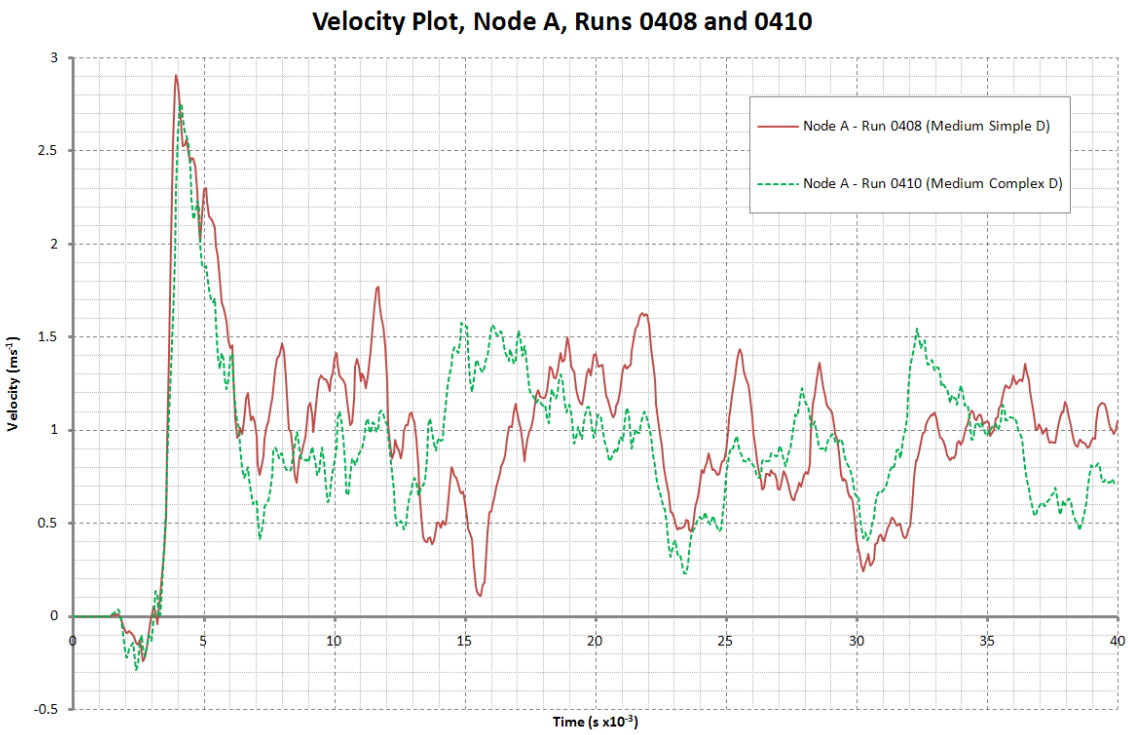

Figure D. 6 - Plot of Node A, Runs 0408 and 0410 (Simple vs. Complex)

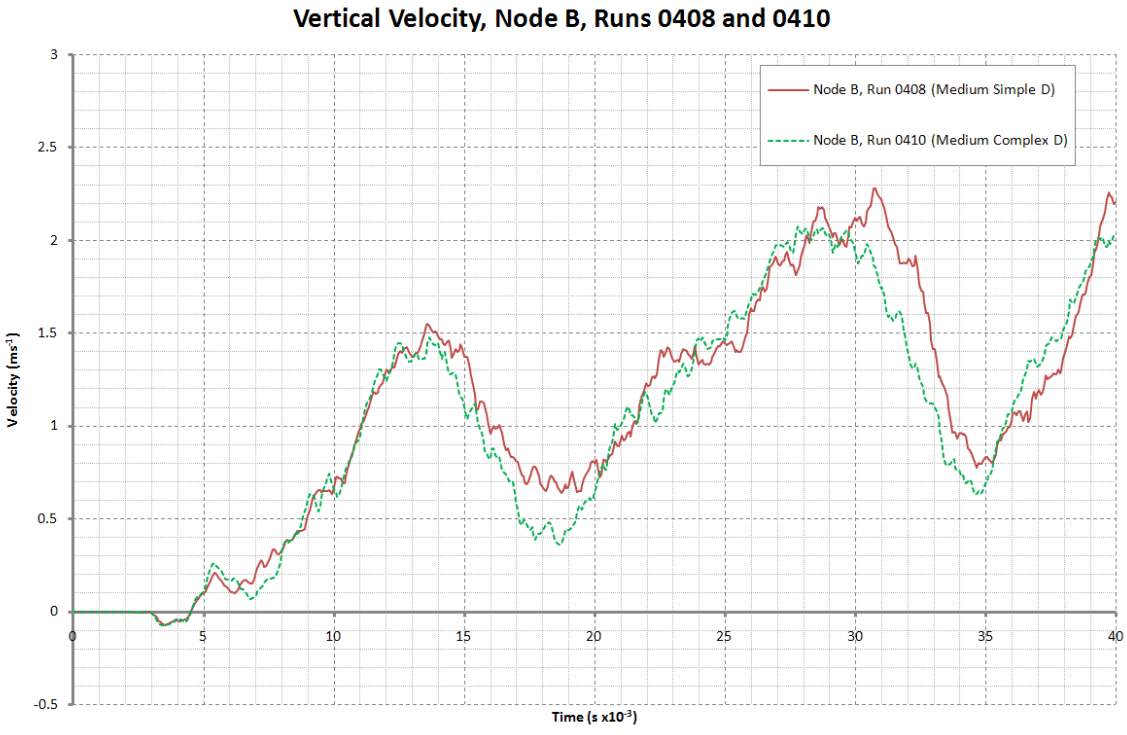

Figure D. 7 - Plot of Node B, Runs 0408 and 0410 (Simple vs. Complex)

D.3.b Structural model size

Simulating an entire ship is a very time-consuming process, both to build the model and to execute the simulation. Two comparative tests were conducted to determine whether a section of ship shorter than the full length could give results comparable to the whole ship.

The first test compared a full-length prismatic model with a model which contained only one compartment length on either side of the output nodes. To construct the full-length model, the Medium Simple model described above was replicated five times to give ten compartments over 100m, the approximate length of a J/K/N-Class destroyer. This model is referred to as the Long Simple model.

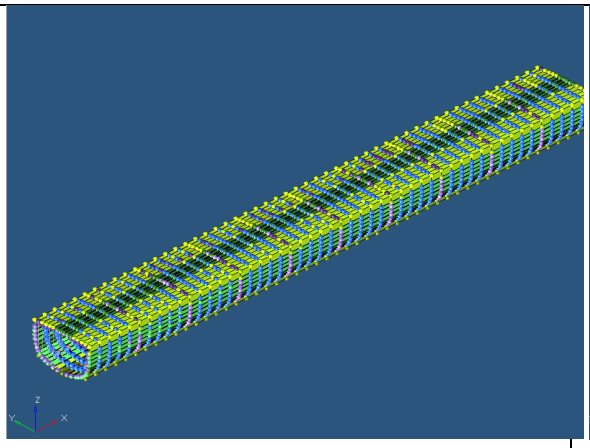

Figure D. 8 - Long Simple JAVELIN model (transverse bulkheads not shown)

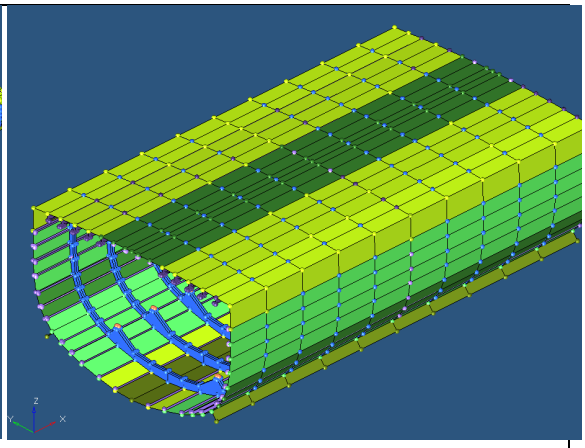

Figure D. 9 - Medium Simple JAVELIN model (transverse bulkheads not shown)

The Long Simple and Medium Simple models were compared:

Runs:

- 0407 –Long Simple model run with Shot D
- 0408 –Medium Simple model run with Shot D

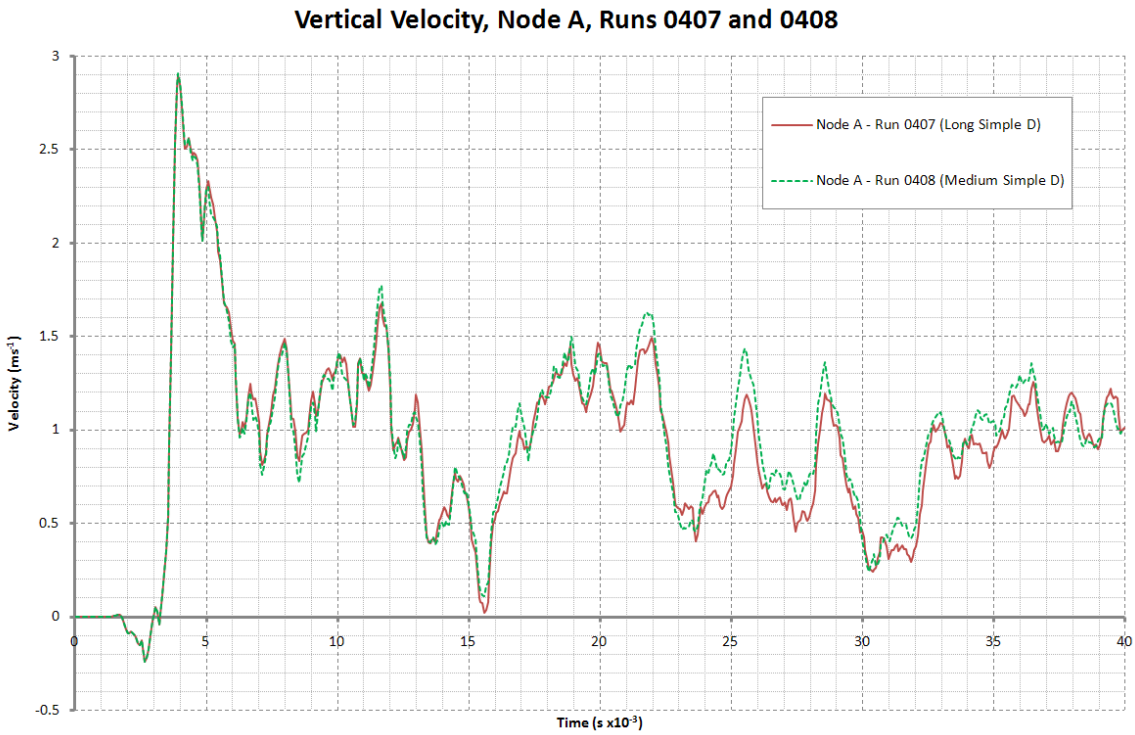

Figure D. 10 - Velocity Plot of Node A, Runs 0407 and 0408 (Long vs. Medium)

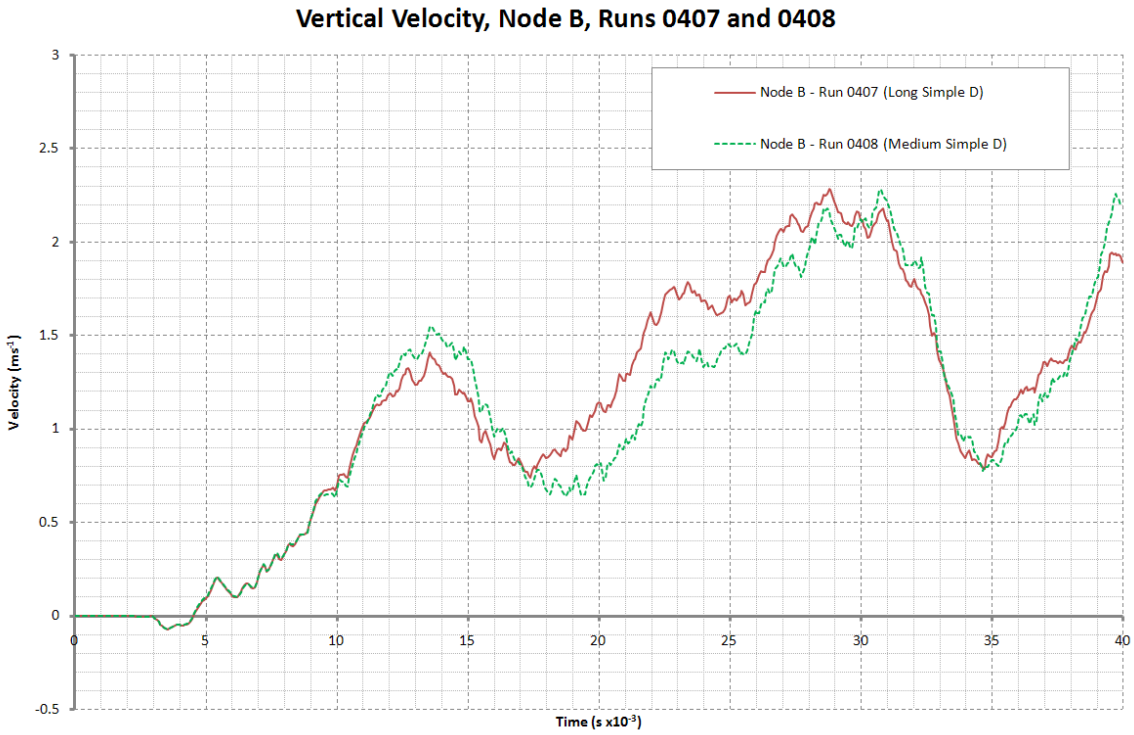

Figure D. 11 - Velocity Plot of Node B, Runs 0407 and 0408 (Long vs. Medium)

Figures D.10 and D.11 show close agreement between the results of the two models, suggesting that a three-compartment model provides a good representation of the behaviour of the longer model.

The second test compared the Medium model, with one compartment on either side of the output nodes, to a Short model, with one frame space on either side of the output nodes.

The shortened model was based on a 6m section of the Medium Complex model around the central bulkhead. The model included the frame on which the output nodes were located, and the adjacent frame and bulkhead. An additional half frame space of shell plating was included on each end, in order to reduce the asymmetric loading on the outer frame and the bulkhead.

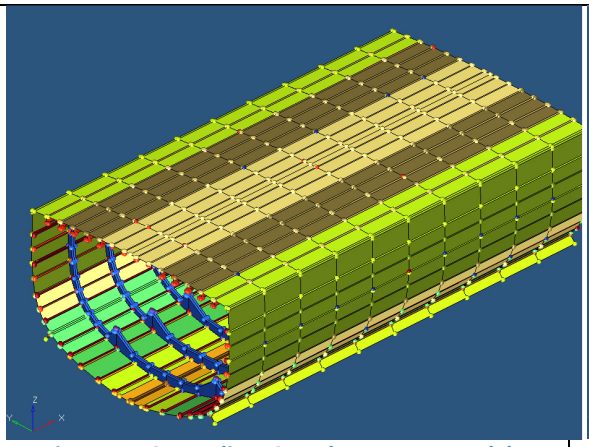

Figure D. 12 - Medium Complex JAVELIN model (transverse bulkheads not shown)

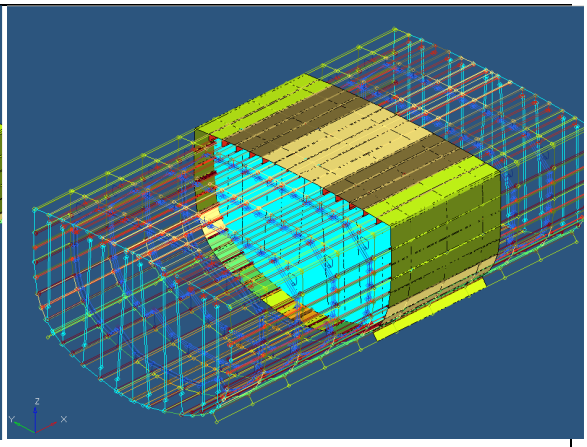

Figure D. 13 - Short Complex JAVELIN model (transverse bulkheads not shown)

Runs:

- 0401 – Medium Complex model run with Shot A
- 0402 – Short Complex model run with Shot A

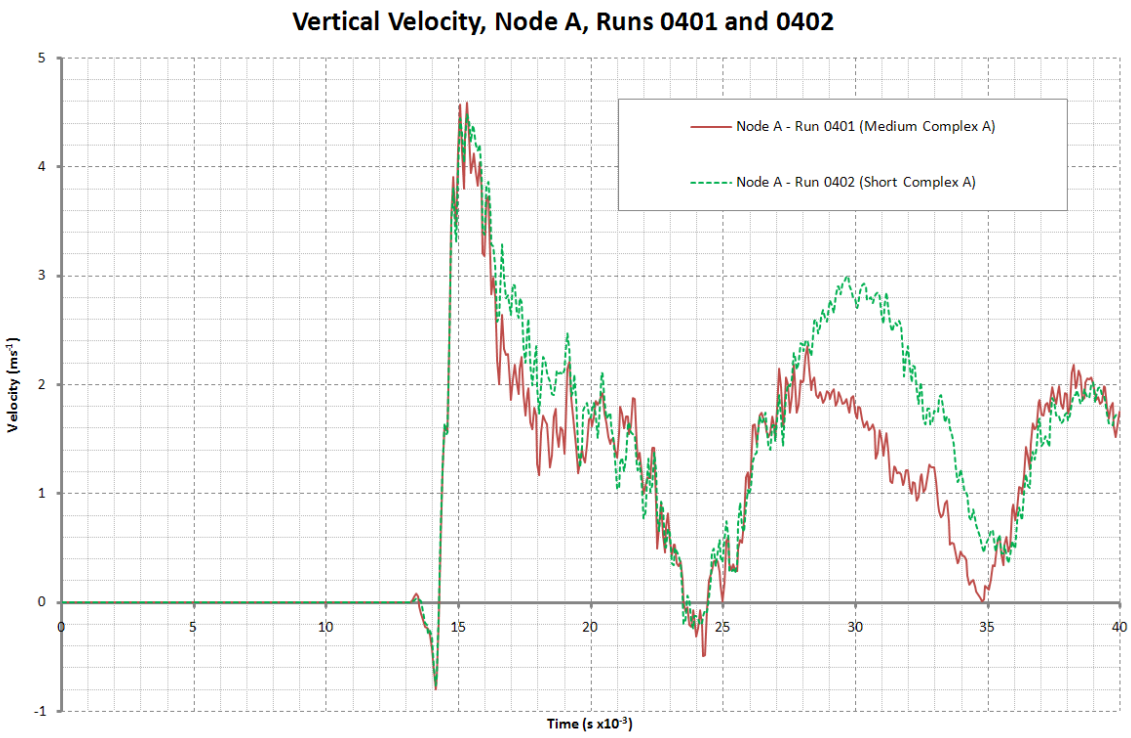

Figure D. 14 - Velocity Plot of Node A, Runs 0401 and 0402 (Medium vs. Short)

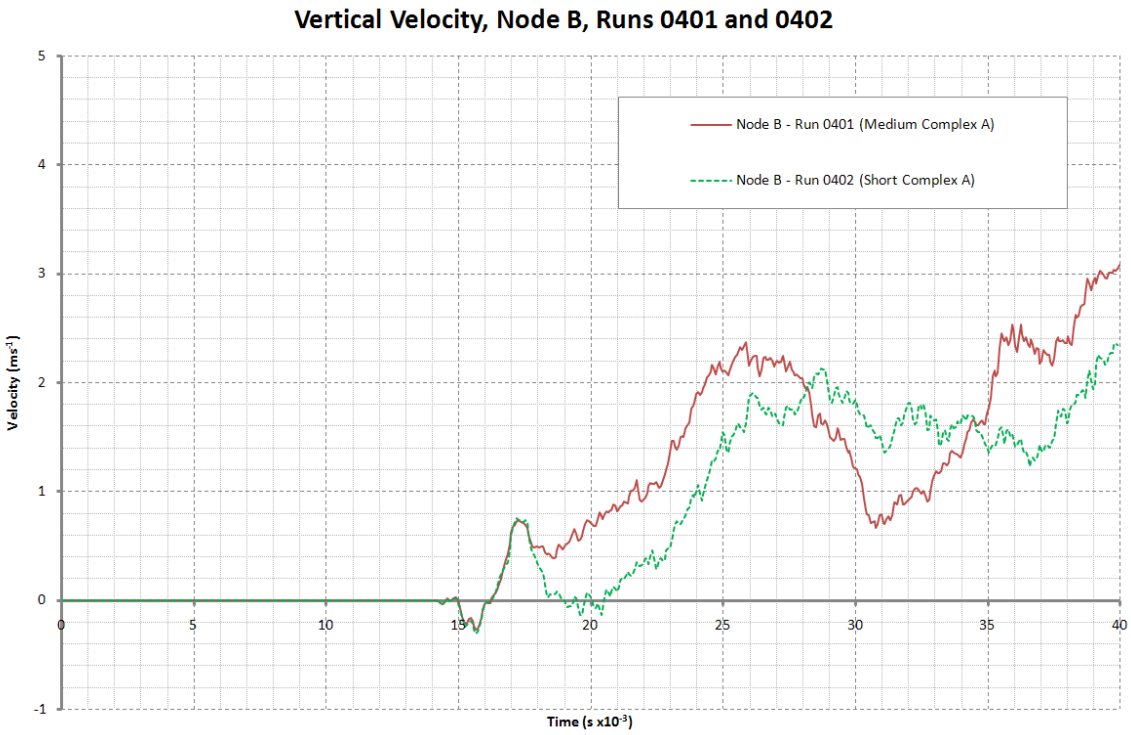

Figure D. 15 - Velocity Plot of Node B, Runs 0401 and 0402 (Medium vs. Short)

Figures D.14 and D.15 show poor agreement between the responses of the models, suggesting that a model two frame bays in length does not provide a good representation of the behaviour of the longer model.

D.3.c Structural Assumptions

Three details of structure were unclear from the JAVELIN plans provided by the National Maritime Museum: the thickness of the bulkhead plating, frame webs and frame flanges. Sensitivity studies were conducted to explore the effects of varying these parameters from the values assumed in all the models previously mentioned.

Variants of the Medium Complex model were created with increased and decreased values of bulkhead thickness, frame web thickness and frame flange thickness. All were subjected to Shot A.

Runs

- 0401 – Medium Complex model run with Shot A
- 0404a – Medium Complex model (3mm bulkhead plating) run with Shot A
- 0404b – Medium Complex model (10mm bulkhead plating) run with Shot A
- 0404c – Medium Complex model (5mm frame web thickness) run with Shot A
- 0404d – Medium Complex model (15mm frame web thickness) run with Shot A
- 0404e – Medium Complex model (5mm frame flange thickness) run with Shot A
- 0404f – Medium Complex model (15mm frame flange thickness) run with Shot A

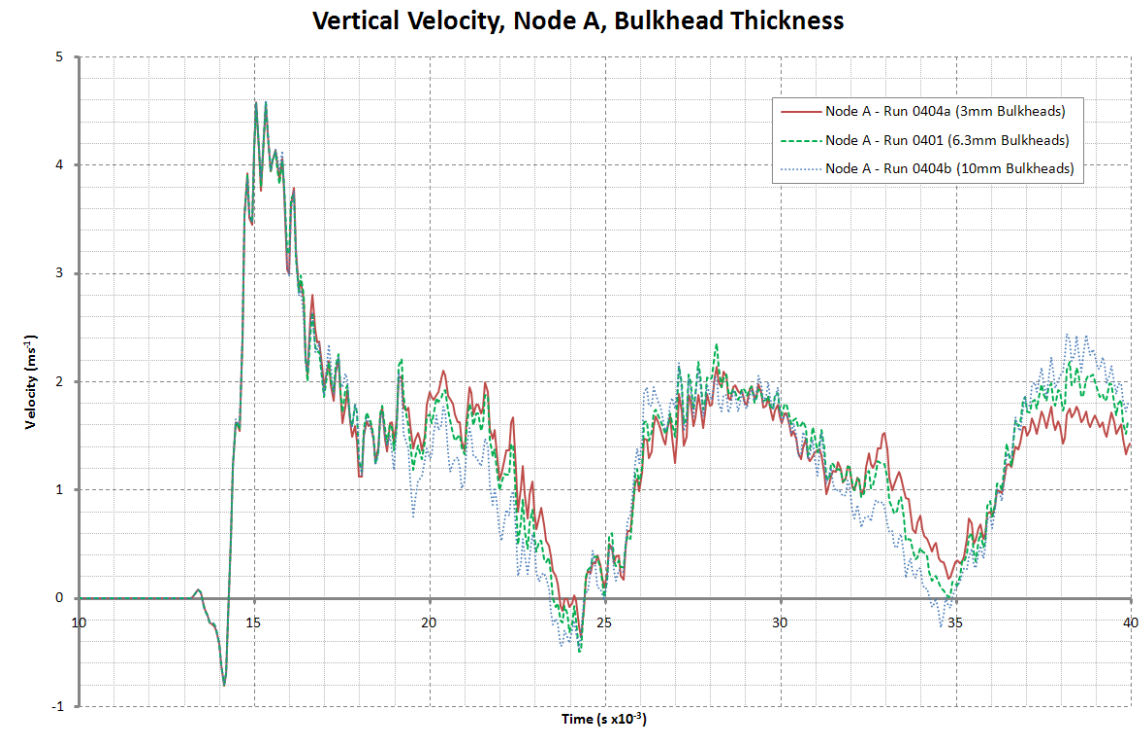

Figure D. 16 - Velocity Plot of Node A, Runs 0404a, 0401 and 0404b (Varying bulkhead thickness)

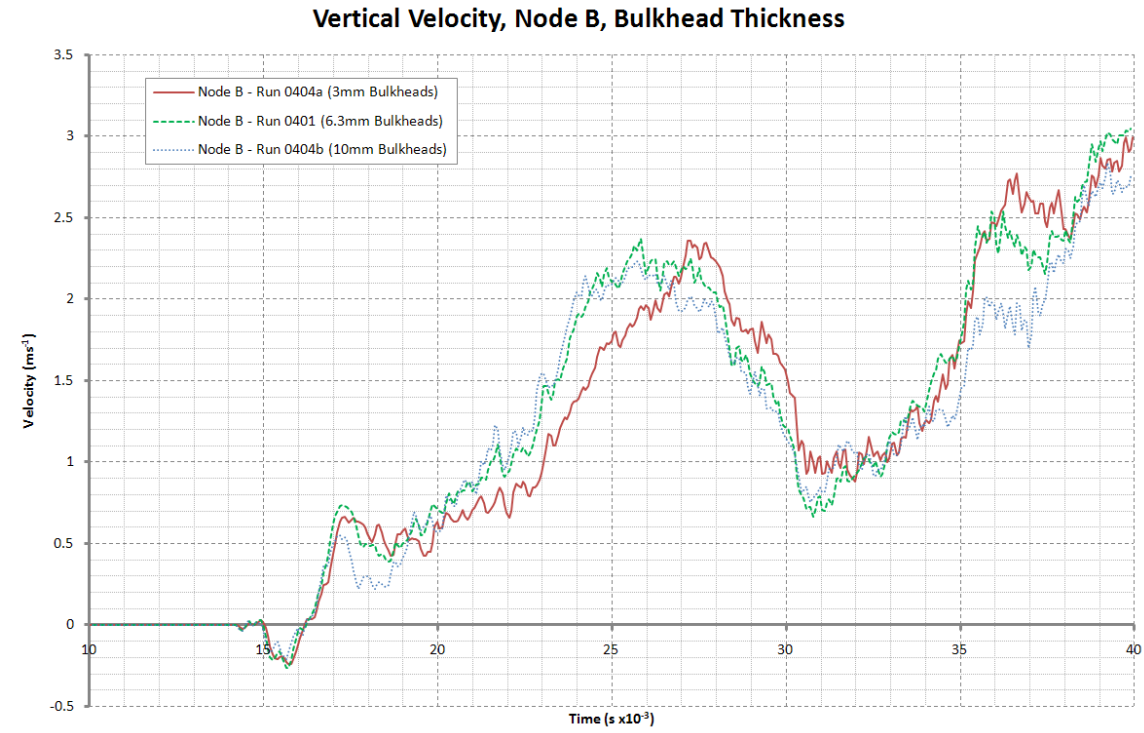

Figure D. 17 - Velocity Plot of Node B, Runs 0404a, 0401 and 0404b (Varying bulkhead thickness)

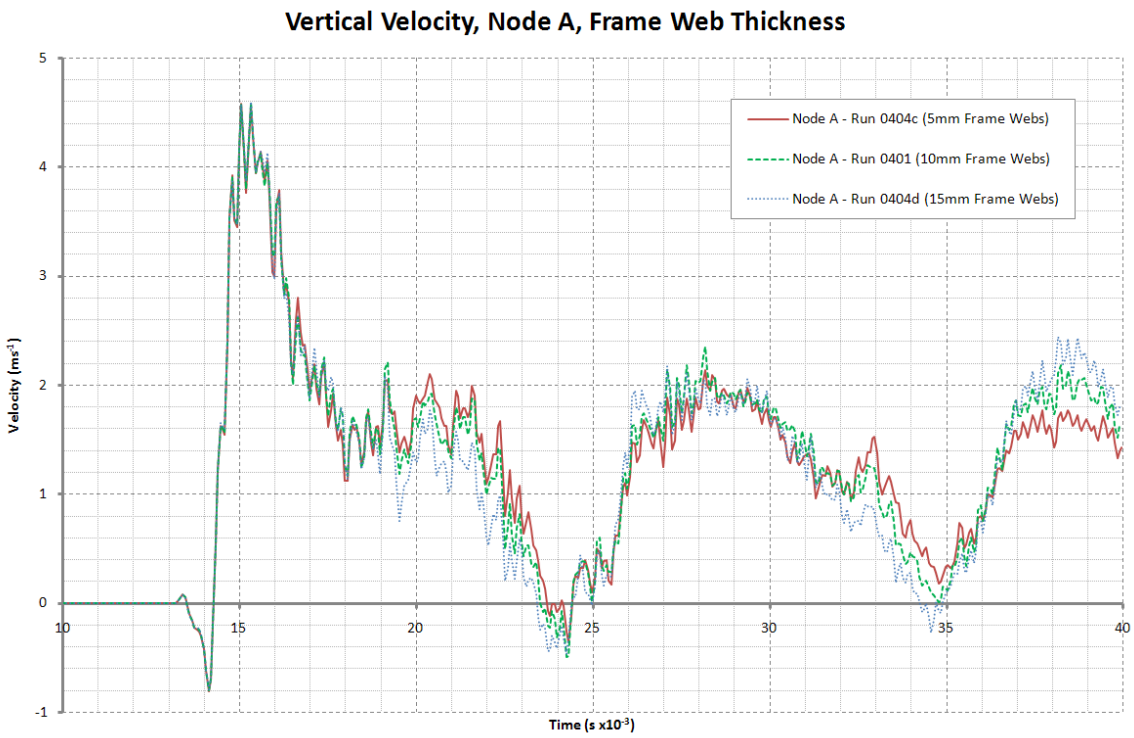

Figure D. 18 - Velocity Plot of Node A, Runs 0404c, 0401 and 0404d (Varying frame web thickness)

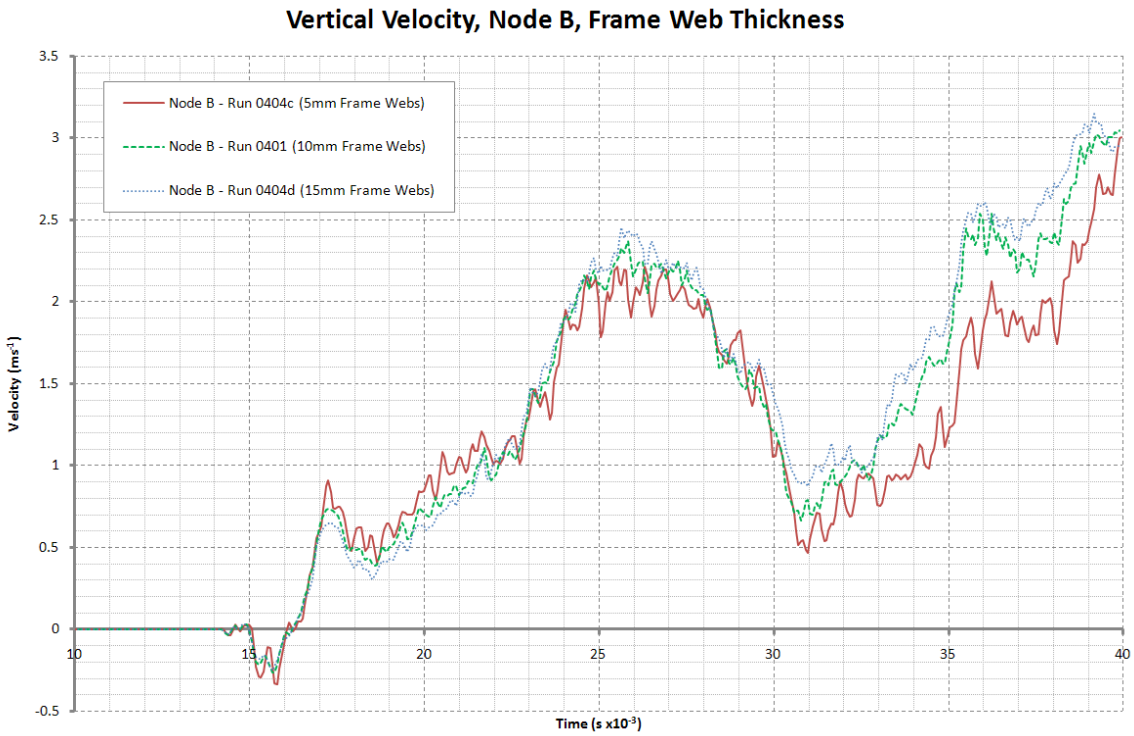

Figure D. 19 - Velocity Plot of Node B, Runs 0404c, 0401 and 0404d (Varying frame web thickness)

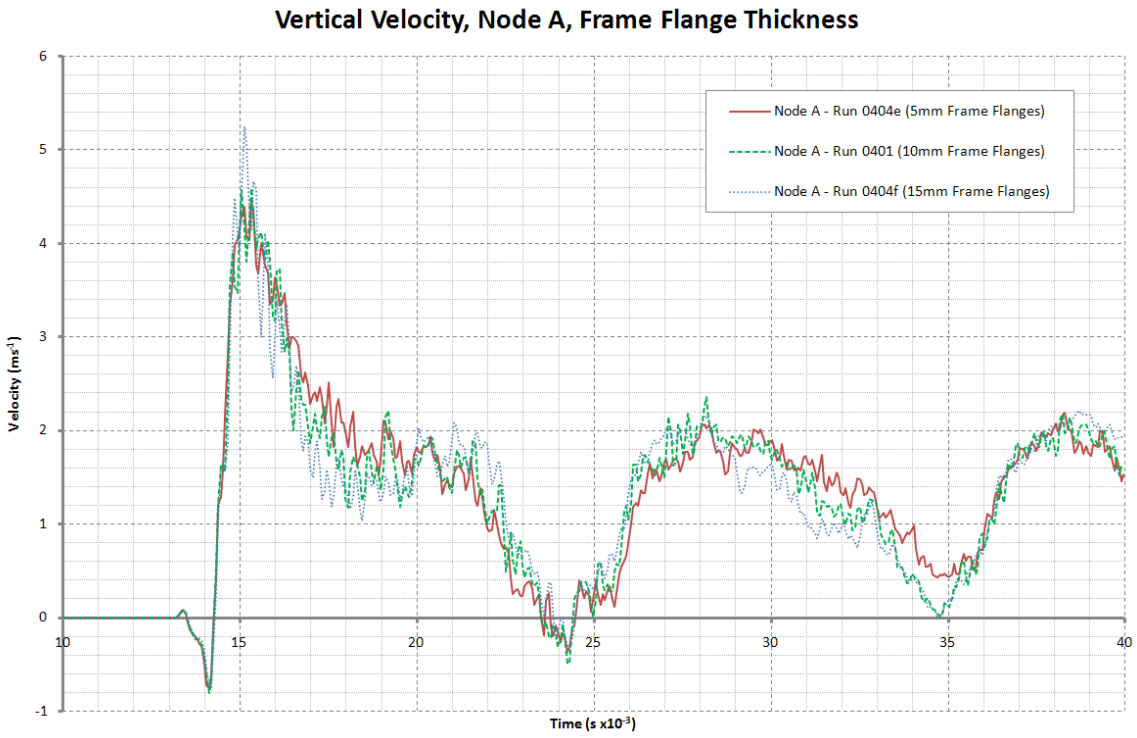

Figure D. 20 - Velocity Plot of Node A, Runs 0404e, 0401 and 0404f (Varying frame flange thickness)

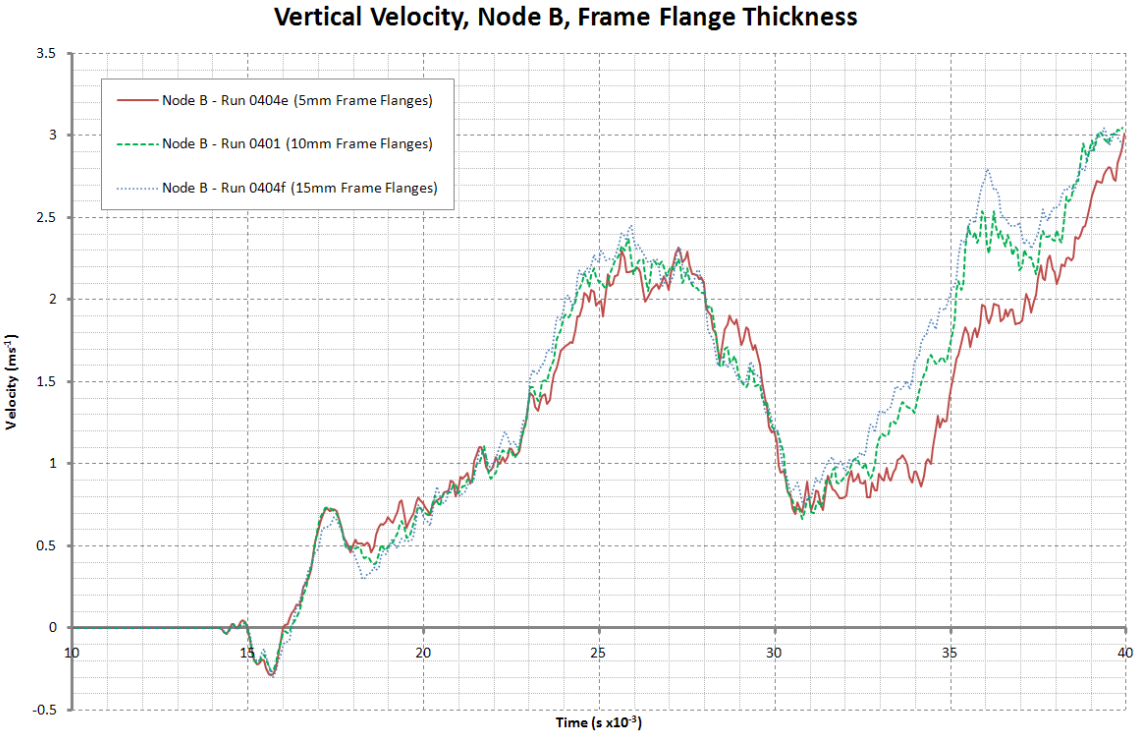

Figure D. 21 - Velocity Plot of Node B, Runs 0404e, 0401 and 0404f (Varying frame flange thickness)

Figures D.16 through D.21 suggested that the models were reasonably insensitive to variation in the parameters under consideration and, therefore, any errors in estimating those parameters would be unlikely to have a significant impact on the simulated response of the ship. This allowed confidence in the validation studies which compared the response of models of this ship (which could have included such errors) against full-scale trials data.

Appendix E Corvette Baseline Ship Design

In order to explore the difference in shock response between longitudinal and transversely stiffened structure, it was necessary to design a smaller ship than the NFR-90. In ships longer than approximately 100m, the structural design tends to be dominated by longitudinal bending and shearing of the main hull girder, while in shorter ships local pressure loads dominate. Since there was no suitable existing ship for which the required data was readily available, a design was worked up from scratch. This appendix contains a description of the process by which that design was developed, up to the concept level.

The Design Building Block Method (Andrews and Pawling, 2003) was used to develop a weight- and space-balanced model to the 200-block level. Stability, powering, layout and survivability considerations were addressed. The payload was selected to be typical for a modern, well-armed corvette designed for action against air and surface targets:

i. 1 x OTO Melara Super Rapid 76mm gun
ii. 1 x RTN-10X Radar/EO director
iii. 2 x 16-cell Vertical Launch System silos for CAMM surface-to-air missile
iv. 2 x 4-cell launcher for MM40 Exocet surface-to-surface missile
v. 2 x MSI Seahawk DS-30B 30mm guns
vi. 2 x DAGAEI Decoy Launchers
vii. 1 x IAI ELTA ELM-2238 STAR L-band surveillance radar
viii. 2 x MF/HF Tx, 4 x MF/HF Rx, 4 x VHF Tx/Rx, 1 x INMARSAT antenna
ix. Flight deck for 10-tonne helicopter (e.g. SH-60 Seahawk)

The design was developed in the Paramarine Early Stage Ship Design (ESSD) environment, a software tool designed to support the Design Building Block Method.

E.1 Super Building Block Stage

Building blocks were created for the payload systems, engine rooms and other, layout-critical spaces (compass platform, SCC, galley and dining halls, boat bays, operations room). Roughly thirty blocks were produced.

A hullform was produced using a Hull Generator-based tool produced by McDonald (2010). Similarly to Pawling's Quickhull-based tool used for developing the NFR-90 model (Pawling,

2009), this uses van Griethuysen's model (Van Griethuysen, 1992) to produce a coherent set of hull dimensions, to which a hull is then fitted as well as possible. Unlike Quickhull, Hull Generator produces a cage of B-Splines which define a NURBS surface, allowing arbitrary geometry.

A number of different arrangements were explored. A single block superstructure was chosen, which allowed a convenient arrangement of payload systems. Initial hullform parameters were chosen, and powering was estimated using Fun and Liebman's method (Fung and Liebman, 1995). A CODOG arrangement of prime movers was selected and engine rooms sized approximately. Bulkhead positions were set based on the need to meet the two-compartment damage stability standard specified in DEFSTAN 02-109, the limit state being submergence of the No. 1 deck.

E.2 Building Block Stage

The remaining building blocks were generated using the Frigate Development Kit, a Paramarine ESSD template developed by the candidate to allow rapid development of surface combatant designs (Bradbeer, 2010). This kit includes pregenerated building blocks containing space and weight algorithms taken from the UCL Ship Design Data Book (UCL, 2011), allowing rapid sketching and auditing of layouts.

The design was developed to the level of 194 building blocks. The layout was further developed, with the access philosophy based around a single passage on No. 2 Deck, doglegged to limit blast transmission and to pass around machinery uptakes/downtakes.

The hullform parameters were fixed and a firm estimate of powering made, allowing the prime movers to be sized. Structural weight was estimated based on scaling formula (Chalmers, 1993 p103) to allow for design balance before the structure was designed. A stability analysis was conducted against the criteria defined in DEFSTAN 02-109 for intact and damaged stability.

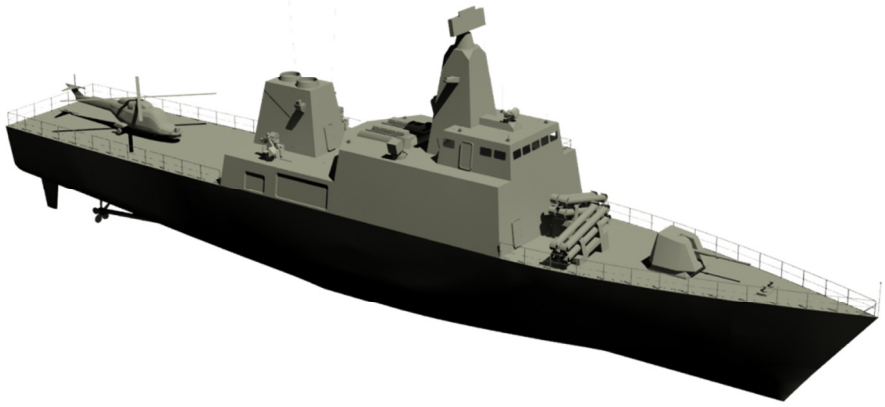

Figure E. 1 - Visualisation of the baseline corvette design

Hull girder bending load and shear force were estimated using the tools in ESSD. To calculate a load distribution, the hull was divided into 21 strips. All items having a mass of 3 tonnes or more were allocated to strips as a distributed weight. This accounted for roughly 15% of the deep displacement. The remainder was distributed assuming a constant density throughout the ship. Bending moment and shear force were estimated using the same method as was used in designing the frigate model (see Section 5.2.)

The following ship characteristics were taken forward to drive the structural model:

i. Bending Moment (Hogging): 68.5 MNm
ii. Bending Moment (Sagging): -98.4 MNm
iii. Shear Force: 2.7 MN
iv. Rule Length: 72m
v. Top speed: 30 knots
vi. Midships draught: 2.9m
vii. Block Coefficient 0.495

Appendix F Data Extraction from EPSA Output

This Appendix presents the MATLAB code used to extract data from the EPSA output files and convert it from the proprietary format used into a simple tabulated form.

```
function [ output ] = TapeParserUD( folder)
% Tape Parser UD fuction
% By Nick Bradbeer, 2011
% This function reads data from a WAI EPSA Tape6 output file and
converts it into a form more suitable for analysis
starttime = clock;
%TapeParser - reads in a Tape98 and Tape5 from the subfolder
'folder' and returns all points within the specified region in
the format:
%Row 1: Node Number
%Row 2: X Co-Ordinate
%Row 3: Y Co-ordinate
%Row 4: Z Co-Ordinate
%Row 5: Maximum Velocity
%Row 6: Maximum Acceleration
%Row 7: Rise Time to peak velocity
%Row 8: Velocity Zero-Zero period
%Row 9+: Velocity-time trace
%The UD version of TapeParser does not chop up data into regions
and does not apply the low-pass filter.

%PART 1 - Read in Data from Tape98
% Routine to read in a tape98 file and assign traces to a matrix
disp('Starting Part 1');
finishtime = clock;
disp(finishtime);
%Open files with identifier id
t98path = [folder '/tape98']
t5path = [folder '/tape5']

tape98 = fopen(t98path);
tape5 = fopen(t5path);
%Handle time/curves headers
header = fgetl(tape98); %Gets title line
linein = fgetl(tape98); %Gets curves line
curves = sscanf(linein, '%d');
     % curves(1) is number of curves.
     % curves(2) is number of data points per curve
linein = fgetl(tape98); %Gets the $DXP$ line
linein = fgetl(tape98); %Gets the time units line (time sec)
linein = fgetl(tape98); %Gets the unknown line (0, 1e-3)
linein = fgetl(tape98); %Gets the timesteps line
timestep = sscanf(linein, '%f');
     % timestep(1) is timestep length
     % timestep(2) is number of timesteps
%Create time column for graphing against
timeaxis = (linspace(0,timestep(1),curves(2)-1))';
%FOR EACH CURVE IN TAPE98
for c = 1:curves(1)
     %Strip out header data
     linein = fgetl(tape98); %Gets the CURVE.... line
```

```
          rawnodes(c,1)=(str2num(linein(28:34)));  %strips  out
the node number and assigns it to rawnodes(c,1)
          rawnodes(c,2:4)=linein(24:26); %Assigns a type code
(either "  w" for velocity or "zdf" for displacement to rawnodes
(c,2:4)
          % Note that rawnodes must store nodes by rows not by
columns, to allow for the storage of type strings in columns 2:4
     linein = fgetl(tape98); %Gets the units line (displacement
m)
     linein = fgetl(tape98); %Gets the min/max/start line
          minmax(:,c)  =  str2num(linein);  %Strips  out  the
minimum, maximum and starting values for this curve
               %minmax(1,c) is minimum value for curve c
               %minmax(2,c) is maximum value for curve c
               %minmax(3,c) is starting value
          range(c)=minmax(2,c)-minmax(1,c); %Sets data range
               %range(c) is the range of data from min to max
     %For each line in data block:
     for  ln  =  1:ceil(curves(2)/20);  %This  is  the  number  of
lines per curve, since tape98 fits 20 points per line
          if ln == 1
               clear datastring;
               datastring  =  [fgetl(tape98)];  %Gets  the  first
line of the block
               else
               datastring = [datastring, fgetl(tape98)]; %Gets
the nth line of data, appends to datastring
               end
          end
          %Import entire data block into tape
          %trace    =    fscanf(tape98,    '%1[1234567890    ]',
5*timestep(2));
          %Scan through trace in blocks of five importing each
block into rawdata(n,c)
          for n = 1:curves(2);
               data= (str2num(datastring((n*5)-4:(n*5))));
               rawdata(n,c)                                    =
((data/100000)*range(c))+minmax(1,c);
               end
          end
     fclose(tape98);
clear c data datastring header tape98 linein ln minmax n range;

% PART 2
% AT THIS POINT, ALL TAPE98 DATA HAS BEEN READ IN BUT NOT SORTED
% Sort through rawdata and grab only the velocity lines
disp('Starting Part 2');
finishtime = clock;
disp(finishtime);
NextVelDataCol=1;
for c = 1:curves(1);  %Loop once per line in rawdata
     if rawnodes(c,2:4) =='  w'
          %i.e. if the line corresponds to an upward velocity
trace
                    veldata(:,NextVelDataCol)  =  rawdata(:,c);
     %Copy line to veldata(:,c)
                    velnodes(1,NextVelDataCol)                =
rawnodes(c,1);                  %Copy     node     number     to
velnodes(1,c).
                    % Note that velnodes stores one node per
column like veldata, while rawnodes stored one node per row
                    NextVelDataCol = NextVelDataCol + 1;
                    end
```

```
     end
clear c nextveldatarow rawdata rawnodes NextVelDataCol;

% PART 3
% Load tape5 and locate x,y&z co-ordinate values for all nodes
in velnodes
% co-ordinates go into rows 2,3&4 of velnodes

% Scan through file and grab co-ordinates of all nodes held in
velnodes
disp('Starting Part 3');
finishtime = clock;
disp(finishtime);

while 1;
    linein = fgetl(tape5); %grabs next line

    if linein == -1 %check for file end
        break
    end

    if linein(1:6) == 'node   '; %discard line if not a node
definition. If it is a node definition, check if we are
interested

        thisnode = str2num(linein(10:16)); %grab the node number
from linein
        for n = 1:size(velnodes,2) %run through list of nodes of
interest
            if thisnode == velnodes(1,n) %if the node number of
linein is this node of interest
                velnodes(2,n) = str2num(linein(17:29)); %grab x
                velnodes(3,n) = str2num(linein(30:42)); %grab y
                velnodes(4,n) = str2num(linein(43:55)); %grab z
            end
        end
    end
  end

  fclose(tape5);
  clear n linein tape5 thisnode;

  % PART 4
  % Apply Low-Pass Filter to the velocity data to smooth it
  % Using tenth order Butterworth filter at cutoff frequency of
100 Hz
disp('Starting Part 4');
finishtime = clock;
disp(finishtime);


%Choose cutoff frequency:
%fcutoff = 100; %in Hz
%Half of sampling frequency:
%fhalfsampling = 0.5/timestep(1);
%Normalised frequency:
%fnorm = fcutoff / fhalfsampling;
%[b a] = butter(10, fnorm, 'low');
%veldatalpf = filtfilt(b,a,veldata);
veldatalpf = veldata;                       % REMOVE THIS LINE IF
LOW-PASS FILTERING IS DESIRED
```

```
  clear fcutoff fhalfsampling fnorm a b;

 % PART 5 - Calculate Accelerations
 for n=1:timestep(2)-1;
    accdata(n,:) = veldatalpf(n+1,:)-veldatalpf(n,:);
    accdata(n,:) = accdata(n,:)./timestep(1);
end

disp('Starting Part 5');
finishtime = clock;
disp(finishtime);

%PART 6 - Divide the acceleration traces up by geographically
defined regions
disp('Starting Part 6');
finishtime = clock;
disp(finishtime);

counter=0; % This counts how many have been sorted into the
region.

for c = 1:size(veldata,2);                  % Cycle through each
node, sorting each one
                counter = counter+1;
                sorted_accdata(:,counter)=accdata(:,c);
                sorted_summarydata(1,counter)  =  velnodes(1,c);
%Stuff the node number into row 1
            sorted_summarydata(2:4,counter)=    velnodes(2:4,c);
%Pass XYZ co-ords to data rows 2:4

     sorted_summarydata(5,counter)=max(veldatalpf(:,c));   %Pass
max vel to data row 5
                sorted_summarydata(6,counter)=max(accdata(:,c));
%Pass max accel to data row 6
                [risetime,              period]               =
findperiod(veldatalpf(:,c));%Invoke  Findperiod  to  derive  rise
time and zero-zero period of the velocity curve
            sorted_summarydata(7,counter)                     =
risetime.*timestep(1); %Pass rise time to data row 7
                sorted_summarydata(8,counter)                 =
period.*timestep(1); %Pass period to data row 8
                sorted_veldatalpf(:,counter)  =  veldatalpf(:,c);
%Put the trace into sorted_veldatalpf
                    end             %End of the C-loop


output = [sorted_summarydata; sorted_veldatalpf];

finishtime = clock;
runtime = finishtime - starttime;
disp('Start Time');
disp(finishtime(1,4:6));
disp('Run Time');
disp(runtime(1,4:6));

figure;
plot3(output(2,:), output(3,:), output(4,:),'.');
title('Plot of XYZ Co-ordinates of nodes');
disp('1: Node Number');
disp('2: X Co-Ordinate');
disp('3: Y Co-ordinate');
disp('4: Z Co-Ordinate');
disp('5: Meximum Velocity');
```

```
disp('6: Maximum Acceleration');
disp('7: Rise Time to peak velocity');
disp('8: Velocity Zero-Zero period');
disp('9+: Velocity-time trace');
end
```

Appendix G MATLAB Code Used to Develop SRS Plots

This Appendix presents the MATLAB code, adapted from (Irvine, 2006), used to develop SRS plots:

```
function[x_pos, x_neg] = SRSnb(time_input, acc_input, freq_range,
wantplot, damp)
%disp(' ')
%disp(' srs.m   ver 2.0   July 3, 2006')
%disp(' by Tom Irvine   Email: tomirvine@aol.com')
%disp(' ')
%disp(' This program calculates the shock response spectrum')
%disp(' of an acceleration time history, which is pre-loaded into
Matlab.')
%disp(' The time history must have two columns: time(sec) &
acceleration')
%disp(' ')
% Version modified by Nick Bradbeer Jan 2012
% Modified version reads in a time history, acceleration history and
frequency range, and returns an SRS spectrum
%
clear t;
clear y;
clear yy;
clear n;
clear fn;
clear a1;
clear a2
clear b1;
clear b2;
clear jnum;
clear THM;
clear resp;
clear x_pos;
clear x_neg;
%
%disp(' ')
%disp(' Select file input method ');
%disp('   1=external ASCII file ');
%disp('   2=file preloaded into Matlab ');
%file_choice = input('');
%
%if(file_choice==1)
%    [filename, pathname] = uigetfile('*.*');
%    filename = fullfile(pathname, filename);
%%
%    fid = fopen(filename,'r');
%    THM = fscanf(fid,'%g %g',[2 inf]);
%    THM=THM';
%else
%    THM = input(' Enter the matrix name:  ');
%end

%
t=double(time_input);
y=double(acc_input);
%
tmx=max(t);
tmi=min(t);
n = length(y);
%
%out1 = sprintf('\n  %d samples \n',n);
```

```
%disp(out1)
%
dt=(tmx-tmi)/(n-1);
sr=1./dt;
%
%out1 = sprintf(' SR  = %g samples/sec    dt = %g sec \n',sr,dt);
%disp(out1)
%
%Starting frequency is 1 Hz
fn=freq_range;
nsteps = size(freq_range,1);
%
%Set damping %age
%damp=0;
%Damp now inherited from inputs
%
%
tmax=(tmx-tmi) + 1./fn(1);
limit = round( tmax/dt );
n=limit;
yy=zeros(1,limit);
for i=1:length(y)
        yy(i)=y(i);
end
%
%disp(' ')
%disp(' Calculating response..... ')
%
%  SRS engine
%
for j=1:nsteps
%
    omega=2.*pi*fn(j);
    omegad=omega*sqrt(1.-(damp^2));
    cosd=cos(omegad*dt);
    sind=sin(omegad*dt);
    domegadt=damp*omega*dt;
%
 %Kelly-Richman Algorithm
        a1(j)=2.*exp(-domegadt)*cosd;
        a2(j)=-exp(-2.*domegadt);
        b1(j)=2.*domegadt;
        b2(j)=omega*dt*exp(-domegadt);
        b2(j)=b2(j)*(      (omega/omegad)*(1.-2.*(damp^2))*sind      -
2.*damp*cosd );
        b3(j)=0;
%

    forward=[ b1(j),  b2(j),  b3(j) ];
    back   =[     1, -a1(j), -a2(j) ];
%
    resp=filter(forward,back,yy);
%
    x_pos(j)= max(resp);
    x_neg(j)= min(resp);
%
end
%
%   Convert to pseudo velocity
%
for j=1:nsteps
    x_pos(j)=x_pos(j)/(2.*pi*fn(j));
    x_neg(j)=x_neg(j)/(2.*pi*fn(j));
end
%

%Want to plot?
if wantplot == 1
```

```
      %Set srs_max to the max of the pos plot and neg plot, to scale
the graph
      srs_max = max(x_pos);
      if max( abs(x_neg) ) > srs_max
            srs_max = max( abs(x_neg ));
      end


      %Set srs_min to the lowest value from the pos plot and the neg
plot to scale the graph
      srs_min = min(x_pos);
      if min( abs(x_neg) ) < srs_min
            srs_min = min( abs(x_neg ));
      end
      %
      %PRODUCE Pseudo-Velocity Plot
      plot(fn,x_pos,fn,abs(x_neg),'-.');
      %
      ylabel('Velocity (m/sec)');
      xlabel('Natural Frequency (Hz)');
      title(' Pseudo Velocity Shock Response Spectrum - Undamped');
      grid;
      set(gca,'MinorGridLineStyle','none','GridLineStyle',':','XScale'
,'log','YScale','log');
      legend ('positive','negative',2);


      fmax=max(fn);
      fmin=fmax/10.;
      fmax= 10^(round(log10(fmax)+0.5));

      ymax= 10^(round(log10(srs_max)+0.8));
      ymin= 10^(round(log10(srs_min)-0.6));
      axis([1,1e4,ymin,ymax]);

end

%Output SRS curves
output = x_pos;

end
```

Appendix H Shock Response Spectrum Envelope Plots by Shock Region of Each Model Simulated

H.1 Model 1801 (T-bar stiffeners spaced at 600mm x 1500mm)

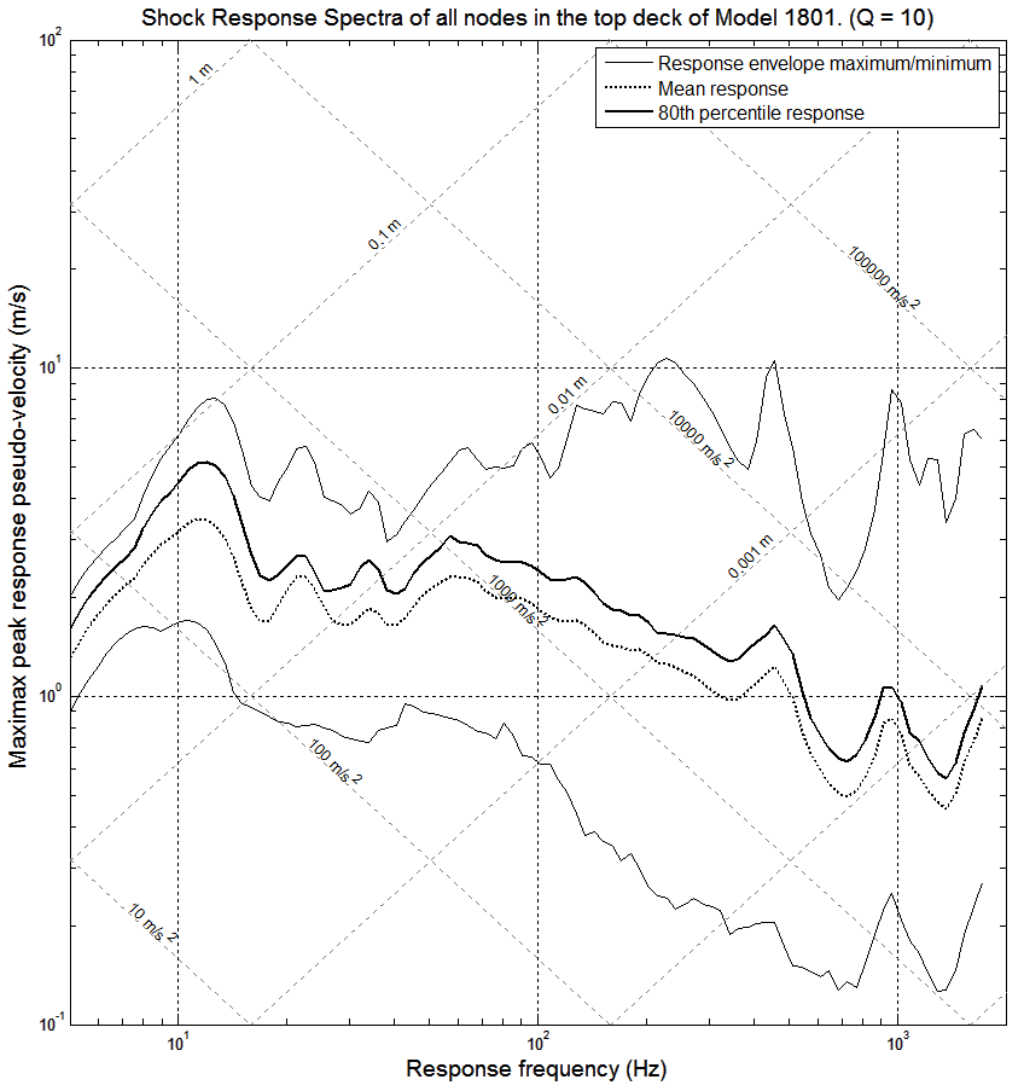

Figure H. 1 - Shock Response Spectrum of all nodes in the Top Deck region of Model 1801 (600mm x 1500mm T-bar stiffeners)

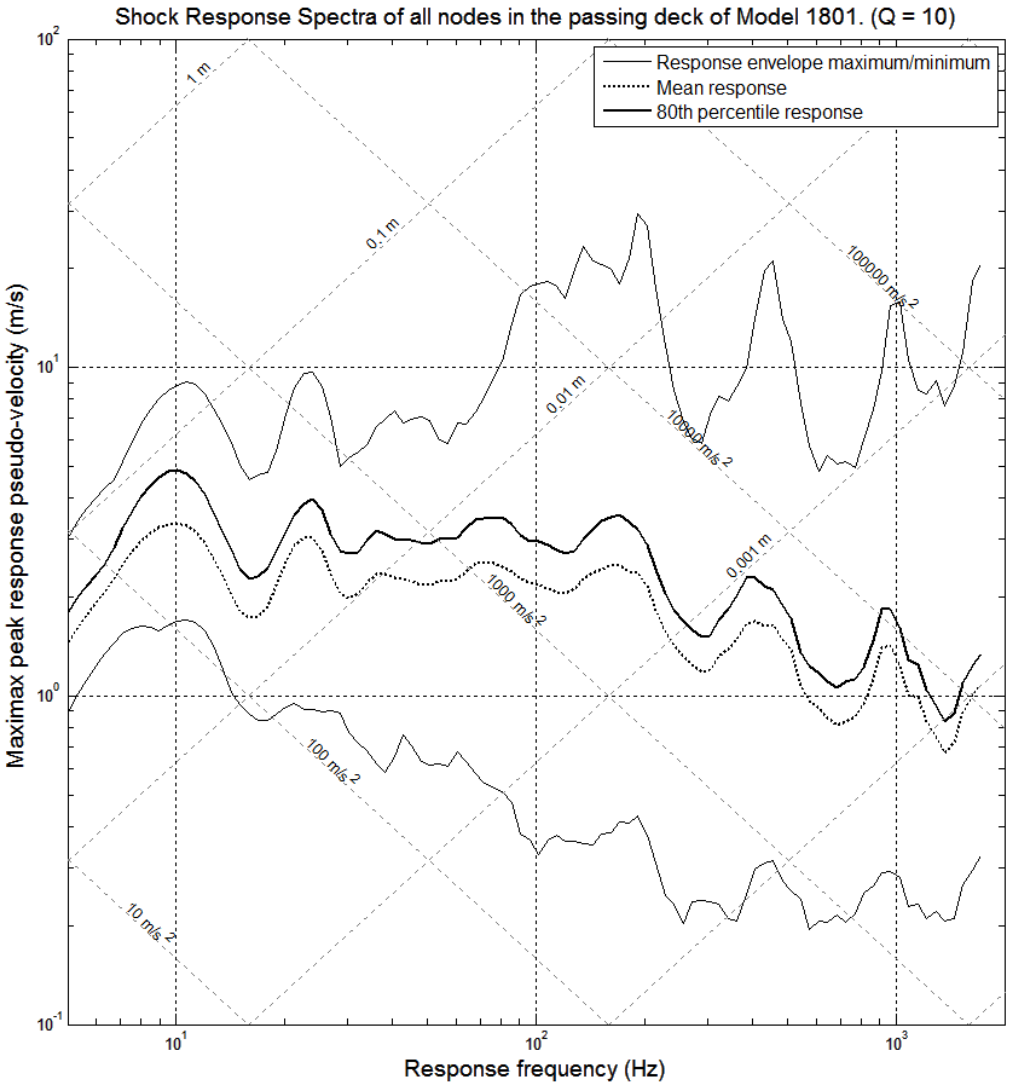

Figure H. 2 - Shock Response Spectrum of all nodes in the Passing Deck region of Model 1801 (600mm x 1500mm T-bar stiffeners)

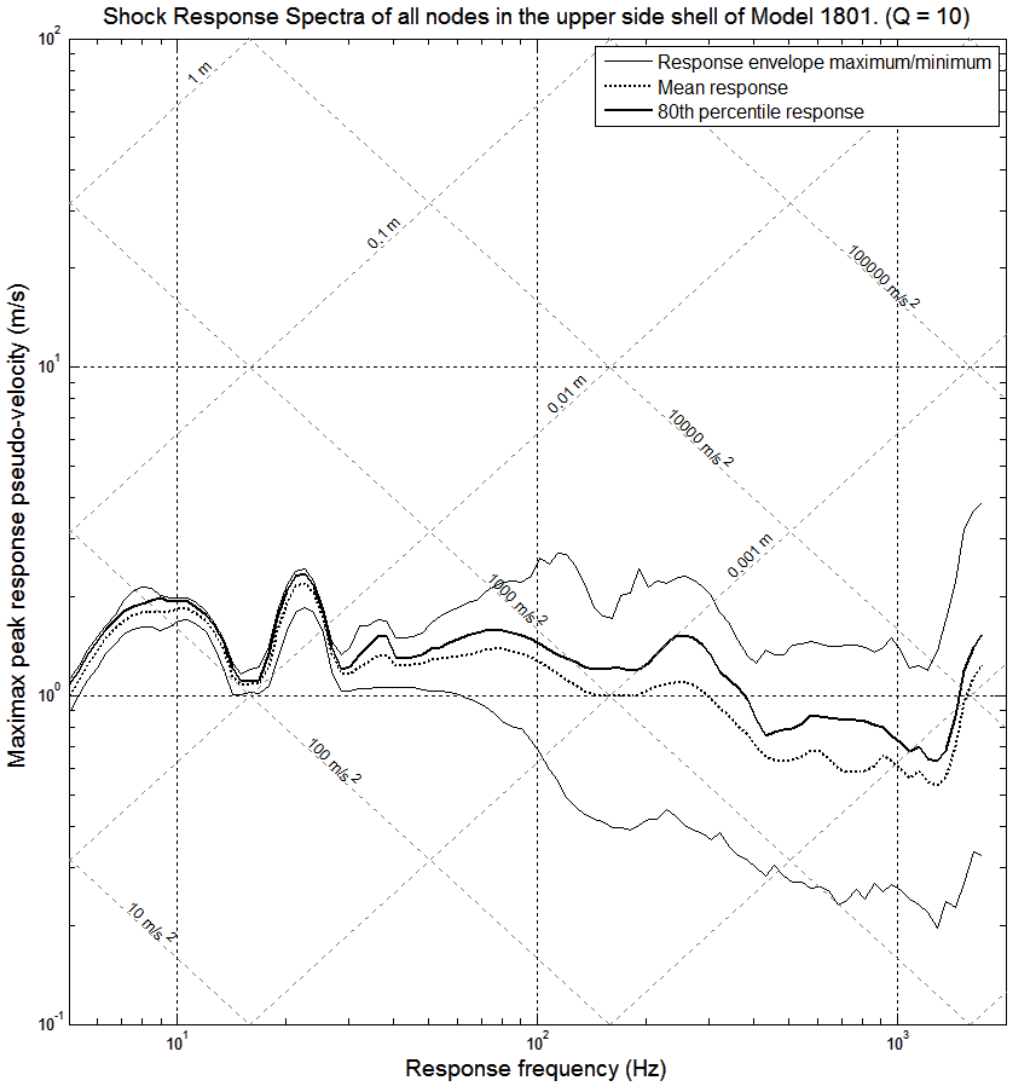

Figure H. 3 - Shock Response Spectrum of all nodes in the Upper Side Shell region of Model 1801 (600mm x 1500mm T-bar stiffeners)

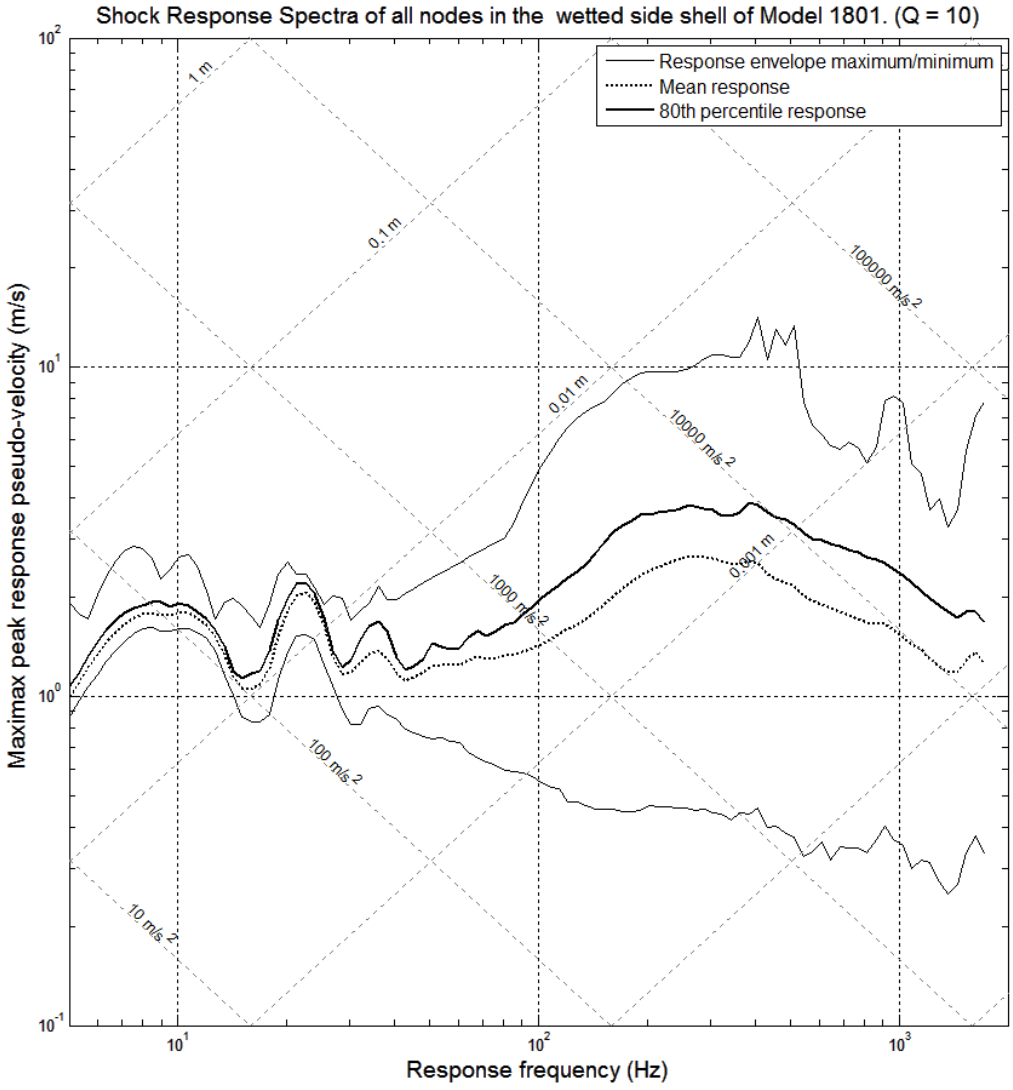

Figure H. 4 - Shock Response Spectrum of all nodes in the Wetted Side Shell region of Model 1801 (600mm x 1500mm T-bar stiffeners)

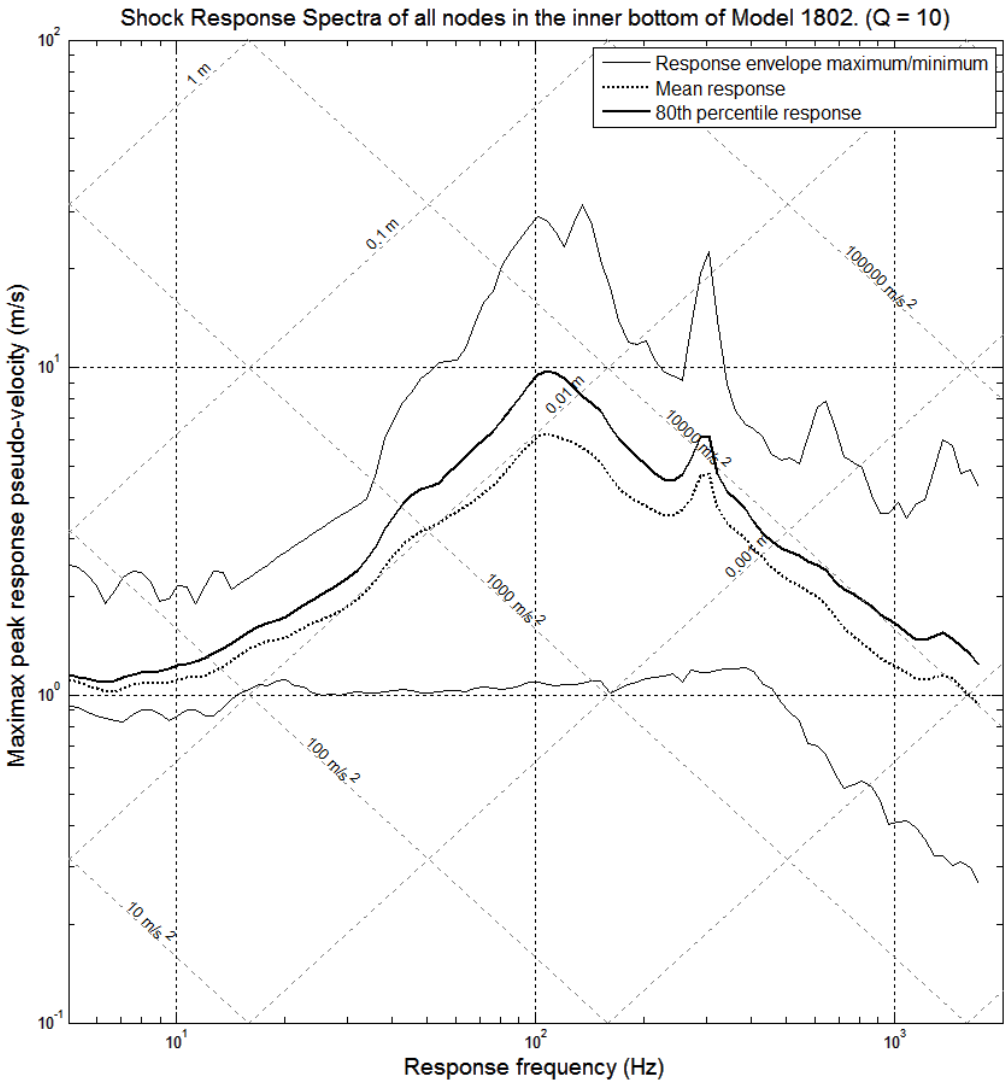

Figure H. 5 - Shock Response Spectrum of all nodes in the Inner Bottom region of Model 1801 (600mm x 1500mm T-bar stiffeners)

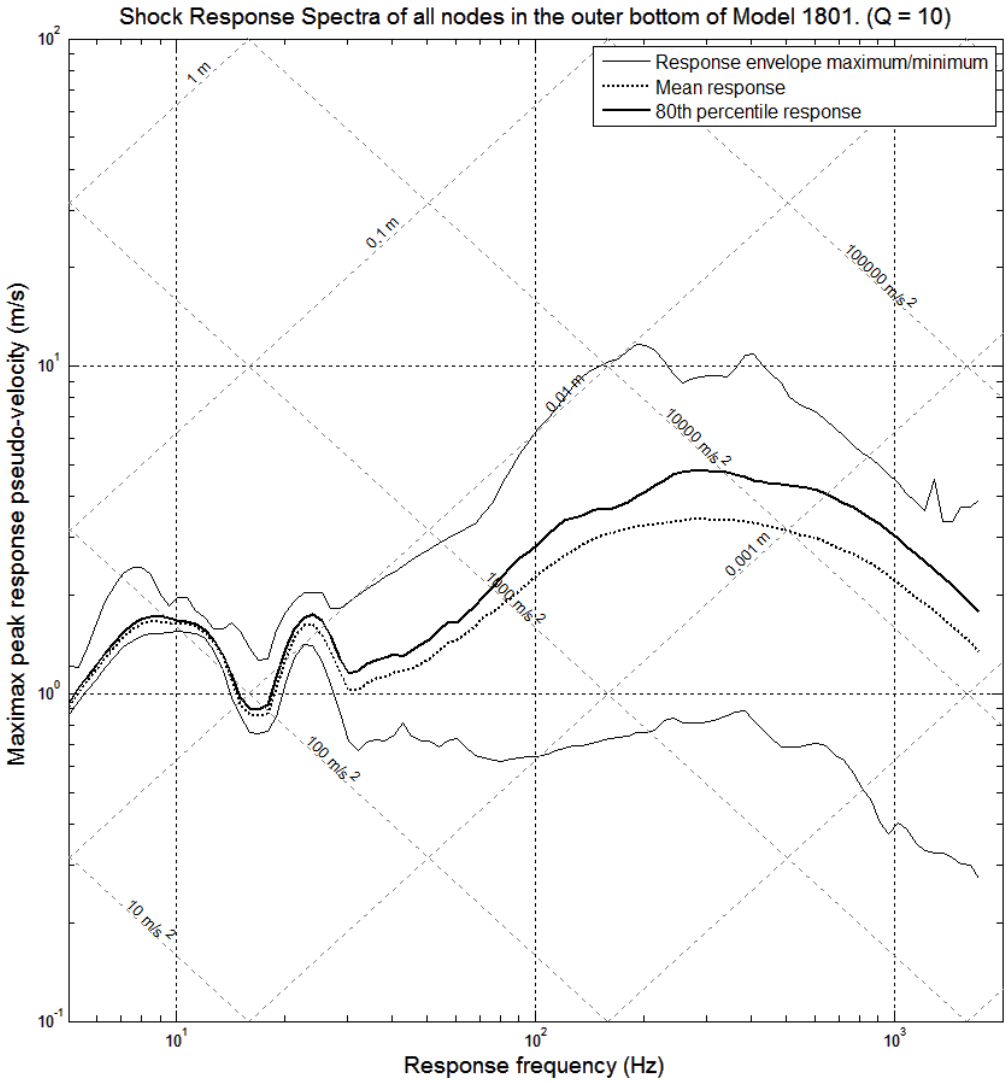

Figure H. 6 - Shock Response Spectrum of all nodes in the Outer Bottom region of Model 1801 (600mm x 1500mm T-bar stiffeners)

H.2 Model 1802 (T-bar stiffeners spaced at 800mm x 2000mm)

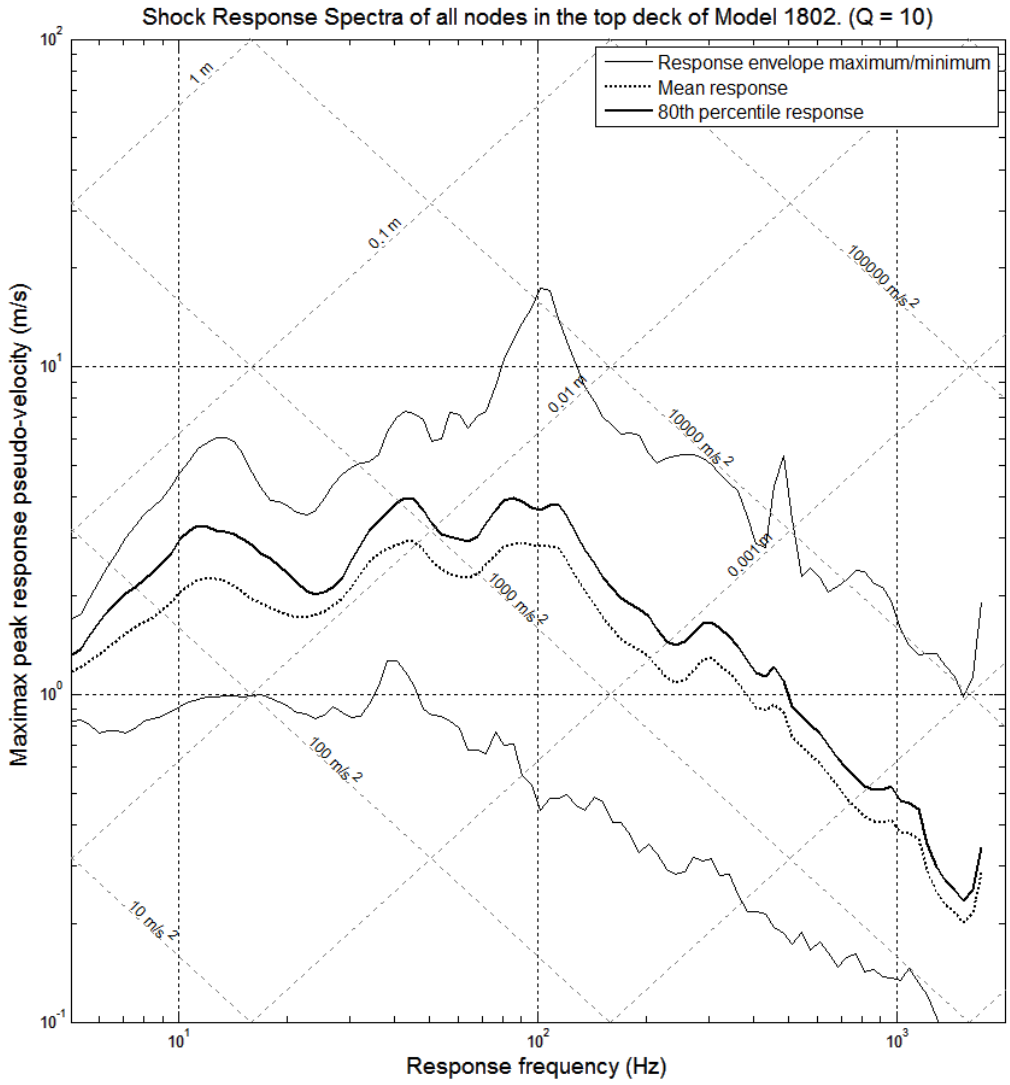

Figure H. 7 - Shock Response Spectrum of all nodes in the Top Deck region of Model 1802 (800mm x 2000mm T-bar stiffeners)

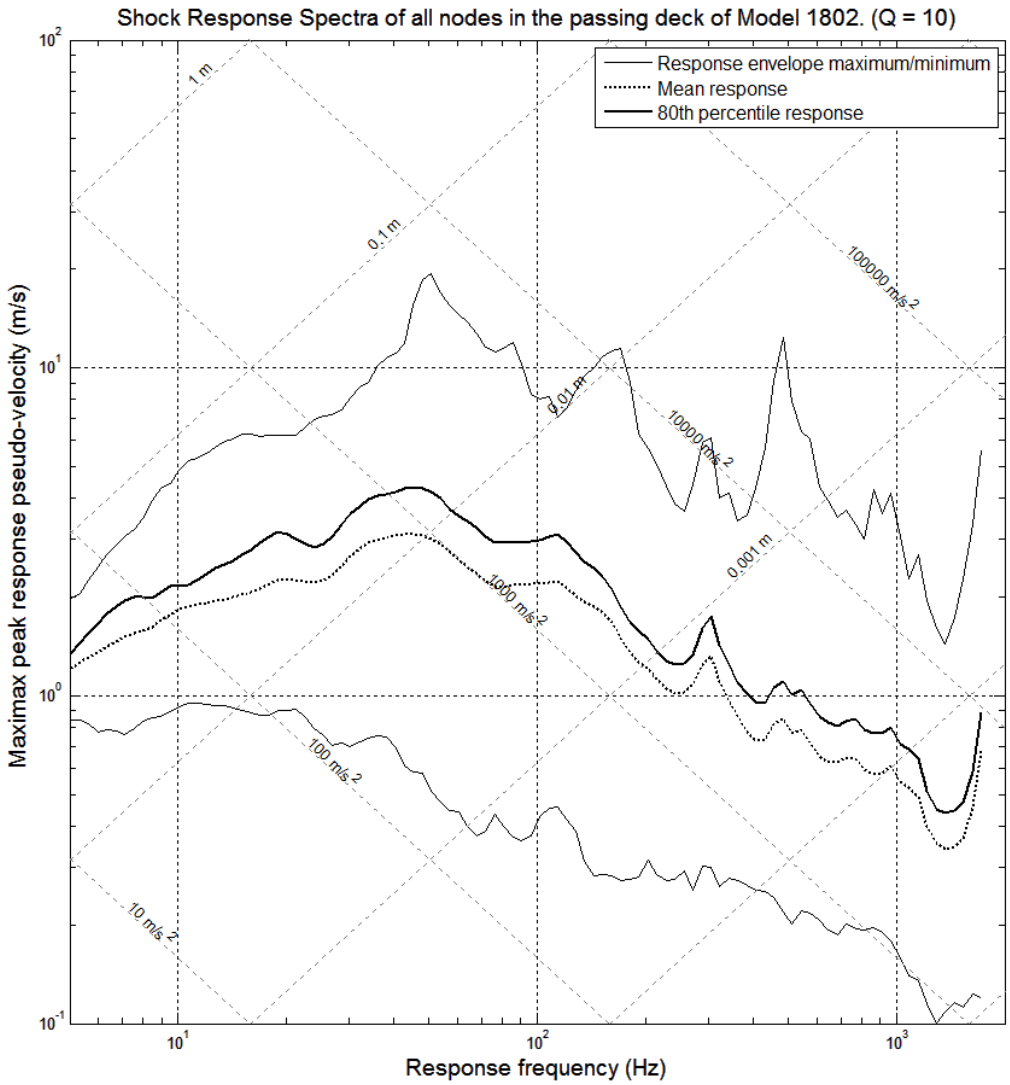

Figure H. 8 - Shock Response Spectrum of all nodes in the Passing Deck region of Model 1802 (800mm x 2000mm T-bar stiffeners)

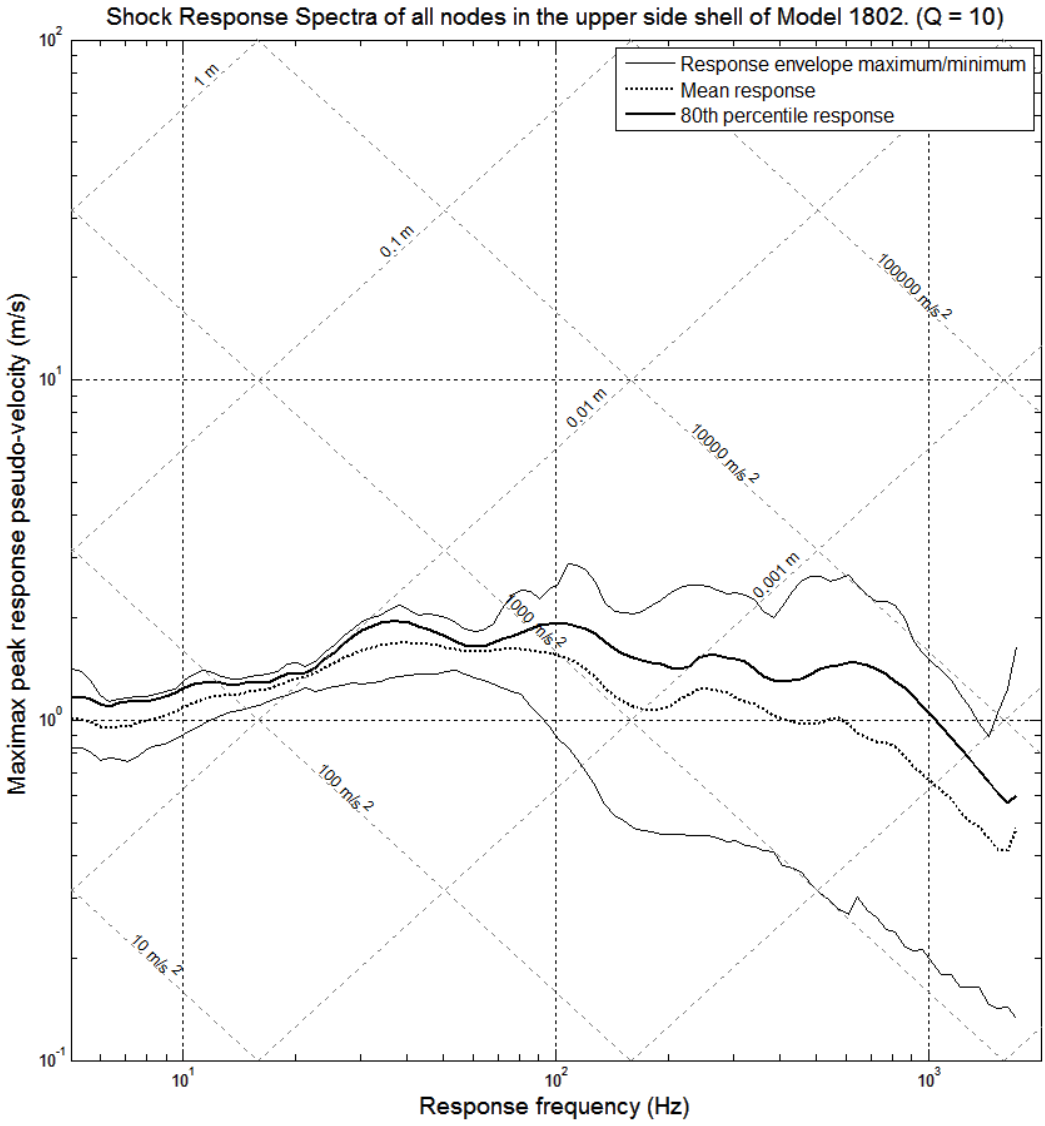

Figure H. 9 - Shock Response Spectrum of all nodes in the Upper Side Shell region of Model 1802 (800mm x 2000mm T-bar stiffeners)

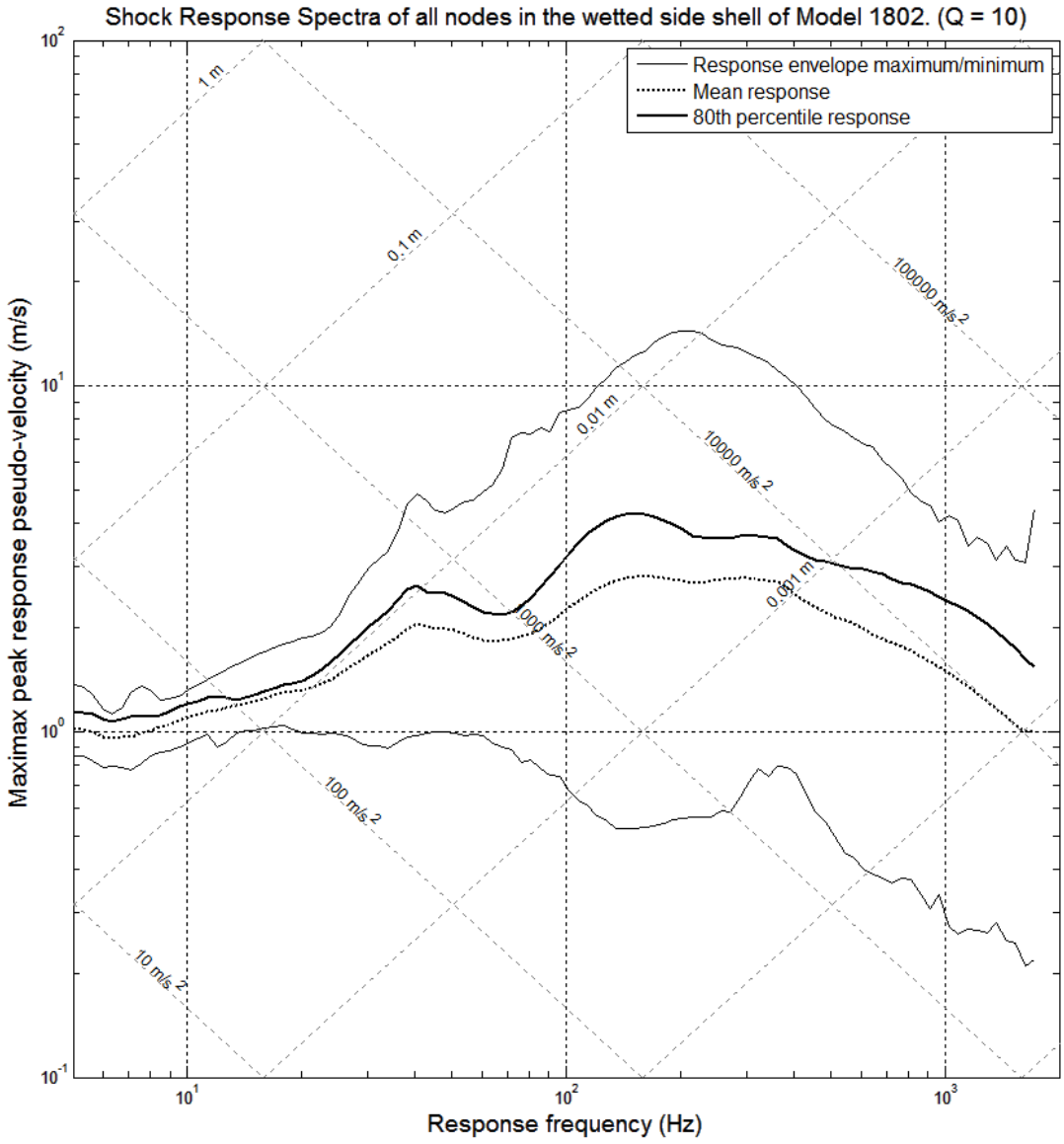

Figure H. 10 - Shock Response Spectrum of all nodes in the Wetted Side Shell region of Model 1802 (800mm x 2000mm T-bar stiffeners)

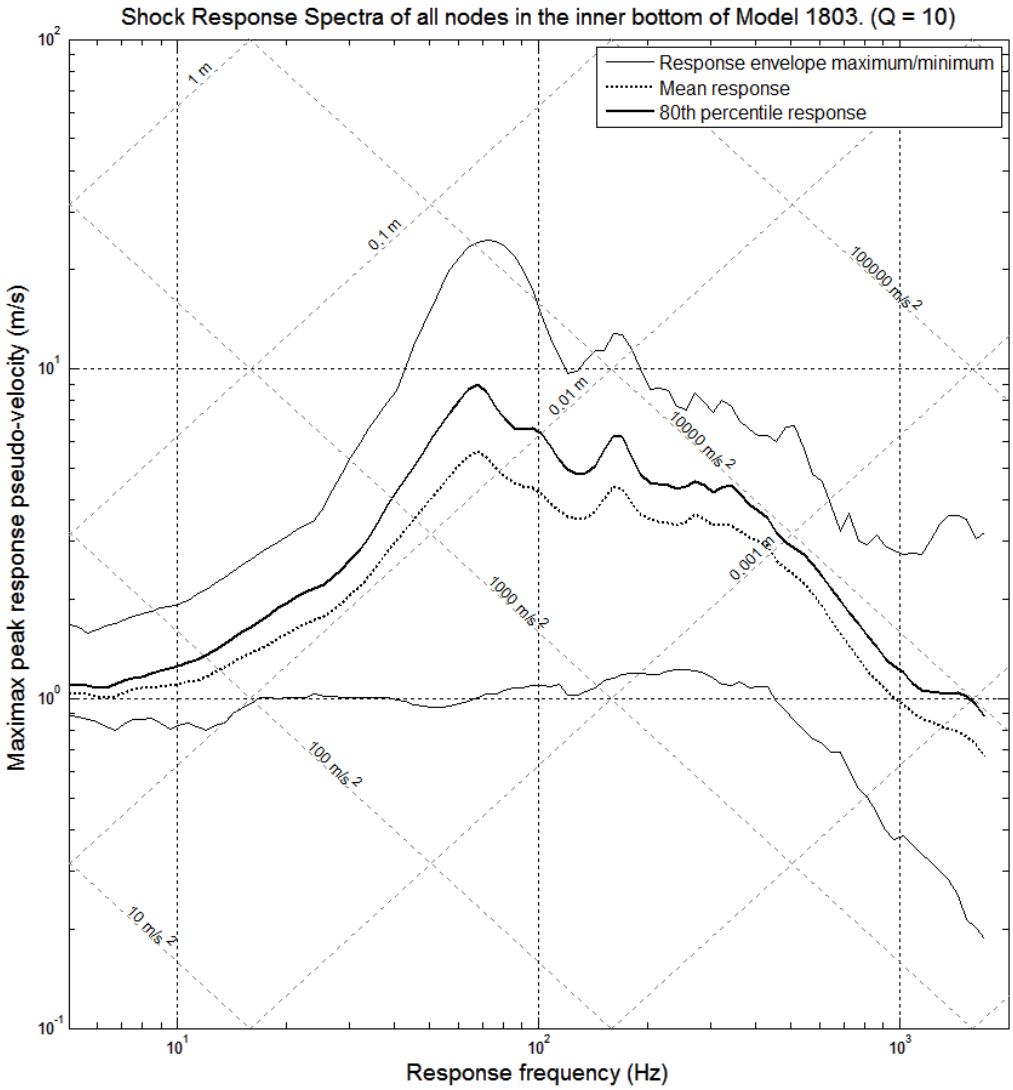

Figure H. 11 - Shock Response Spectrum of all nodes in the Inner Bottom region of Model 1802 (800mm x 2000mm T-bar stiffeners)

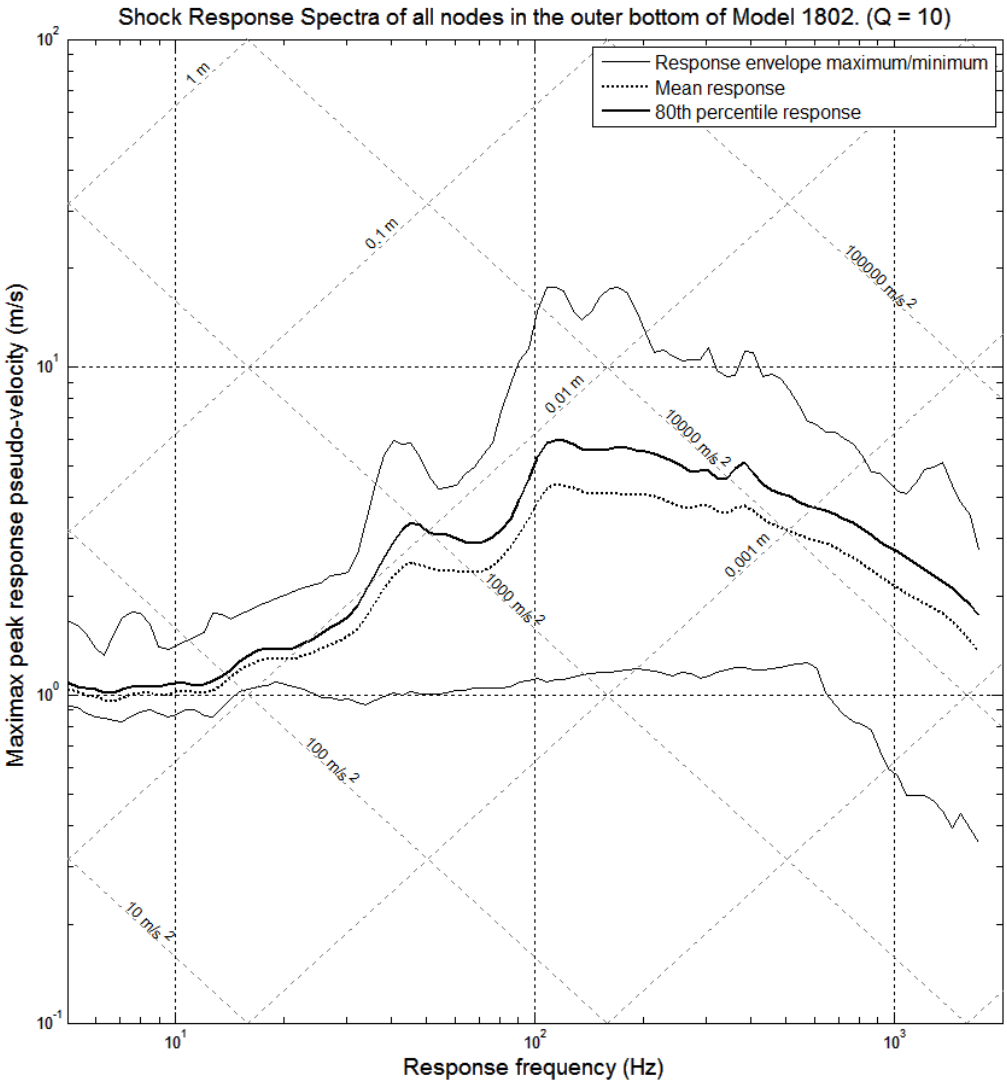

Figure H. 12 - Shock Response Spectrum of all nodes in the Outer Bottom region of Model 1802 (800mm x 2000mm T-bar stiffeners)

H.3 Model 1803 (T-bar stiffeners spaced at 1200mm x 3000mm)

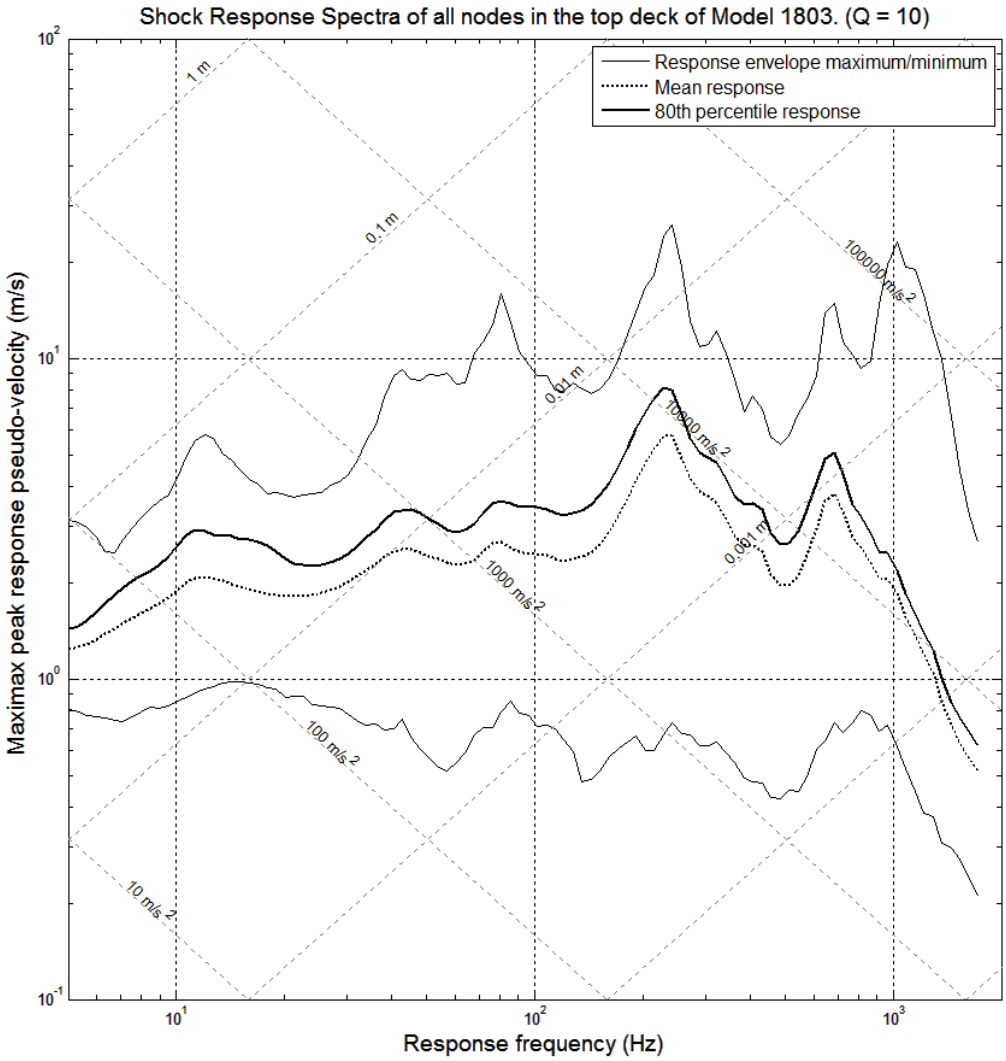

Figure H. 13 - Shock Response Spectrum of all nodes in the Top Deck region of Model 1803 (1200mm x 3000mm T-bar stiffeners)

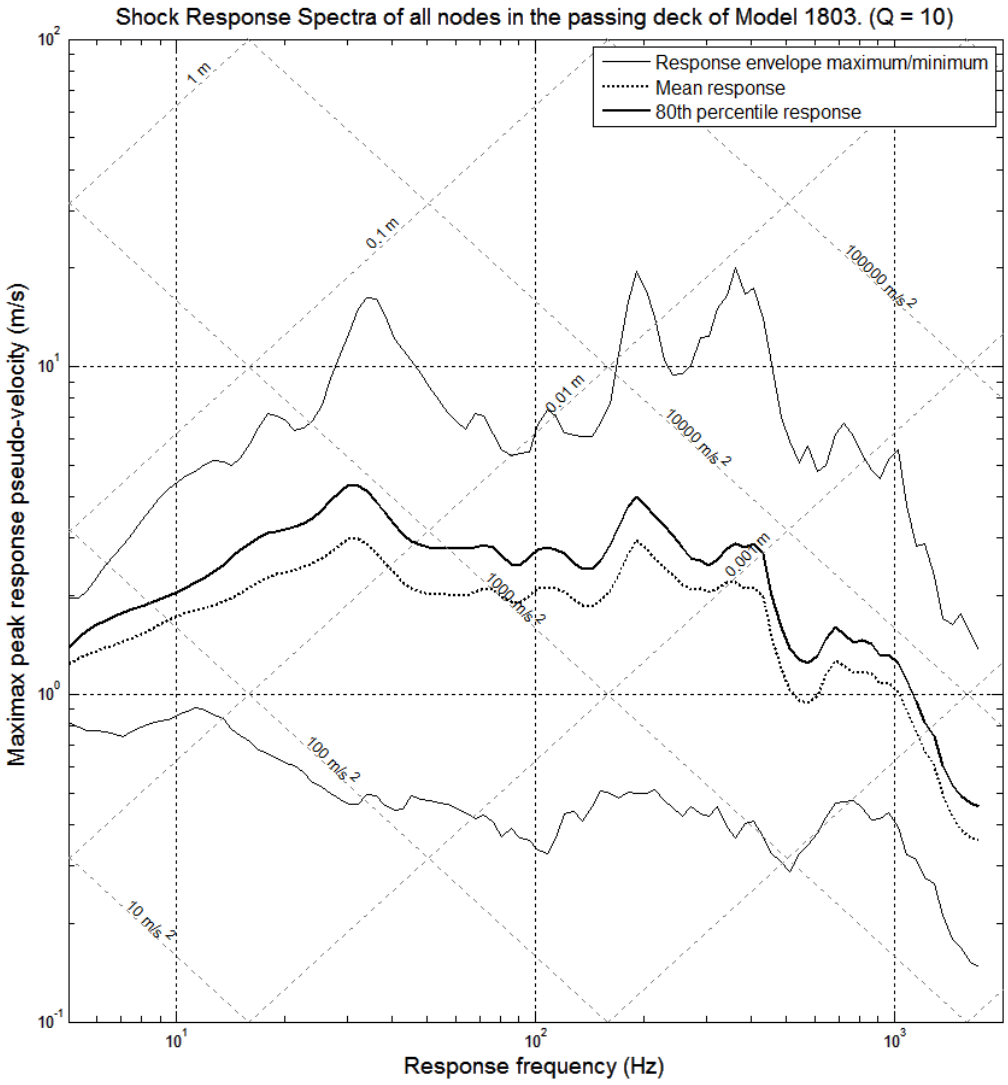

Figure H. 14 - Shock Response Spectrum of all nodes in the Passing Deck region of Model 1803 (1200mm x 3000mm T-bar stiffeners)

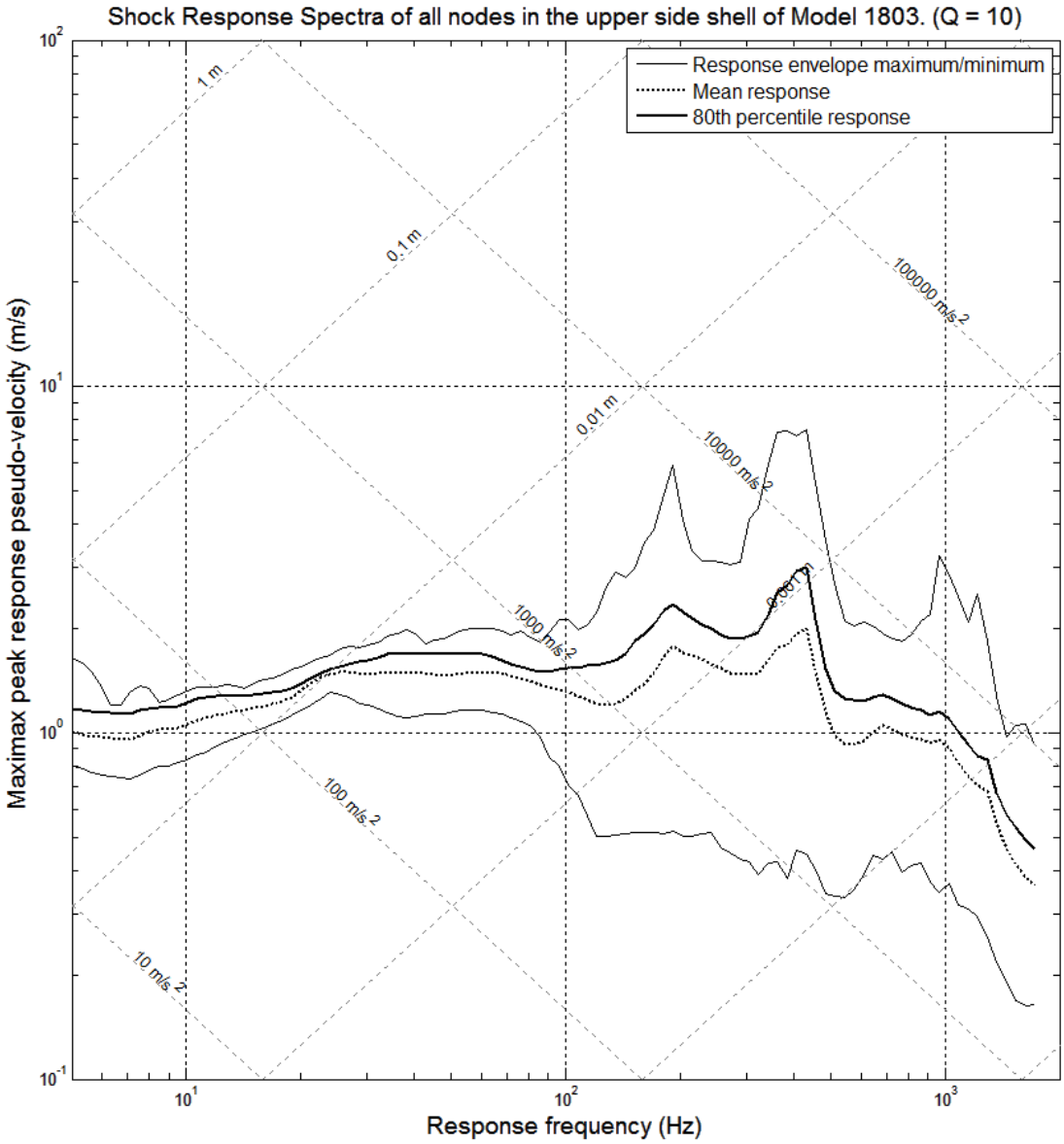

Figure H. 15 - Shock Response Spectrum of all nodes in the Upper Side Shell region of Model 1803 (1200mm x 3000mm T-bar stiffeners)

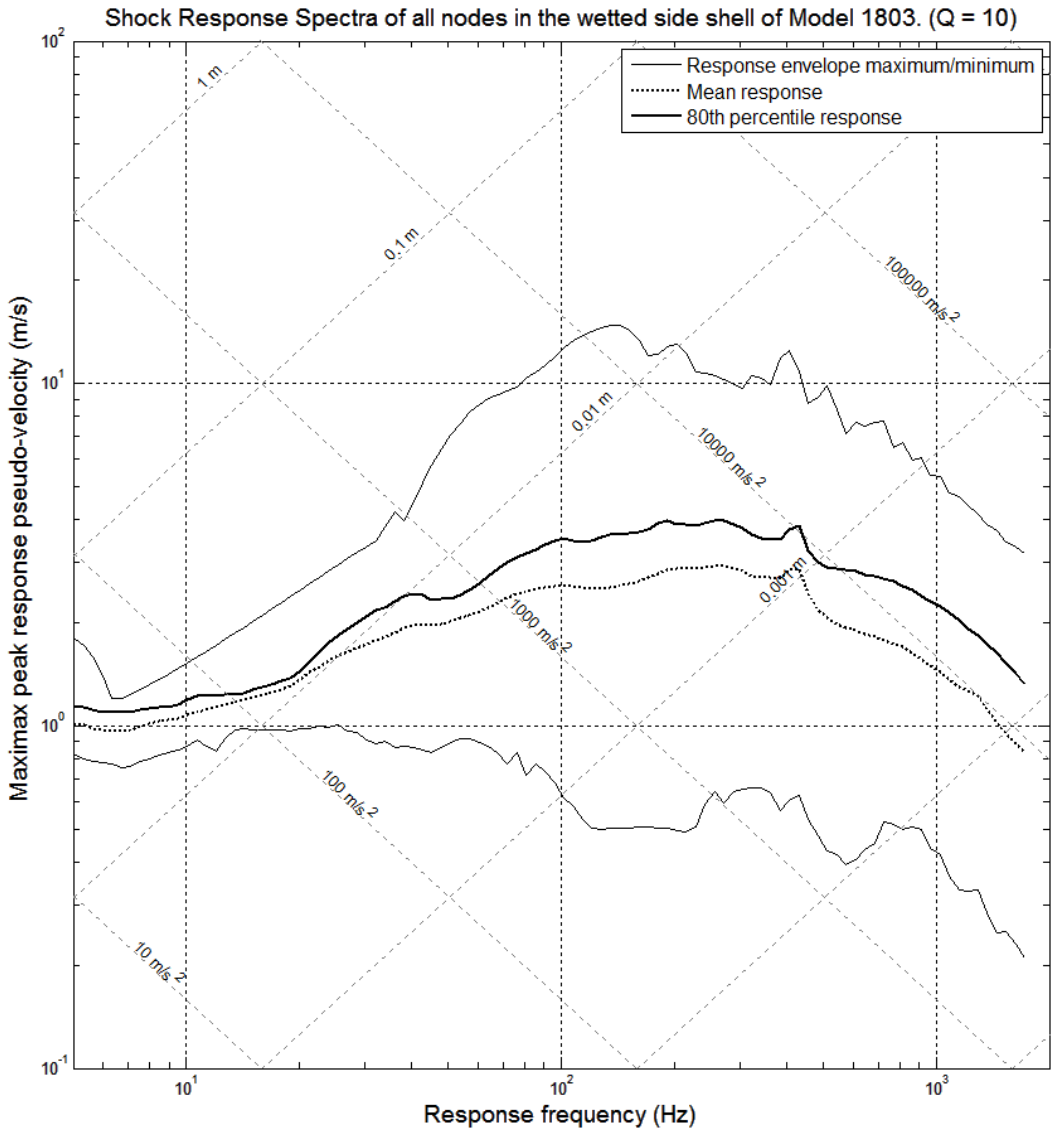

Figure H. 16 - Shock Response Spectrum of all nodes in the Wetted Side Shell region of Model 1803 (1200mm x 3000mm T-bar stiffeners)

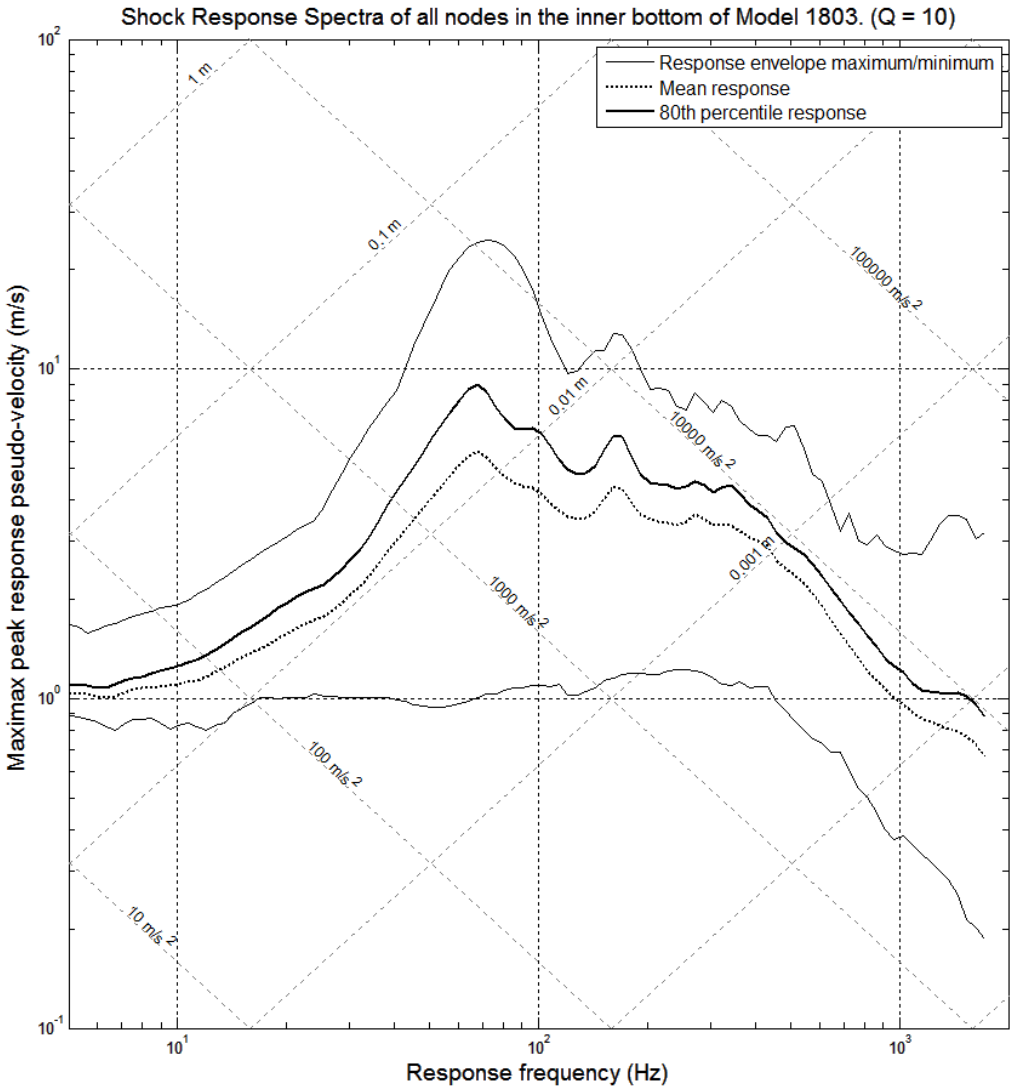

Figure H. 17 - Shock Response Spectrum of all nodes in the Inner Bottom region of Model 1803 (1200mm x 3000mm T-bar stiffeners)

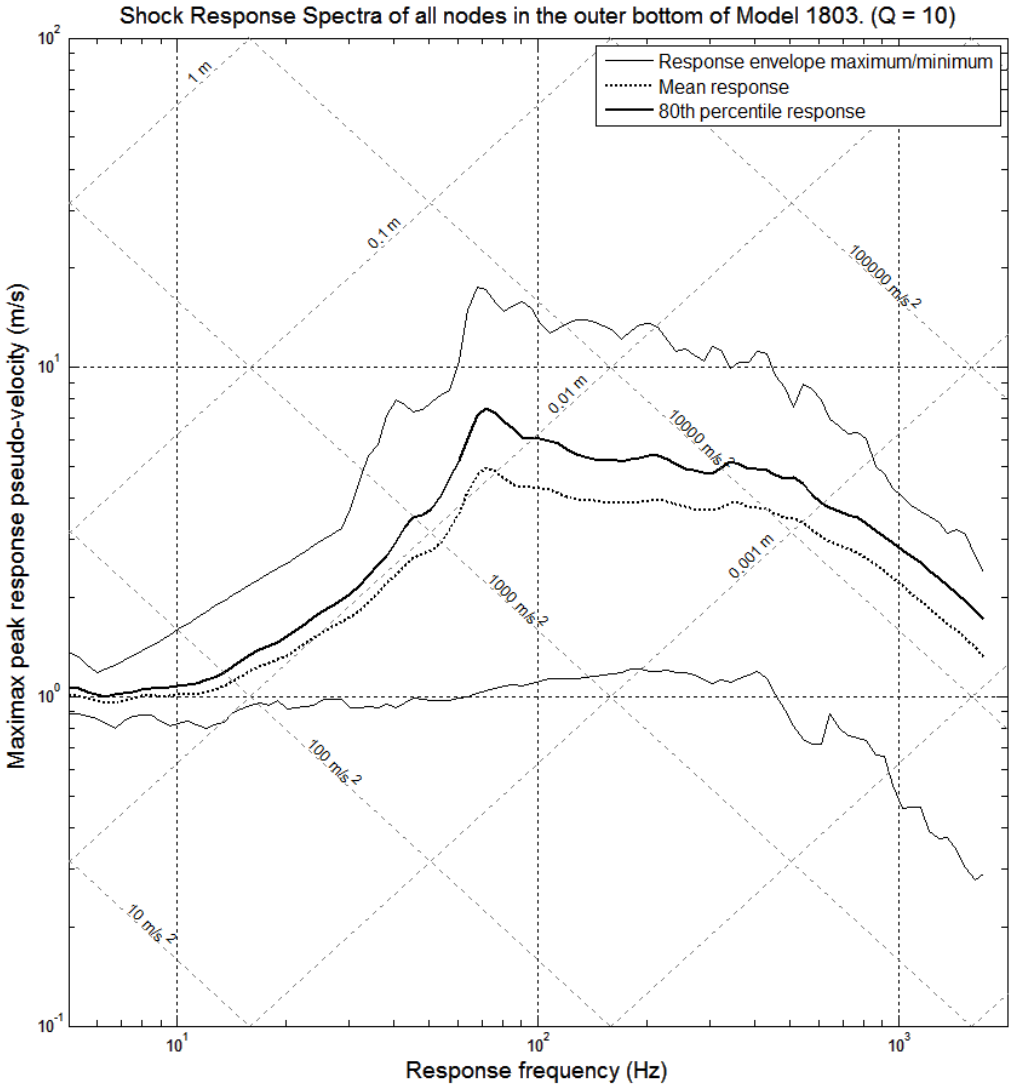

Figure H. 18 - Shock Response Spectrum of all nodes in the Outer Bottom region of Model 1803 (1200mm x 3000mm T-bar stiffeners)

H.4 Model 1804 (Offset Bulb Plate stiffeners spaced at 600mm x 1200mm)

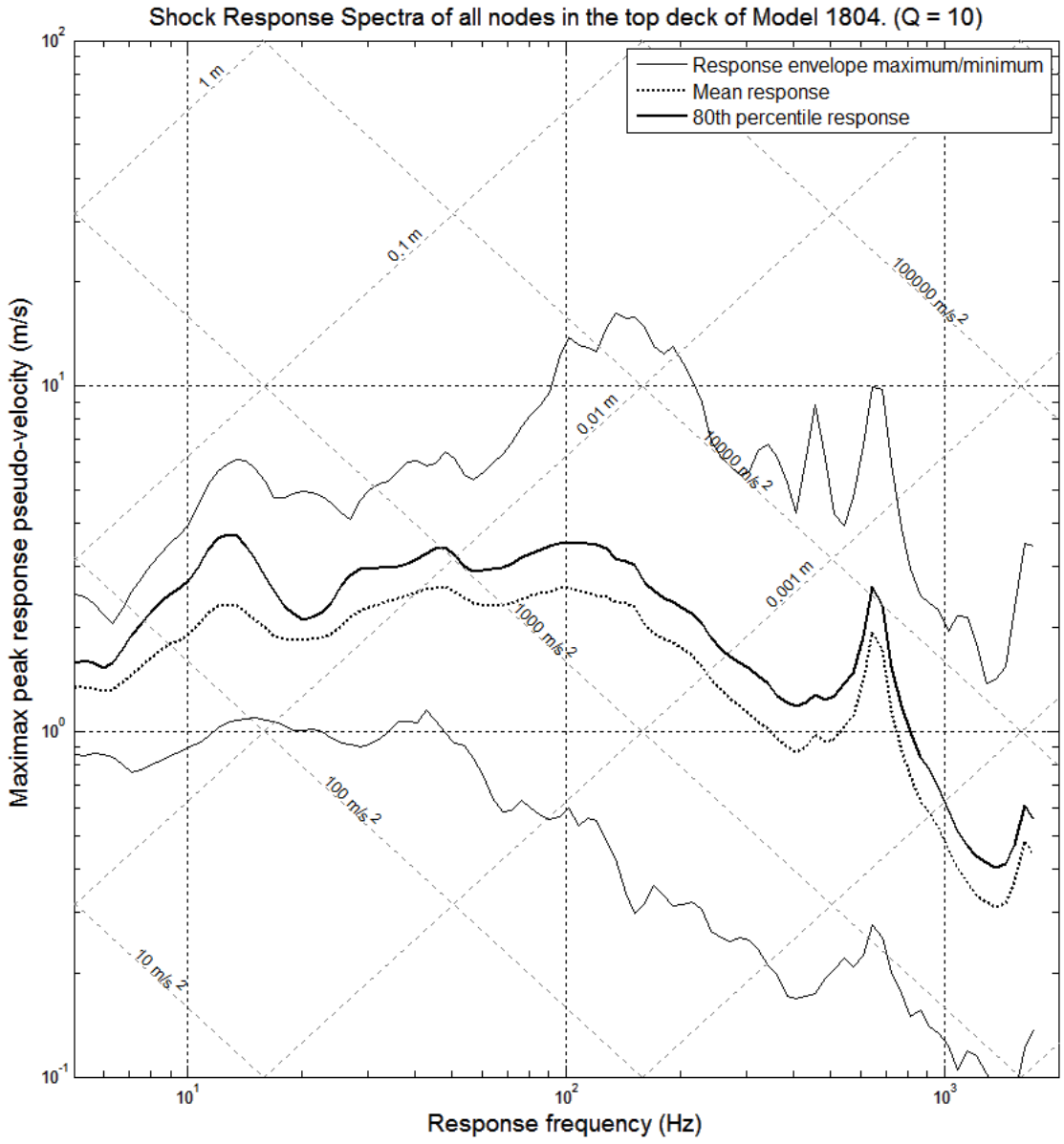

Figure H. 19 - Shock Response Spectrum of all nodes in the Top Deck region of Model 1804 (600mm x 1500mm Offset Bulb Plate stiffeners)

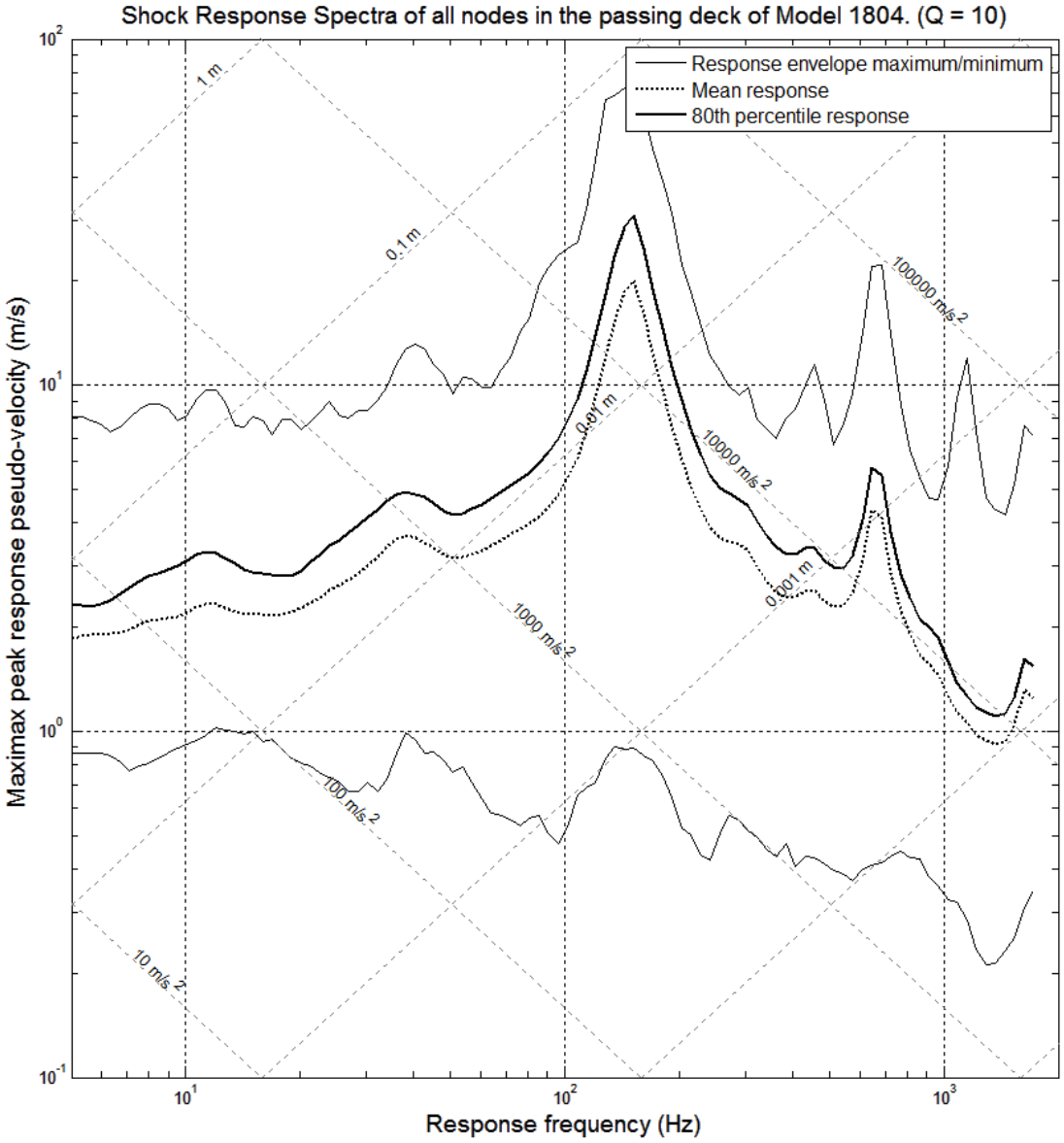

Figure H. 20 - Shock Response Spectrum of all nodes in the Passing Deck region of Model 1804 (600mm x 1500mm Offset Bulb Plate stiffeners)

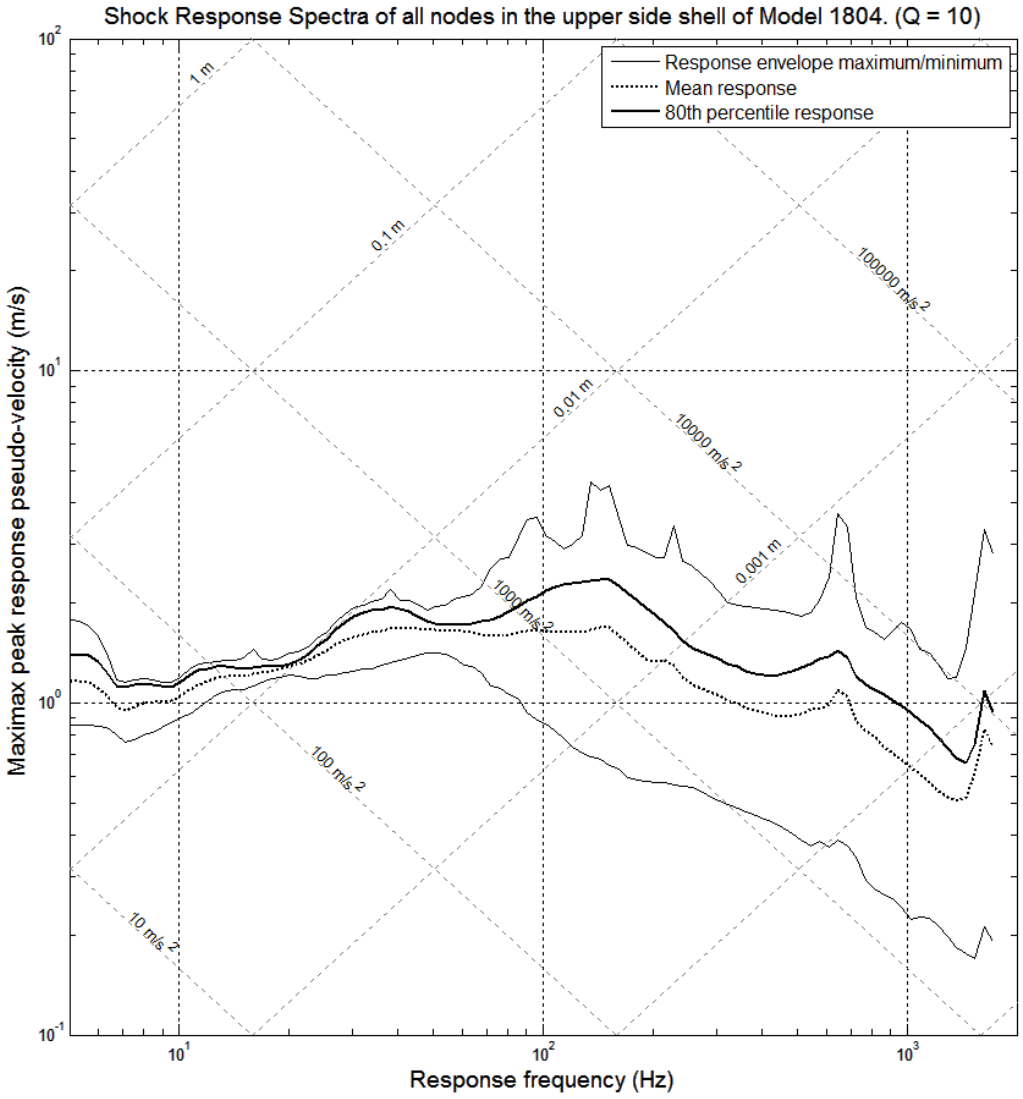

Figure H. 21 - Shock Response Spectrum of all nodes in the Upper Side Shell region of Model 1804 (600mm x 1500mm Offset Bulb Plate stiffeners)

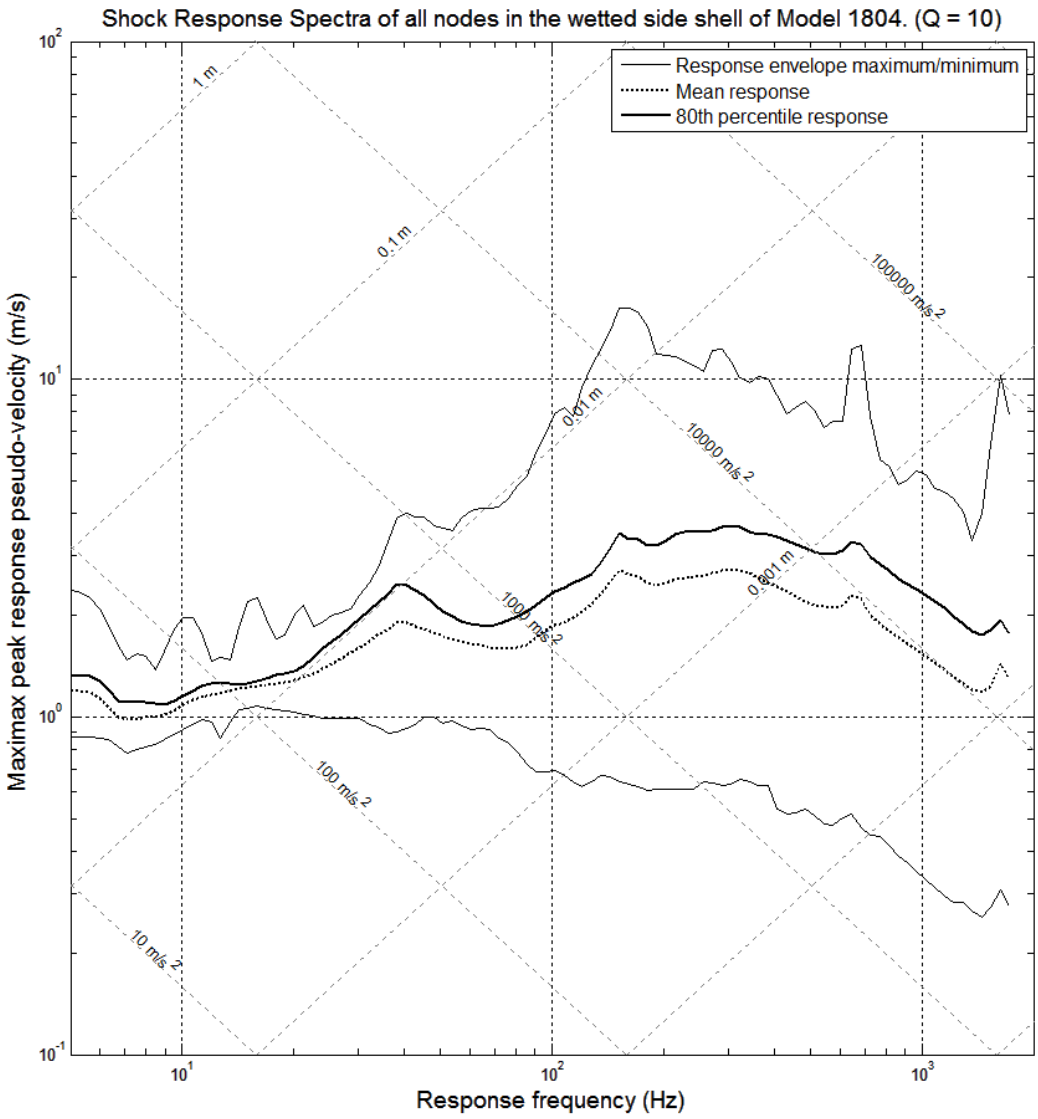

Figure H. 22 - Shock Response Spectrum of all nodes in the Wetted Side Shell region of Model 1804 (600mm x 1500mm Offset Bulb Plate stiffeners)

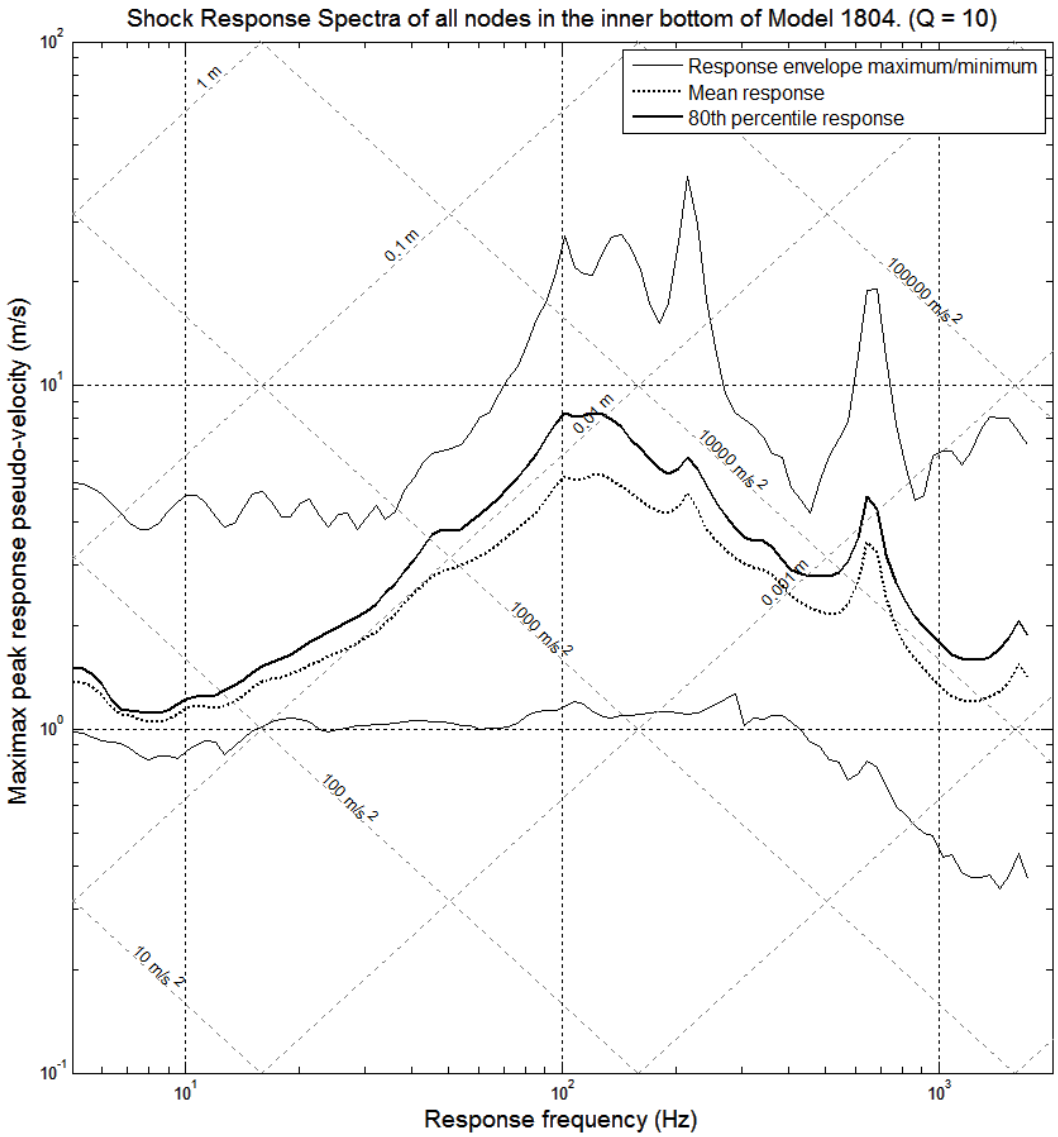

Figure H. 23 - Shock Response Spectrum of all nodes in the Inner Bottom region of Model 1804 (600mm x 1500mm Offset Bulb Plate stiffeners)

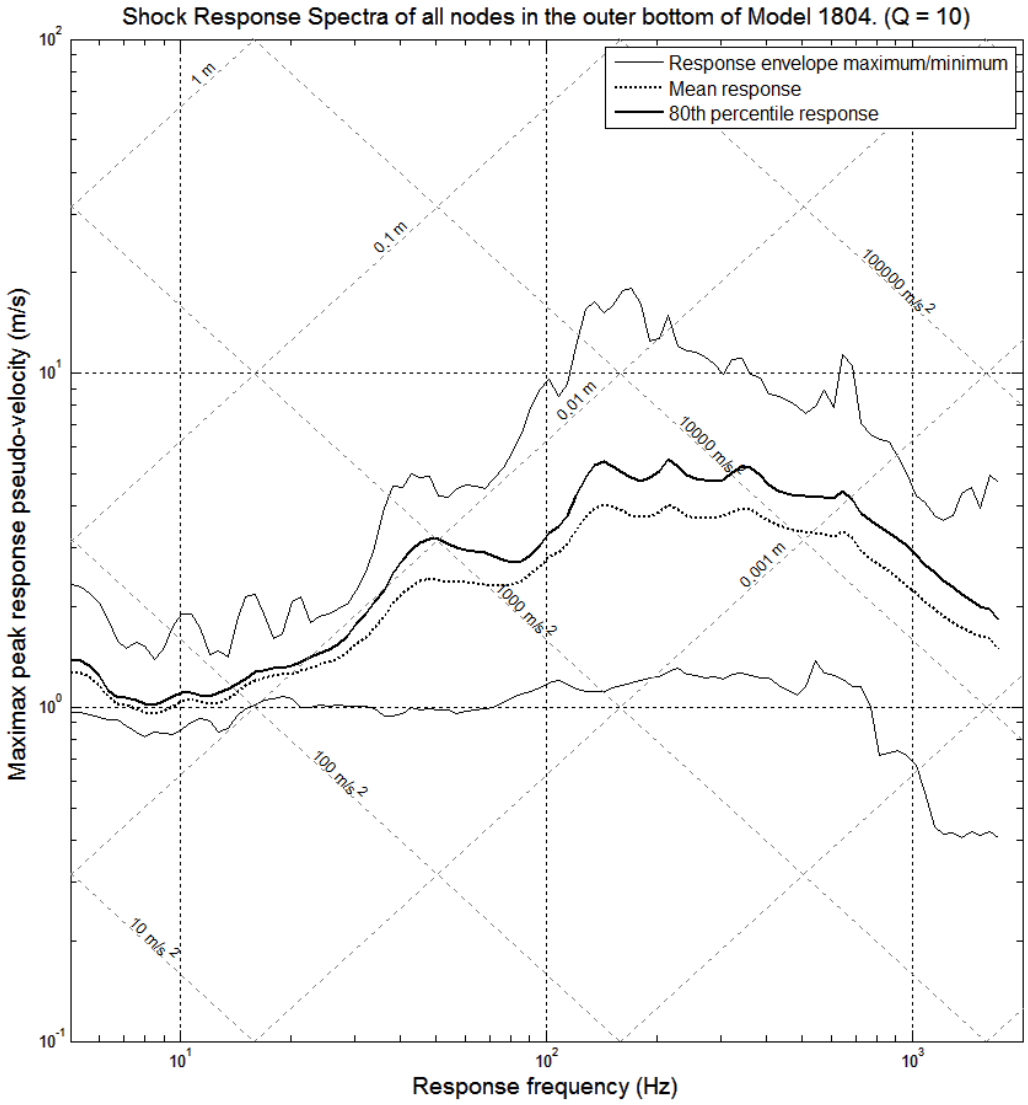

Figure H. 24 - Shock Response Spectrum of all nodes in the Outer Bottom region of Model 1804 (600mm x 1500mm Offset Bulb Plate stiffeners)

H.5 Model 1807 (flat bar stiffeners spaced at 600mm x 1200mm)

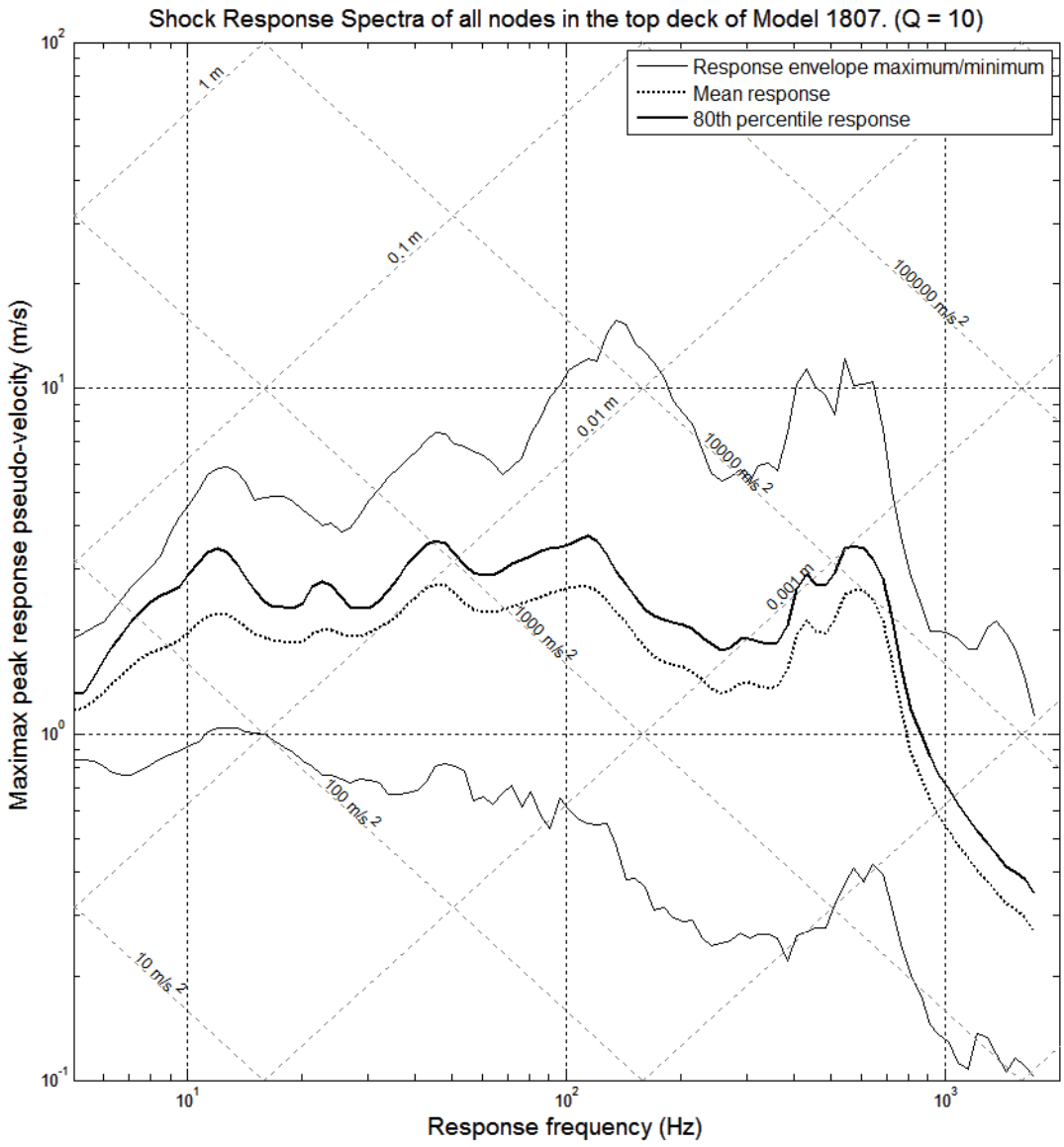

Figure H. 25 - Shock Response Spectrum of all nodes in the Top Deck region of Model 1807 (600mm x 1500mm flat bar stiffeners)

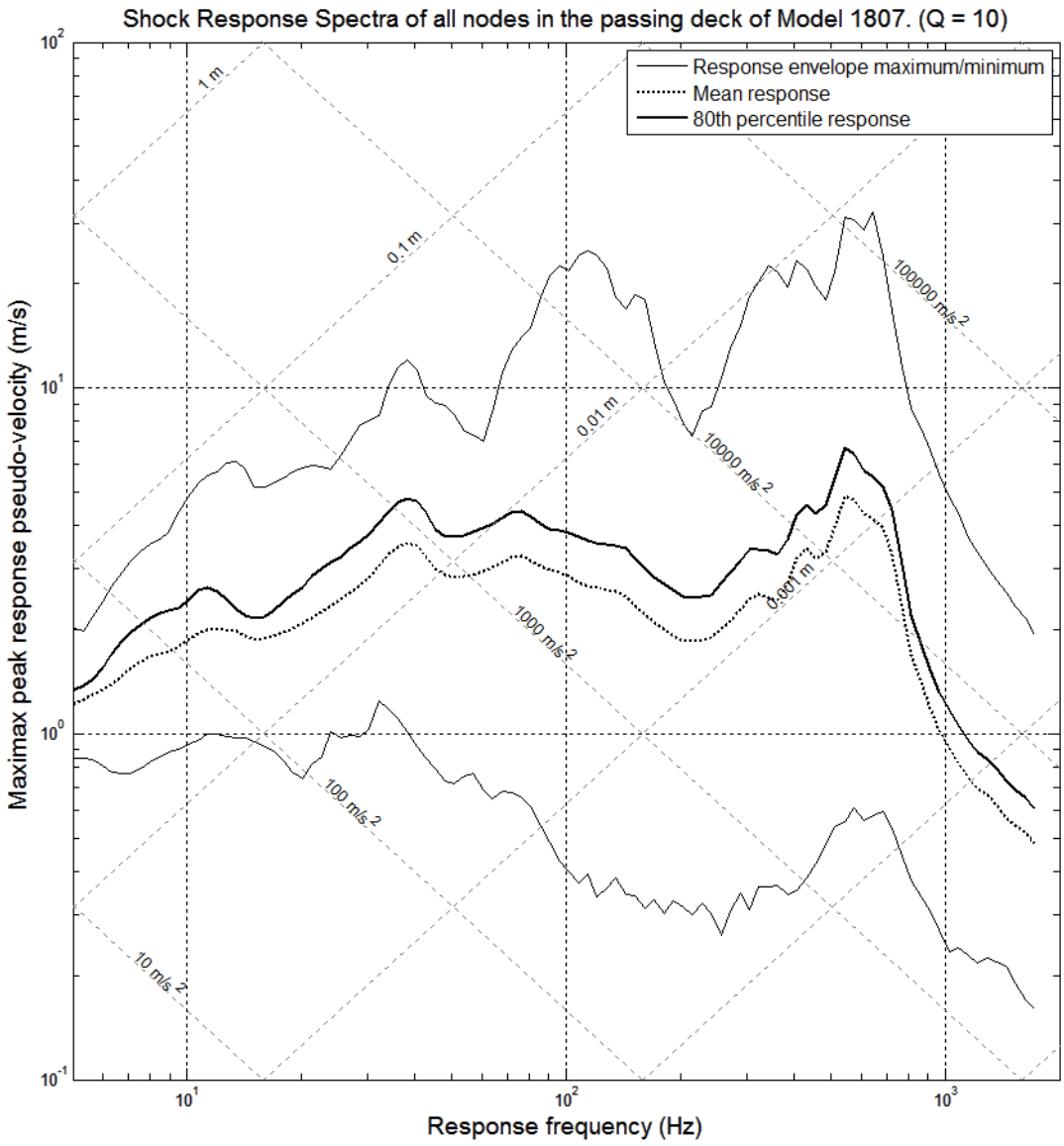

Figure H. 26 - Shock Response Spectrum of all nodes in the Passing Deck region of Model 1807 (600mm x 1500mm flat bar stiffeners)

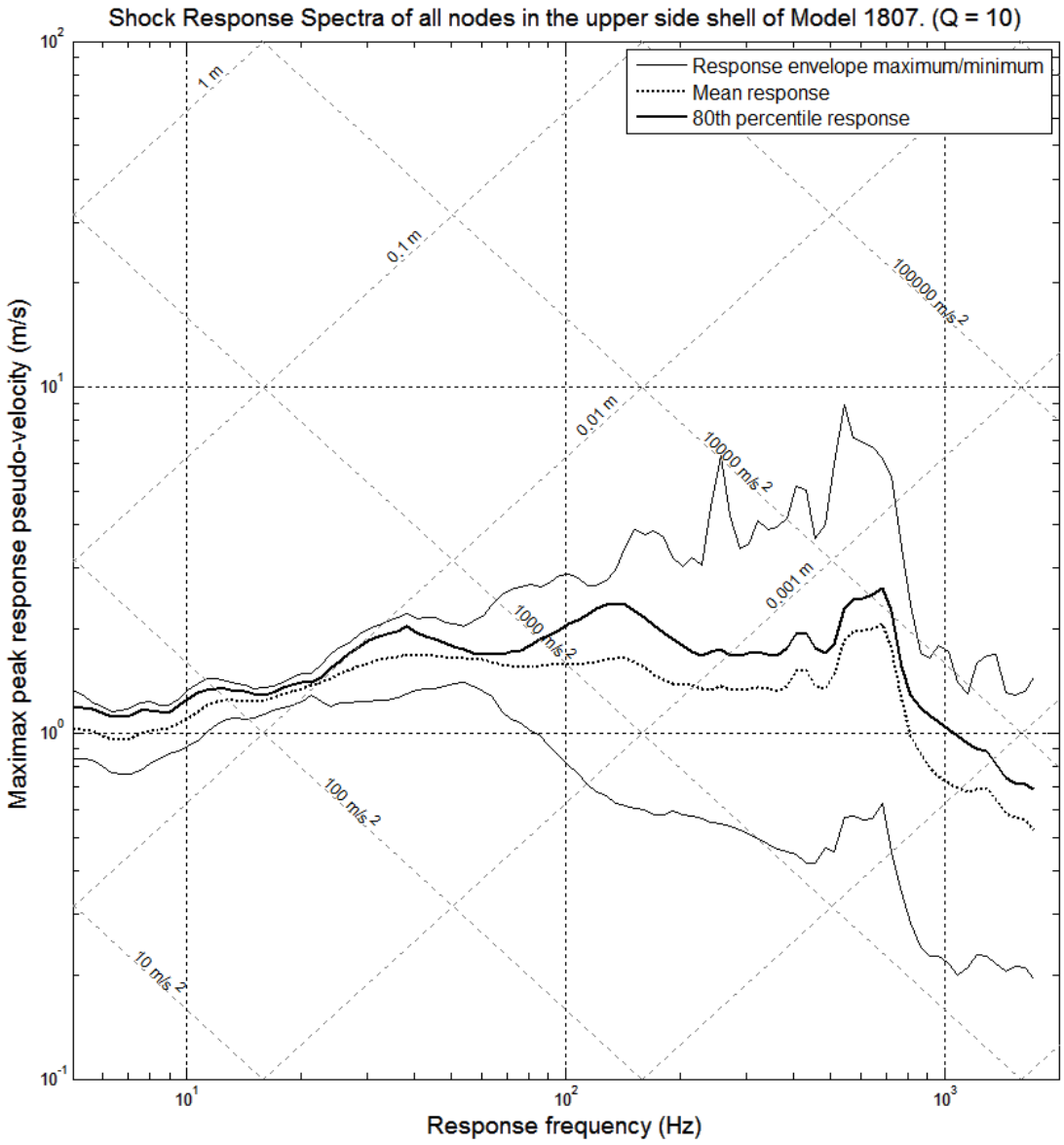

Figure H. 27 - Shock Response Spectrum of all nodes in the Upper Side Shell region of Model 1807 (600mm x 1500mm flat bar stiffeners)

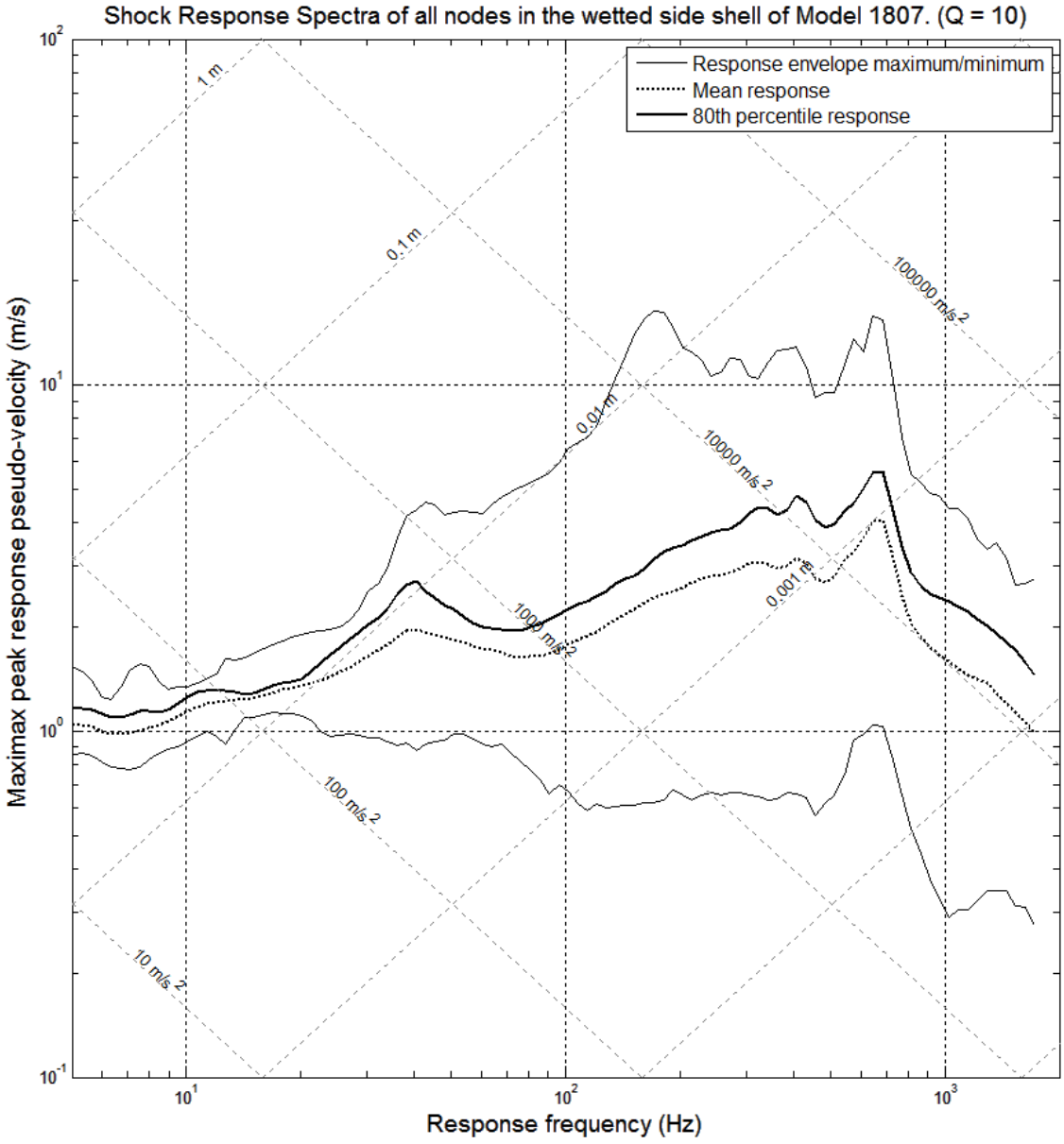

Figure H. 28 - Shock Response Spectrum of all nodes in the Wetted Side Shell region of Model 1807 (600mm x 1500mm flat bar stiffeners)

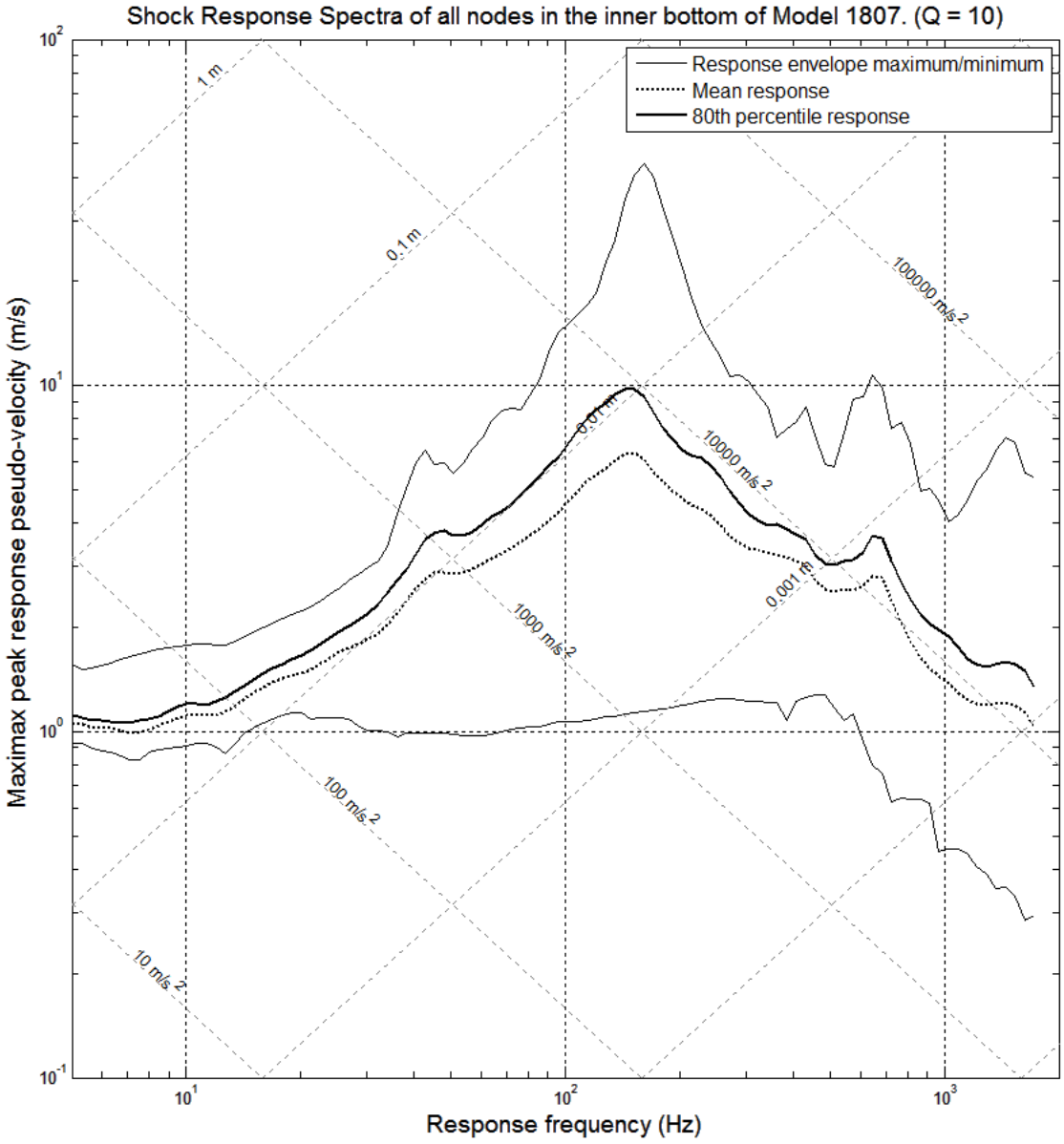

Figure H. 29 - Shock Response Spectrum of all nodes in the Inner Bottom region of Model 1807 (600mm x 1500mm flat bar stiffeners)

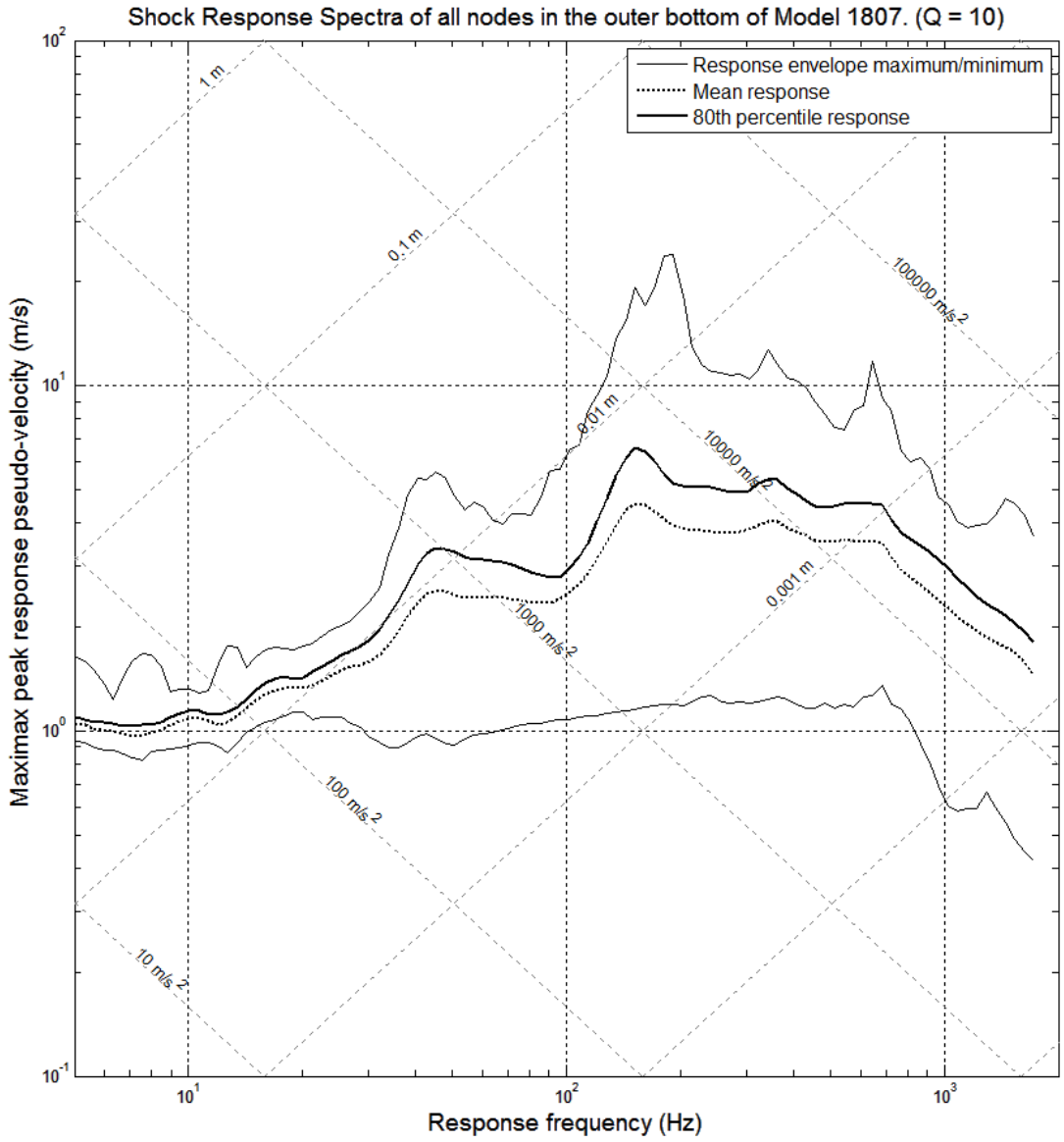

Figure H. 30 - Shock Response Spectrum of all nodes in the Outer Bottom region of Model 1807 (600mm x 1500mm flat bar stiffeners)

H.6 Model 1851 (Corvette model with longitudinal stiffening)

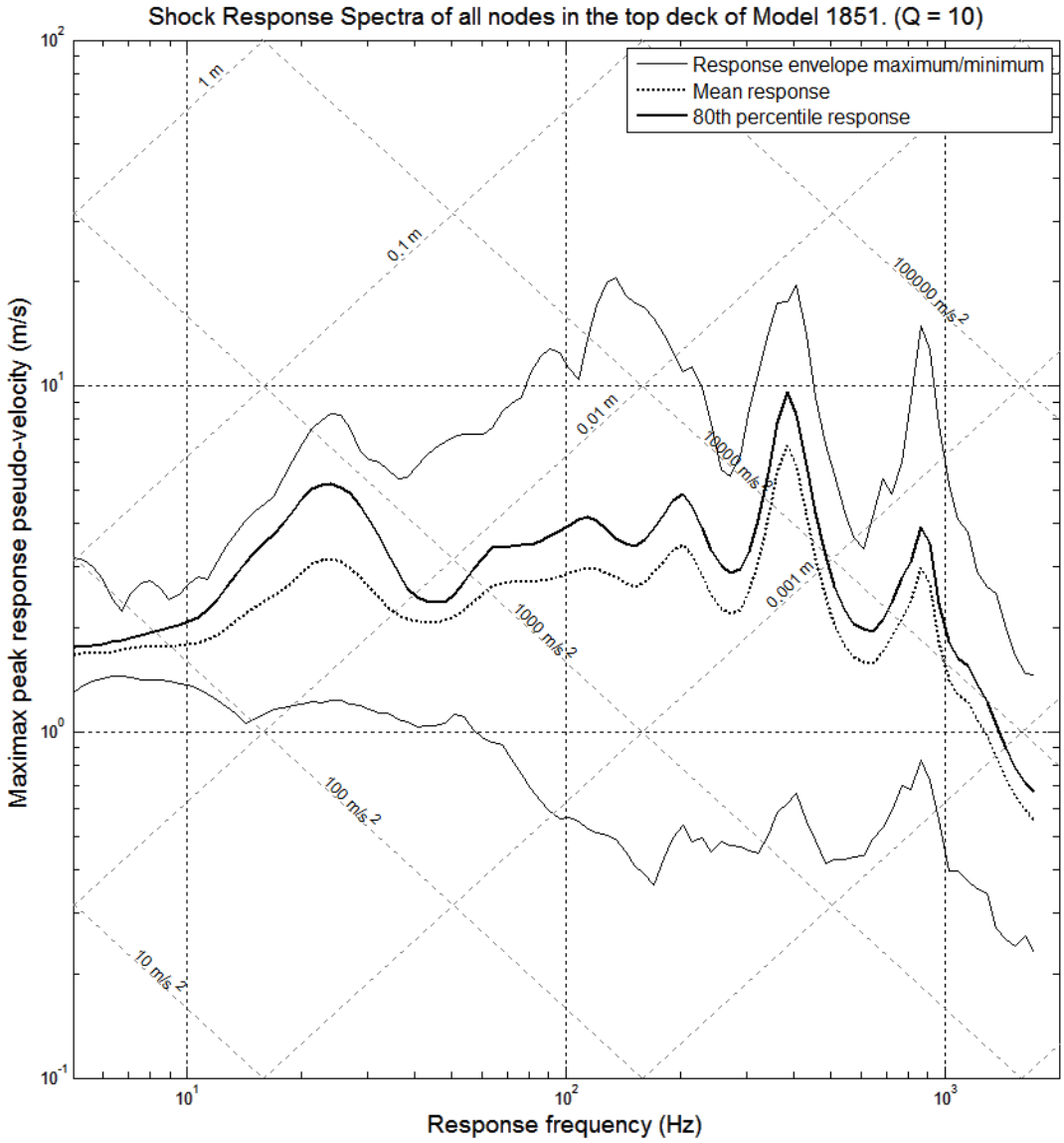

Figure H. 31 - Shock Response Spectrum of all nodes in the Top Deck region of Model 1851 (Corvette model with longitudinal T-bar stiffeners spaced at 600mm x 1500mm)

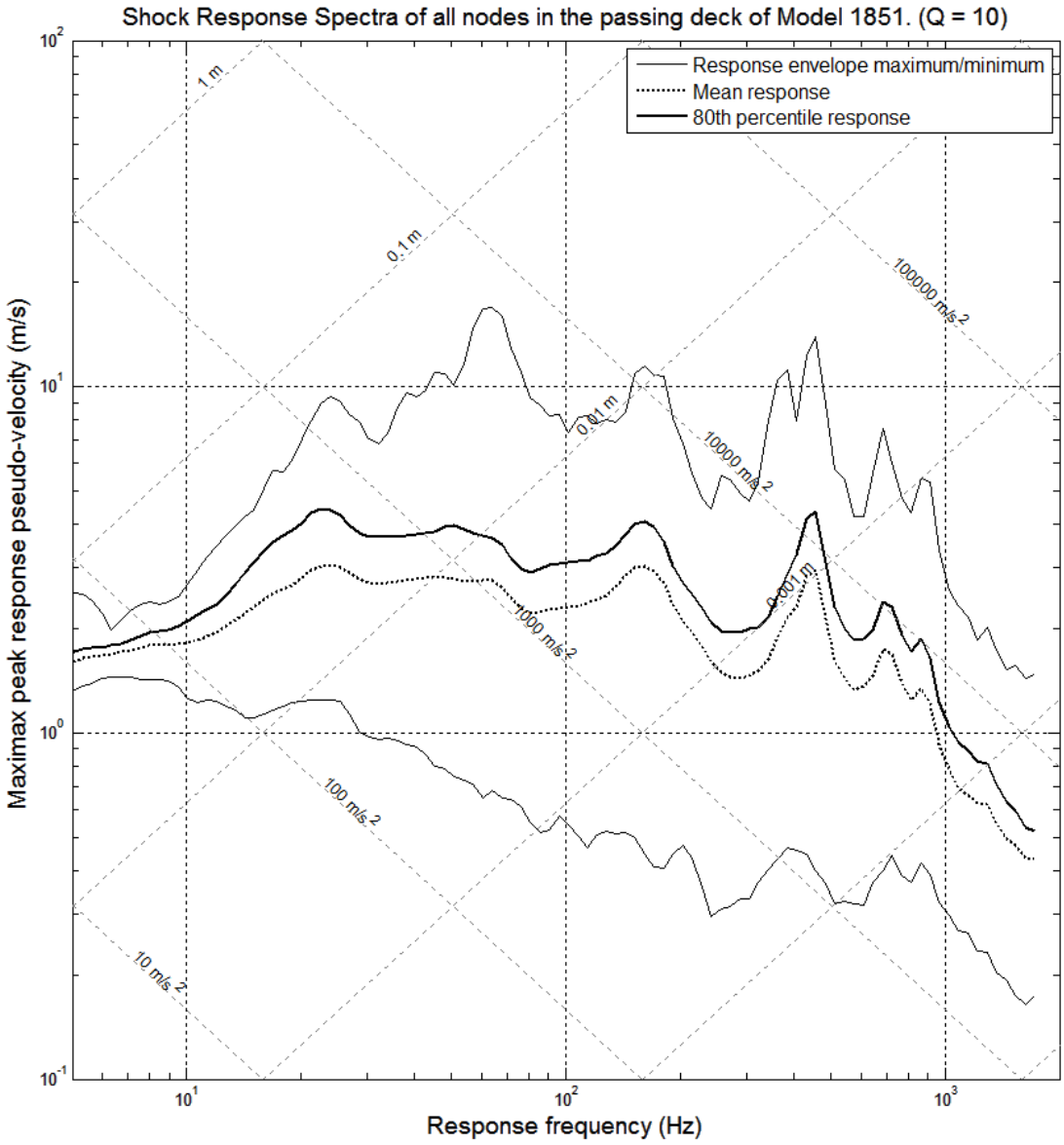

Figure H. 32 - Shock Response Spectrum of all nodes in the Passing Deck region of Model 1851 (Corvette model with longitudinal T-bar stiffeners spaced at 600mm x 1500mm)

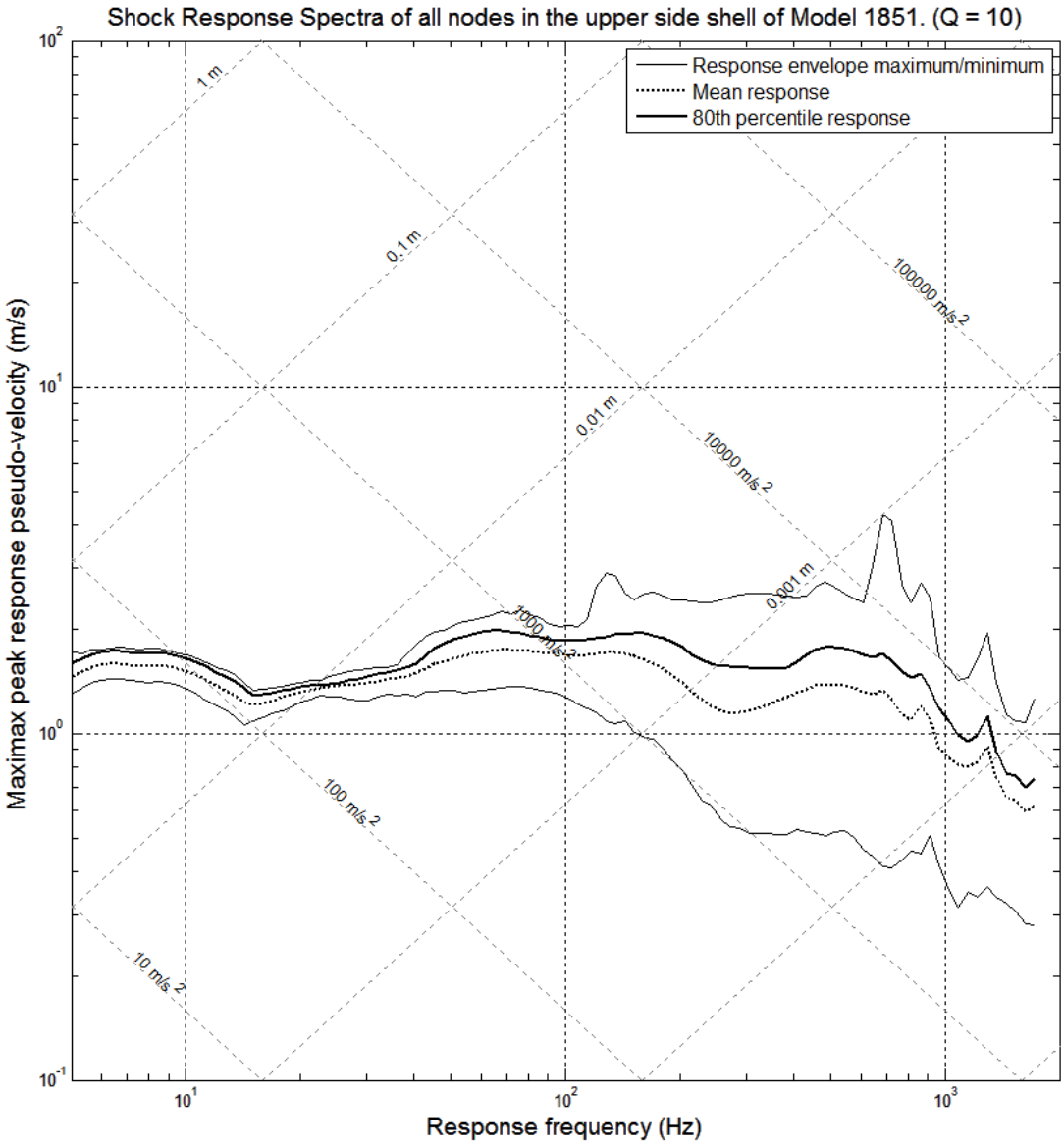

Figure H. 33 - Shock Response Spectrum of all nodes in the Upper Side Shell region of Model 1851 (Corvette model with longitudinal T-bar stiffeners spaced at 600mm x 1500mm)

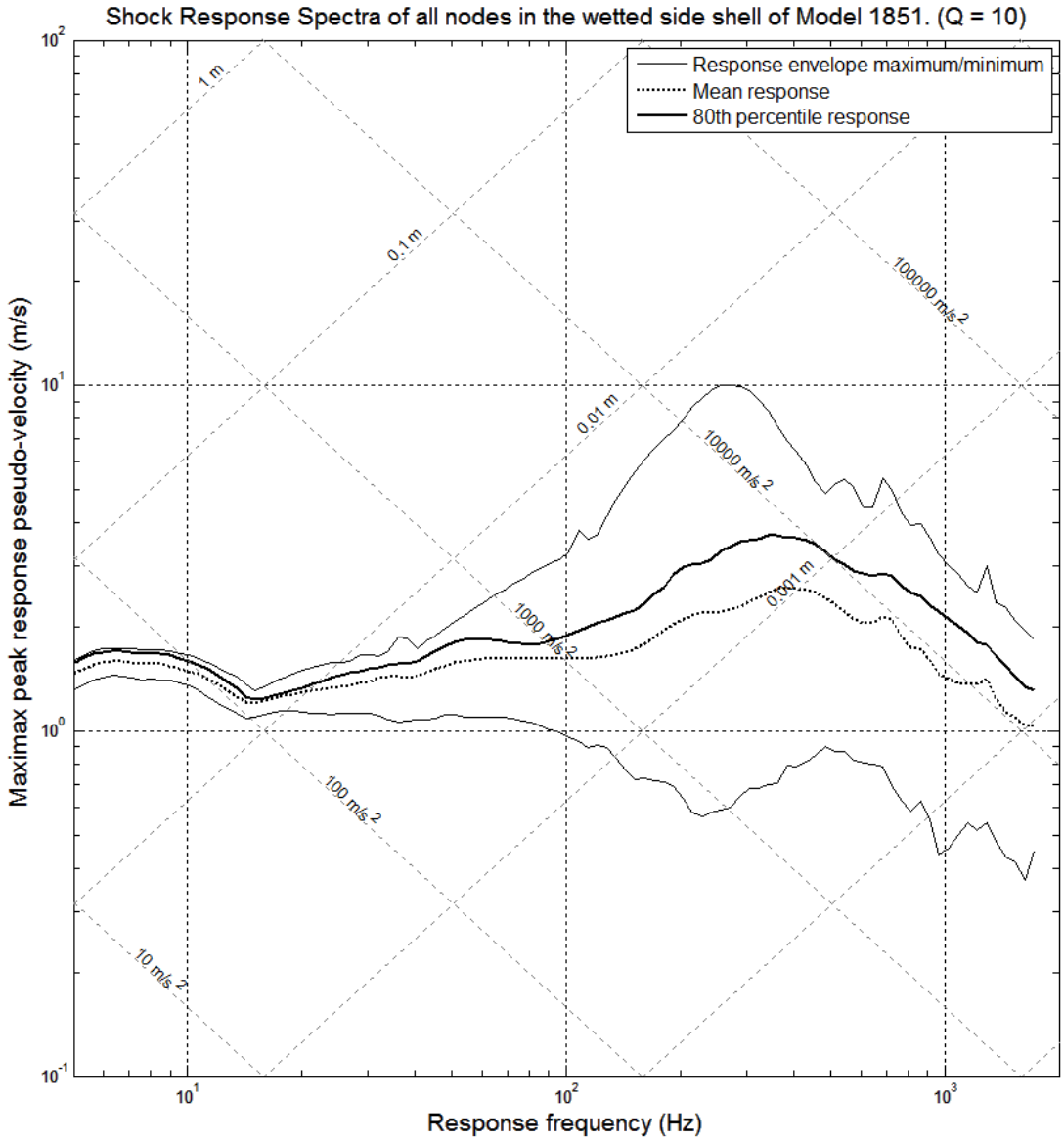

Figure H. 34 - Shock Response Spectrum of all nodes in the Wetted Side Shell region of Model 1851 (Corvette model with longitudinal T-bar stiffeners spaced at 600mm x 1500mm)

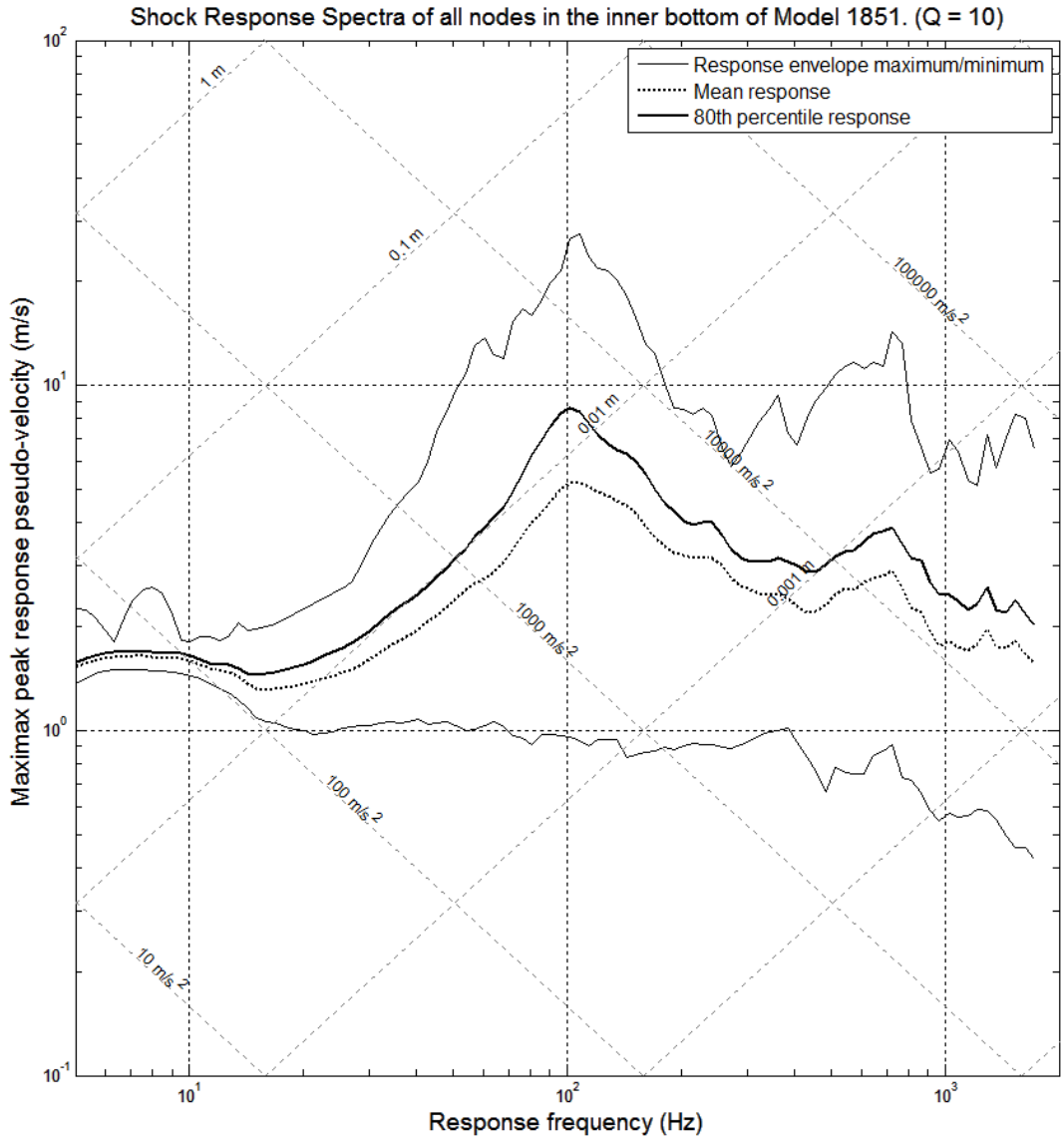

Figure H. 35 - Shock Response Spectrum of all nodes in the Inner Bottom region of Model 1851 (Corvette model with longitudinal T-bar stiffeners spaced at 600mm x 1500mm)

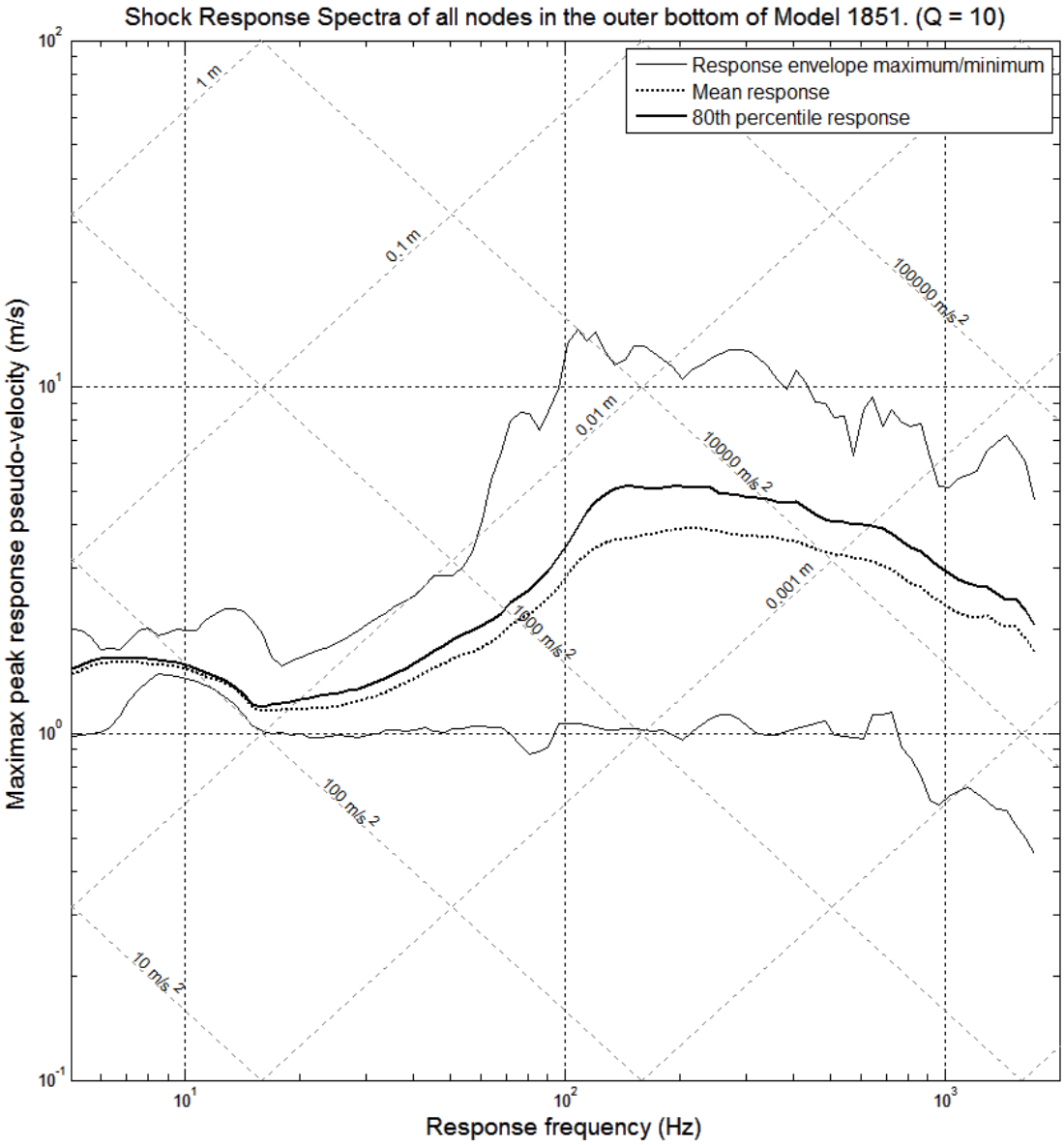

Figure H. 36 - Shock Response Spectrum of all nodes in the Outer Bottom region of Model 1851 (Corvette model with longitudinal T-bar stiffeners spaced at 600mm x 1500mm)

H.7 Model 1852 (Corvette model with transverse stiffening)

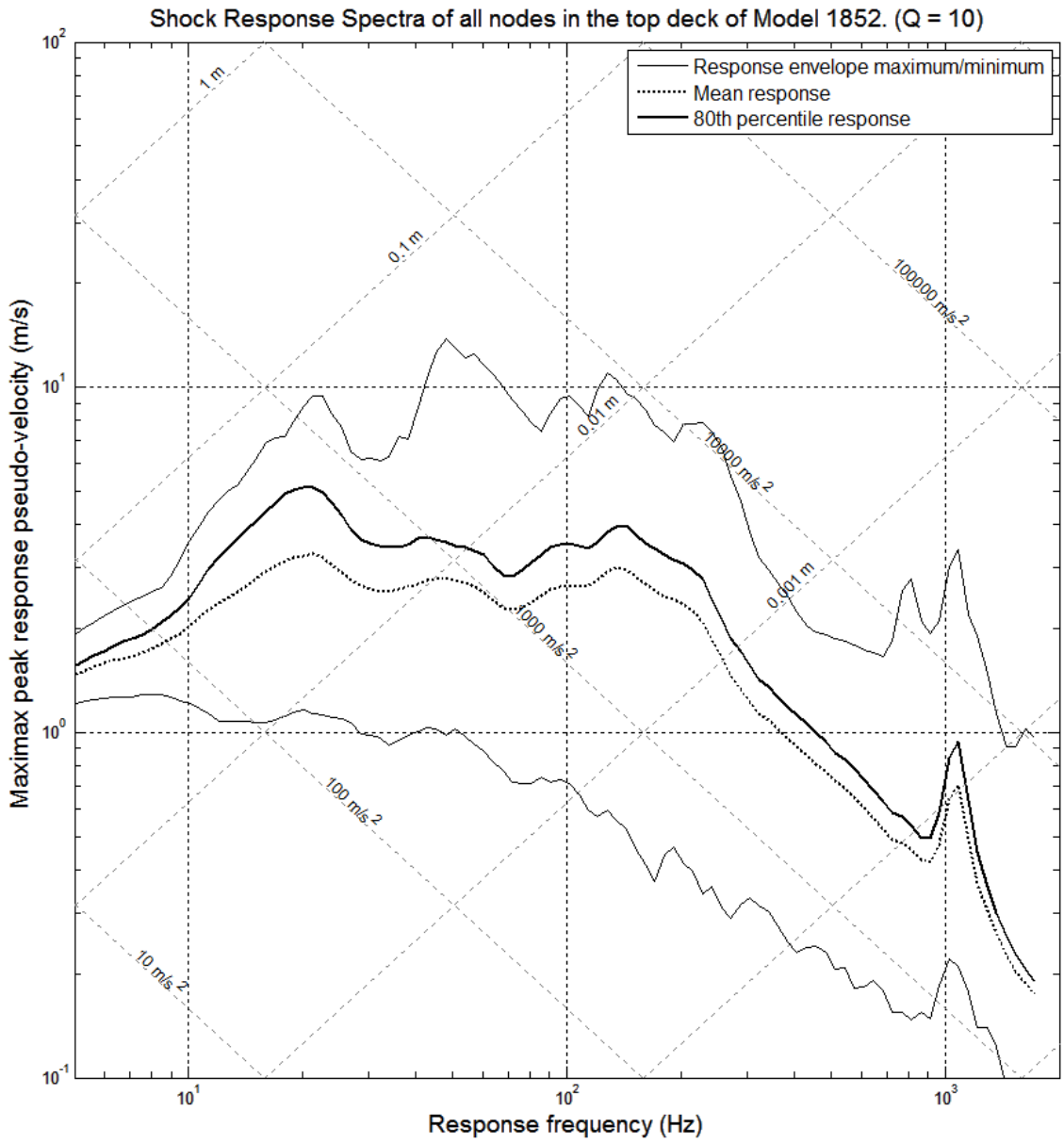

Figure H. 37 - Shock Response Spectrum of all nodes in the Top Deck region of Model 1852 (Corvette model with transverse stiffening spaced at 1500mm)

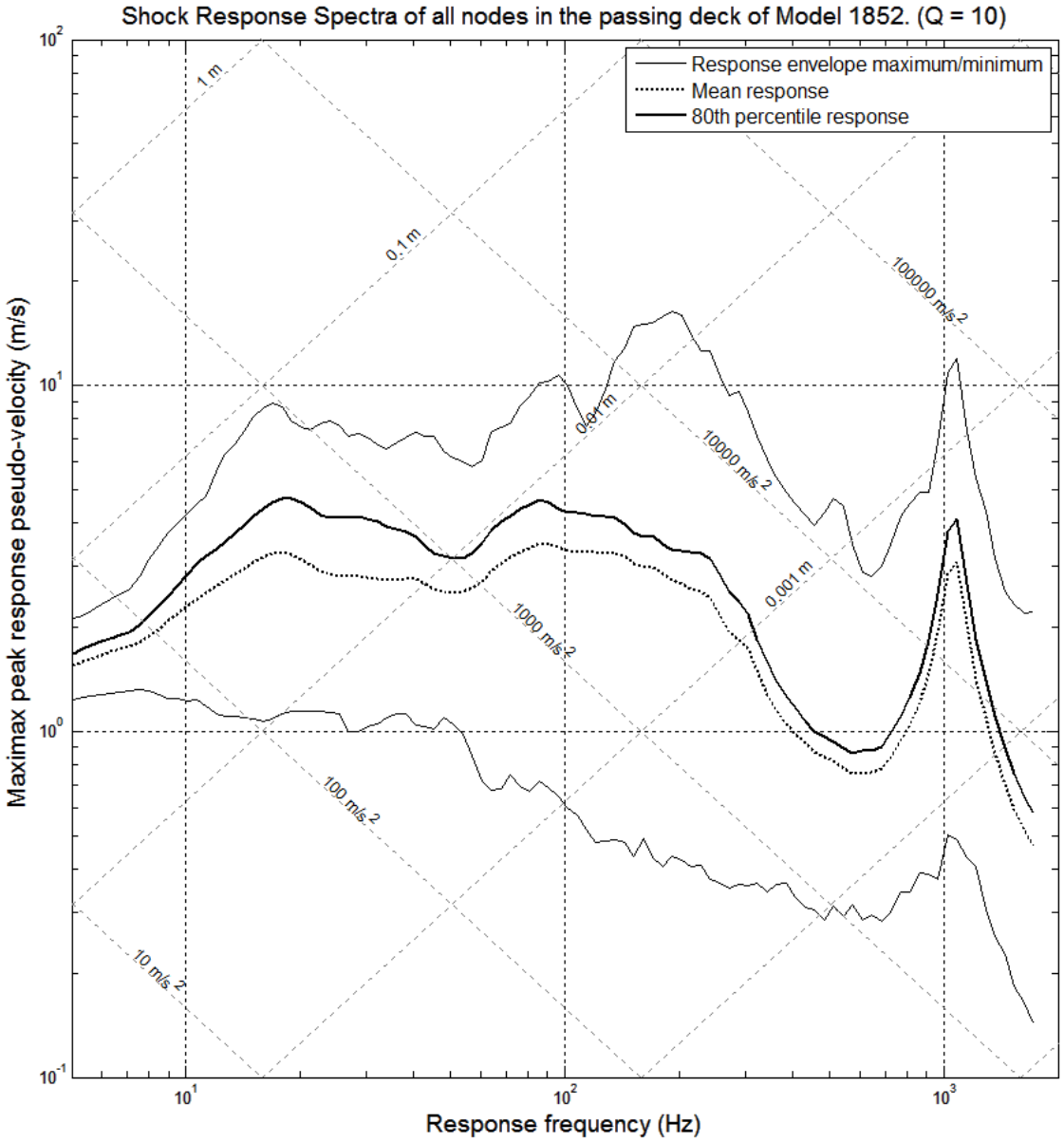

Figure H. 38 - Shock Response Spectrum of all nodes in the Passing Deck region of Model 1852 (Corvette model with transverse stiffening spaced at 1500mm)

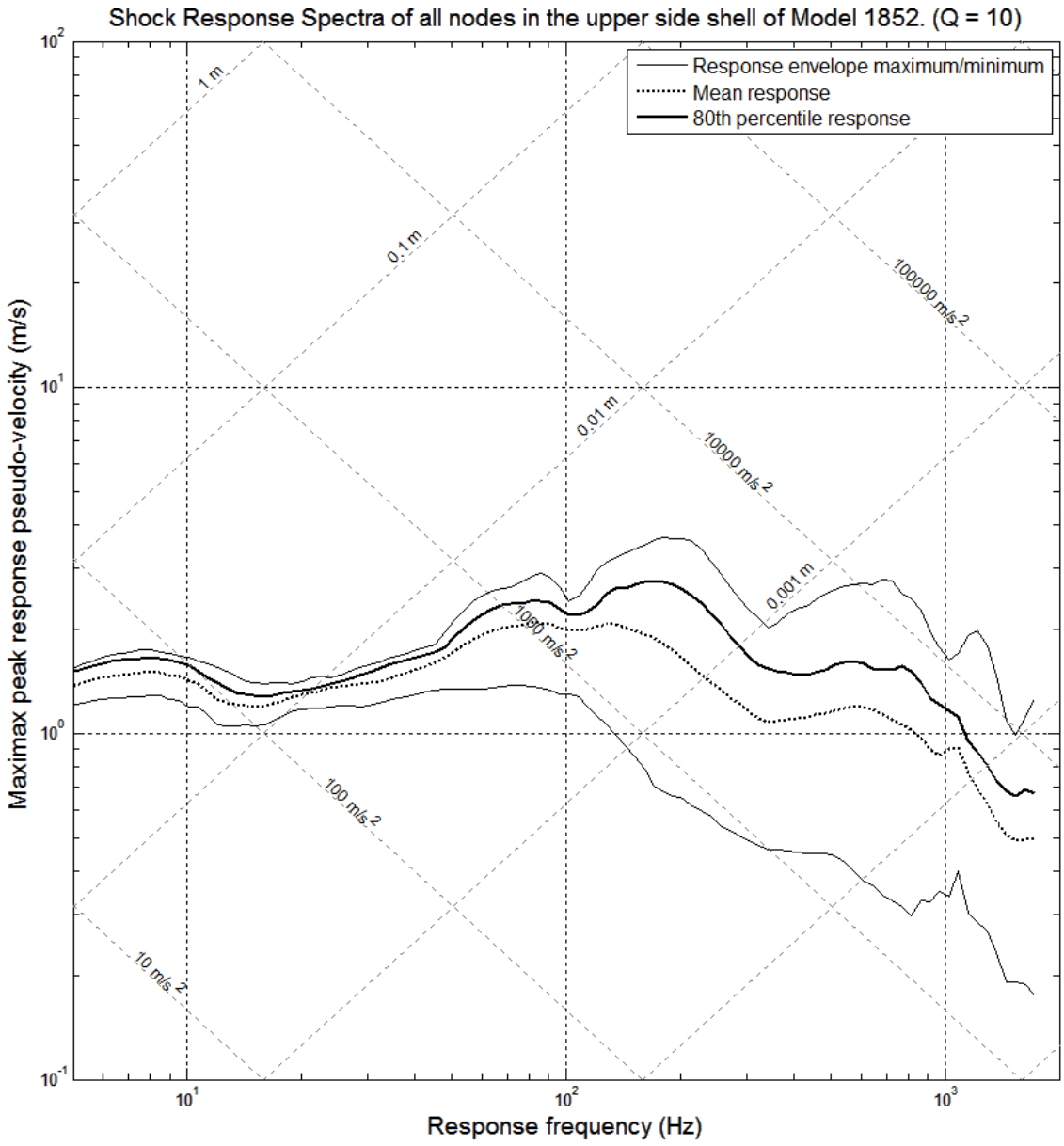

Figure H. 39 - Shock Response Spectrum of all nodes in the Upper Side Shell region of Model 1852 (Corvette model with transverse stiffening spaced at 1500mm)

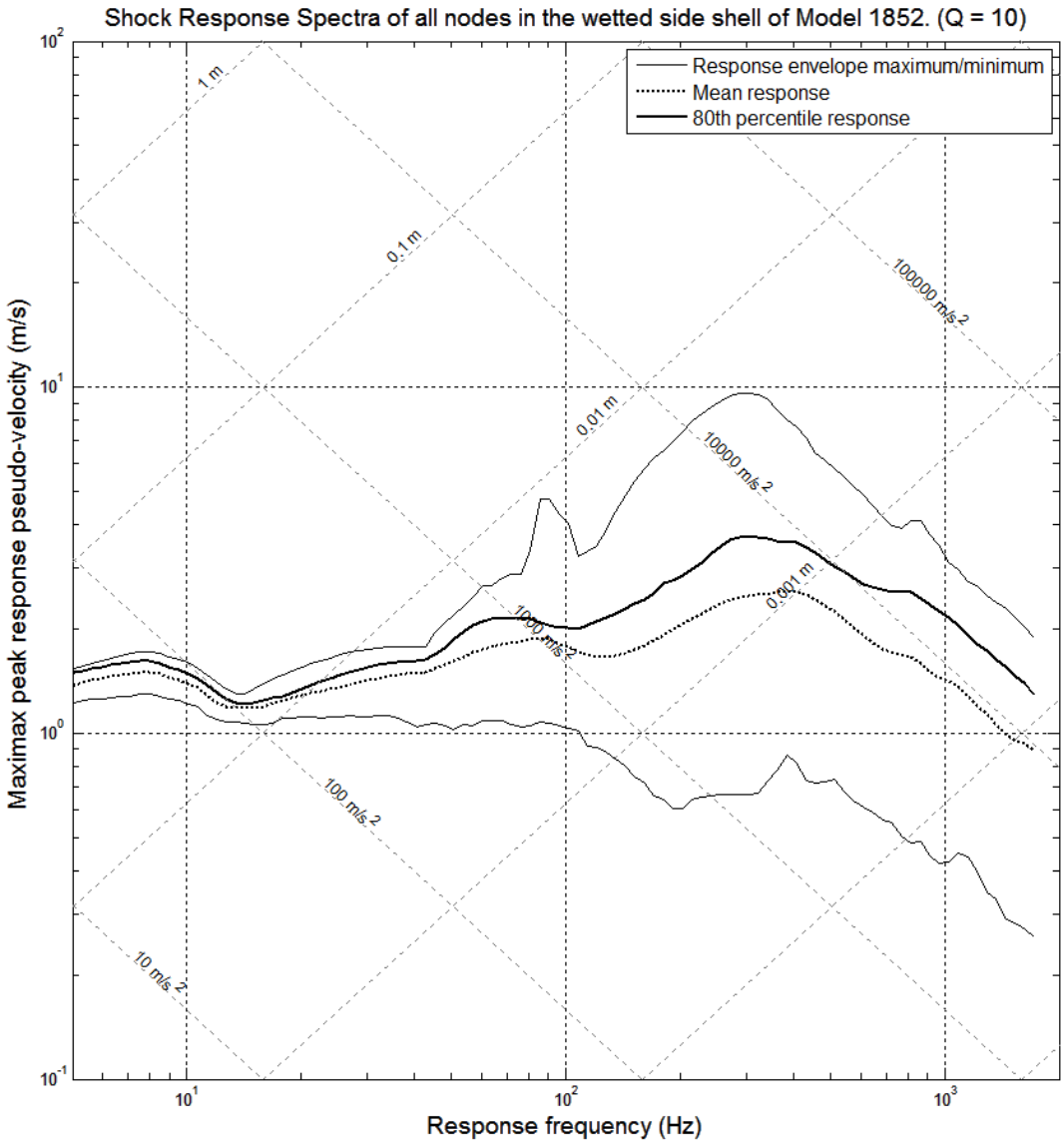

Figure H. 40 - Shock Response Spectrum of all nodes in the Wetted Side Shell region of Model 1852 (Corvette model with transverse stiffening spaced at 1500mm)

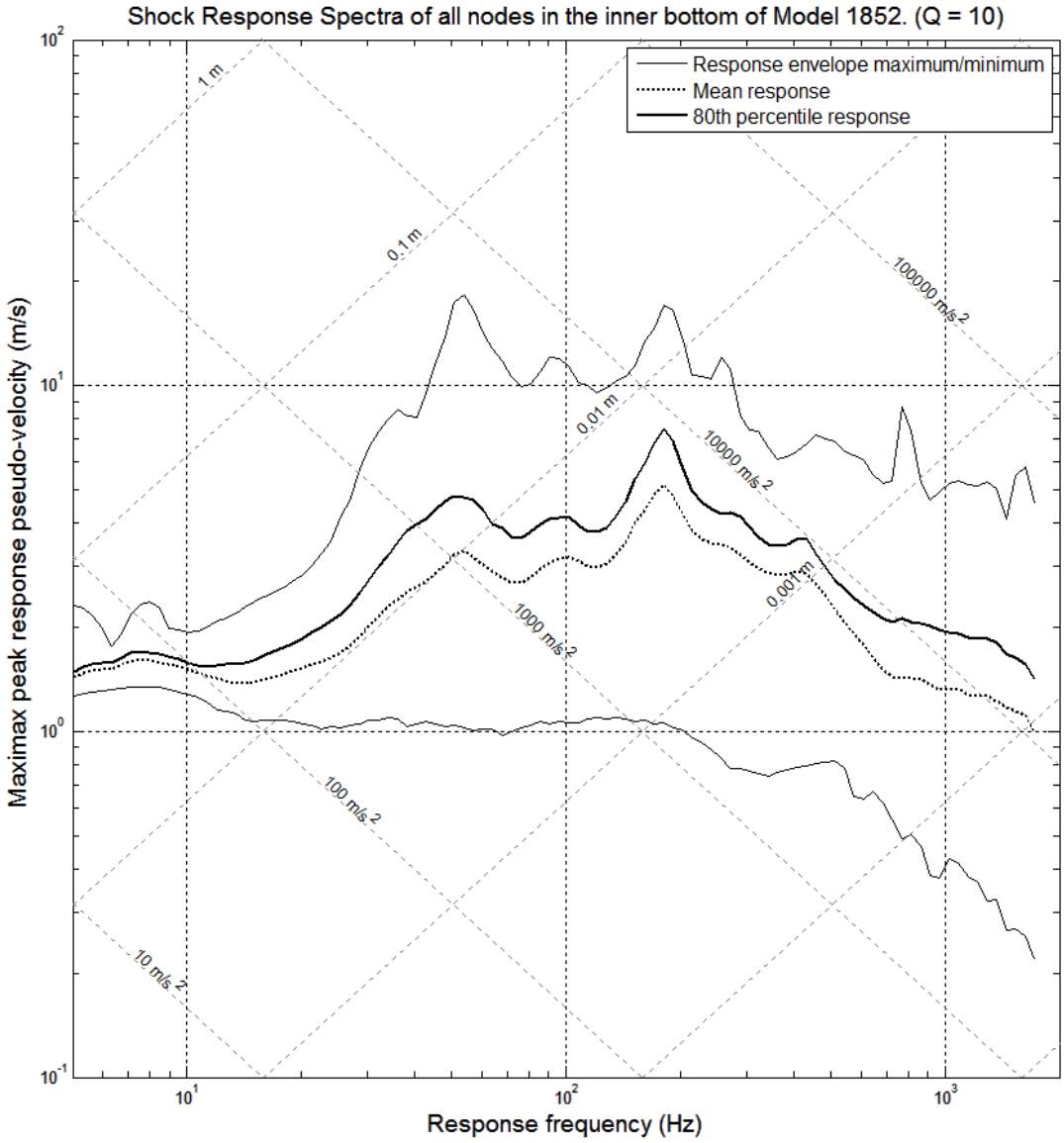

Figure H. 41 - Shock Response Spectrum of all nodes in the Inner Bottom region of Model 1852 (Corvette model with transverse stiffening spaced at 1500mm)

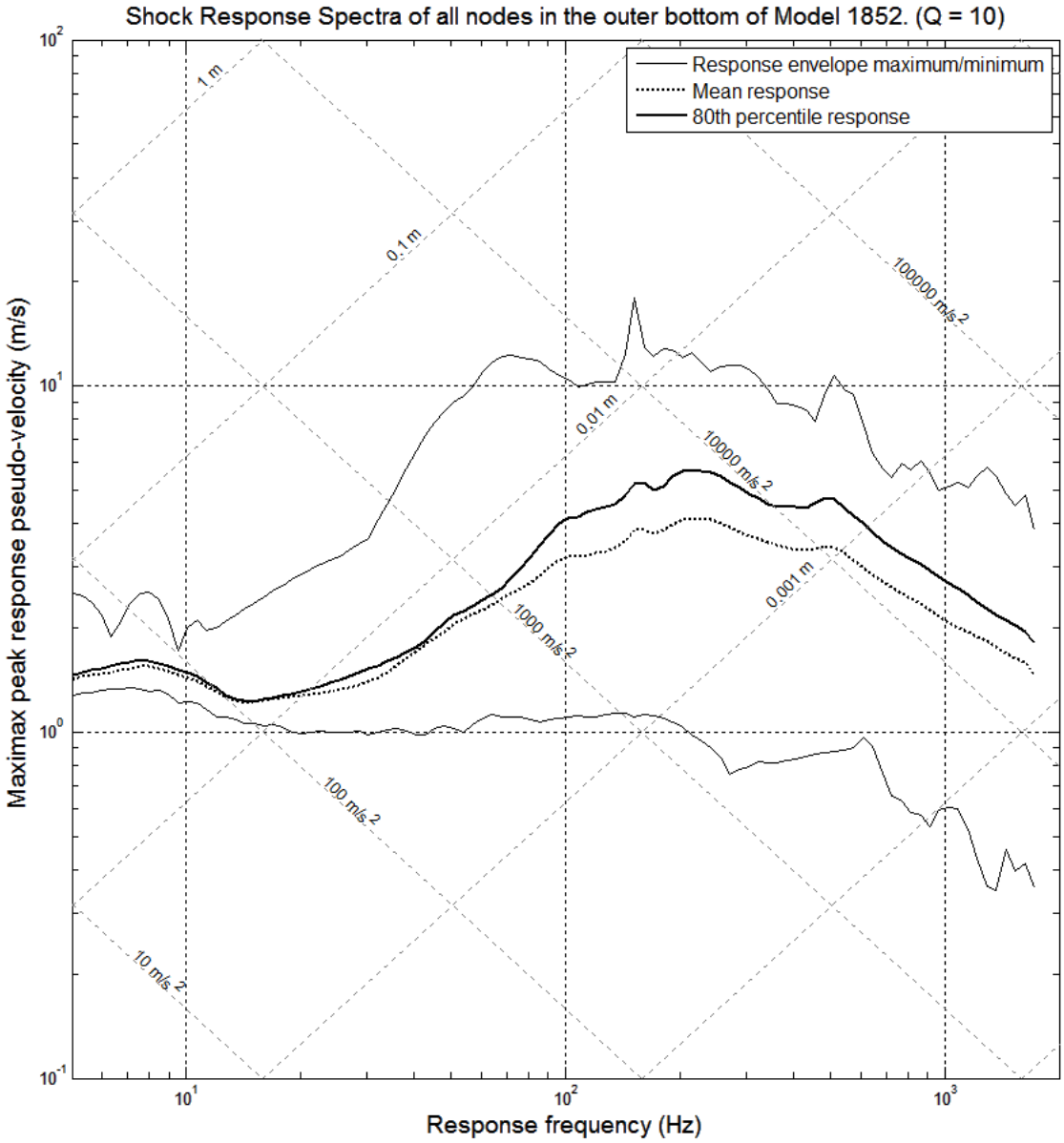

Figure H. 42 - Shock Response Spectrum of all nodes in the Outer Bottom region of Model 1852 (Corvette model with transverse stiffening spaced at 1500mm)